# Role of Topoisomerases in mitochondrial biology of the human malaria parasite Plasmodium falciparum

A Thesis

Submitted to the University of Hyderabad for partial fulfilment of the award of a Ph.D. degree in the Department of Biotechnology and Bioinformatics, School of Life Sciences,

University of Hyderabad

Вy

Priyanka Singh

17LTPH05





Department of Biotechnology and Bioinformatics

School of Life Sciences

University of Hyderabad

Hyderabad-500046 Telangana, India

**Date** 

**July 2023** 



## UNIVERSITY OF HYDERABAD

Department of Biotechnology and Bioinformatics

School of Life Sciences

#### DECLARATION

I, Priyanka Singh, hereby declare that this thesis entitled, "Role of Topoisomerases in mitochondrial biology of the human malaria parasite Plasmodium falciparum" submitted by me under the guidance and supervision of Dr. Sunanda Bhattacharyya, is an original and independent research work. I also declare that it has not been submitted previously in part or in full to this University or any other University or Institution for the award of any degree or diploma.

(Research Supervisor)

Priyanka Singh

(17LTPH05)

(Research Scholar)



# UNIVERSITY OF HYDERABAD

# Department of Biotechnology and Bioinformatics

## School of Life Sciences

#### CERTIFICATE

This is to certify that this thesis entitled, "Role of Topoisomerases in mitochondrial biology of the human malaria parasite *Plasmodium falciparum*" is a record of bona fide work done by Priyanka Singh, a research scholar for the Ph.D. program in Department of Biotechnology and Bioinformatics, School of Life Sciences, University of Hyderabad under my guidance and supervision. The thesis is free from plagiarism and has not been submitted previously in part or in full to this or any other University or Institution for the award of any degree or diploma.

## A. Part of this thesis has been published in the following journals:

- Priyanka Singh, Wahida Tabassum, Nupur Fangaria, Sandeep Dey, Siladitya Padhi, Mrinal K. Bhattacharyya, Kota Arun Kumar, Arijit Roy, and Sunanda Bhattacharyya\*, Plasmodium Topoisomerase VIB and Spo11 Constitute Functional Type IIB Topoisomerase in Malaria Parasite: Its Possible Role in Mitochondrial DNA Segregation (2023), Microbiology Spectrum, doi: https://doi.org/10.1128/spectrum.04980-22
- 2) Shephali Bansod, Navneet Bung, Priyanka Singh, Niranjan Suthram, Himashree Choudhury, Arijit Roy, Gopalkrishnan Balusu, Sunanda Bhattacharyya\*, Elucidation of an essential function of the unique charged domain of *Plasmodium* topoisomerase III (2020), Biochemical Journal, doi: 10.1042/BCJ20200318

#### B. Part of the work has been presented in the following conferences:

- 1. Poster presentation entitled, 'Study of mitochondrial import and mt-DNA recruitment of Plasmodium falciparum topoisomerase VI' in Molecular parasitology meeting, MPM XXXII 2021, Marine Biological Laboratory, Woods Hole, Massachusetts, United States, October 5-9, 2021.
- 2. Lightning talk entitled "Plasmodium Topoisomerase VIB and Spo11 constitute functional type IIB topoisomerase in the malaria parasite, Future of Malaria Research Symposium, 2022, Johns Hopkins Bloomberg School of Public Health, Baltimore, Maryland, United States, October 28th, 2022.
- 3. Oral presentation entitled, 'Topoisomerase VI: a functional type II mitochondrial topoisomerase in the malaria parasite Plasmodium falciparum' in BioAnveshna, Symposium on frontiers in Biotechnology and Bioinformatics, Department of Biotechnology and Bioinformatics, University of Hyderabad, November 7-8, 2022.

#### C. Publications from other projects:

- 1. Nupur Fangaria, Khushboo Rani, Priyanka Singh, Sandeep Dey, Kota Arun Kumar, and Sunanda Bhattacharyya\*, DNA damage-induced nuclear import of HSP90a is promoted by Aha1 (2022), Molecular Biology of the Cell, doi:10.1091/mbc. E21-11-0554
- 2. Priyanka Singh, Khushboo Rani, Akanksha Gotmare, Sunanda Bhattacharyya\*, A tale of topoisomerases and the knotty genetic material in the backdrop of Plasmodium biology (2022), Bioscience Reports, doi: 10.1042/BSR20212847
- 3. Wahida Tabassum, Priyanka Singh, Niranjan Suthram, Sunanda Bhattacharyya\*, Mrinal Kanti Bhattacharyya\*, Synergistic action between PfHsp90 inhibitor and PfRad51 inhibitor induces elevated DNA damage sensitivity in the malaria parasite (2021), Antimicrobial Agents and Chemotherapy, doi:10.1128/AAC.00457-21

(DOBB)

Dept. of Biotechnology & Bioinformatics University of Hyderabad Hyderabad.

Dept. of Biotechnology & Bioinformatics
School of Cafe States Sor
University of Hyderabad
Gachibowli, Hyderabad-500 046.

(School of Life, S जीव विज्ञान राकाय / School of Life Scien

हैदराबाद विश्वविद्यालय/University of Hydera हैदरावाद / Hyderabad-500 046

SI No. 1840 Notification No. 1

## हैदराबाद विश्वविद्यालय

## **UNIVERSITY OF HYDERABAD**

(A Central University Established by an Act of Parliament)

P.O. CENTRAL UNIVERSITY, GACHIBOWLI, HYDERABAD - 500 046 (INDIA)

SEMESTER GRADE TRANSCRIPT

**REGULAR EXAMINATION** 

REG. NO. 17LTPH05

NAME OF THE STUDENT PRIYANKA SINGH

MONTH AND YEAR OF NOV 2018 SEMESTER 1

COURSE Ph.D. BIOTECHNOLOGY

PARENT'S NAME HARNARAYAN SINGH /

COURSE NO	TITLE OF THE COURSE	CREDITS	RESULTS
BT801	RESEARCH METHODOLOGY/ANALYTICAL TECHNIQUES	4	PASS
BT802	RESEARCH ETHICS, BIOSAFETY, DATA ANALYSIS AND	4	PASS
BT803	SCIENTIFIC WRITING AND RESEARCH PROPOSAL	4	PASS

SEMESTER GRADE POINT AVERAGE (SGPA):10.0

(In words) :TEN POINT ZERO

DEPUTY REGISTRAR (ACAD & EXAMS)

Date Of Result Notification : Jan 9, 2019

Date Of Download: Jul 10, 2023

This is system generated certificate issued by O/o The Controller of Examinations, University of Hyderabad

### Acknowledgements

I would like to utilize this opportunity to thank everyone who helped make my thesis possible.

Firstly, I want to thank everyone for their kindness and support, which enabled me to conduct this research project and the fortitude to see it through to a successful end.

I would like to extend my thanks to my PhD advisor, Dr. Sunanda Bhattacharyya, for enabling me to take part in this project and for careful scrutinising my development, and for her significant guidance throughout my PhD programme.

I am grateful to Prof. Mrinal Bhattacharyya for his critical inputs, timely suggestions and providing useful commendations during my Ph.D. I want to express my sincere thanks to my doctoral committee members, Prof. Anand K Kondapi, and Prof. Mrinal K Bhattacharyya for their valuable advice during my research.

I thank the Head of department, Biotechnology, and bioinformatics Prof. J.S.S Prakash, and the former heads, Prof. K.P.M.S.V Padmasree, Prof. Anand Kondapi and Prof. Niyaz Ahmed, for allowing us to make use of all the research facilities within the department.

I show my gratitude to the Dean of School of Life Sciences, Prof. N. Siva Kumar, and the former Deans, Prof S. Dayananda Prof. R.P. Sharma, Prof. P. Reddanna, and Prof. KVA Ramaiah for supporting us with all the research amenities.

Using this opportunity, I would want to express my gratitude to Dr. Arijit Roy of TCS Innovation Labs for his assistance with my computational modelling and structural analysis. I appreciate the assistance and support of the entire School of Life Sciences team, both teaching and non-teaching. I want to thank CSIR (Council of Scientific & Industrial Research) for supporting my research financially for five years.

I would like to thank the funding organizations DBT, DST-SERB, CSIR, DST-FIST, and UGC-SAP for their support to the lab financially.

I am grateful for the money provided by DST-FIST, DBT-CREBB, UGC-SAP, and DST-PURSE to the school and department for shared facilities that supported my research.

A sincere thanx to my dear lab mates and seniors Dr. Niranjan Suthram and Dr. Wahida Tabassum for your tremendous encouragement, pep-talks, inspiration, and humour. Also, I would like to show gratitude to my seniors Dr, Shephali Bansod, Dr. Nupur Fangaria, and also to my lovely, enthusiastic juniors Abhilasha, Tanishka, Khushboo, Akanksha, Iman, Shradha, Pooja, Jyoti, and Deepak for their timely help, support, and for keeping the environment energetic in the lab.

I thank all the present M.Sc. Project students from the Bhattacharyya's lab, Shreyasee, Deepanshu, Tiyas, Apeksha, Maria and Pallavi for their help and co-operation.

I want to thank our lab attender Mr. Ramesh for his help in the lab.

I honestly appreciate all my SLS friends' contributions to scientific debates, advice, and enjoyable conversations.

I appreciate a lot of people, but I want to thank my family for their support and encouragement. I am indebted to my parents for the invaluable and unwavering love. To my dad, the late Mr. Har Narayan Singh: I will succeed if I can muster half your courage. I hope that you are proud of me. I want to thank my mother for always being an inspiration to me—a woman who is full of love and determination. I want to show my sincere admiration to my brother for always being there and supporting my decisions in life. Immense thanks to my best friend and my life partner, Anjulesh, we both know I could not have done this without you. Thanks for keeping me on my toes.

At last, Finally, I thank staff of Health Centre, University of Hyderabad for helping me in this journey.

\*Priyanka Singh\*\*



### **Table of Content**

## Chapter 1. Introduction and scope of the thesis

1.1. History of malaria and Global malaria burden	14
1.2. The social and economic burden of malaria parasite	14
1.3. Ecology of malaria parasite	15
1.3a. Malaria Parasite and its transmission	15
1.3b. Dual host life cycle	16
1.4. Challenges in malaria control and treatment	19
1.4a. Antimalarial drug resistance	19
1.4b. Antigenic variation	19
1.4c. Current scenario in malaria research	19
1.5. Understanding parasite biology from a molecular perspective to develop new anti-mal	arial targets
1.5a. Replication and Cell division in malaria parasite: Endoreduplication	21
1.6. Malaria parasite organelle development	24
1.6.1. Mitochondria of malaria parasite	24
1.6.1a. TCA cycle of the malaria parasite	25
1.6.1b. Mitochondrial Electron transport chain	27
1.6.1c. Inhibition of Mitochondrial Electron transport chain by Atovaquone	29
1.7. Topoisomerases: Molecular Scissors of the DNA	30
1.7.1. Classification of Topoisomerases	30
1.7.1.1. Type I DNA topoisomerases	31

1.7.1.1a. Topoisomerase III in other eukaryotes	34
1.7.1.1b. Topoisomerase III of human malaria parasite	35
1.7.2. Type II DNA topoisomerases	39
1.7.2a. Topoisomerase VI a vital protein in many eukaryotes	41
1.7.2b. Topoisomerase VI of human malaria parasite	43
1.7.2c. Topoisomerases as target	46
1.7.2d: Radicicol-a Topoisomerase VI inhibitor	47
1.8. Objectives of the study	49
1.9. Specific Aims	50
1.10. Significance of the Study	51
Chapter 2. Materials & Methods	53
2.1 Molecular Biology techniques	53
2.1.1 Bacterial competent cell generation	53
2.1.2 Bacterial transformation	53
2.1.3 Plasmid DNA isolation method	54
2.1.4 Site-directed mutagenesis	55
2.1.5 Western Blotting	55
2.1.6 FAIRE	56
2.1.7 Co-IP	57
2.1.8 ChIP	58
2.2. Cell Biology	59
2.2.1. Immunofluorescence assay and Fluorescence Microscopy	59

2.3 Yeast genetic techniques	60
2.3.1. Yeast Competent Cell generation	60
2.3.2. Yeast transformation	61
2.3.3. Protein isolation from yeast cells and western blot analysis	61
2.3.4. Yeast strains generation and Yeast Sporulation	62
2.3.5. Yeast-two hybrid analysis	63
2.4 Methods in <i>Plasmodium falciparum</i> culture	64
2.4.1 Red Blood cells washing	64
2.4.2 Freezing of <i>Plasmodium</i> parasites	64
2.4.3 Thawing of malaria parasites	64
2.4.4. Genomic DNA isolation from <i>Plasmodium falciparum</i>	65
2.4.5. Maintenance of <i>Plasmodium in vitro</i> culture	65
2.4.6. Synchronization of <i>Plasmodium</i> parasites by sorbitol method	66
2.4.7. RNA isolation and Real-time analysis	66
2.4.8. Isolation of Protein from parasite	67
2.5 Drug assays in <i>Plasmodium</i> culture	67
2.5.1 Drug Inhibition assay in <i>Plasmodium</i>	67
2.5.2 Fixed ratio method to determine interaction between Radicicol and ATQ/CQ	68
2.6 Bioinformatics analysis	69
2.6.1. Sequence- and structure-based comparison of PfTopoVIB and HsTopoVIBL	69

## Chapter 3

Specific Aim 1: To evaluate whether PfTopoVI (PfSpo11 and PfTopoVIB) participates in	n the
mitochondrial DNA segregation of the malaria parasite	71
3.1. To investigate whether PfSpo11 is the catalytic subunit of TopoVI enzyme	71
3.2. To determine whether PfTopoVI is expressed at the stage where mitochondrial segreg	ation
occurs	75
3.2.1. The transcriptional expression of <i>PfTopoVIB</i> and <i>PfSPO11</i> display a unique patter	rn
compared to the other Type II topoisomerases of P. falciparum	75
3.2.2. PfTopoVIB and PfSpo11 protein expression were induced at the late Schizont stage	ge of
the parasite	76
3.2.3. Stage-specific compactness of <i>PfSPO11-1_UAS</i> and <i>PfTOPOVIB_UAS</i>	80
3.2.4. The enrichment of activation and repression histone marks at the promoter-prox	kimal
region of PfTOPOVIB and PfSPO11 at the LS stage of the parasite	82
3.3. Whether PfSpo11 and PfTopoVIB constitute the functional holoenzyme within the parasite	85
3.4. Whether PfTopoVI is a mitochondrial topoisomerase of the malaria parasite	88
3.4.1. PfTopoVIB and PfSpo11 both associate with the mitochondrial DNA of the ma	ılaria
parasite	88
3.4.2. PfTopoVI recruits uniformly throughout the mt-genome of <i>Plasmodium falciparu</i>	m 91
3.4.3. PfTopoVIB inhibitor Radicicol and Atovaquone potentiate each other	93
3.4.4. The PfTopoVIB inhibitor Radicicol interacts with Atovaquone in a synergistic	
manner	93
3.4.5. Atovaquone reduces mitochondrial import of PfTopoVIB and PfSpo11 in a continuous continuous accordance in the continuous cont	dose-
dependent manner	96
3.4.6. Atovaquone reduces mtDNA recruitment of PfTopoVIB and PfSpo11 in a continuous continuous and PfSpo11 in a continuous continuo	dose-
dependent manner	101

3.5. Computational analysis predicts structural differences between PfTopoVIB and HsTopoVIBL	
	103
Discussion-Specific Aim-1	106
Chapter 4	
Specific Aim 2: To decipher whether PfTopoIII participates in the mitochondri	al DNA
segregation of the malaria parasite	111
4.1. To study the stage specific expression of <i>PfTOPOIII</i> at different replicative stages of	
Plasmodium	112
4.2. To study whether PfTopoIII is a part of the mitochondrial replisome	114
4.3. To study whether PfTopoIII is associated with the mitochondrial genome of the malaria	ı
parasite	114
Discussion Specific Aim-2	121
References	
5. Appendix	
A. Cloning of <i>PfSPO11</i> in yeast centromeric expression plasmid <i>pHCA</i>	127
B. Cloning of <i>PfSPO11</i> <sup>Y65F</sup> in yeast centromeric expression plasmid <i>pHCA</i>	129
C. Cloning of <i>ScSpo11</i> in yeast centromeric expression plasmid <i>pHCA</i>	130
D. Cloning of Full Length <i>PfmtDNAPolymerase</i> in <i>pGADC1</i> Yeast two-hybrid Vector	131
List of Figures in the study:	
Figure 1: The malaria-causing parasite <i>Plasmodium falciparum's</i> life cycle	18
Figure 2: The fundamental distinction between the endocycle and the typical mitotic cell of	cycle are
shown in this diagram	23

Figure 3: Diagrammatic illustration of the <i>Plasmodium falciparum</i> mitochondrial TCA cycle	26
Figure 4: <i>Plasmodium falciparum's</i> electron transport chain (ETC)	28
Figure 5: A schematic representation depicting the mechanisms of action for Type I and Ty	ype II
topoisomerases	33
Figure 6: Domain organisation of DNA topoisomerase III (TopoIII) in human and Plasmo	odium
falciparum	38
Figure 7: Schematic representation showing the decatenation of catenated/ supercoiled DNA by	by the
enzyme Type II topoisomerases, resulting in the formation of relaxed or decatenated DNA	40
Figure 8: Illustration of different domains present in <i>Plasmodium</i> TopoVIB and Spo11	45
Figure 9: PfSpo11 complements the sporulation defect of the diploid Δspo11 strain	73
Figure 10: Plasmodium falciparum TopoVIB and Spo11 display a unique expression pa	attern
compared to the other type II topoisomerases of <i>P. falciparum</i>	78
Figure 11: PfTopoVIB and PfSpo11 are induced at the LS stage of the parasite	79
Figure 12: Stage-specific compactness of the promoters of PfTopoVI subunits	81
Figure 13: Stage-specific promoter activity of PfTopoVI subunits	84
Figure 14: PfTopoVIB and PfSpo11 form the functional holoenzyme in the parasite	87
Figure 15: PfTopoVIB and PfSpo11 are recruited specifically to the mitochondrial genome but	not to
the apicoplast genome	89
Figure 16: PfTopoVIB and PfSpo11 are evenly distributed to the mitochondrial genome	92
Figure 17: IC <sub>50</sub> determination of Atovaquone and Radicicol in 3D7 parasite	94
Figure 18. PfTopoVIB inhibitor Radicicol and Atovaquone show synergism with each other	98

Figure 19. Atovaquone reduces mitochondrial import of PfTopoVIB and PfSpo11 in a	dose-
dependent manner	99
Figure 20. Atovaquone reduces mtDNA recruitment of PfTopoVIB and PfSpo11 in a dose-depe	ndent
manner	102
Figure 21. Multiple-sequence alignment of TopoVIB/TopoVIBL proteins	104
Figure 22. Structural alignment of the Bergerat fold region of PfTopoVIB and HsTopoVIBL	from
different angles	105
Figure 23. Diagrammatic demonstration of the interaction between <i>Plasmodium</i> Topoisomerase	e VIB
and Spo11, forming a functional type IIB topoisomerase complex in the malaria parasite	109
Figure 24. Expression analysis of PfTopoIII at different Schizont stages of the malaria parasite	113
Figure 25. PfTopoIII interacts with PfmtDNApolymerase	116
Figure 26. PfTopoIII interacts with mitochondrial genome	117
Figure 27. PftopoIII( $\Delta$ 259–337) shows poor association with mtDNA	120
Figure 28. Cloning of <i>PfSPO11</i> , into <i>pHCA</i> vector	127
Figure 29. Cloning of <i>PfSPO11</i> <sup>Y65F</sup> , into <i>pHCA</i> vector	130
Figure 30. Cloning of ScSPO11, into pHCA vector	131
Figure 31. Cloning of <i>PfmtDNAPolymerase</i> in <i>pGADC1</i> vector	132
List of Tables used in this study:	
Table 1: IC <sub>50</sub> for strain 3D7 of Radicicol in combination with Atovaquone and <i>vice versa</i>	95
Table 2: FIC values for strain 3D7 for the combinations of Atovaquone and Radicicol/ Radicicol	ol and
Chloroquine	95

Table 3: List of Yeast strains used in the study

Table 4: List of primers used in the study

135

6. Synopsis

#### **Abbreviations:**

A. thaliana Arabidopsis thaliana

ACT Artemisinin-based Combination Therapy

Ade Adenine

AP Apurinic or apyrimidinic

ATP Adenosine triphosphate

B. fold Bergerat fold

BIN4 Brassinosteroid-insensitive 4

bp Base pair

CAP Catabolite Activator Protein

CQ Chloroquine

DEPC Diethyl pyrocarbonate

DHA Dihydroartemisinin

DHODH Dihydroorotate dehydrogenase

DMSO Dimethyl sulfoxide

DNase Deoxyribonuclease

DSB DNA double strand break

dsDNA Double-Stranded DNA

DTT Dithiothreitol

EDTA Ethylenediamine tetra acetic acid

ETC Electron transport chain

FAD Flavin adenine dinucleotide

FIC Fractional Inhibitory Concentration

G1 Gap 1

G2 Gap 2

gDNA Genomic DNA

His Histidine

HU Hydroxyurea

IC<sub>50</sub> Half maximal inhibitory concentration

IgG Immunoglobulin G

IPTG Isopropyl-β-D-1-thiogalactopyranoside

iRBC Infected Red blood cell

kDa Kilo Dalton

Leu Leucine

M phase Mitosis Phase

MCT Monocarboxylate transporter

MDS Molecular dynamics simulation

mETC Mitochondrial electron transport chain

Mg Milligram

min Minutes

ml Milliliter

mM

MMS Methyl Methane Sulphate

MQO Malate quinone oxidoreductase

Millimolar

mtDNA Mitochondrial DNA

MTS Mitochondrial targeting sequence

mV Milli Volt

NADH Nicotinamide adenine dinucleotide + Hydrogen

N-gate Entry gate

nM Nanomolar

°C Degree Celsius

OD Optical Density

P. falciparum Plasmodium falciparum

P. malariae Plasmodium malariae

P. ovale Plasmodium ovale

P. vivax Plasmodium vivax

PAGE Poly-acrylamide gel electrophoresis

PCIA Phenol chloroform isoamyl alcohol

PEG Polyethylene glycol

BLM Bloom syndrome

EMP1 Erythrocyte membrane protein 1

Topo I Topoisomerase I

TopoII Topoisomerase II

TopoIII Topoisomerase III

TopoVI Topoisomerase VI

P. knowlesi Plasmodium knowlesi

PMSF Phenylmethylsulfonylfluoride

Qo Ubiquinol oxidation site

RHL1 Root hairless-1

RNA Ribonucleic acid

RNase Ribonuclease

Rpm Rotations per minute

RPMI Roswell Park Memorial Institute

S. cerevisiae Saccharomyces cerevisiae

S Synthesis phase

SC Synthetic complete

SDS Sodium dodecyl sulphate

SP Sulfadoxine-pyrimethamine

ssDNA Salmon sperm DNA

TCA Tricarboxylic acid

TOPRIM Topoisomerase-Primase

Tyr Tyrosine

Ura Uracil

WHO World health organization

WT Wild Type

YNB Yeast nitrogen base

YPD Yeast extract, peptone, dextrose

 $\Delta \Psi m$  Mitochondrial membrane potential

μF Micro Faraday

μg Microgram

μl Microliter

μm Micrometre

μM Micromolar

Chapter 1

Introduction

#### 1.1. History of malaria and Global Malaria burden

Mosquitoes trapped in amber from the Palaeogene period, around 30 million years ago, provided the first indication of malaria parasites. The malaria that affects human is an African disease that coevolved with the ones that infect non-human primates and birds. Malaria is unique in historical records (1). It was named "King of Diseases" according to the writings of the Vedic period (1500 to 800 BC). In Medieval Italian, it originated as mala ria- "poor air." In the 20th century, malaria alone killed between 150 to 300 million people (2). It is widespread as a deadly infectious disease among all the continents. Although malaria researchers have received numerous Nobel Prizes for their work, the illness still affects over two hundred million people per year and claims more than 600,000 lives. Science and medicine have been focusing on its prevention and treatment. Research interest has since been directed towards the biology of both the parasites that cause it and the mosquitoes that transmit it.

According to the WHO, World Malaria Report 2022, Malaria cases were projected to be 247 million in 2021. An estimated 6,19,000 deaths were reported due to malaria. Among them, African region accounted for a significant global malaria burden and children under the age of 5, made up approximately 80% of all malaria-related deaths in the area (3). Malaria appears in these tropical and subtropical regions due to multiple factors like higher transmission rate, local weather conditions and socio-economic instability.

#### 1.2. The social and economic burden of malaria parasite

Malaria hampers the development in a variety of ways, including effects on reproduction, population growth, saving/investing, worker productivity, illness, premature mortality, and medical costs. Malaria is associated with lower economy in sub-Saharan African nations due to the labour force absenteeism, which eventually hampers all the sectors including education and health. In the past, nations with a high malaria burden have seen slower annual growth rate than the nations without

malaria transmission. The main factors here are the direct costs, such as the money spent on prevention and treatment by individuals and by the government, as well as the indirect costs, such as the income or productivity lost because of disease or death.

#### 1.3. Ecology of the malaria parasite

#### 1.3a. Parasite and its transmission

Malaria is a severe disease caused by a parasite of the genus *Plasmodium*, which infects through the bites of infected female *Anopheles* mosquitoes. There are approximately 400 species of *Anopheles* across the world, out of them, 60 are vectors for malaria parasite under standard condition. *Anopheles* mosquitoes are easily distinguished during the resting state, when the proboscis, head, and the body are kept on a straight line to each other but keeping an angle with the surface. Female *Anopheles* mosquitoes take blood from the host. The effective growth of the malaria parasite in the mosquito (from the "gametocyte" to the "sporozoite") depends on numerous factors. The ambient temperature and humidity (higher temperatures accelerate parasite growth inside the mosquito) are the critical factors for the parasite to complete its life cycle within the mosquito host. Unlike human hosts, mosquito hosts do not noticeably suffer from the presence of parasites. Before the parasite spreads to other people during the blood meals, it must go through a lifecycle shift within the mosquito. Given the lifespan of the mosquito and the length of time needed for that life-cycle change, transmission becomes significantly less likely when the temperature falls below 18°C (4). Thus, proper maintenance of the temperature is essential for the transmission.

This malaria parasite causes a significant extent of morbidity and mortality. Over 100 species of malaria parasites can infect a wide variety of animal species, including reptiles, birds, and various mammals, but only five parasites like *Plasmodium falciparum*, *Plasmodium vivax*, *Plasmodium ovale*, *Plasmodium malariae* and *Plasmodium knowlesi* can infect human under natural conditions.

These species vary in their morphology, immunological pattern, geographic distribution, recurrence, and drug response. Out of the five parasitic species that cause malaria in humans, - P. falciparum and P. vivax are of the greatest risk. Plasmodium falciparum is the causative agent of acute and potentially fatal malaria and the leading cause of malaria-related deaths among the young children in Africa. The least common malaria parasite is P. ovale, which is confined to West Africa, although P. malariae occurs worldwide. The most common malaria parasite is P. vivax, but its infection is rarely fatal (5). P. ovale and P. vivax are dormant liver stage parasites, also identified as hypnozoites. They can persist in the organ for years prior to the beginning of a new infection, which results in the relapses of malaria infection.

#### 1.3b. Dual host Life cycle

Malaria parasite develops and undergoes morphological changes between the two hosts: the mosquito, and the human (Figure 1). The liver is where the malaria parasite first begins to develop before moving on to infect human red blood cells. Sporozoites transferred by the blood meal of mosquito into the human host, infect liver cells and mature into schizonts, further rupturing and releasing merozoites. These merozoites infect the red blood cells, which marks the asexual development of the parasite. During this asexual blood stage, the parasite undergoes maturation from Ring stage (because of its ring shape morphology) to the Trophozoite stage (https://www.cdc.gov/malaria/about/biology/index.html). Trophozoite develops into a multinucleated structure known as Schizont, which ruptures and releases more merozoites into the blood and establishes the blood stage infection. Few of the Ring stage parasites differentiate into female and male gametocytes through an unknown signal. These gametocytes are taken up by the blood meal of the female Anopheles mosquito. The gametocytes fuse within the mosquito, generating a diploid zygote, which further develop to become an ookinete. These ookinetes migrate to the midgut of the mosquito and develop into oocysts. The oocysts undergo a maturation process, resulting in the production of sporozoites. Subsequently, these sporozoites migrate to the salivary glands of the

mosquito, facilitating the perpetuation of the malaria transmission cycle upon the mosquito's bite on a human host.

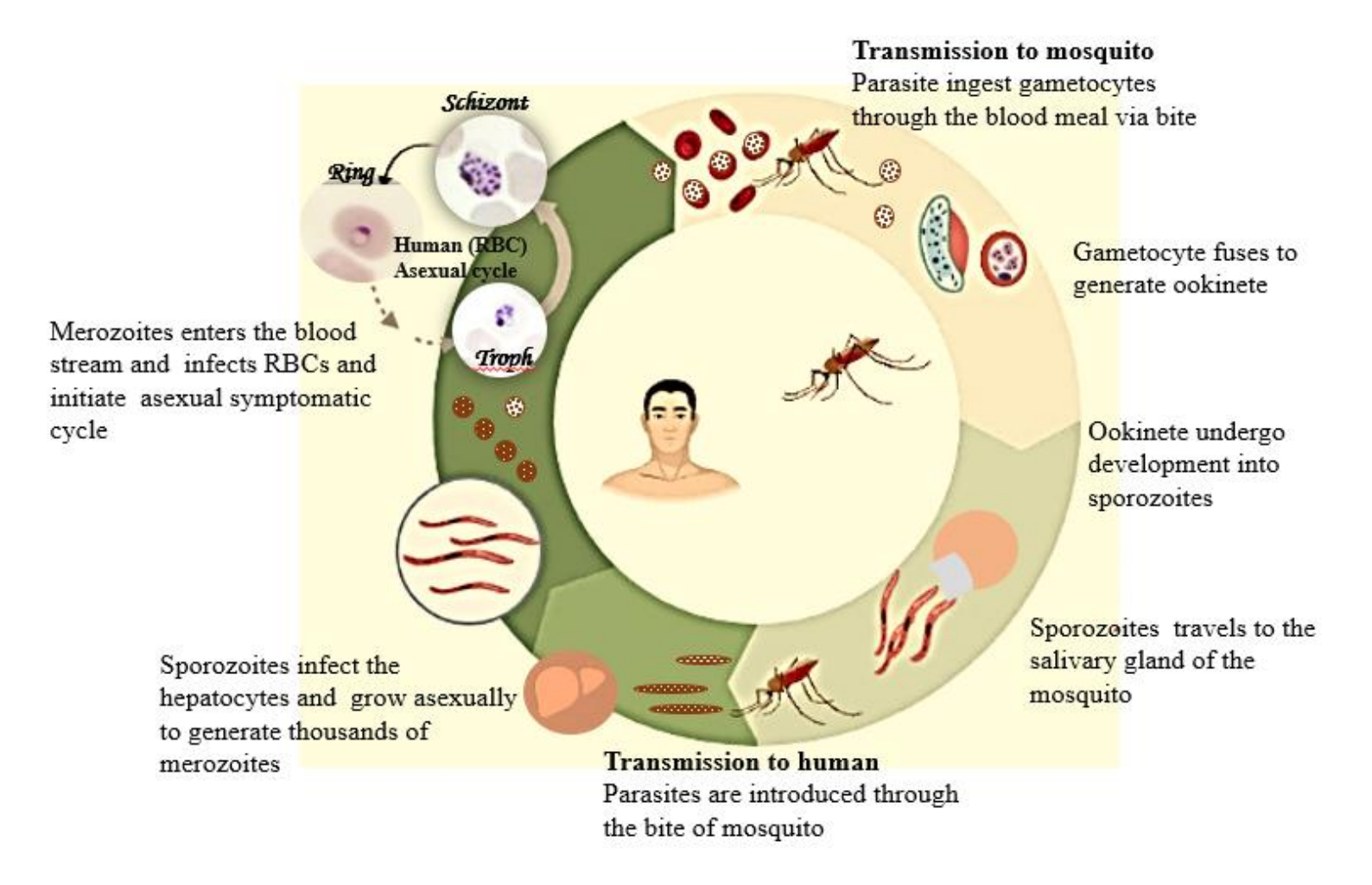


Figure 1: The malaria-causing parasite Plasmodium falciparum's life cycle. Two hosts are involved in the life cycle: Anopheles mosquitoes and human. The parasite goes through several phases in the human host, including sporozoite, merozoite, ring, trophozoite, schizont, and gametocyte, which result in the appearance of malarial clinical signs. The parasite reproduces sexually in the mosquito host, producing sporozoites, that can be transmitted to a new human host by the mosquito bite. The picture offers a thorough representation of each step of the life cycle and illustrates the parasite life cycle.

#### 1.4. Challenges in malaria control and treatment

#### 1.4a. Antimalarial drugs and resistance

Despite more than half a century of malaria research, antimalarial drug resistance remains an ongoing threat to the global burden against malaria. From the Chloroquine (CQ)-based therapies to Artemisinin-based combination therapies (ACTs), which are the present first-line agents for the treatment, malaria has developed resistance to all the current antimalarial. The primary cases of suspected quinine resistance were reported in 1910 (6). Later, quinine-based combination therapy was replaced with CQ monotherapy. CQ was extensively utilized as a first-line treatment for malaria during 1940s. Resistance to CQ was first developed in Southeast Asia in the late 1950s and subsequently it spread to other parts of the world. By the 1990s, CQ resistance became a foremost problem in several parts of the world.

Sulfadoxine-pyrimethamine (SP) was introduced as an antimalarial drug in the 1960s. Resistance to SP first emerged in 1970s and subsequently spread to Africa. By the 1990s, SP resistance had become widespread in many parts of Africa, leading to a change in treatment policies. Artemisinin-based combination therapies (ACTs) are presently the most efficient antimalarial drugs and are recommended as first-line treatments by the World Health Organization (WHO). Resistance to Artemisinin was first reported in 2008. Recently, the range of *P. falciparum* drug-resistant strains remain variable across the globe.

#### 1.4b. Antigenic variation

Antigen variation is another challenge to the treatment of malaria. Malaria parasite establishes the persistent re-infection due to the antigenic variation. The surface antigen protein allows malaria parasites to stay masked through immune clearance. The parasite contains a vast number of genes that are employed to produce various surface proteins, enabling it to alter its surface antigen frequently and evade immune system recognition. This antigenic variation is due to the sporadic exchange of the variants of the major surface antigen PfEMP1, which is also responsible for

parasite cytoadherence. The *var* gene family contains members that encode several versions of PfEMP1. The *P. falciparum* genome has about 60 *var* genes, allowing parasites to cycle through their repertoire of surface proteins while varying their antigenic signature by selecting a different *var* gene for expression. Parasites can make the most of their array of variant antigens by restricting exposure to a single version of PfEMP1 at a time and switching to a new variant after the host has developed a successful immune response. Therefore, to ensure that genes express themselves in ways that are mutually exclusive, persistent infection requires both a very diversified repertoire of antigen-coding genes and a sophisticated system of coordinated gene activation and silencing (7). Due to the essential role of this surface antigen protein in pathogenesis and developing protection against the diseases, it is one of the major foci of malaria research and treatment (8).

#### 1.4c. Current scenario in malaria research

A lot of work is being done in the field of malaria research to create efficient preventative, diagnostic, and therapeutic measures. New vaccine candidates, enhanced diagnostic equipment, and innovative therapeutic targets have all been developed recently in malaria research. The global goal of eliminating malaria is, however, seriously hampered by the evolution of drug-resistant strains of the malaria parasite and insecticide-resistant mosquito populations. Comprehending the epidemiology of disease and its effect on human health, researchers are also researching the interactions between the malaria parasite and its host. Additionally, there are continuous initiatives to create innovative technologies and techniques, including as gene drive systems and novel insecticides, for the control of malaria. High-throughput chemical library screening, genetic research to pinpoint essential genes for the parasite's life cycle, bioinformatics analysis to pinpoint protein-protein interactions and metabolic pathways are all methods employed to find novel targets.

Novel promising drug targets are being explored on everyday research to conquer and eradicate malaria. Focusing on enzyme/protein and metabolic pathways that are unique to the parasite and not present in the human host is a potential method for discovering new antimalarial targets.

# 1.5. Understanding parasite biology from a molecular perspective to develop new anti-malarial targets

#### 1.5a. Replication and Cell division in malaria parasite: Endoreduplication

*Plasmodium*, in contrast to the binary fission, undergoes multiple genome replication within the same cytoplasm prior to cytokinesis, that results in many-and not necessarily 2n-daughter cells, called merozoites. Schizogony causes all the pathology associated with malaria by first occurring in hepatocytes and then in erythrocytes. This process is crucial for treating patients because erythrocyte development rates define parasitaemia, which frequently links to the severity of the disease (9). A merozoite invades a fresh erythrocyte to start the cycle, and for the first 24 hours after invasion, the parasite only has one haploid nucleus, which is in interphase or G1. Chromosome replication begins as the centriolar plaque (CP) duplicates, signalling the transition from growth to replication. Recently, a new model is put forth for the growth process of malaria parasite where subsequent rounds of genome replication are associated with genome segregation, followed by final division (10). A global cell cycle regulator may be involved which controls the transcriptional regulation of *Plasmodium*. The signal that triggers this cytokinesis is yet unknown, although it may be caused by a lack of nutrients or space in the host erythrocyte. The malaria parasites experience an approximately threefold increase in size during the Ring and Trophozoite stage, and a roughly seven-fold increase during the complete proliferative blood stage (11). The replication machinery in malaria parasite acts to be an excellent drug target as the mechanism and regulators are divergent from that of the human host (10). The synchronization of gene expression, targeted proteolysis of cell cycle regulators posttranslational modification, are all necessary for maintaining the balance between cell proliferation, cell cycle arrest, and differentiation that are required to maintain the development. Eukaryotic cells develop by a process known as the "mitotic cell cycle," in which the genome is duplicated just once before the cell divisions. There are two separate phases in the cell cycle: Interphase including G1, S and G2 phase, and the second phase including M phase (mitosis). The S

(synthesis phase) marks the DNA replication, and the M (mitotic phase) refers to the time the cell divides.

The parasite that causes severe malaria in human, starts multiple cell cycle progressions to support multiple growth during its life cycle. Malaria parasite does not develop through a conventional mode of cell division (**Figure 2**), instead, undergoes a non-canonical mode (endoreduplication), which includes schizogony (where a multinucleate structure is formed before the cytokinesis) and sporogony (10). Through the process of endoreduplication, a singular parasite has the capacity to generate tens of thousands of progeny cells within a single cell. As a result, it can undergo development from a haploid to a polyploid state, carrying multiple copies of its genome (12). *P. falciparum* reproduces asexually both in erythrocytes and in hepatocytes (liver cells) by schizogony, where multiple cycles of DNA replication take place, followed by the nuclear division without subsequent cytoplasmic division (13). In mammalian hepatocytes and erythrocytes during schizogony, as well as in mosquito oocysts during sporogony, the endoreduplication process takes place. The mitotic division observed in this scenario is unusual, as there is no distinct G2 cell cycle observed during schizogony. The second type of mitotic division occurs during male gametogenesis. The fusion of the female gamete results in the formation of a diploid zygote, initiating the process of meiosis(14). Endoreduplication is the most crucial source of polyploidy in plants and other eukaryotes (15), (16).

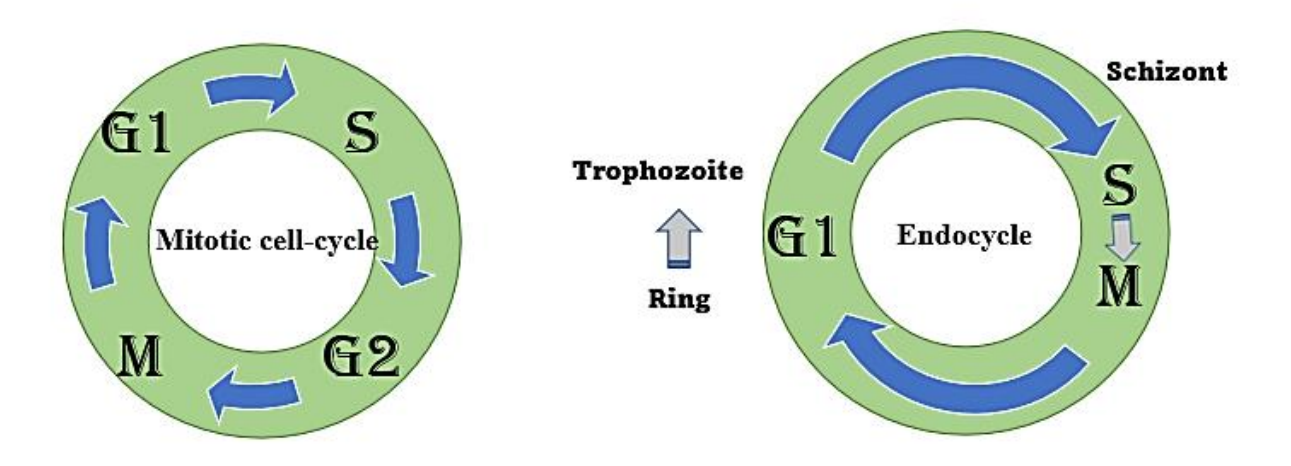


Figure 2: The fundamental distinction between the endocycle and the typical mitotic cell cycle are shown in this diagram. A) There are four distinct phases that make up the mitotic cell cycle: G1 (gap 1), S (DNA synthesis), G2 (gap 2), and M (mitosis). The mitotic cell cycle is shown as a circular pattern in the figure, with arrows denoting the movement from one stage to the next. DNA replication characterises the S phase and the cell prepares for mitosis during G2 and splits into two daughter cells during M. B), The endocycle, in malaria parasite consists of G1 phase that marks the Ring to mid-Trophozoite stage parasite. The end of Trophozoite stage to Schizogony marks the S-Phase of the cycle immediately followed by the M-Phase. There is no G2 phase in this endocycle. This figure shows the essential distinctions between the endocycle and the regular mitotic cell cycle.

#### 1.6. Malaria parasite organelle development

Electron microscopic studies showed that, during the development of the parasite in the asexual life cycle, each mitochondrion is subsequently paired with an apicoplast (17). The development of mitochondrial and apicoplast organelles in merozoite daughters was investigated with the transfected double parasite line expressing fluorescent proteins that target mitochondria and apicoplast. Three distinct stages in the schizonts were identified. The early and mid-schizont stages are marked by the initiation of nuclear and apicoplast division, respectively. Conversely, mitochondrial division occurs just before cell division during late-schizont stage. Proper segregation of the mitochondrial genome into the daughter cells after replication is vital for the survival of the organism. However, the molecular mechanism behind the proper segregation and protein machinery required for appropriate genome segregation are still unidentified.

#### 1.6.1. Mitochondria of malaria parasite

Mitochondria is a symbiotic organelle produced from alphaproteobacteria. Two primary functions of mitochondria in a eukaryotic cell are TCA (tricarboxylic acid) cycle and mETC (mitochondrial electron transport chain). The mitochondria of the malaria parasite are highly divergent from the human host. It has been demonstrated that the mtDNA of *Plasmodium* follows the rolling circle mode of replication like that of *Saccharomyces cerevisiae*. The malaria parasite's mitochondrial genome consists of approximately 20 copies per cell organized in the form of linear concatemers. This small mitochondrial DNA replicates with several single-stranded copies of the DNA produced in a head-to-tail arrangement called concatemer. *Pf*mtDNA contains a small 6 kb genome that encodes three proteins: cytochrome *c* oxidase subunits 1, 3 and cytochrome *b*. All three genes are essential for various processes, such as maintenance of mitochondrial membrane potential, heme and coenzyme Q biosynthesis, pyrimidine biosynthesis, *etc*. Defects in the mitochondrial DNA maintenance may serve for severe metabolic defects and respiratory failures in the protozoan parasite (18).

#### 1.6.1a.TCA cycle of malaria parasite

The TCA cycle, also called the Krebs cycle occurs in the mitochondria and contributes to the production of ATP by oxidising carbon sources. It initiates with the production of malate via anaplerotic reactions and 2-oxoglutarate is formed from glutamine as well as from the conversion of acetyl-CoA to citrate. In general, pyruvate, the product of glycolysis, is transported *via* the monocarboxylate transporter (MCT) family. The change of pyruvate to acetyl-CoA takes place, after which citrate enters the cycle (**Figure 3**). Malate is converted to oxaloacetate by MQO (malate quinone oxidoreductase), a membrane-associated protein that is FAD (Flavin adenine dinucleotide)-dependent. Quinones of the mtETC accept electrons, and NAD acts as an electron donor. Mammals do not have MQO, but *Plasmodium* and several bacteria have it. The *Plasmodium* MQO may thus be a target for therapeutic development. Eventually, citrate is converted into succinate *via* the production of isocitrate, alpha-ketoglutarate and succinyl-coA. The succinate is converted to malate. The cycle then restarts when malate is changed back into oxaloacetate (**Figure 3**).

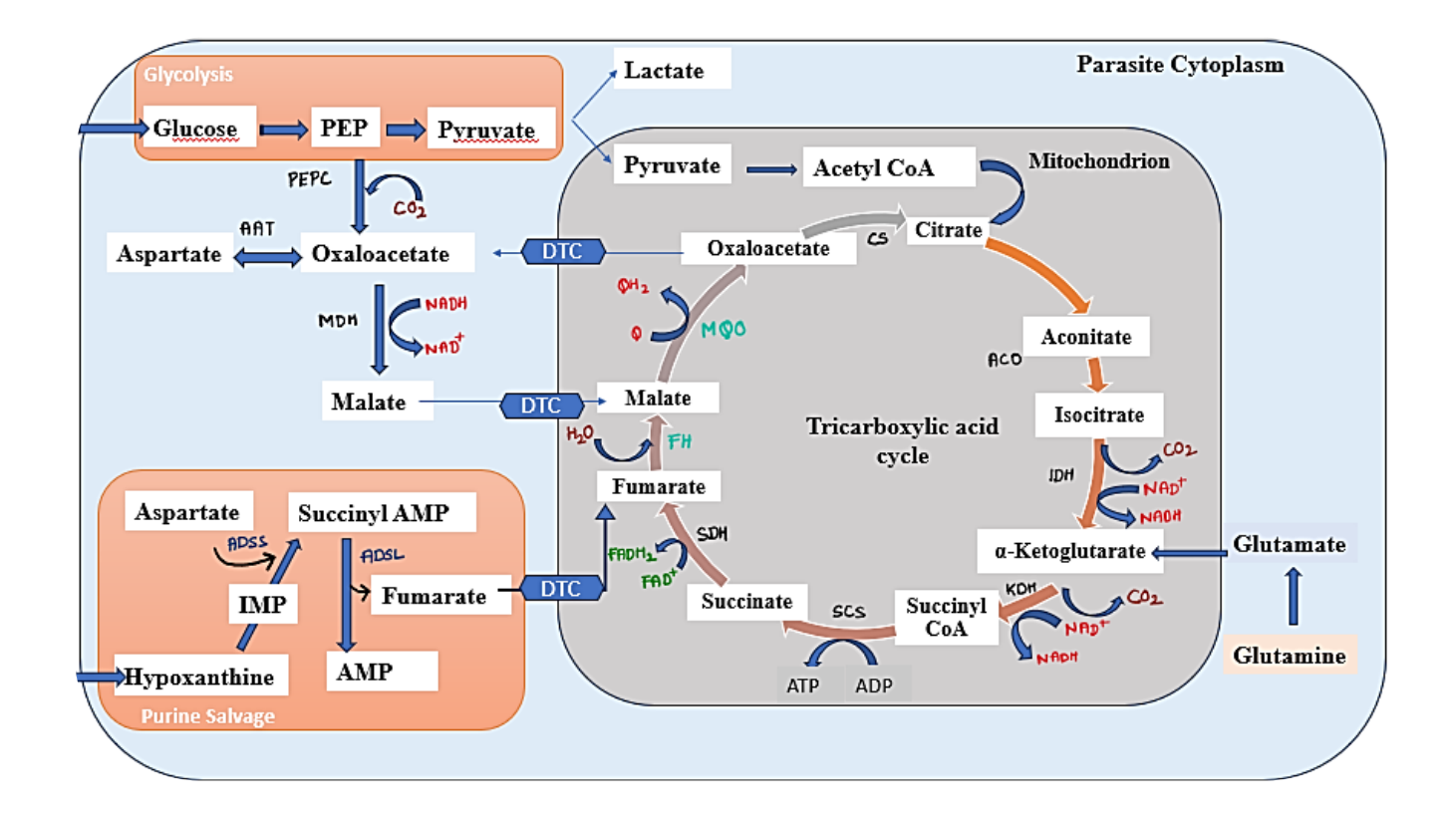


Figure 3: Diagrammatic illustration of the Plasmodium falciparum mitochondrial TCA cycle. A hexose transporter imports glucose into the parasite, where it is then transformed by glycolysis to pyruvate. A minute portion of the pyruvate is carried to the mitochondrion which is transformed into the two-carbon acetyl CoA, which subsequently enters the TCA cycle, while the bulk is fermented anaerobically to lactate. Glutamate serves as the primary source of carbon for the TCA cycle, serving it in the form of ketoglutarate. Succinyl-CoA is then further converted into succinate, which make fumarate. Fumarate undergoes conversion to malate which further produces oxaloacetate. At the end, Oxaloacetate conversion to citrate using citrate synthase, completes one TCA cycle.

#### 1.6.1b. Mitochondrial Electron transport chain:

The primary function of the mitochondrial electron transport chain extends beyond energy metabolism to include the generation of a transmembrane proton gradient across the inner membrane of the mitochondria, which is crucial for the survival of the unicellular parasite. The significant percentage of eukaryotic cells need the mtETC to produce proton-motive force that is crucial for oxidative energy metabolism. However, for malaria parasite and some other parasites, ETC plays a critical role by transferring electrons to the Dihydroorotate dehydrogenase (DHODH) during the pyrimidine biosynthesis process. The mitochondrion also produce several additional metabolites in addition to pyrimidine production (19). The inner membrane's electron transport chain is the metabolic engine that propels several mitochondrial and cellular operations. The mtETC of the higher eukaryotes is composed of four important membrane enzyme complexes namely, NADH: ubiquinone oxidoreductase (Complex I), succinate: ubiquinone oxidoreductase (Complex II), ubiquinol: cytochrome c oxidoreductase (Complex III, also known as cytochrome bc1), and cytochrome c oxidase (Complex IV), with ubiquinone (Coenzyme Q) and cytochrome c which are the mobile electron carriers between the complex. Plasmodium does not harbour the large multi-subunit Complex I located in the inner membrane but maintains the electron transfer from Complex II through complex IV (Figure 4). In comparison to their counterparts in human and yeast, the mitochondrial electron transport chain complexes of the malaria parasite have substantially fewer subunits. Electron transport chain of malaria parasite is the primary source of the mitochondrial proton electrochemical gradient. As the parasite shows sensitivity towards inhibition of the mitochondrial electron transport chain, it implies its essentiality for the survival of the parasite. The final energy-saving step among the numerous eukaryotic species that depend on oxidative phosphorylation is ATP production, however it is unclear if this procedure is used by P. falciparum parasites. P. falciparum, oxidative phosphorylation process does not seem to serve as a source of cellular ATP.

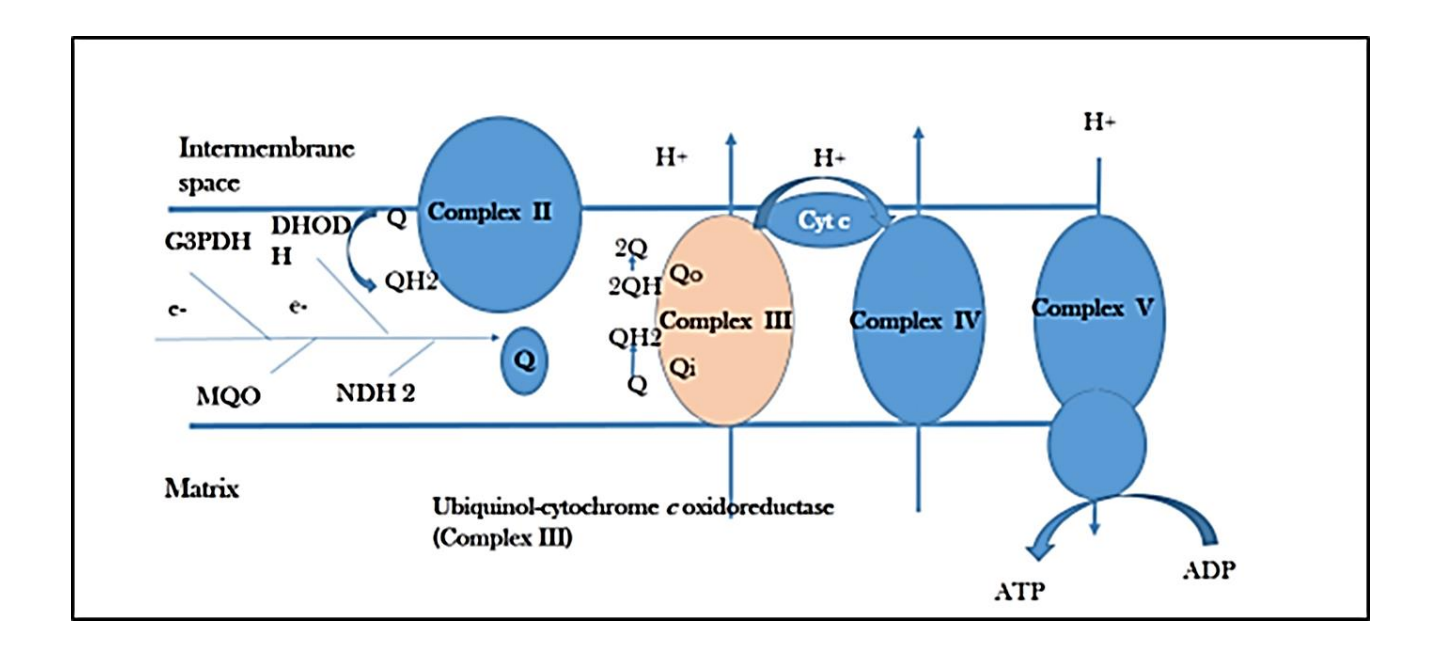


Figure 4: Plasmodium falciparum's electron transport chain (ETC). ETC of malaria parasite comprises of numerous protein complexes, incorporating NADH dehydrogenase, cytochrome b, cytochrome c, and cytochrome oxidase. They work mutually to transport electrons to molecular oxygen, producing a proton gradient i.e., difference in proton concentration across the mitochondrial membrane. Complex III and IV of the mtETC translocate protons from the matrix to the intermembrane space. Potential generated is sourced to drive the synthesis of ATP. The ATP synthase of the parasite, which differs significantly from that of the host, is put together as a large dimeric complex.

#### 1.6.1c. Inhibition of Mitochondrial Electron transport chain by Atovaquone

The mitochondrial proton electrochemical gradient is produced by the mtETC. Atovaquone is a naphthoquinone that shows broad-spectrum antiprotozoal action. It is a structural analogue of the mitochondrial electron transport chain protein Ubiquinone. Atovaquone is used in combination with Proguanil for treating malaria. Study shows that Atovaquone inhibits electron transport in malaria parasites and collapses the mitochondrial membrane potential ( $\Delta \Psi m$ ). The collapse of mitochondrial membrane potential ( $\Delta \Psi m$ ) can have extensive implications beyond the inhibition of electron transport. Proguanil enhances the ability of Atovaquone to induce the collapse of  $\Delta \Psi m$ , thereby reducing the concentration of Atovaquone required to effectively eradicate the parasites. The specific molecular mechanisms underlying the synergistic activity of Proguanil remain unclear, but this phenomenon has been observed at concentrations achievable through pharmacological means (20). In addition to its role in electron transport inhibition, Atovaquone acts as a site-specific protonophore, destabilizing the cytochrome bc1 complex and promoting proton leakage through this particular site. In *Plasmodium* species, its mode of action has been illuminated (18). Aping the structure of ubiquinone, it accepts electrons from the mitochondrial ETC enzymes and transfers them to cytochromes. Atovaquone inhibits the growth of Dd2 parasite lines with an IC<sub>50</sub> concentration of 1 nM, without Proguanil, and 0.2 nM in combination with Proguanil (18). Atovaquone has a high degree of selectivity when it comes to the ubiquinol oxidation site (Qo) of cytochrome b. Unfortunately, there was a strong correlation between mutations at cytochrome b position 268 (Tyr) which contributes to the formation of Qo site and elevated levels of Atoyaquone resistance. Numerous parasite enzymes associated with the mitochondrial electron transport chain are therefore affected. Dihydroorotate dehydrogenase (DHOD) is one such enzyme required in the biosynthesis of pyrimidines and essential for parasite survival because Plasmodium cannot go through pyrimidines biosynthesis (21).

## 1.7. Topoisomerases: Molecular Scissors of the DNA

DNA supercoiling is crucial for DNA packaging inside the cells. However, the process of DNA replication and transcription can create difficulties in terms of DNA structure due to the excessive coiling of the DNA double helix. This torsion eventually prevents the DNA or RNA polymerases from moving along the DNA helix. A class of enzymes known as DNA topoisomerase, is found in all living organisms, including human and unicellular protozoan parasites, which is involved in maintaining the topology of the DNA. These topoisomerases are magicians, that catalyse necessary topological changes in the DNA by changing the DNA linking number, during all the essential biological processes.

## 1.7.1. Classification of topoisomerases

There are four categories of DNA topoisomerases, classified based on their mechanism of action (Figure 5). Type I topoisomerase enzymes relax DNA by creating a single strand break, allowing the other strand to pass through before re-joining the broken strand. They change the DNA linkage number by 1 and do not require ATP for their activity. Type I topoisomerases can be divided into two subtypes, IA, and IB. Mg2+ is necessary for the functioning of type IA topoisomerases. and preferentially relax negative supercoiling of the DNA, while type IB topoisomerases can relax both positive and negative DNA supercoils and are independent of Mg<sup>2+</sup>. Type II Topoisomerases are further divided into Type IIA and Type IIB topoisomerases. Type IIA topoisomerases create double-strand breaks in DNA by temporarily cleaving the two strands in one DNA duplex, forming an enzyme-operated DNA gate that enables a second DNA helix to pass through, changing the DNA linkage number by 2. This class of enzymes catalyses the relaxation of positively and negatively supercoiled DNA and possesses a potent DNA decatenating activity. Nuclear genome of the malaria parasite encodes both type I and Type II topoisomerases. The Type I, family members present in the genome of the malaria parasite *Plasmodium falciparum* are Topoisomerase III (PfTopoIII) along with Topoisomerase IB (PfTopoI). Type IIA, topoisomerases encoded by *Plasmodium falciparum* 

genome are, Topoisomerase II (PfTopoII) and Gyrase (PfGyrase). Topoisomerase VI (PfTopoVI) belongs to the Type IIB topoisomerases in malaria parasite (22).

# 1.7.1.1. Type I DNA Topoisomerase

Topoisomerases of this class are monomeric enzymes and are classified into three subgroups, namely A, B, and C, based on their structure and mode of action. Within the A-family, there are two enzymes called Topo IA and Topo III. These enzymes exhibit a temporary association with the 5'-phosphoryl group and necessitate the presence of divalent cations for binding to DNA, as illustrated in (Figure 5). On the other hand, the B and C families (23, 24), encompass Topo IB along with Topo V, respectively. These enzymes maintain their association with the 3'-phosphoryl group, and do not require divalent metal cations for the purpose of DNA binding. Topo IA creates a DNA gate by binding to the broken DNA, allowing another DNA strand to pass through. It is specifically involved in relaxing negative DNA supercoils (25). In contrast, Topo IB performs a rotational movement of the nicked DNA strand in relation to the complementary strand. Both topoisomerases (Type IB and IC) possess the ability to relieve both positive and negative DNA supercoiling, as depicted in (Figure 5). Unlike Type IA, Type IB topoisomerase initiates a single-strand nick in the DNA, which is a distinct mechanism compared to the strand-passage reaction employed by Type IA Further, single strand break makes it possible for DNA to rotate, the rate of which is governed by the friction within the enzyme cavity before the strand is re-ligated. The Type IC topoisomerase, TopoV, was isolated from the hyperthermophilic methanogen *Methanopyrus kandleri* (23). The 61-kDa N-terminal segment of M. kandleri Topo V, which served as the first Topo V structure, was distinct from every other topoisomerases (24). The activity of Topoisomerase V is both ATP- and Mg<sup>2+</sup>-independent, and it can effectively relax both negative and positive supercoils. The covalent TopoV: DNA complex is formed with the 3' phosphate of the DNA backbone. A single molecule approach was used to observe that Topo V causes the relaxation of DNA using controlled rotation (26). For this, Topo V, that was initially regarded as Type IB, since been proposed as a new Type IC class due to its structural and

biochemical differences (24, 27). In addition, Topo V possesses the ability to function as an AP-lyase, participating in the repair of abasic DNA damage while also engaging in DNA repair activities(28).

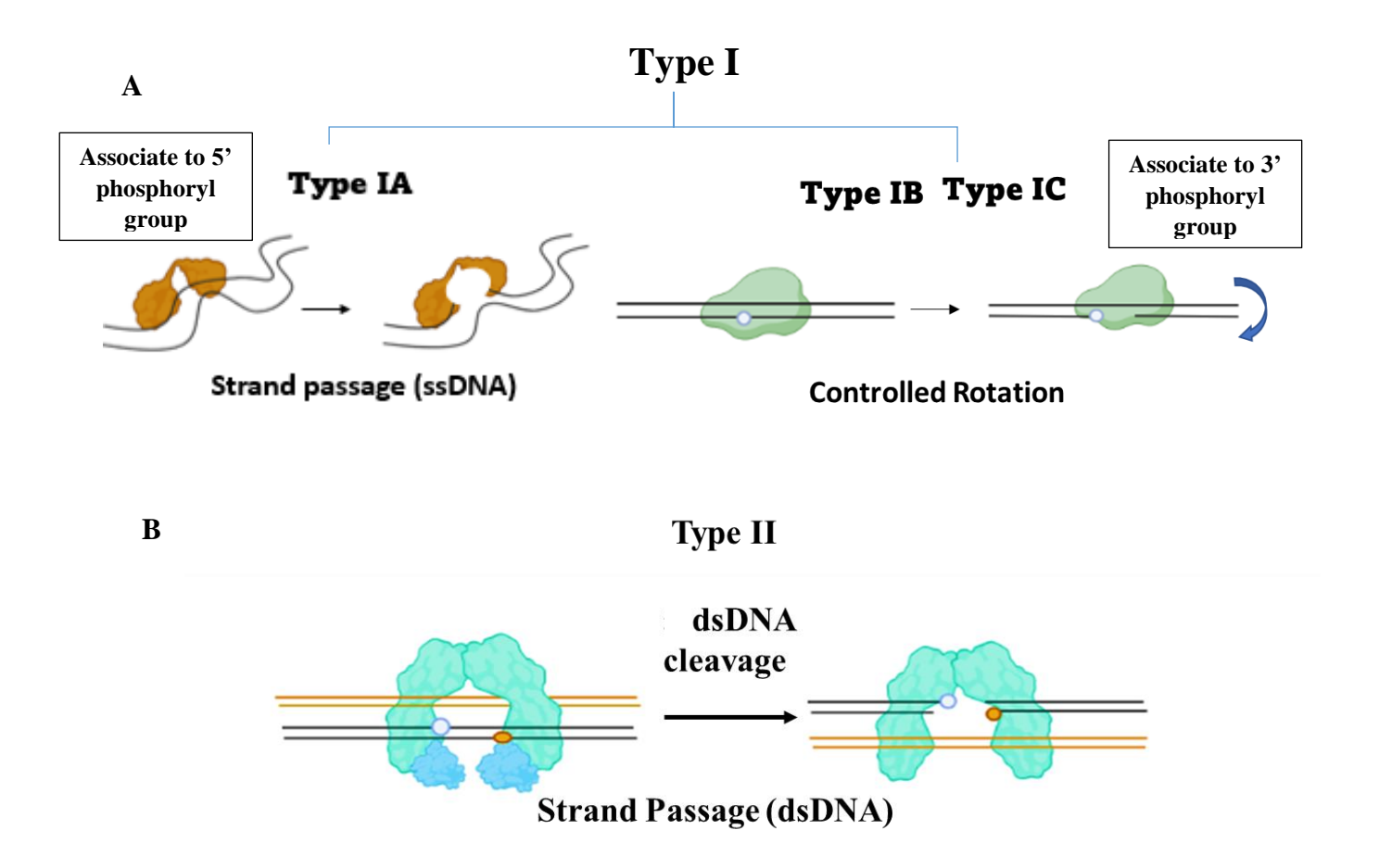


Figure 5: A schematic representation depicting the mechanisms of action for Type I and Type II topoisomerases. (A) Type I Topoisomerase: The figure demonstrates the steps involved in the activity of Type I topoisomerases. Initially, the topoisomerase enzyme binds to the DNA duplex, recognizing a specific site. It then generates a transient single-strand break in one DNA strand, allowing the other strand to pass through the break Upon the passage of the DNA strand, the topoisomerase enzyme reconnects the broken ends, resulting in the relaxation of DNA supercoiling or the removal of a single DNA interlink. (B) The figure depicts the sequential stages that Type II topoisomerases take to function. First, a particular point on the DNA duplex is recognized and bound by the topoisomerase enzyme. Then it causes a DSB in the DNA, opening a gate for an additional DNA fragment to flow through. The enzyme binds to the broken ends of the DNA by the creation of a covalent intermediate in this process. The enzyme re-ligates the DNA strands after the passage of the DNA segment, resolving any DNA supercoiling or interlinking.

The ability of TopoV to repair DNA is not influenced by its topoisomerase activity, as demonstrated by the fact that mutating the active site tyrosine does not affect its capacity to carry out DNA repair. (28). While all topoisomerases are indirectly engaged in DNA repair and maintenance, only Topo V possesses the specific capability to directly mend abasic DNA damage(29).

Topo III, a Type-I topoisomerase being the main attention of this research, is discussed in depth in a following section.

## 1.7.1.1a. Topoisomerase III in other eukaryotes

Along with the prokaryotic lineages, archaeal and eukaryotic organisms also share topoisomerase III. The TopoIII mutants were initially isolated in yeast and found to promote recombination between the repetitive sequences (30-32). DNA sequencing analysis revealed that it is homologous to the bacterial topoisomerases, i.e., TopA and TopB (31). It was observed that budding yeast cells that do not possess topoisomerase III are able to survive; however, their growth rate was reduced by two-fold due to the accumulation of cells in the late S/G2 phase of the cell cycle (30). Furthermore, diploid cells with both copies of the topoIII gene completely removed (topoIII-/topoIII-) in yeast exhibit an inability to undergo the process of sporulation (30, 31). There are two homologous genes for TopoIII in vertebrates (TopoIIIα and TopoIIIβ). Inactivation TopoIIIα in mice during the embryonic stage results in the death of the embryos (33). It was observed that Yeast TopoIII and human TopoIIIα have a direct physical connection with Sgs1 and Blm, respectively. They work together to resolve double Holliday junctions that form when the replication fork suddenly stops, and sister chromosomes are being replicated. Thus TopoIII aids in suppressing genetic crossover (34). TopoIIIα is also essential for the decatenation and segregation of human mitochondrial DNA after the replication process (34). TopoIIIa is of significant importance in human cells for the maintenance of mitochondrial DNA (mtDNA). It is specifically responsible for decatenating hemicatenane structures that arise during the replication of mtDNA (35). Depletion of TopoIIIα results in a significant decrease in monomeric

mtDNA and the formation of large catenated networks, leading to impaired segregation of the mitochondrial genome in humans (34).

TopoIIIβ is the only RNA topoisomerase that relieves topological stress generated during the transcription by specifically binding to a group of mRNAs. The absence of Topo IIIβ showed cognitive defects and psychiatric disorders in mice (36).

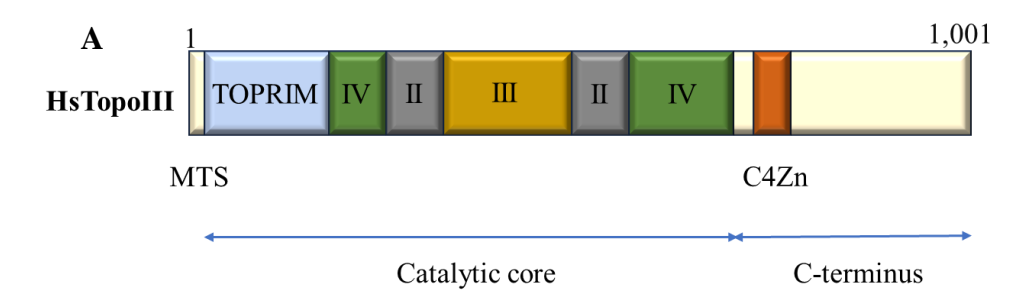
Topo III and Topo IB, which belong to the Type I topoisomerase family, are found in the genome of *Plasmodium*. In *P. falciparum*, the orthologs of Topo III and Topo IB have been identified as closely linked with their counterparts in other *Plasmodium* species, throughout evolution, and they were unique from those in yeast and higher eukaryotes (22). In this study we have focused to study the role of Topoisomerase III in mitochondrial biology of the malaria parasite.

#### 1.7.1.1b. TopoIII of Human Malaria Parasite

The *Plasmodium* genome encodes for Topoisomerase III (Gene ID: PF3D7 1347100), a member of Type I family of topoisomerases, which codes for a 710 amino acid containing protein. Significant differences can be observed in the amino acid sequences of human TopIIIα and PfTopoIII, as depicted in (**Figure 6**). The sequence identity between PfTopoIII and its human orthologue is approximately 39%. Topoisomerase/primase (Toprim) domain, which contributes to the substrate binding and metal ion coordination (37) activity is present in the N-terminal end of both human TopoIII and PfTopoIII. There is a unique mitochondrial targeting sequence (MTS) at the N-terminal end of the human TopoIII, but no such sequence is present in PfTopoIII. HsTopoIII also contains a characteristic Zinc Finger motif at its C-terminal domain, which is absent in PfTopoIII. In our research laboratory, we utilized the I-TASSER server to model the structure of PfTopoIII, employing human TopoIIIα (PDB ID: 4CGY) as a template. Analysis of PfTopoIII domains revealed the presence of an additional charged region within domain II, spanning an 85-amino-acid stretch (**Figure 6**). Notably, this charged domain is absent in Topo III enzymes of all eukaryotic. However, Topo III enzymes of bacteria possess a shorter charged loop composed of 17 amino acids. Previous investigations have

demonstrated the critical role of the charged domain in efficient DNA binding of E. coli TopoIII (38). PfTopoIII possesses conserved residues in the TOPRIM domain, and the catalytic tyrosine residue is also conserved in the GYISYPRTET motif. The Molecular Dynamic Simulations (MDS) showed that the PfTopoIII structure was stable, but the charged domain displayed large fluctuations (38). The molecular dynamics simulation (MDS) of PfTopoIII in complex with a DNA octamer revealed that the enzyme undergoes a structural change upon binding to DNA. Initially, PfTopoIII-ssDNA adopts a closed conformation like when it is not bound to DNA (apo enzyme). However, over time, the movement of domain III and the Toprim domain creates a central cavity, allowing the DNA to fit in. This movement of domains is often referred to as protein-mediated gate dynamics (39) and has significant implications for the enzyme's biochemical activities. The stability of the DNA octamer is maintained by hydrogen bonding and stacking interactions between the DNA bases and positively charged residues in the charged domain of PfTopoIII. Therefore, it can be concluded that the charged domain contributes to the effective binding of PfTopoIII with DNA, suggesting that it plays a crucial role in the enzyme's catalytic mechanism. However, the functional significance of PfTopoIII charge linker region was never comprehended. Semi-quantitative RT-PCR analysis revealed that PfTOPOIII transcript is expressed at the schizont stage of the parasite (38). It was also demonstrated that the spatiotemporal expression of PfTopoIII take place in the nucleus and in the mitochondria during the actively replicating stage of the parasite (39). The interaction of PfTopoIII with both PfBLM (Bloom syndrome protein) along with PfWRN (Werner syndrome protein) within malaria parasite was confirmed through the application of the yeast two-hybrid assay (38). Furthermore, the restoration of normal growth rate and the reduction in sensitivity to MMS (methyl methane sulfonate) were observed upon the introduction of full-length PfTopoIII into the \( \Delta\text{topoIII} \) yeast strain (38). The replication fork stalls as a result of HU treatment, which eventually results in the formation of chicken foot like structures (40), and significantly reduces cell viability. It was observed that the treatment with hydroxyurea (HU) results in the arrestation in parasite growth with concomitant induction of

PfTopoIII expression (38). In addition, it was observed that a transgenic parasite line, which ectopically expressed PfTopoIII, successfully rescued the toxicity induced by HU (hydroxyurea). In contrast, the mutant lacking the charged domain was unable to provide the same rescue effect (38). These genetic studies indicate the essential role of the charged domain in the proper functioning of PfTopoIII, although its precise mechanism has yet to be determined



В

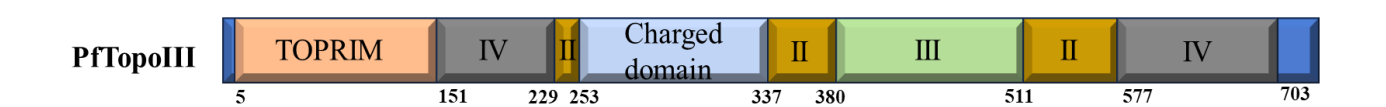


Figure 6: Domain organisation of DNA topoisomerase III (TopoIII) in human (A) and Plasmodium falciparum (B). A) Domain organisation of Human TopoIII, distinguished as Catalytic core domain and C-terminal domain. MTS directs the mitochondrial targeting sequence, and Conserved domains are indicated as roman numerals. B) Structure of Plasmodium falciparum TopoIII. Domains are marked as follows: Toprim (Red), The other two domains, II and IV are coloured in yellow and grey, respectively. A unique charged linker domain to Plasmodium falciparum is shown in blue.

## 1.7.2. Type II DNA topoisomerases

Type II DNA topoisomerases are evolutionarily conserved and are indispensable for several biological processes like transcription, replication, recombination, and DNA repair and thus survival of every living being. The capacity to relax negatively supercoiled DNA is a characteristic shared by all known eukaryotic topoisomerases. The knotting and unknotting as well as catenation and decatenation processes (Figure 7) on intact duplex DNA can also be catalysed by type II topoisomerases (41). The type II topoisomerases are enzymes that exist as dimers and can be classified into Type IIA and IIB based on their domain organization. These enzymes are responsible for creating a temporary double-strand break in the DNA (42). Type IIA topoisomerases form homodimers and utilize three protein interphases, namely N-gate, DNA-gate, and C-gate protein interphases, during the process of DNA decatenation. The N-gate, which acts as the entry gate, is the point where the DNA segment to be cleaved enters the enzyme, forming an enzyme-bound DNA duplex known as the G-Segment. Upon binding of ATP, the amino-terminal domain initiates dimerization, causing the temporary closure of the N-gate, cleavage of the G segment, and subsequent release of the second DNA duplex, referred to as the T segment, through the C-gate, which serves as the third gate. After that, the G section is ligated (43). The domain organization of Type IIB topoisomerases is different from Type IIA topoisomerases. Type IIB topoisomerases, carry out their action through two protein gates and do not possess C-gate. Upon cleaving the G segment, the Type IIA topoisomerases expeditiously release the T segment through the G gate. This type of topoisomerase has two subunits, A and B; The A subunit contains DNA binding and cleavage domains, whereas the ATPase domain is located within the B subunit. The ATPase domain folds into the Bergerat fold identical to the GHKL ATPase domain family protein (Gyrase, Hsp90, Histidine kinase, and MutL) (44). The other domains, like DNA cleavage and re-joining domain TOPRIM (Topoisomerase-Primase) and, the DNA binding domain CAP (Catabolite Activator Protein), also share considerable similarities between the two sub-classes.

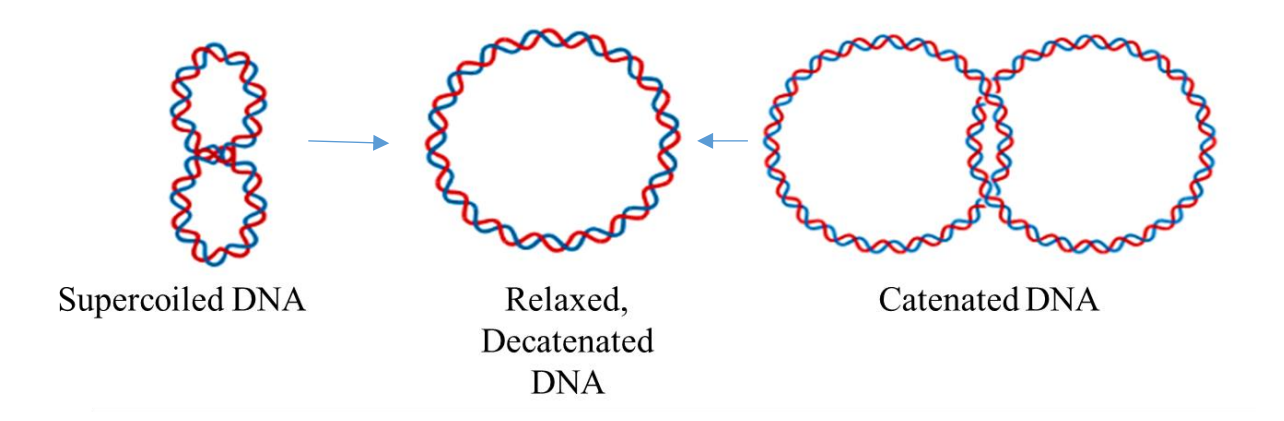


Figure 7: Schematic representation showing the decatenation of catenated/supercoiled DNA by the enzyme Type II topoisomerases, resulting in the formation of relaxed or decatenated DNA. This figure is a basic representation for descriptive purposes only and does not show the actual scale or complexity of the DNA molecules or the enzymatic process.

## 1.7.2a. Topoisomerase VI a vital protein in many eukaryotes

Topoisomerase VI is the only known member of the type IIB class of the topoisomerase family until recently in 2020, two more members of this family were identified, as the Topo VIII and the Mini-A (45). Topoisomerase VI is comprised of two subunits, TOPOVIA (Spo11) and TOPOVIB. The Spo11 protein is a eukaryotic homolog of the subunit A of TopoVI from archaebacteria. Several studies have proposed that the formation of double-strand breaks (DSBs) during meiosis in S. cerevisiae is attributed to a Topoisomerase II-like activity known as Topoisomerase VI (TopoVI). It has been observed that mutations in the Spo11 gene result in the absence of both meiotic DSB induction and meiotic recombination (46). Interestingly, a conserved tyrosine residue (tyrosine 135 in Spo11) is found in all eukaryotic homologs of Topoisomerase VIA, highlighting its conserved role in this biological process. This tyrosine might be critical for Spo11 and facilitates the cleavage of the DNA. Site-directed mutagenesis of this tyrosine to phenylalanine showed defects in the formation of meiotic DSBs at transient DNA fragments in the mutant strains (47). Reduced spore formation and low spore viability were observed in the mutants of *spo11* in *yeast*. Thus, Spo11 might generate the DSBs that initiate meiotic recombination by a cleavage reaction in S. cerevisiae similar to the one catalysed by archaeal TopoVI (48),(49). Mutations of SPO11 genes in fungi and mice (50) cause defects in meiotic recombination. In S. cerevisiae, nine additional proteins are indispensable for Spo11 activity, i.e., Spo11-Ski8, Rec102-Rec104, Mei4-Mer2-Rec114, and Mre11-Rad50-Xrs2; however, nothing is known about how these group of proteins are recruited on the site of DSBs and function in a concert (51).

Topoisomerase VI has been shown to play various functions in plants. In *A. thaliana*, three *SPO11* homologs are present (*AtSPO11-1*, *AtSPO11-2*, and *AtSPO11-3*), which are ancient paralogs of the other ones and are thought to be evolved by gene duplication (52). *AtTOPOVI* interacts with two auxiliary proteins, BIN4 (brassinosteroid-insensitive 4) and RHL1 (root hairless-1), and their mutants (bin4 and rhl1) showed defects in endoreduplication of the plant. Loss of *BIN4* elicits an ATM- and

ATR-dependent DNA damage response in post-mitotic cells, leading to an early arrest of endoreduplication (53). The basis behind the interaction between these two proteins with TopoVI is not yet known.

To detect the male sterile genes in the rice plant, a mutant library was constructed via exposing the rice cultivar 9522 of Oryza sativa with gamma-ray radiation and it led to the finding of two allelic male sterile mutants named as Oryza sativa meiotic topoisomerase VIB-like proteins; osmtopVIB-1 and osmtopVIB-2. Plants carrying the mutant allele were sterile in reproductive growth, but showed no effect on vegetative development (54). Tetrads of unusual size and shape were observed in the anther locus of VIB mutants which indicates that *OsmtopVIB* is indispensable for the initiation of the recombination during meiosis. In plants, it was found that *OsmtopVIB* interacts with *OsSPO11-1* and *OsSPO11-4* proposing they could associate together to form a hetero-tetrameric complex like that of the archaeal Topo VI (55).

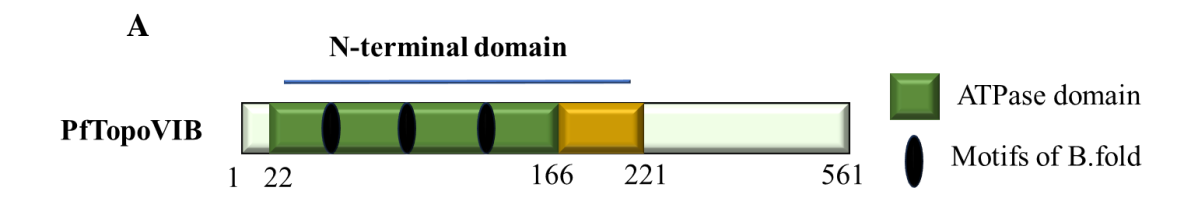
Mice contain two splice variants of *SPO11* (*SPO11* α and β). There is a 82% identity amongst putative mouse and human proteins (56). The mRNA splicing isoform present in human is like that of mouse Spo11α and Spo11β. Spo11β expression is at the early meiosis stages in contrast to Spo11α. Using *A. thaliana TOPOVIB* as a query, the mouse gene Gm960 was identified, which codes for approximately 63.8 kDa protein, that exhibits a strong similarity to *AtMTOPVIB*. However, *Mus musculus* TopoVIBL (TopoVIB Like protein) shows a low level of identity and similarity (11 and 19%), respectively with *S. shibatae* TopoVIB. Yeast two-hybrid assay showed mouse TOPOVIBL protein interacts with SPO11β but not with SPO11α. TOPOVIBL and SPO11β showed the formation of an enzyme complex (57). Meiotic DSBs are catalysed by a complex of SPO11 and TOPOVIBL in the mouse. Disruption of *SPO11* resulted in infertility in the mouse (50). Spo11<sup>-/-</sup> deficient spermatocytes showed defects in undergoing synapsis. Its accumulation in foci at the leptotene stage gives an indication of the DSB formation. Similarly, Mice TopoVIBL also plays a role in meiotic DSB formation. In comparison, the wild-type male homozygous mutant of TopoVIBL-<sup>/-</sup> showed

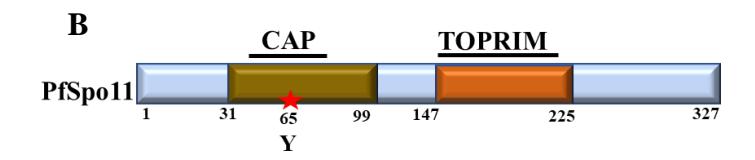
disrupted spermatogenesis in most of the seminiferous tubules (58). These effects were further confirmed by reduced  $\gamma$ H2AX levels and indiscernible RPA foci, indicating defective DSB formation in the mutants (58).

## 1.7.2b. Topoisomerase VI of human malaria parasite

The uncertainty existed whether a bona fide TopoVI occurs in *Plasmodia* until the identification of TopVIA (Pf3D7\_1217100.1), i.e., PfSpo11 encoding 327 amino-acid and TopoVIB (Pf3D7\_1365600) encoding 561 amino-acid long protein in the genome of *Plasmodium falciparum* (59). However, Spo11-2 (PF3D7 1027600), a different putative paralog, exists and codes for a 336 amino-acid containing protein. It has been noted that while human organisms do not possess orthologs of Topoisomerase VIB (TopoVIB), a human protein known as Topoisomerase VIB-like (TopoVIBL) has been identified. Notably, the sequence similarity between TopoVIBL and Plasmodium TopoVIB is only around 10%. TopoVIB of *Plasmodium* shows 31.5% similarity with *Sulpholobus shaibatae* SsTopoVIB. It harbours ATP binding and a transducer domain that communicates with the ATP binding site and interacts with the TopoVIA subunit to form a holoenzyme complex. The ATPbinding domain of *Plasmodium* topoisomerase VIB, ranging from amino acids 22 to 166, shares similarity with the Bergerat fold-forming domain identified in the GHKL ATPase protein family (60) (Figure 8A). The CAP and TOPRIM domains found in PfTopoVIA (PfSpo11) have sequence similarities to SsTopoVIA with 34.8% and 57%, respectively. TOPRIM (Topoisomerase-Primase), domain is a conserved DNA cleavage and re-joining domain, and the CAP (Catabolite Activator Protein) is a DNA binding domain, where the catalytic tyrosine residue at the 65<sup>th</sup> aa (as represented by the red star) (Figure 8B). The expression of both PfTOPOVIA and PfTOPOVIB was investigated in different stages (Ring, Trophozoite, Schizont, and Gametocyte) of P. falciparum using semiquantitative RT-PCR analysis. The findings revealed that both genes express specifically during the schizont stage of parasite development (44). According to the yeast two-hybrid analysis, PfTopoVIA and VIB interact with each other. Subcellular fractionation analysis established the

localization of topoisomerase VIB, both in the nuclear and organelle fractions; but not in the cytoplasmic fraction of the parasite (59). Based on genetic data, it has been demonstrated that the coexistence of PfTopoVIA and PfTopoVIB can restore the lethal phenotype observed in yeast topoII mutants. Conversely, PfTopoVIB alone does not possess the ability to accomplish the same rescue effect (60). This shows that both PfTopoVIA and PfTopoVIB contain Type II topoisomerase-like activity. However, the specific function of this enzyme complex in malaria parasite was never explored before.





★ Active Tyrosine Residue

(A) Diagrammatic representation of PfTopoVIB. Amino acid 22 to 161 resembles the ATP binding region of PfTopoVIB. Bergerat fold (B. fold) conserved motifs are represented in black colour. (B) TOPRIM (Topoisomerase-Primase), domain is a conserved catalytic domain, DNA cleavage and re-

Figure 8: The figure illustrates the different domains present in Plasmodium TopoVIB and Spo11.

joining domain, and DNA binding domain, CAP (Catabolite Activator Protein). Sequence analysis

revealed similar catalytic residue present at 65th aa position (red) of PfSpo11 protein.

## 1.7.2c. Topoisomerases as target

Targeting topoisomerases as a method of preventing malaria has been suggested by several research. *Plasmodium* parasite replication and transcription have been shown to be disrupted by inhibition of Topo I and Topo II activities (22, 60). Furthermore, structural research has shed light on the distinctive characteristics of *Plasmodium* topoisomerases, indicating that inhibitors could be developed to preferentially target the parasite enzymes while minimising off-target effects on human topoisomerases (22). Although Type IIA and Type IIB topoisomerases exhibit similarities in terms of their domain arrangements and functions, but differences are notable during their mechanisms of action. Consequently, inhibitors designed to selectively target Type IIA topoisomerases are usually ineffective on Type IIB topoisomerases. Topoisomerase II poisons and catalytic inhibitors are two subcategories of Type II topoisomerase inhibitors. Etoposide and doxorubicin are the examples of Topoisomerase II poisons, that trap the enzyme in a covalent bond with DNA, causing doublestranded breaks which subsequently result in cell death. These inhibitors are frequently used to treat several malignancies, such as leukaemia, lymphoma, and solid tumours. On the other hand, catalytic inhibitors like ICRF-187 and dexrazoxane are non-cleavable complex-forming inhibitors of DNA topoisomerase that do not produce protein-linked DNA strand breaks (61). They effect the DNA replication and cell division, as they bind to the enzyme and prevent it from performing its catalytic activity. ICRF-187 was found to act by a rare mechanism in which the drug does not compete for the ATP-binding pocket of topoisomerase, but bridges and further stabilizes a transient dimer interface between two ATPase protomers (62). Researchers conducted a screening of different analogues of 9anilinoacridine to assess their potential to inhibit the decatenation activity of Type II topoisomerases. During this process, they identified a derivative called 3,6-diamino-1'-amino-9-anilinoacridine. This particular compound with IC<sub>50</sub> concentration of 25 nM within parasite culture, exhibited significant effectiveness(63). However, the mechanism by which it inhibits the activity remains unidentified.

Topoisomerases are also being considered as molecular targets for various antibacterial and anticancer therapeutics (64). Anticancer agents perform their function utilizing two main mechanisms: a) stabilization of the ternary DNA-enzyme-drug covalent complex and resulting in the inhibition of DNA double helix re-integration, which can lead to apoptosis; b) they inhibit the catalytic cycle of the enzyme without any direct interference with the topoisomerase-DNA complex. A topoisomerase I inhibitor like nemorubicin (MMDX), which is a third-generation anthracycline derivative, shows its affectivity against a wide-ranging spectrum of tumour models and is now being studied in phase I/II clinical trials (64). DNA topoisomerase II are the targets of a wider and more diversified class of antineoplastic agents, including the amacrines and actinomycin. DNA gyrase has been identified as the target of antibacterial drugs like coumarin and quinolone (65, 66).

## 1.7.2d. Radicicol-a Topoisomerase VI inhibitor

Radicicol, also recognized as monorden, is a natural product that binds to Hsp90 (67). It binds to the ATPase domain of Hsp90 and prevents the maturation of Hsp90 clients and thus leading to proteasomal degradation (67). Earlier studies have provided evidence for the inhibitory properties of Radicicol on both the decatenation of kinetoplast DNA (kDNA) and the relaxation of supercoiled plasmid DNA mediated by archaeal Topo VI (67). To gain insights into the underlying mechanism, researchers utilized X-ray crystallography to examine the structural foundation of Radicicol-induced inhibition. The findings revealed that Radicicol and ATP engage in competitive binding to the ATPase pocket situated within the Bergerat fold of TopoVIB. This competition effectively hampers the nucleotide-dependent dimerization of TopoVIB subunits (68).

In a previous study, we generated an in-silico model of PfTopoVIB based on the SsTopoVIB template. Our analysis revealed that Radicicol interacts with the ATP binding pocket of PfTopoVIB in a manner similar to its binding to SsTopoVIB (69). Biochemical experiments displayed that Radicicol inhibits the relaxation and the decatenation activity of both *Plasmodium falciparum* and *Sulfolobus shibate* topoisomerase VIB (60, 68). Our previous study utilized a yeast cell-free extract

containing PfTopoVIB and PfSpo11, which demonstrated that Radicicol exhibits dose-dependent inhibition of PfTopoVI's decatenation activity (60). In cultures of *P. falciparum* 3D7, Radicicol exhibited inhibitory effects on parasite growth, with an IC<sub>50</sub> value of 8 µM (59). Notably, when exposed to sublethal doses of Radicicol, the parasites were transiently arrested in the Schizont stage, inhibiting their progression to the Ring stage. While Radicicol did not affect the ploidy of the treated *Plasmodium*, it significantly reduced the mitochondrial genome content, even at sublethal doses (59). These observations suggest that target protein of Radicicol plays a crucial role in replication of mitochondria, despite being inessential for nuclear replication.

In a separate study, we designed various analogues of Radicicol and using bioinformatics tools, monitored which of the Radicicol derivatives would bind precisely to the PfTopoVIB but not to PfHsp90 (69). Out of the 97 analogues of Radicicol that were tested for their ability to dock on PfTopoVIB as well as on PfHsp90, we identified three such analogues that show a strong affinity for PfTopoVIB (69) and don't bind to PfHsp90 at all. In future, synthesis and utilization of these analogues might reduce the off-target activity of the Radicicol and might be employed to study the function of PfTopoVIB in the biology of the malaria parasite.

## Objectives of the study

Malaria is a major public health concern that needs special attention. To date, just a handful of antimalarial agents are utilized to target malaria and parasites exhibit resistance to all the antimalarial. Therefore, active research is required to identify new target and target proteins. Protozoan topoisomerases are currently being examined as potential therapeutic targets in the hunt for more efficient treatments. These enzymes are crucial for the life of the eukaryotic organism since they are needed for DNA replication, transcription, and genome recombination. The malaria parasite undergoes a non-canonical mode of replication i.e., endoreduplication, in which multiple cycles of nuclear, mitochondrial, and apicoplast genome duplication occur without concurrent division of the cytoplasmic contents. Given that the process of endoreduplication is significant for the survival of the malaria parasite, it is important to identify topoisomerases that are crucial in this process.

We hypothesise that PfTopoIII, a Type I topoisomerase, and PfTopoVI (PfSpo11 and PfTopoVIB), a Type II topoisomerases, are engaged in the decatenation of replicated chromosomes *i.e.*, segregation of chromosomes during endoreduplication.

We developed the following specific aims, which provided the framework for the investigation. With various independent approaches, we have determined whether PfTopoIII and PfTopoVI (PfSpo11 and PfTopoVIB) participate in the mitochondrial DNA maintenance of the malaria parasite.

## **Specific Aims**

- 1. To evaluate whether PfTopoVI (PfSpo11 and PfTopoVIB) participate in the mitochondrial DNA segregation of the malaria parasite
- 1.1. To investigate whether PfSpo11 is the catalytic subunit of TopoVI enzyme
- 1.2. To determine whether PfTopoVI is expressed at the stage where mitochondrial segregation occurs
- 1.3. Whether PfSpo11 and PfTopoVIB constitute the functional holoenzyme within the parasite
- 1.4. Whether PfTopoVI is a mitochondrial topoisomerase of the malaria parasite
- 1.5. Computational analysis between PfTopoVIB and HsTopoVIBL
- 2. To decipher whether PfTopoIII participates in the mitochondrial DNA segregation of the malaria parasite
- 2.1. To study the stage specific expression of *PfTOPOIII* at different replicative stages of *Plasmodium*
- 2.2. To study whether PfTopoIII is a part of the mitochondrial replisome
- 2.3. To study whether PfTopoIII is associated with the mitochondrial genome of the malaria parasite

# Significance of the study

Through our research, we have discovered and characterized *Plasmodium* topoisomerase VIB and Spo11 as functional Type IIB topoisomerase. We also proved that *Plasmodium* Topoisomerase III is a mitochondrial Type I topoisomerase in the malaria parasite. Through our investigation, we identified a potential role for these proteins that occurs specifically during the late-schizont stage of the malaria parasite, facilitating the mitochondrial genome segregation This could have implications for better understanding the parasite biology and treatment of malaria as the maintenance and proper distribution of genome during the parasite's life cycle is essential for its infectivity.

# Chapter -2 Materials and Methodology

## 2.1 Molecular Biology techniques

## 2.1.1. Bacterial competent cell generation:

To prepare the initial inoculum, a single colony of bacterial cells was inoculated into 5 ml of LB (Luria Broth) medium supplemented with the relevant antibiotics. The culture was incubated overnight at 37°C with continuous shaking at 200 rpm in an incubator. One millilitre (1 ml) of the primary inoculum was added to 50 ml of LB media with the appropriate antibiotics and allowed to grow under the same conditions until the OD<sub>600</sub> reached 0.5–0.7. Cells were harvested by centrifuging them for 8 minutes at 8000 rpm, at 4°C. After that, the pellet was dissolved in 25 ml of 0.1 M CaCl<sub>2</sub> (ice-cold). Centrifugation was carried out for 8 minutes at 8000 rpm, at 4°C. The pellet was once more re-suspended in 12.5 ml of 0.1 M ice-cold CaCl<sub>2</sub> solution, and it was then incubated for 4 to 8 hours at 4°C. Cells were then centrifuged for 8 minutes at 8000 rpm, at 4°C. The pellet was then redissolved in 1.07 ml of 0.1 M ice-cold CaCl<sub>2</sub> solution, along with 170 μl 100 % glycerol. Liquid nitrogen was used to freeze 100 μl of suspension into pre-chilled microfuge tubes. Cells were frozen and stored to -80°C for long-term preservation.

#### 2.1.2. Bacterial transformation

One vial of competent cells was retrieved from -80°C and thawed on ice. The plasmid DNA (25–50 ng) was put to the top of the cells and incubated for 30 minutes on ice. Following incubation, the cells were given heat shock for 30 or 90 seconds (depending on the expression strain) and the tube was immediately placed on ice for two minutes. LB medium (900 µl) was added in the tube, which was then incubated for an hour at 37 °C, 200 rpm in a shaker incubator. After 2 minutes of spinning the cells at 10,000 rpm to pellet them down, most of the supernatant was discarded. The residual supernatant was used for the resuspension the pellet, which was then disseminated over an LB-agar plate with the proper antibiotic. The plate was then incubated at 37°C incubator for 16 hours till the growth was observed.

#### 2.1.3. Plasmid DNA isolation method

The primary inoculum consisting of a single bacterial colony, containing the desired plasmid, was cultured in 5 ml of LB medium supplemented with the suitable antibiotic. The culture was incubated overnight at 37°C in a shaking incubator set at 200 rpm. Cells were harvested by centrifuging for 5 minutes at 4000 rpm, at 4°C. The pellet achieved was re-suspended in 200 µl of pre-chilled solution-I (25 mM Tris pH 8.0, 10 mM EDTA pH 8.0) and after mixing properly cells were transferred to a microfuge tube. 200µl of solution II (0.2 M NaOH, 1 % SDS) was mixed by inverting several times. Cells were incubated at RT for 5 minutes. Then, 150µl of solution 3 (3 M NaOAc pH 5.2) was added and further incubated on the ice for the duration of 5 minutes along with occasional mixing. Sample was then centrifuges at 12000 rpm, for 15 minutes, and the supernatant was collected. To this, 2.2 volumes of 100 % alcohol was added and incubated at -20°C for 90 minutes followed by spinning of the samples for 30 minutes at 12000 rpm, 4°C. Centrifugation process, precipitated the DNA. Washing of the pellet was done using 70 % alcohol and further spun for 5 minutes at 12000 rpm, 4°C. The pellet was air-dried and re-suspended in 30 µl of 1X TE (10 mM Tris pH 8.0, 1 mM EDTA pH 8.0) at room temperature, and RNase treatment was done by adding 5µl (10 mg/ml) of RNase and incubated for 30 minutes at 37°C water bath. After incubation, sample volume was made up to 400 μl by adding 1X TE, and 400μl of PCIA (Phenol: Chloroform: Isoamyl alcohol) solution to it. The sample was vortexed for 3 minutes and further centrifuged at 12000 rpm for 15 minutes, at room temperature. The aqueous top layer was collected in new tube, followed by addition of 1/10th volume of solution-III (3M Sodium acetate pH 5.2) and 2.2 volume of 100 % alcohol to precipitate the DNA. The sample was incubated for 4 hours at -80°C. Final precipitation of plasmid DNA was performed by centrifuging samples for 30 minutes at 12000 rpm, at 4°C. Finally, Pellet was washed by adding 70 % alcohol (500 µl) and centrifuged at 12000 rpm, at 4°C for 5 minutes. After air-drying the samples, pellet was resuspended in 30 µl of 1X TE buffer.

## 2.1.4. Site-directed mutagenesis:

The splicing by overlap extension (SOE) PCR technique was employed to introduce a point mutation (Y to F) within the catalytic tyrosine residue of *PfSPO11*, which is situated at the 65th amino acid position. This was achieved by changing the TAC codon to TTT. To perform mutagenesis, the coding sequence was amplified into two segments. The initial segment was obtained from a cDNA template and amplified using the primer pair OSB (645 and 652). The subsequent segment was acquired using the primer pair OSB (653 and 646). The obtained segments were subsequently utilized as templates in amplifying the complete-length *PfSPO11* along with Y65F mutation. This amplification was achieved using the primer pair OSB (645 and 646) (see Table 4). The amplified product was subsequently cloned into the yeast expression vector *pHCA* (70). The successful introduction of the mutation was confirmed through DNA sequencing.

## 2.1.5. Western blotting

Tightly synchronized ES, MS, and LS stage-specific *P. falciparum* 3D7 cultures were then harvested, and protein was isolated as mentioned before (39). SDS-PAGE was used to run the protein samples, which were then transferred to the Poly Vinylidene di Fluoride (PVDF) membrane. The membrane was treated with methanol for the time duration of 20 seconds, followed by water for 2 minutes, and then with 1X transfer buffer (5.86 glycine, 11.64 gm Tris-base, and 0.75 gm SDS) for 5 minutes prior to the transfer. Protein was transferred using a semi-dry technique under 240 mA of current for 80 minutes. Following the transfer, the botting membrane was blocked for two hours at room temperature using a 5 % concentration of the blocking buffer (5 g of skim milk powder and 100 ml of 1X TBS (0.2 Molarity Tris base, 9% NaCl, pH 7.6, 0.1 % Tween-20). During the blotting procedure, different primary antibodies were used for specific experiments. The antibodies utilized for probing TopoVIB and Spo11 were rabbit anti-TopoVIB antibody (60) along with a rabbit antihuman Spo11 (anti-hSpo11) antibody (Invitrogen). These antibodies were used at dilutions of 1:500

and 1:3,000, respectively. The blot was incubated overnight at 4°C on a rocker. To normalize the results, a mouse anti-human actin antibody (Abcam) at a dilution of 1:5000 was used. The secondary antibodies, horseradish peroxidase (HRP)-conjugated anti-rabbit IgG (Promega) and anti-mouse (Santa Cruz Biotechnology), were utilized at a dilution of 1:10,000. In order to evaluate the protein concentration in the presence of atovaquone, cytochrome c (Cyt c) was employed as a marker for mitochondrial proteins. The parasite proteins were probed with an anti-mouse anti-Cytc antibody (Abcam) at a dilution of 1:3,000. Chemiluminescence detection was performed using a Pierce kit to visualize the western blots. The experiments were repeated three times with different cell batches, and band intensities were quantified using Image J software. The average relative densities were plotted using GraphPad Prism software.

## 2.1.6. Formaldehyde-assisted isolation of regulatory elements (FAIRE)

The FAIRE assay was conducted based on a previously described protocol (71). Briefly, synchronized parasite cultures at different stages (early-stage, mid-stage, and late-stage) were segregated into two different parts: one as a Ref (Reference) sample and another as a Test sample. For the time duration of 10 minutes the samples were centrifuged at 3,000 rpm. For the test cultures at each stage, 1% formaldehyde (37% concentration) was added and incubated in an orbital shaker at 25°C and 80 rpm for 20 minutes. To quench the formaldehyde, glycine was added at a final concentration of 125 mM and incubated for an additional 10 minutes at the same temperature. The parasite cultures were then centrifuged again at 3,000 rpm for 10 minutes. The obtained pellets were washed with phosphate-buffered saline (PBS) containing phenylmethylsulphonyl fluoride (Sigma) for each stage, repeating the washing step twice. Finally, for the time duration of 15 minutes the cells were centrifuged at 3,500 rpm and rapidly frozen with the help of liquid nitrogen. The cells were then further processed by resuspending them in the volume of total 1 mL of the lysis buffer comprising the following components: (2 % Triton X-100, 1 % SDS, 100 mM NaCl, 10 mM Tris-HCl, pH 8.0, 1 mM EDTA) per 0.4 g of cells and incubating for 1 h for both the reference and test samples. The

samples were then subjected to six sessions of 10-s burst sonication, followed by five minutes on ice. The cells were then centrifuged at 16,000 g for 20 min at 4°C. The obtained supernatant was processed with phenol, chloroform, and isoamyl alcohol (PCIA). Following PCIA treatment, the aqueous top layer was moved into a new tube and precipitated with the help of two volumes of 100 % ethanol and one volume of sodium acetate. The PCR analysis involved the use of primer pairs OSB (463 and 464) and OSB (563 and 564), which were designed to target the promoters of *PfTOPOVIB* and *PfSPO11*, respectively (**refer to Table 4**). For normalization purposes, control primers OSB 177 along with OMKB 418, targeting the *PfCOX* promoter, were also employed (**see Table 4**).

## 2.1.7. Coimmunoprecipitation (Co-IP)

Adhering to the manufacturer's instructions, the Thermo Scientific Pierce cross-link immunoprecipitation kit was used to conduct the Co-IP procedure. To begin, the anti-PfSpo11 antibody was bound to 50 µl of Pierce protein A/G Plus agarose beads (Provided inside immunoprecipitation kit) through a 2-hour incubation on a rotator at room temperature. The beads and antibody were then cross-linked using disuccinimidyl suberate (DSS) solution for 90 minutes at room temperature. Subsequently, the beads were washed according to the protocol, using 100 µl of elution buffer and 200 µl of wash buffer to neutralize the cross-linking. To prepare the samples, a total of 80 ml of tightly synchronized Late-Schizont stage parasite culture was harvested using 0.15% saponin treatment. The parasites were subsequently lysed with an IP lysis buffer (composed of 0.025 M Tris, 0.15 M NaCl, 0.001 M EDTA, 1% NP-40, and 5% glycerol at pH 7.4). The lysate was separated from cellular debris through centrifugation at 13000 g and 4°C for 10 minutes. The precleaned lysate was incubated overnight with antibody-bound beads. The column was positioned in a collection tube, and flow-through was gathered. The antigen antibody-bound beads were then subjected to washing, using washing buffer, and conditioning buffer. Bound antigen was eluted by elution buffer and further subjected to the western blot analysis. All buffers used were provided in the kit.

## 2.1.8. Chromatin immunoprecipitation assay (ChIP)

Synchronized ES, MS, and LS stage-specific 3D7 parasites were harvested, each with 7 to 8 % parasitemia, and we followed the standard procedure as described previously (39). Briefly, formaldehyde (37 %) was added to the parasite culture so that its final concentration reached 0.5 %, and then the culture was incubated at 37°C for 10 min. Late-Schizont stage culture was divided into two parts, one cross-linked with formaldehyde and another one non-cross linked with formaldehyde. To assess the non-specific recruitment, a negative control culture without a crosslinking agent was utilized. Following that, sonication was performed at a frequency of 37 Hz using an Elma S-60H sonicator, generating smaller chromatin fragments by following the established technique. Selective immunoprecipitation of protein-DNA complexes was performed using 8 µl of anti-PfTopoVIB antibody and anti-PfSpo11 antibody (procured from Invitrogen). To reverse the cross-linking, a 5 M NaCl solution was employed, followed by DNA extraction through proteinase K-phenol chloroform treatment. Utilizing particular primer pairs that cover several 1-kilobase sections (A to F) from the *Plasmodium falciparum* mitochondrial genome, following the previously described protocol (39). The quantification of PfTopoVIB and PfSpo11 recruitment to mtDNA was conducted. Collective coverage of the entire mitochondrial genome was done by each primer pair from A to F amplifying fragments of 1-kb length. Moreover, to amplify the junctional sequence, primer pair F was uniquely designed with the purpose of targeting the intended sequence, generating an amplicon from either circular mtDNA or concatemers formed by the fusion of two monomeric mtDNA units. To determine the specificity of TopoVI enzymes recruitment to the mitochondrial genome and the presence of both subunits across the apicoplast genome, two primer sets (P1 and P2) were utilized. Primer set P1 targets a region of 214 bp, while primer set P2 targets 310 bp region of apicoplast genome. The ChIP assay included the use of rabbit IgG as a control. To quantify the association with mitochondria, specific primer pairs were utilized to perform real-time quantitative PCR (qPCR) analysis. The primer pairs employed for amplifying regions A to F were as follows: A (OMKB 540 and OSB 596), B (OSB 493

and OSB 597), C (OMKB 615 and OSB 598), D (OSB 599 and OSB 600), E (OSB 601 and OSB 602), and F (OMKB 620 and OSB 603) (refer to Table 4). The effect of Atovaguone treatment on the recruitment of PfTopoVIB and PfSpo11 was examined by treating tightly synchronized midtrophozoite parasite cultures (7 to 8% parasitemia) with varying concentrations of Atovaquone (0, 0.5, 1.2, and 2.4 nM). The cultures were subsequently maintained and allowed to progress until they reached the late schizont (LS) stage. Following that, cultures specifically enriched with LS stage parasites were harvested and subjected to chromatin immunoprecipitation (ChIP). To investigate the recruitment of H3K4me3 and H3K9me3 on PfSPO11\_UAS and PfTOPOVIB\_UAS, chromatin immunoprecipitation (ChIP) assays were conducted using parasite samples from the early schizont (ES), mid-schizont (MS), and late schizont (LS) stages. The assessment of histone mark recruitment was conducted on the C-terminal end (CTE) of the relevant genes, serving as a control group within the experimental procedure. 8µl of each antibody against H3K4me3 (Millipore) and H3K9me3 (Millipore), respectively was used for the assay. The quantification of recruitment was performed using the primer pairs OSB (463 and 464) for PfTOPOVIB\_UAS and OSB (563 and 564) for PfSPO11\_UAS (listed in Table 4). Additionally, to assess the recruitment of activation and repression marks to CTE\_PfTOPOVIB and CTE\_PfSPO11, the primer pairs OSB 548 and OSB 549, and OSB 589 and OSB 590, respectively (provided in Table 4), were used. In the experiments, Rabbit IgG was employed as a negative control.

## 2.2. Cell Biology

## 2.2.1. Immunofluorescence assay and fluorescence microcopy

Synchronous stage-specific cultures of *Plasmodium* with a parasitemia of 6% were collected at the early schizont (ES), mid-schizont (MS), and late schizont (LS) stages. The cultures were washed with 1X PBS and for the duration of 15 minutes were fixed with 4% paraformaldehyde. Following that, PBS was used to wash them once more, after which they were subjected to permeabilization using a

combination of ice-cold acetone and methanol in a ratio of 1:3 for a duration of 15 minutes. To block non-specific binding, a 3% bovine serum albumin (BSA) solution was applied. The parasites were then incubated with primary antibodies at the following dilutions: anti-mouse anti-cytochrome c (from Abcam) at a dilution of 1:50, anti-rabbit anti-TopoVIB at a dilution of 1:25, and anti-rabbit anti-Spo11 at a dilution of 1:25. The incubation was carried out for 1 hour at 37°C. Afterward, the slides were washed three times with 1X PBS and PBS-Tween 20 (PBST) for a time duration of 15 minutes each. For protein detection, a secondary antibody cocktail was prepared, consisting of Alexa Fluor 488-conjugated goat anti-mouse IgG (green) at a dilution of 1:250, Alexa Fluorophore 594-conjugated chicken anti-rabbit IgG (red) at a dilution of 1:250, and DAPI (blue) (from Invitrogen) at a dilution of 1:50. The slides underwent three consecutive washes. Following the experimental procedures, the parasites were mounted using an antifade solution (Life Technologies). Subsequently, the fluorescence signals of PfCyt-c (green) and PfTopoVIB/PfSpo11 (red) were analyzed and captured using a Nikon Eclipse NiE AR fluorescence microscope. To determine the correlation between the immunofluorescence images and calculate the Pearson correlation coefficient (PCC), JaCoP plugin integrated into the ImageJ software (version 1.52s) was utilized.

## 2.3. Yeast genetic techniques

## 2.3.1. Yeast competent cell generation

For yeast competent cell preparation, the primary inoculum was prepared by inoculating the desired yeast strain in 5 ml of yeast growth medium and the culture was grown overnight at 30°C, in a shaking incubator at 200 rpm. Next day, a small volume was taken out from the primary inoculum to give secondary inoculum in a 40 ml growth medium. The volume of primary culture to be added in the secondary inoculum was determined using the formula:

Volume needed = (Volume of secondary culture x  $0.5 \text{ OD}_{600}$ )/ (Overnight OD<sub>600</sub> of primary culture x  $2^n$ ), in which, n= no. of generations.

The secondary culture was grown until  $OD_{600}$  reaches 0.6 to 0.8. Cells were the centrifuged at 3500 rpm, at 4°C, and the pellet was then washed with 10 ml autoclaved Milli-Q water to remove the residual media. Lastly, the cells were re-suspended in 300 $\mu$ l of Lithium acetate solution (1X Tris-EDTA, 1X Lithium Acetate) to attain the competency.

#### 2.3.2. Yeast transformation:

To approximately 200 µl of competent yeast cell, about (0.5-1)µg of desired DNA was mixed along with the 10 µg of carrier DNA (salmon sperm DNA). PEG solution containing 10X LiOAc (Sigma), 10X TE, 50 % PEG 2000 (Sigma) of about 1.2 ml was added to the cells, and was incubated for 30 minutes, at 200 rpm, in a 30°C shaking incubator. After incubation, heat shock was given to the cells at 42°C for 15 mins and kept on ice immediately for 2 minutes. The cells were then centrifuged at 5000 rpm for 1 minute, and the supernatant was removed. The obtained pellet was re-suspended in 200µl of 1X Tris-EDTA buffer and spread on the desired plate. The plate was then kept in a 30°C incubator for growth of the colonies.

#### 2.3.3. Protein isolation from yeast cells and western blot analysis:

Inoculated yeast cells were grown overnight at 30°C at 200 rpm in 5 ml of the appropriate medium. The primary culture, grown overnight was used to inoculate fresh 20 ml of suitable media, and continued to grow until the  $OD_{600}$  reached 0.5. The secondary culture was centrifuged at 3000 rpm for 5 minutes to harvest the cells. TCA (Trichloroacetic Acid) wash was performed after washing the pellet in 500  $\mu$ l of autoclaved water. The pellet was resuspended in TCA after the supernatant was removed. The cells were lysed by adding glass beads (Sigma), and the solution was vigorously vortexed. Protein-containing supernatant was collected in a fresh 1.5 ml microfuge tube. With intermittent chilling on ice and vortexing, the mixture of cells and glass beads was washed with TCA. The supernatant was then once more collected into the same tube. After centrifuging the sample, the supernatant was discarded. In 60  $\mu$ l of 1X sample buffer (Tris-HCl, pH 6.8, 2 % SDS, and

bromophenol blue), the precipitated protein was dissolved. The sample was next boiled for three to five minutes, followed by centrifugation for five minutes, and then the protein samples were subjected to SDS-PAGE, which were then transferred to the Poly Vinylidene di Fluoride (PVDF) membrane. Protein was transferred using a semi-dry technique under 240 mA of current for 80 minutes. Following the transfer, the membrane was blocked for two hours at room temperature using a 5 % blocking buffer (5 g of skim milk powder and 100 ml of 1X TBS (0.2 M Tris base, 9 % NaCl, pH 7.6, 0.1 % Tween-20). Blot was probed with different primary antibodies. The ScSpo11 and PfSpo11 proteins were probed using a rabbit anti-human Spo11 (anti-hSpo11) antibody obtained from Invitrogen, diluted at 1:500. To ensure accurate loading control, a mouse anti-Nsp1 antibody obtained from Abcam was used at a dilution of 1:5000.

## 2.3.4. Yeast strains generation and Yeast sporulation:

The spo11Δ BY4743 strain of diploid yeast (**Table 3**) was transformed with the following constructs: empty pHCA vector, *pHCA-PfSPO11*, *pHCA-Pfspo11Y65F*, and *pHCA-ScSPO11*. This transformation resulted in the creation of four strains: *PSY4*, *PSY1*, *PSY2*, and *PSY3* (**Table 3**). To initiate sporulation, each strain was first cultured in histidine dropout medium and allowed to grow overnight at 30°C while shaking. The next morning, the cells were transferred to pre-sporulation medium, which contained 1% potassium acetate, 1% yeast extract, 2% peptone, 0.003% uracil, and 0.005% leucine. The cultures were then incubated for 18 hours at 30°C while shaking. Once the optical density of the cultures reached 0.5 at 600 nm (OD<sub>600</sub>), the cells were washed with sterile Milli-Q water and resuspended in sporulation medium, which contained 1% potassium acetate, 0.003% uracil, and 0.005% leucine. The cells in sporulation medium were incubated in a shaking water bath at 18°C for 48 hours. Following the designated incubation period, the cells were subjected to staining using the nuclear marker DAPI. The assessment of sporulation efficiency involved the examination of a total of 1,000 cells from each strain. The sporulation efficiency was determined by calculating the percentage of cells that exhibited 3 or 4 asci out of the total number of diploid cells observed.

Three independent experiments were performed for each strain, and fluorescence microscopy was utilized for cell counting and analysis. Sporulation efficiency was calculated using the formula:

## % of sporulation = (cells containing 3 or 4 asci/total no. of diploid cells counted) \* 100

GraphPad Prism 6 was used to plot the standard deviation (SD) for each strain. *P*-values were calculated using the two-tailed Student's t test.

## 2.3.5. Yeast-two hybrid analysis

To perform yeast two-hybrid analysis, the *PJ69-4A* strain was used. All fusion constructs were transformed in the *PJ694A* strain to generate *PSY5*, *PSY6*, *PSY7* and *PSY8*. In *PJ69-4A*, as a control, empty *pGADC1* and empty *pGBDUC1* were transformed to generate *PSY5*. Next, we transformed *pGADC1-PfmtDNApolymerase* and *pGBDUC1*, in *PJ69-4A* to generate *PSY6*; *pGADC1* and *pGBDUC1-PfTopoIII* to *PJ69-4A* to generate *PSY7* and *pGADC1-PfmtDNApolymerase* and *pGBDUC1-PfTopoIII* to *PJ69-4A* to generate *PSY8*. All, Yeast strain genotypes are tabulated in the **Table 3**. Yeast two hybrids analysis was carried out as mentioned previously (72). In SC-Ura-Leu medium, the strains *PSY5*, *PSY6*, *PSY7* and *PSY8* were grown till logarithmic phase. Following that, they were serially diluted and patched in SC-Ura-Leu-His and SC-Ura-Leu-Ade medium. For 3–4 days, the plates were incubated at 30°C. In our investigation, the *PSY5* strain served as the negative control.

## 2.4. Methods in *Plasmodium falciparum* culture

#### 2.4.1. Red blood cell washing

Blood was collected in a 15 ml tube and was centrifuged at 15,000 rpm for 15 minutes. The top player containing serum and white buffy coat was removed using the pasture pipette. To the volume of RBC, equal volume of incomplete medium (RPMI-1640 without Hypoxanthine and Albumax) (Lonza) was added and mixed properly. The blood was then centrifuged at 3000 rpm for 15 minutes. Washing of the RBC's pellet was repeated twice with incomplete medium by simultaneous removal of the supernatant after the wash. To get 50 % hematocrit, washed RBSs were further mixed gently with equal volumes of incomplete medium and stored that 4°C.

#### 2.4.2. Freezing of *Plasmodium* parasites

The early ring-stage parasites with a parasitaemia of about (2-4) % were put into a 15 ml falcon tube and centrifuged for 10 minutes at 2500 rpm. The supernatant was aspirated, and an equal volume of freezing solution (5 % glycerol, 1.6 % sodium lactate, 0.03 % KCl, and 25 mM sodium phosphate) was then added dropwise (1 drop/second) to the estimated PCV (packed cell volume). After a gentle mixing, the mixture was left undisturbed for five minutes. Dropwise additions of 1.3 volume of the freezing solution were made. Each cryo-vial was then filled with 1ml of the sample. These cryo-vials were moved to an isopropanol container for progressive freezing. Overnight, the freezing container was kept at -20°C. The following day, the vials were moved into a liquid nitrogen tank for long-term storage.

## 2.4.3. Thawing of malaria parasite

Frozen parasites were taken out from liquid nitrogen tank and thawed by partially dipping the vial containing parasites in 37°C warmed water for (2-3) minutes. The vial was sanitized with 70 % alcohol and wiped. The thawed parasites were transferred into 50 ml centrifuge tube and Solution-I (1.4 M NaCl) (0.2 ml of solution-I/1ml of parasite culture) was added one drop per second, with

gentle mixing, followed by incubation for 5 minutes. Next, 10 ml of solution-II (1.6 % NaCl) per 1 ml of thawed parasites was added while gently mixing. The tube was then centrifuged at 1000 rpm for 10 minutes at room temperature and aspirated the supernatant using pasture pipette. The parasite pellet was made loose by gentle tapping and solution-III (0.9 % NaCl and 0.2 % Glucose) was added per 1 ml of the parasite in a drop wise manner followed by gentle mixing. The sample was again centrifuged at 1000 rpm for 10 minutes and supernatant was removed. Pellet obtained was resuspended in 3 ml of complete media and 200 µl of washed blood was added and culture was maintained in the 6-well plate, in a candle jar (37°C) incubator (73).

## 2.4.4. Genomic DNA isolation in Plasmodium falciparum

5 ml of 3D7 parasite culture was taken and centrifuged at 3000 rpm. 0.15 % Saponin was added to the parasite pellet and incubated at 37°C for 20 min. After saponin treatment, parasites were lysed using lysis buffer (40mM Tris HCL, 80mM EDTA and 2 % SDS) containing proteinase K and incubated at 37°C water bath for 3hr, with intermittent vortexing. After incubation, PCIA treatment was performed twice, and the aqueous layer was transferred into a new 1.5 ml tube. Genomic DNA was precipitated overnight at -80°C using 2.2 volumes of 100 % ethanol and one-third volume of sodium acetate.

## 2.4.5. Maintenance of *Plasmodium in vitro* culture

Plasmodium strains were maintained *in vitro* using the candle jar method (73). Albumax-II (5 mg/ml) and Hypoxanthine (0.5 mg/ml) in RPMI-1640 complete medium was used for the maintenance and growth of the parasite culture. When the parasitemia reached 2.5 %, sub-culture was done while maintaining the hematocrit of RBC at 5 %. In cultures, fresh medium and blood were added to reduce parasitemia to 0.5 %. In accordance with this, the volume of the culture was changed to 5 ml. The amount of parasitemia was estimated by Giemsa staining.

### 2.4.6. Synchronization of *Plasmodium* culture using Sorbitol

The culture containing 5 ml of early ring-stage parasites was centrifuged for 10 minutes at room temperature at 2000 rpm. After removing the supernatant, the pellet was dissolved in 0.5 ml of prewarmed 5 % sorbitol solution. The pellet was incubated in a water bath for 20 minutes at 37 °C with 5 minutes of intermittent mixing. Following incubation, 5 ml of incomplete medium was added in the pellet and centrifuged for 10 minutes at 2500 rpm, room temperature. Three washing cycles were performed after aspirating the supernatant. The pellet was then moved into a fresh 6-well culture plate, re-suspended in complete media, and maintained in a candle jar in a 37°C incubator.

### 2.4.7. RNA isolation and real-time analysis

Using established protocols, total RNA was extracted from the Early-Schizont, Mid-Schizont, and Late-Schizont stages of the 3D7 parasite (39). To eliminate DNA contamination from the RNA samples, DNase I treatment (Fermentas) was conducted. Reverse transcription of 1 mg of total RNA was carried out using a reverse transcriptase enzyme (Qiagen), and the resulting cDNA was amplified using gene-specific primers. The *ARP* gene-specific primers OSB (94 and 95), **Table 4** were used to amplify the cDNA product. For assessing *PfSPO11* expression, gene-specific primers OSB (589 and 590) (**Table 4**) were used. *PfTOPOVIB* expression was examined using gene-specific primers OSB (548 and 549) (**Table 4**). Additional gene-specific primer pairs, OSB (578 and 579) (**Table 4**) for *PfTOPOII* (PF3D7\_1433500), OSB (580 and 581) for *PfGYRA* (PF3D7\_1223300), and OSB (582 and 583) (**Table 4**) for *PfGYRB* (PF3D7\_1239500), were utilized. The cDNA was diluted at a 1:50 ratio and subjected to real-time PCR analysis using Takara RT-PCR and the Applied Biosystems 7500 Fast real-time PCR machine. To determine the Ct values for each topoisomerase transcript, the ARP transcript was used as a normalizing control. ΔCt values were calculated for each topoisomerase transcript, and the relative mRNA levels were obtained using the formula (change in mRNA level

 $[2^{\Delta Ct}]$ ). The mean values along with the standard deviation (SD) were plotted using GraphPad Prism 6 software.

### 2.4.8. Isolation of Protein from parasite

Harvesting of 10ml samples of tightly synchronized ES, MS, and LS stage parasite cultures was carried out when the parasitaemia reached 5%. The cultures were then subjected to centrifugation at room temperature for 10 minutes at 3000 rpm. This process resulted in the formation of pellet, which were utilized for subsequent analyses. The pellet was given two packed cell volume of 0.15 % saponin and was incubated for 20 minutes in a water bath at 37°C with periodic mixing. The sample was resuspended with 5 volumes of pre-warmed incomplete medium and centrifuged at 4000 rpm for ten minutes at 4°C. The achieved parasite pellet was further washed with 1x PBS (3-4) times to remove the traces of saponin. Finally, 1X Laemmli buffer (63 mM Tris-HCl, pH 6.8, 10 % Glycerol, 0.0005 % Bromophenol blue, and 0.1 % 2-Mercaptoethanol) was used to resuspend the parasite pellet.

#### 2.5. Drug assays in *Plasmodium* culture

### 2.5.1. Drug Inhibition assay in *Plasmodium*

Tightly synchronized parasites (3D7) having parasitaemia 1 % were used for the assays. Total 1 ml of the culture volume was used in a sterilized Eppendorf tube. The culture was then centrifuged at 2500 rpm for five minutes, and the acquired supernatant was discarded. 1ml complete medium containing varying drug (in appropriate vehicle solvent) concentrations, was added to the cell-pellet, and transferred to 24 well culture plates for the growth. The plate was then incubated for 48 hr in a 37°C incubator. Cell survivability was calculated by both Giemsa staining method as well as SYBR Green-I based assay as previously described (59). In this method, the fluorescent dye SYBR Green I (Takara) intercalate between the base stacks of parasite DNA, consequently the calculated fluorescent intensity is directly proportional to the number of parasites present. Briefly, 100 μl of in vitro culture was taken in 96-well plate containing 100μl of lysis buffer having SYBR Green reagent (20 mM Tris-

HCl (pH 7.5), 5 mM EDTA, 0.008 % saponin, and 0.08 % Triton X-100) and was incubated at room temperature in dark for 60 minutes. Fluorescence intensities were calculated using the multimode reader (Spectramax m2e) at excitation and emission wavelengths of 485 and 530 nm, respectively. Each assay was replicated three times for reproducibility. Corrected fluorescent readings were obtained by subtracting the background readings of the culture without parasites. Dose-response curves were plotted with the help of GraphPad 6 software to calculate the 50 % inhibitory concentration (IC<sub>50</sub>) of Radicicol/Atovaquone.

### 2.5.2. Fixed ratio isobologram method to determine interaction between Radicicol and Atovaquone/Chloroquine

To investigate the interaction between Radicicol (Sigma) and Atovaquone (Sigma) in vitro, we employed a fixed ratio isobologram method. The IC<sub>50</sub> value of Radicicol was determined by treating synchronized schizont stage-specific 3D7 parasites with various concentrations of Radicicol for 48 hours at 37°C. Similarly, for the determination of the IC<sub>50</sub> value of Atovaquone, synchronized trophozoite-specific 3D7 parasites were exposed to different concentrations of Atovaquone for 48 hours at 37°C. The percentage of parasite inhibition was assessed using both Giemsa staining and SYBR Green-based staining with a plate reader (Spectramax m2e). The IC<sub>50</sub> values were calculated by plotting the percentage of inhibition against the drug concentration on a semi-log graph using GraphPad Prism 6 software. To investigate the potential interaction between Radicicol and Atovaquone, we conducted experiments combining the two drugs at four fixed ratios (4:1, 3:2, 2:3, and 1:4), following a previously published protocol (74). Each drug combination, along with its 2fold serial dilutions, was evaluated in triplicate to assess its impact on parasite development. We used a 96-well plate, with each well containing a total reaction volume of 200 ml comprising 100 ml of culture (1% parasitemia and 5% hematocrit) and 100 ml of medium with or without the specific drug. The plates were then incubated at 37°C for 48 hours, followed by parasite counting using the SYBR Green I-based method. The IC<sub>50</sub> value for each drug combination was determined by plotting a semilog graph. Additionally, we calculated the fractional inhibitory concentration (FIC) for each drug using an appropriate equation.

### $FIC = IC_{50}$ of the drug in mixture/IC<sub>50</sub> of the drug alone

The interaction between Radicicol and Atovaquone was evaluated by calculating the  $\Sigma$ FIC (Summation of Fractional Inhibitory Concentration) value using the equation FIC = (IC<sub>50</sub> of Radicicol in combination / IC<sub>50</sub> of Radicicol alone) or (IC<sub>50</sub> of Atovaquone in combination / IC<sub>50</sub> of Atovaquone alone). The resulting values were used to construct an isobologram using GraphPad Prism software. A  $\Sigma$ FIC value of less than 1 indicates synergism, values between 1 and 2 represent an additive interaction (no interaction), and a value of 2 or higher suggests antagonism. The same methodology was employed to determine the drug interaction between TopoVIB inhibitor Radicicol and Chloroquine (Sigma).

### 2.6. Bioinformatic Analysis:

### 2.6.1. Sequence- and structure-based comparison between PfTopoVIB and HsTopoVIBL

The sequences of all TopoVIB/TopoVIBL proteins were retrieved from the UniProt database (75). *S. shibatae*, *P. falciparum*, *P. berghei*, *Mus musculus*, and *Homo sapiens* were used for the analysis and their UniProt ID numbers are as follows, O05207, Q8ID53, A0A509AMZ8, J3QMY9, and Q8N6T0, respectively. Clustal V was employed to perform multiple-sequence alignment. PfTopoVIB & HsTopoVIBL like structures were retrieved from the Alpha Fold database (76). Furthermore, structural alignment was performed with the help of Visual Molecular Dynamics (VMD) (77).

### Chapter 3

**Results** 

Specific Aim-1

3. Specific Aim 1: To evaluate whether PfTopoVI (PfSpo11 and PfTopoVIB) participates in the mitochondrial DNA segregation of the malaria parasite

#### 3.1. To investigate whether PfSpo11 is the catalytic subunit of TopoVI enzyme

We attempted to express and purify the recombinant PfSpo11 protein in multiple bacterial systems to examine the functionality of PfSpo11; However, our attempts were unsuccessful, leading us to employ yeast as an alternative surrogate system. Our aim was to determine whether the putative PfSpo11 could complement the functions of *S. cerevisiae* Spo11 (ScSpo11). It is widely acknowledged that diploid budding yeast go through meiosis in response to nitrogen deprivation condition, resulting in the production of haploid nuclei during the process of meiosis, which are subsequently enclosed in spores (78). In yeast, the initiation of meiosis is facilitated by ScSpo11, which catalyses the breakage of double-stranded DNA. This DNA breakage is then repaired through recombination among the paternal chromosomes. In plants, Spo11 and TopoVIB function as a complex, while ScSpo11 catalyses double-strand breaks (DSBs) by interacting with several other proteins in the absence of TopoVIB (51). Sequence analysis revealed that the active site tyrosine ScSpo11 is essential for its DSB induction activity (79).

To understand whether there is any similarity between the sequences of PfSpo11 and ScSpo11 we performed pairwise sequence alignment analysis. We identified that PfSpo11 possesses the conserved CAP (catabolite activating protein) domain involved in DNA binding and the TOPRIM domain responsible for the metal binding. These domains exhibit 42.7% and 59.5% sequence similarity, respectively, with their counterparts in ScSpo11 (Figure 9A), respectively (60). Furthermore, the catalytic tyrosine residue at 65<sup>th</sup> position, that is essential for its function, is conserved in the *Plasmodium* Spo11 protein. To conduct the genetic complementation assay, we cloned *Plasmodium* falciparum SPO11 and ScSPO11 into a centromeric yeast expression plasmid. Subsequently, we introduced a point mutation (Y to F) at the catalytic tyrosine residue present at 65<sup>th</sup> position of *PfSPO11* employing site-directed mutagenesis, and the mutated gene was inserted into a yeast

centromeric expression plasmid. Using diploid  $\Delta spol1$  yeast strain, we created four isogenic strains by transforming the following four centromeric vectors: an empty vector used as a negative control, PfSPO11, PfSPO11<sup>Y65F</sup>, and ScSPO11 (used as positive control) (**Figure 9B**). The four strains were then allowed to sporulate by growing individually in the sporulation medium and we measured the spore forming ability in each one of them. We stained the nucleus of each strain with a nuclear marker DAPI and, the spore development was observed using a fluorescence microscope (Figure 9C). We noticed that the strain expressing PfSpo11 could overcome the sporulation deficiency observed in the  $\triangle$ spol1 strain, like the strain expressing ScSpol1. Our findings indicated that strains expressing either PfSpo11 or ScSpo11 formed four distinct nuclei. However, the catalytic mutant of *Pfspo11* was unable to undergo sporulation (**Figure 9C**). To exclude the likelihood that the sporulation impairment observed in the PfSpo11Y65F strain was due to a lack of mutant protein expression in yeast, a western blot analysis was performed. Proteins extracted from each of the four strains were subjected to this analysis. A rabbit anti-human Spo11 (anti-hSpo11) antibody from Invitrogen, that cross-react with both PfSpo11 and ScSpo11, was utilized to detect the presence of *Plasmodium* and yeast Spo11. Our study verified the expression of PfSpo11 and its mutant in their respective strains (Figure 9D, first lane from the top), with Nsp1 serving as the loading control (Figure 9D, second lane from the top). We performed a comprehensive analysis by counting more than 1,000 cells in each strain and conducting three separate batches of cell tests to evaluate sporulation efficiency. Our results demonstrated that PfSpo11 could effectively complement the sporulation deficiency observed in the △spo11 strain (1.1%), similar to the strain harbouring ScSpo11. Consistent with our findings, both the strain carrying ScSpo11 (6.6%) and the strain carrying PfSpo11 (8.3%) exhibited high sporulation efficiencies. In contrast, the catalytic mutant strain *Pfspo11Y65F* displayed a significant impairment in sporulation, with an efficiency of only 1.7%, which was comparable to that of the \( \Delta spol1 \) strain (Figure 9E). These findings provide compelling evidence that PfSpo11 functions as a functional ortholog of ScSpo11, and its activity critically depends on the catalytic tyrosine residue

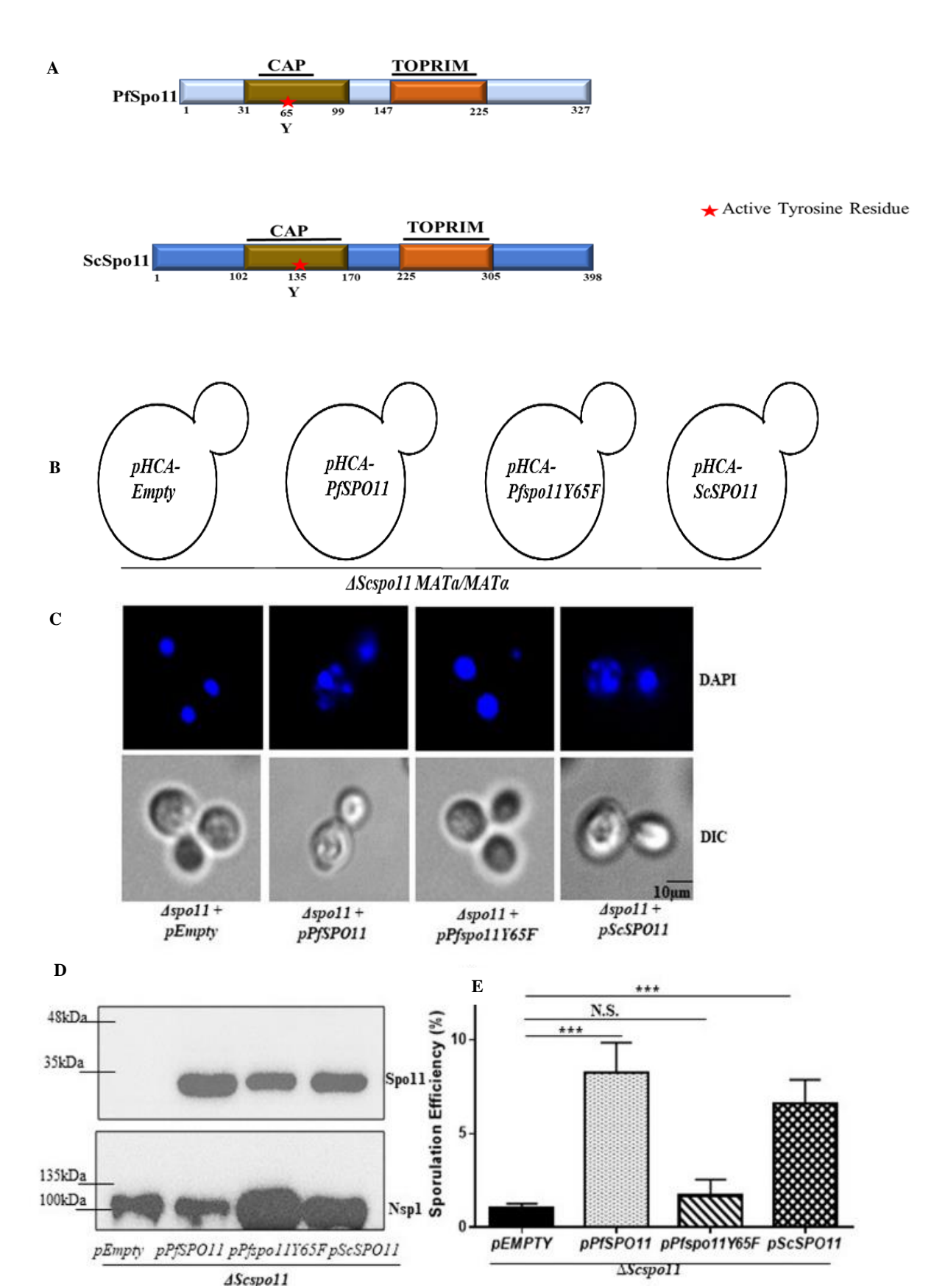


Figure 9: PfSpo11 complements the sporulation defect of the diploid ∆spo11 strain: The figure illustrates the different domains present in both yeast and Plasmodium Spo11 proteins. TOPRIM (Topoisomerase-Primase), domain is a conserved DNA cleavage domain and rejoining domain, and CAP (Catabolite Activator Protein), is the DNA binding domain, where the catalytic tyrosine residue presents at 135th amino-acid, in yeast Spo11 (Red). Sequence analysis revealed similar catalytic residue present at 65th amino-acid position (red) of PfSpo11 protein. (B) A diagrammatic representation depicting the creation of four yeast diploid strains for the sporulation assay:  $\Delta Scspol1$  MATa/MATa-Empty pHCA,  $\Delta Scspol1$ MATa/MATa-pHCA-PfSPO11, ΔScspo11 MATa/MATa-pHCA-Pfspo11Y65F, and ΔScspo11 MATa/MATa-pHCA-ScSPO11.(C) Fluorescence imaging was conducted on the respective diploid strains following sporulation, with nuclei visualized using DAPI staining. The strain expressing PfSPO11 exhibited complementation of the sporulation defect in \( \Delta Scspo11 \) strains, whereas the strain expressing Pfspo11<sup>Y65F</sup> did not. Differential interference contrast (DIC) was utilized.(D) Western blot analysis was performed to verify Spo11 expression in the individual strains, with Nsp1 serving as the loading control.(E) The sporulation efficiency of each strain was determined by counting the number of cells capable of forming mature asci (3 or 4 spores). The experiment was repeated three times using independent cell batches, and a total of 1,000 cells were analysed for each strain. Mean values ( $\pm$  SD) were plotted using GraphPad Prism 6. A two-tailed Student's t-test was used for the statistical analysis (\*\*\*, P < 0.001; N.S., not significant).

### 3.2. To determine whether PfTopoVI is expressed at the stage where mitochondrial segregation occurs

Malaria parasite undergoes various morphological changes during its complex multi-stage life cycle. As said in the 'Introduction' section, there are three distinct schizont stages during the asexual development of the parasite, namely, Early (ES), Mid (MS) and Late-schizonts (LS). The nuclear and apicoplast genome segregation of the malaria parasite take place during the early schizont and mid-schizont stages, respectively, whereas the mitochondrial genome segregation takes place just before the cell division *i.e.*, at the late-schizont stage of the *P. falciparum* (17). We previously discovered that the two PfTopoVI subunits expression were more abundant in the schizont stage than in the ring and the trophozoite stages, respectively. To establish the function of PfTopoVI, we first determined the expression pattern of these two subunits within the three sub-stages of Schizont.

### 3.2.1. The transcriptional expression of *PfTopoVIB* and *PfSPO11* display a unique pattern compared to the other Type II topoisomerases of *P. falciparum*

To investigate the potential role of PfTopoVI during the mitochondrial genome content segregation, we examined the expression of all Type II topoisomerases at different stages of schizont development (22). We used tightly synchronized parasites at the early schizont (ES) stage (35-36 hpi), mid-schizont (MS) stage (39-40 hpi), and late schizont (LS) stage (44-45 hpi) for our experiments (**Figure 10A**). Semi-quantitative RT-PCR analysis was performed using cDNA prepared from these parasite stages. The selection of stages was based on the relative size of the nucleus observed under the microscope. To ensure the absence of genomic DNA contamination, negative reverse transcriptase samples (-RT) were included and subjected to PCR amplification (**Figure 10B**). *ARP*, a constitutively expressed gene was used as a normalization control for all stages (**Figure 10B**, **first lane from the top**). Our results showed distinct expression patterns for *PfTOPOVIB* and *PfSPO11* compared to other Type II topoisomerases like *PfTOPOII*, *PfGYRA*, and *PfGYRB*. At ES and MS stages of the parasite *PfTOPOVIB* and *PfSPO11* were not expressed (**Figure 10B**). However, their expression was

specifically induced at the LS stage, which corresponds to the cessation of nuclear division. Quantitative RT-PCR analysis using two independent batches of parasites confirmed that *PfTOPOVIB* and *PfSPO11* expression levels were negligible during the ES stage compared to the expression levels of *PfTOPOII*, *PfGYRA*, and *PfGYRB* (**Figure 10C**).

These findings suggest that PfTopoVI may not be involved in DNA replication during the ES stage.

# 3.2.2. PfTopoVIB and PfSpo11 protein expression were induced at the late Schizont stage of the parasite

To examine the expression of PfSpo11, we isolated total protein from the early schizont (ES), midschizont (MS), and late schizont (LS) stages of the parasite. We selected a highly antigenic peptide sequence of topoisomerase VIB (CLLNLFTRVKEEYPDEFESI) to generate a primary antibody in rabbits (59). We used a rabbit anti-human Spo11 (anti-hSpo11) antibody (Invitrogen) known to exhibit cross-reactivity with PfSpo11, indicating structural similarity between the two proteins. Western blot analysis was conducted using protein samples acquired from three individual batches of tightly synchronized ES, MS, and LS stage-specific parasites. The blots were probed with the rabbit anti-TopoVIB antibody (diluted at 1:500) and the rabbit anti-human Spo11 (anti-hSpo11) antibody (diluted at 1:3,000) to validate the expression pattern of the proteins. The intensity of each band on the blots was quantified using ImageJ software. The western blot images established the presence of PfTopoVI subunits at the LS stage, with Actin serving as the loading control (Figure 11A, First and second lane from the top). The band intensities of PfTopoVIB and PfSpo11 were normalized against the Actin signal for further analysis. The results demonstrated a significant increase in the expression of PfSpo11 and PfTopoVIB by approximately 5-fold and 10-fold, respectively, during the late schizont (LS) stage compared to the early schizont (ES) and mid-schizont (MS) stages of the parasite (Figure 11B). To validate these findings, an immunofluorescence assay was conducted to visualize the expression of PfTopoVI subunits at the three distinct schizont phases. The red fluorescence signal of both PfTopoVIB and PfSpo11 was observed using an Alexa Red 594-conjugated secondary

antibody and a Nikon Eclipse NiE AR fluorescence microscope. The nucleus was stained with DAPI for visualization. Analysis of numerous cells confirmed that the maximum expression of both subunits occurred during the late schizont stage of the parasite (**Figure 11C & D**). These results suggest that PfTopoVI may play a role in the segregation of the mitochondrial genome rather than in replication.

To further confirm the exclusive expression pattern of PfTopoVI, we utilized two different methods. Firstly, we conducted the FAIRE assay to assess the compactness of the upstream activator sequence of both *PfSPO11* and *PfTOPOVIB*. Secondly, we examined the promoter activity of these subunits at various stages of the schizont.

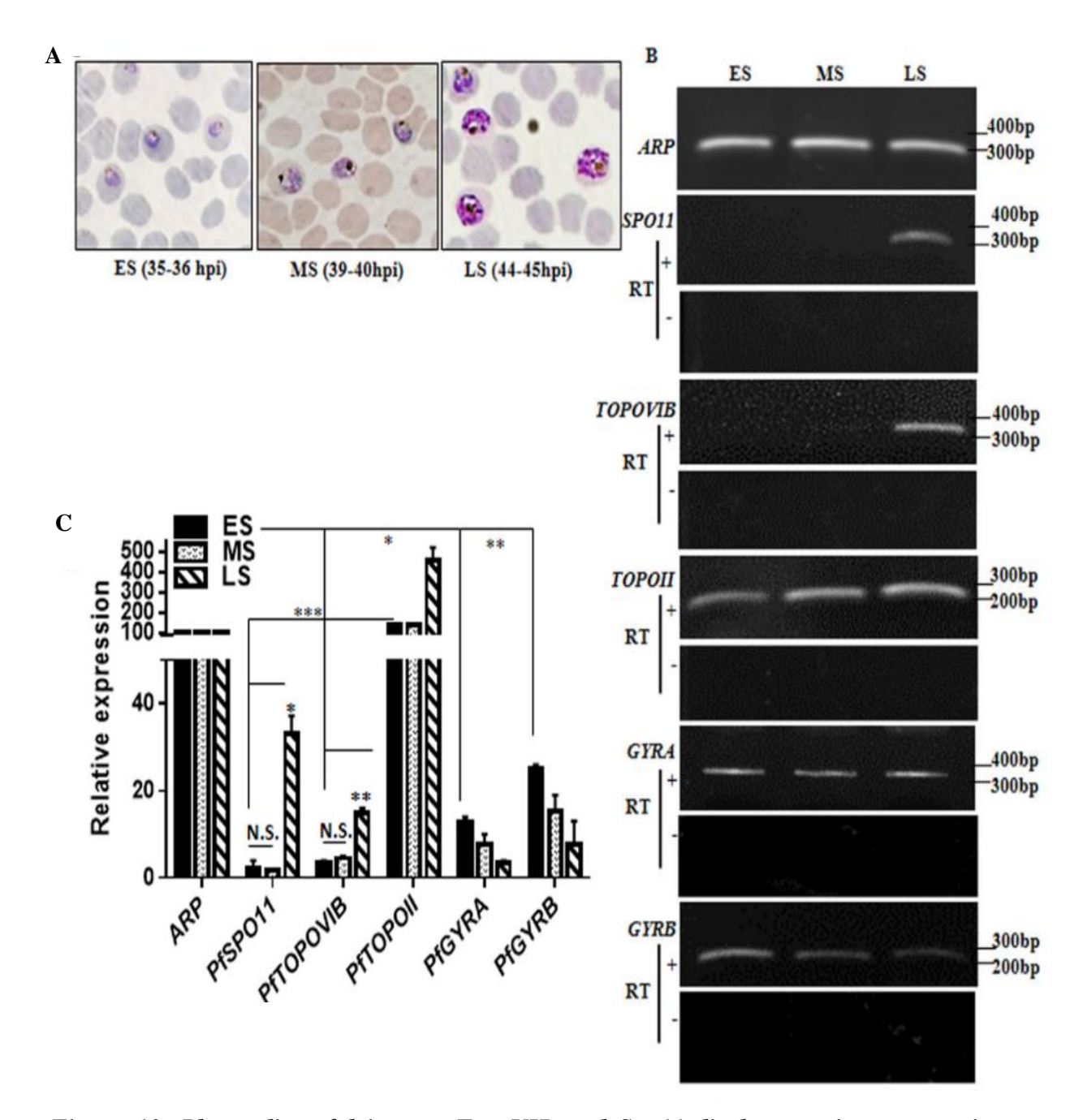


Figure 10: Plasmodium falciparum TopoVIB and Spo11 display a unique expression pattern compared to the other type II topoisomerases of P. falciparum. (A) Figure shows the images of ES (early schizont [35 to 36 hpi]), MS (mid-schizont [39 to 40 hpi]), and LS (late schizont [44 to 45 hpi]) of 3D7 malaria parasites observed after staining with Giemsa. (B) The expression levels of type II DNA topoisomerases (PfTOPOII, PfGYRA, PfGYRB, PfTOPOVIB, and PfSPO11) was analysed using semi-quantitative RT-PCR. cDNA obtained from the ES, MS, and LS stages of the parasites was used for this purpose. Agarose gel images illustrating the results of both positive and negative reverse transcriptase (+ RT and -RT, respectively) samples were provided. (C) Real-time RT-PCR analysis was done to quantify the relative expression levels of all type II topoisomerases in Plasmodium falciparum, compared to the constitutively expressed ARP at the ES, MS, and LS stages. This analysis was conducted using two independent batches of parasites. Statistical significance was determined using a two-tailed Student's t-test, with P-values denoted as \*\*\*, P < 0.001; \*\*, P < 0.05; and N.S., not significant.

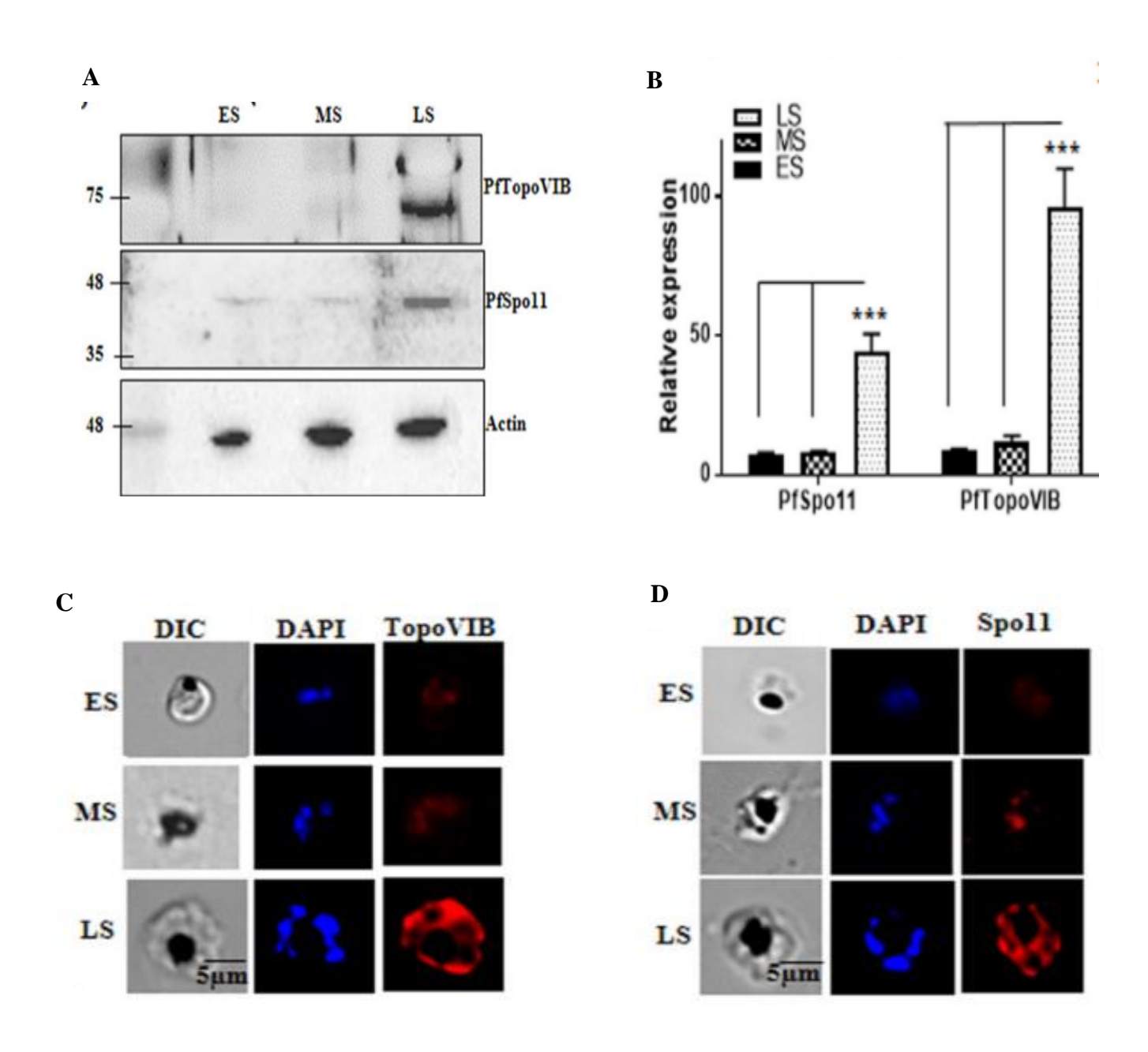


Figure 11: PfTopoVIB and PfSpo11 are induced at the LS stage of the parasite(A) The expression profiles of PfTopoVIB and PfSpo11 were analysed using western blotting, which demonstrated their predominant expression at the Late-Schizont stages of the parasite. Actin was utilized as a reference control for normalization. (B) The relative protein expression levels of PfTopoVIB and PfSpo11 were quantified by analysing western blot data from three independent batches of synchronized parasite proteins obtained at the ES, MS, and LS stages. The mean values ( $\pm$ ) standard deviation (SD) was plotted. Statistical significance was determined using a two-tailed Student's t-test, with p-values indicated as \*\*\*, P < 0.001. (C and D) Immunofluorescence imaging revealed the predominant expression of PfTopoVIB and PfSpo11 at the LS stages of the parasite. Nuclei were visualized using DAPI staining.

#### 3.2.3. Stage-specific compactness of PfSPO11-1\_UAS and PfTOPOVIB\_UAS

To confirm the exclusive expression pattern of PfTopoVI, we looked at the chromatin compaction of the promoter regions of *PfTOPOVIB* and *PfSPO11* at various developmental stages of the parasite. To accomplish this, we have employed FAIRE (Formaldehyde-Assisted Isolation of Regulatory Elements) assay, which enables one to ascertain whether a particular region of chromatin is in the nucleosome free state, or the nucleosome bound state. Our assay was designed to identify whether the promoter regions of *PfTOPOVIB* and *PfSPO11* were indeed active specifically at the LS stage. We utilized two probes located, 620-bp and 311-bp upstream activator sequences (UAS) from the translation start sites (ATG) of *PfTOPOVIB* and *PfSPO11*, respectively, as depicted in (**Figure 12A**). To serve as a control for normalization, we utilized the COX3 promoter sequence, which is not associated with nucleosomes due to its presence in mitochondrial DNA (mtDNA). By employing FAIRE analysis on three tightly synchronized schizont stages of the parasite, we observed that the promoter region of PfTOPOVIB remained in a heterochromatinized state during the ES and MS stages. However, during the LS stage, it underwent a transition to a nucleosome-free state (Figure **12B).** Likewise, the promoter of *PfSPO11* exhibited a similar trend as *PfTOPOVIB\_UAS*, although there was a slight relaxation in chromatin compaction even during the mid-schizont stage. Quantification of the gel images from two independent replicates revealed a 25-fold and 4-fold decrease in chromatin compaction for the *PfTOPOVIB* and *PfSPO11* promoters, respectively, during the LS stage compared to the MS stage of the parasite (Figure 12C).

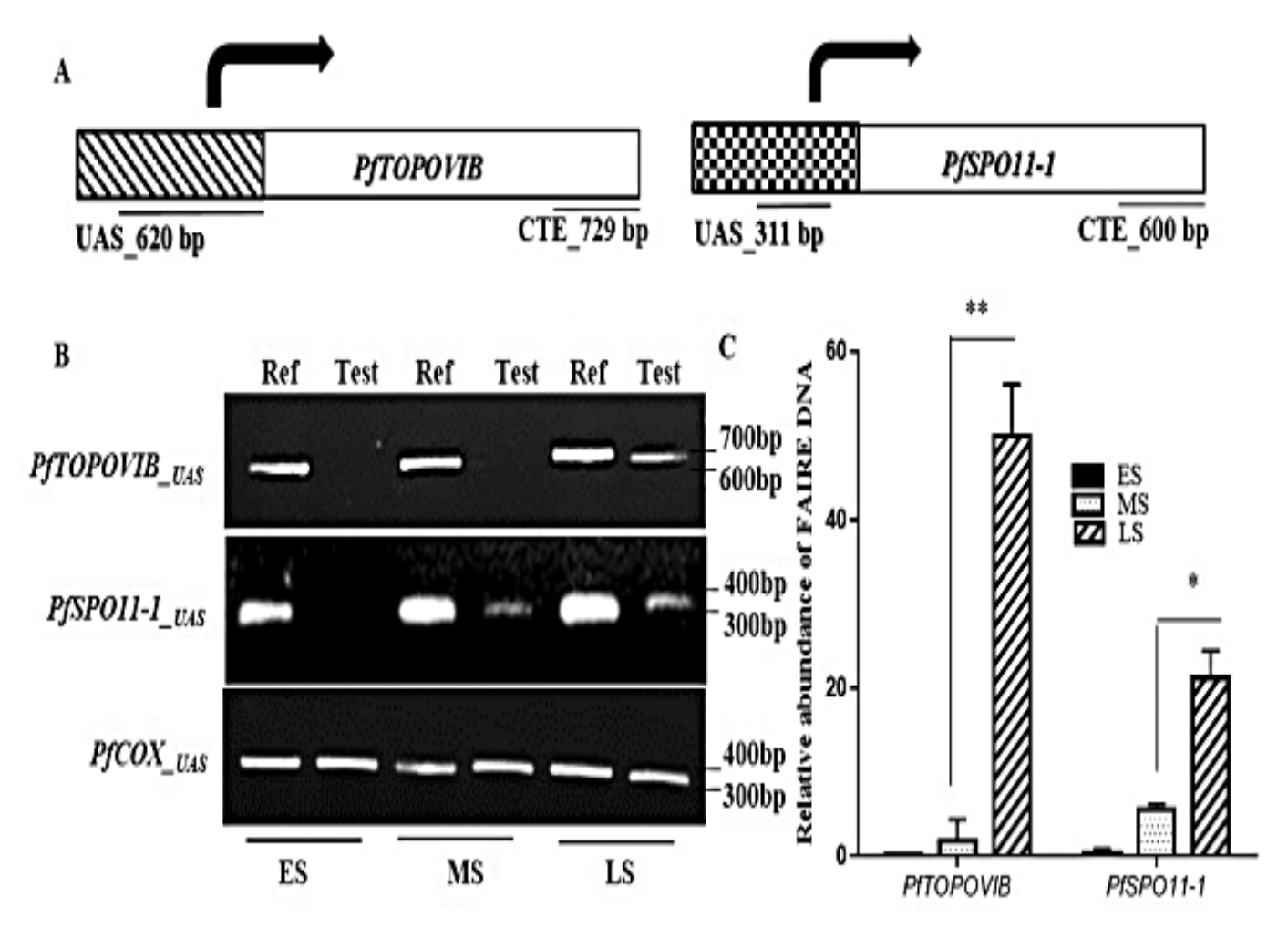


Figure 12: Stage-specific compactness of the promoters of PfTopoVI subunits. (A) The left panel illustrates the locations of the upstream activator sequence (PfToPoVIB\_UAS620) and C-terminal end (729\_CTE) utilized in the FAIRE analysis for PfToPoVIB. Similarly, the right panel shows the positions of the UAS and CTE (PfSPO11-1\_UAS311 and 600\_CTE) utilized in the FAIRE analysis for PfSPO11. (B) The FAIRE analysis was performed on tightly synchronized ES, MS, and LS stages of the parasite, revealing that the chromatin associated with PfToPoVIB\_UAS and PfSPO11-1\_UAS exhibited a relaxed state at the LS stage. The COX3 sequence was employed as a control for normalization. The samples were divided into lanes as follows: lane 1 - ES reference, lane 2 - ES test, lane 3 - MS reference, lane 4 - MS test, lane 5 - LS reference, and lane 6 - LS test. (C) The above-described experiment was replicated using two independent repeats of experiments, and the mean values (±) standard deviation (SD) were plotted. Statistical analysis was conducted using a two-tailed Student's t-test, with significance indicated as \*\*, P < 0.01 and \*, P < 0.05. Both PfToPovib\_UAS and PfSPo11-1\_UAS exhibited a nucleosome-free state at the LS stage

## 3.2.4. The enrichment of activation and repression histone marks at the promoter-proximal region of *PfTOPOVIB* and *PfSPO11* at the LS stage of the parasite

We also assessed the presence of two well-established epigenetic marks, namely the histone activation mark, H3K4me3 and the repression mark H3K9me3, to the promoter-proximal areas of PfTOPOVIB and PfSPO11 at three schizont stages of the parasite. To do this, we used anti-H3K4me3, anti-H3K9me3, or IgG antibodies and performed qPCRs from two independent sets of chromatin immunoprecipitation analysis. Immunoprecipitation with IgG was used as a negative control (Figure 13A, and 13D fourth lane from the top). To access the recruitment of both activation and repression marks on the promoter region of PfTOPOVIB (Figure 13A, first lane from the top) and PfSPO11 (Figure 13D, first lane from the top), inputs samples were normalized for each stage of the parasite. We found that the recruitment of H3K4me3 within the promoter-proximal regions of PfTOPOVIB (Figures 13A, second lane from the top) and that of PfSPO11 (Figure 13D, second lane from the top) increases gradually from ES to LS. Quantitative PCR was done to observe a 6-fold (Figure 13B) and 2-fold (Figure 13E) enrichment within the promoter-proximal regions of PfTOPOVIB and PfSPO11-1 respectively at the LS stage compared to that of the MS stage. On the contrary, recruitment of H3K9me3 in PfTOPOVIB\_UAS (Figure 13A, third lane from the top) and in PfSPO11-1\_UAS (Figure 13D, third lane from the top) were found to decrease considerably from ES to the LS stage. Quantitative PCR analysis showed nearly 3-fold and 10-fold reduction in recruitment of H3K9me3 within the promoter-proximal regions of PfTOPOVIB (Figure 13C) and PfSPO11-1 (Figure 13F) respectively at the LS stage from that of MS stage. To ascertain the specificity of the recruitment of H3K4me3 or H3K9me3 at the promoter-proximal region of PfTOPOVIB/PfSPO11, we performed the ChIP experiment with probes located within the ends of the ORF of the genes (C-terminal end [CTE] probes). Quantitative PCR analysis was performed to calculate the % occupancy of both H3K4me3 and H3K9me3 on the CTE region with respect to the input. However, the levels of recruitment of H3K4me3 at the CTE regions of PfTOPOVIB or

*PfSPO11* were found to be constant, without significant changes throughout ES to at the LS stage (**Figure 13B and E respectively**). Likewise, the recruitment of H3K9me3 remained unaffected at the CTE region of *PfTOPOVIB* or *PfSPO11* at different stages of schizont (**Figure 13C and F respectively**). Collectively, we conclude that the promoter-proximal sequences of *PfTOPOVIB* persist in a hetero-chromatinized condition during the ES/MS stage and undergo active transcription only at the LS stage. In case of *PfSPO11-1\_UAS*, we observe that the promoter-proximal region shows some activity in the Mid-Schizont stage and shows prominent activity in the Late-Schizont stage.

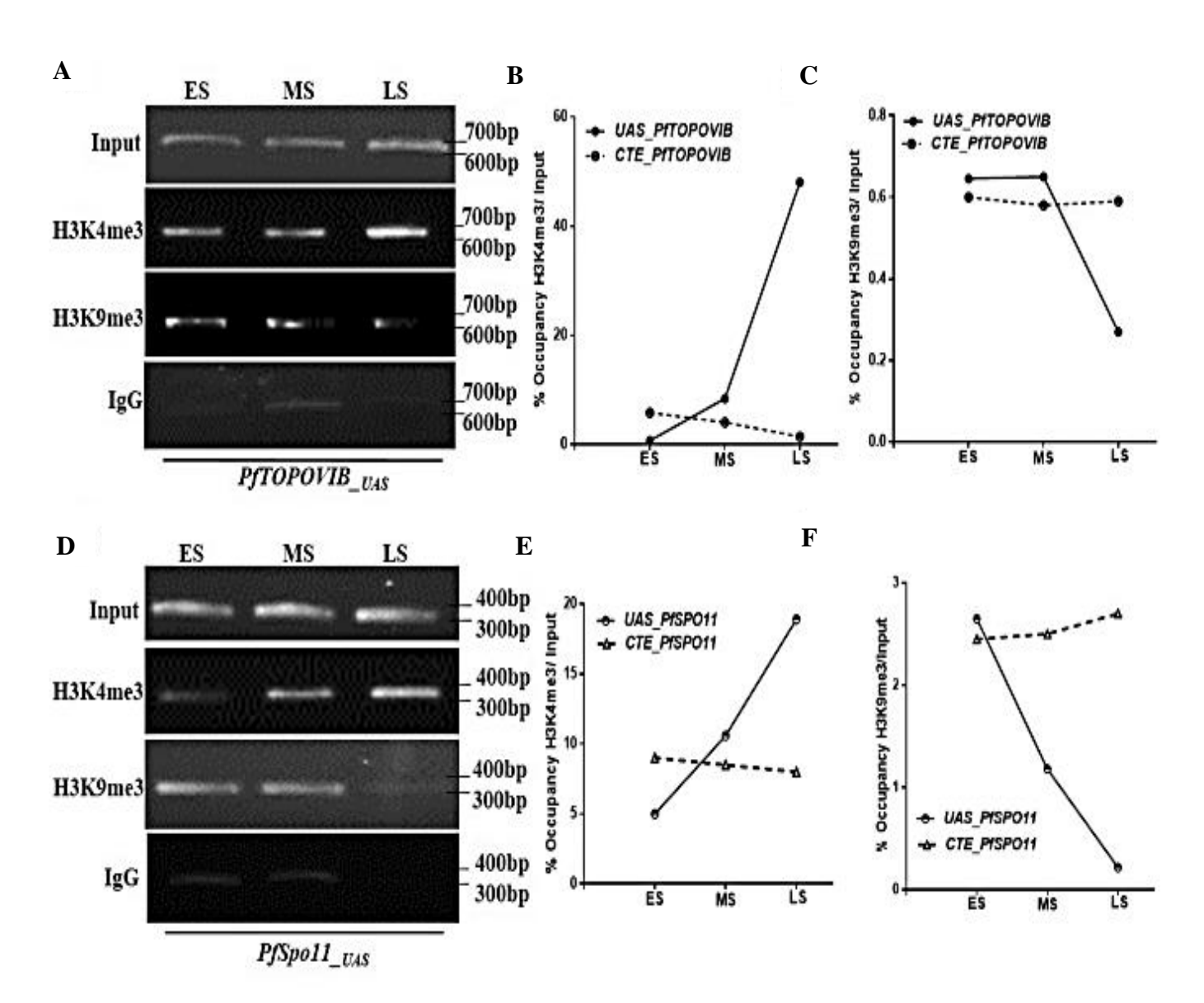
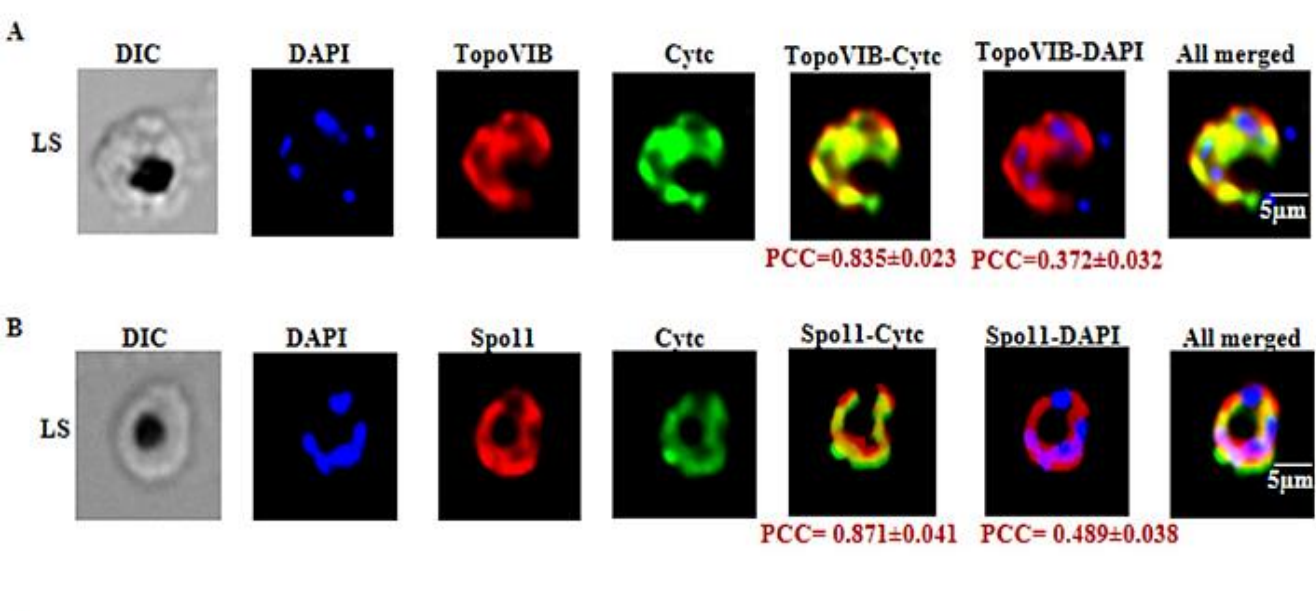


Figure 13: Stage-specific promoter activity of PfTopoVI subunits (A) ChIP assays were conducted on ES, MS, and LS stage parasites using histone mark antibodies, namely: anti-H3K4me3 and anti-H3K9me3 to investigate their occupancy at the PfTOPOVIB\_UAS. Immunoprecipitation with IgG antibody was used as a negative control. (B) Quantitative PCR (qPCR) analysis was performed on two independent sets of ChIP assays performed, and the mean values (±) standard deviation (SD) were plotted. The recruitment of H3K4me3 to PfTOPOVIB\_UAS increased by 6-fold at the LS stage compared to the MS stage, while negligible recruitment of H3K4me3 was observed at CTE\_PfTOPOVIB during the same stage. (C) The recruitment of H3K9me3 to PfTOPOVIB\_UAS decreased by 2-fold at the LS stage compared to the MS stage, whereas the recruitment at CTE\_PfTOPOVIB remained unchanged across the different stages. (D) ChIP assays were performed on ES, MS, and LS stage-specific parasites using anti-H3K4me3/anti-H3K9me3-specific antibodies to examine their binding patterns at the PfSPO11\_UAS. IgG was used as a negative control. (E) qPCR analysis was conducted on two independent sets of ChIP assays, and the mean values  $(\pm)$  standard deviation (SD) were plotted. The recruitment of the activation mark to PfSPO11\_UAS increased by 2-fold at the LS stage compared to the MS stage, while the recruitment at CTE\_PfSPO11 remained unchanged during the different stages. (F) The association of the repressor histone mark exhibited a decreasing trend at PfSPO11\_UAS and was observed almost negligible at the Late-Schizont stage of the parasite culture. However, the repressor mark remained consistently bound at CTE\_PfSPO11 during all schizont stages.

3.3. Whether PfSpo11 and PfTopoVIB constitute the functional holoenzyme within the parasite

We established the expression of individual PfTopoVI subunits within the parasite in the late Schizont stage of the parasite. To determine their subcellular localisation, we harvested LS stage-specific parasites and performed indirect immunofluorescence to visualize PfTopoVIB and PfSpo11 as red fluorescence, as shown in (Figure 11C and D), respectively. We used anti-Cytc antibody to visualize the green fluorescence of mitochondrial protein Cytc. We conclude that there was colocalization of PfTopoVI subunits inside the mitochondria due to overlapping between the red fluorescence of PfTopoVIB/PfSpo11 and green fluorescence of Cyt c, resulting a merged fluorescence of yellow colour. We determined the average Pearson Correlation Coefficient (PCC) for 20-25 images to evaluate whether red-signals specific to PfTopoVIB or PfSpo11 colocalise with the green fluorescence of Cytc. We also calculated the average Pearson Correlation Coefficient (PCC) to evaluate the localisation of PfTopoVIB or PfSpo11 with the nuclear stain DAPI (Figure 14A and B). We observed an average Pearson Correlation Coefficient, PCC=0.835+0.023 for colocalization of PfTopoVIB with Cytc and PCC=0.372±0.032 for colocalization of PfTopoVIB with DAPI. Similarly, we observed an average Pearson Correlation Coefficient, PCC=0.871+0.041 for the colocalization of PfSpo11 with Cytc and PCC=0.489+0.038 for colocalization of PfSpo11 with DAPI. We infer that both the subunits of TopoVI predominantly exist in the mitochondria of the malaria parasite with a stronger correlation with Cytc (PCC > 0.8) and moderate correlation with DAPI (PCC < 0.5). To establish that PfSpo11 and PfTopoVIB forms a holoenzyme complex inside malaria parasite, we verified the physical association between PfTopoVIB and PfSpo11 within the malaria parasite by employing co-immunoprecipitation assay. The LS stage parasites were immunoprecipitated by using PfSpo11 specific antibody as mentioned in the earlier section (Figure 14C, middle lane) and the pellet fraction achieved was probed with PfTopoVIB antibody. We discovered that PfTopoVIB was co-precipitated with PfSpo11, thus establishing a physical association between the two subunits (Figure 14C, first lane from the top). Immunoprecipitation

with Immunoglobulin G antibody was used as a negative control, and we did not detect any PfTopoVIB protein in the IgG pull-down pellet fraction (**Figure 14C, third lane from the top**).



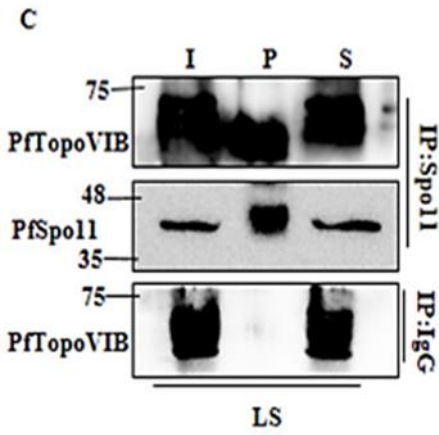


Figure 14: PfTopoVIB and PfSpo11 form the functional holoenzyme in the parasite. (A and B) Indirect immunofluorescence analysis was conducted on LS stage-specific parasites to visualize the localization of PfTopoVIB (red) and PfSpo11 (red) within the parasite nucleus and mitochondria. The average Pearson's correlation coefficient (PCC) values (mean  $(\pm)$  standard error of the mean [SEM], n=25) were calculated to assess the relationship between PfTopoVIB and PfSpo11 fluorescence signals with the nuclear stain DAPI (blue) and Cytc (green). The results showed a moderate correlation (PCC < 0.5) between PfTopoVIB and PfSpo11 fluorescence with DAPI, while a strong correlation (PCC > 0.8) was observed with the mitochondrial marker Cytc. (C) Western blot analysis was performed to examine the coimmunoprecipitation of PfTopoVIB by PfSpo11 in synchronized LS stage parasite lysates. Immunoprecipitation was carried out using anti-PfSpo11 and IgG antibodies. The input fraction (I), immunoprecipitation pellet fraction (P), and supernatant (S) were analysed to detect the presence of PfTopoVIB.

### 3.4. Whether PfTopoVI is a mitochondrial topoisomerase of the malaria parasite

3.4.1. PfTopoVIB and PfSpo11 both associate with the mitochondrial DNA of the malaria parasite. To establish the possible function of PfTopoVI in the segregation of mitochondrial genome, we performed chromatin immunoprecipitation (ChIP) assay to monitor the recruitment of PfTopoVIB and PfSpo11 to the mitochondrial genome in the presence or absence of formaldehyde cross-linking. We found specific binding of PfTopoVIB (Figure 15A, second lane from the top) and PfSpo11 (Figure 15B, second lane from the top) to the mt-genome at the LS-stage specific parasites and found that the mtDNA was only amplified in the sample where formaldehyde was added. Rabbit immunoglobulin G, acted as a negative control in our ChIP experiment (Figure 15A and B, third lane from the top). The IgG values were subtracted from the ChIP recruitment value before plotting. We also monitored the recruitment at synchronous ES, MS and LS stage specific parasites and quantified the percent occupancy of PfTopoVIB to mitochondrial DNA with respect to the input by employing quantitative PCR (qPCR). We observed that PfTopoVIB recruitment to the mt-DNA is positively correlated with its expression and is significantly enriched at the LS stage of the parasites compared to the other stages (Figure 15C). Similarly, the qPCR showed that the percentage of occupancy of PfSpo11 in mtDNA was highest in the LS stage-specific parasites (Figure 15D). To further evaluate whether the recruitment of the PfTopoVI enzyme is specific to the mitochondrial genome or not, we observed the association of both the subunits across the apicoplast genome of the malaria parasite by using two primer sets, P1 and P2, which cover 214 bp and 310 bp, respectively, as presented in (Figure 15E). In the LS stage specific PfTopoVIB and PfSpo11 immunoprecipitated samples, we did not find any occupancy in the apicoplast genome (Figure 15F and G). Together, our data suggest that PfTopoVI may have a role in mitochondrial genome segregation during the late schizont stage of the parasite.

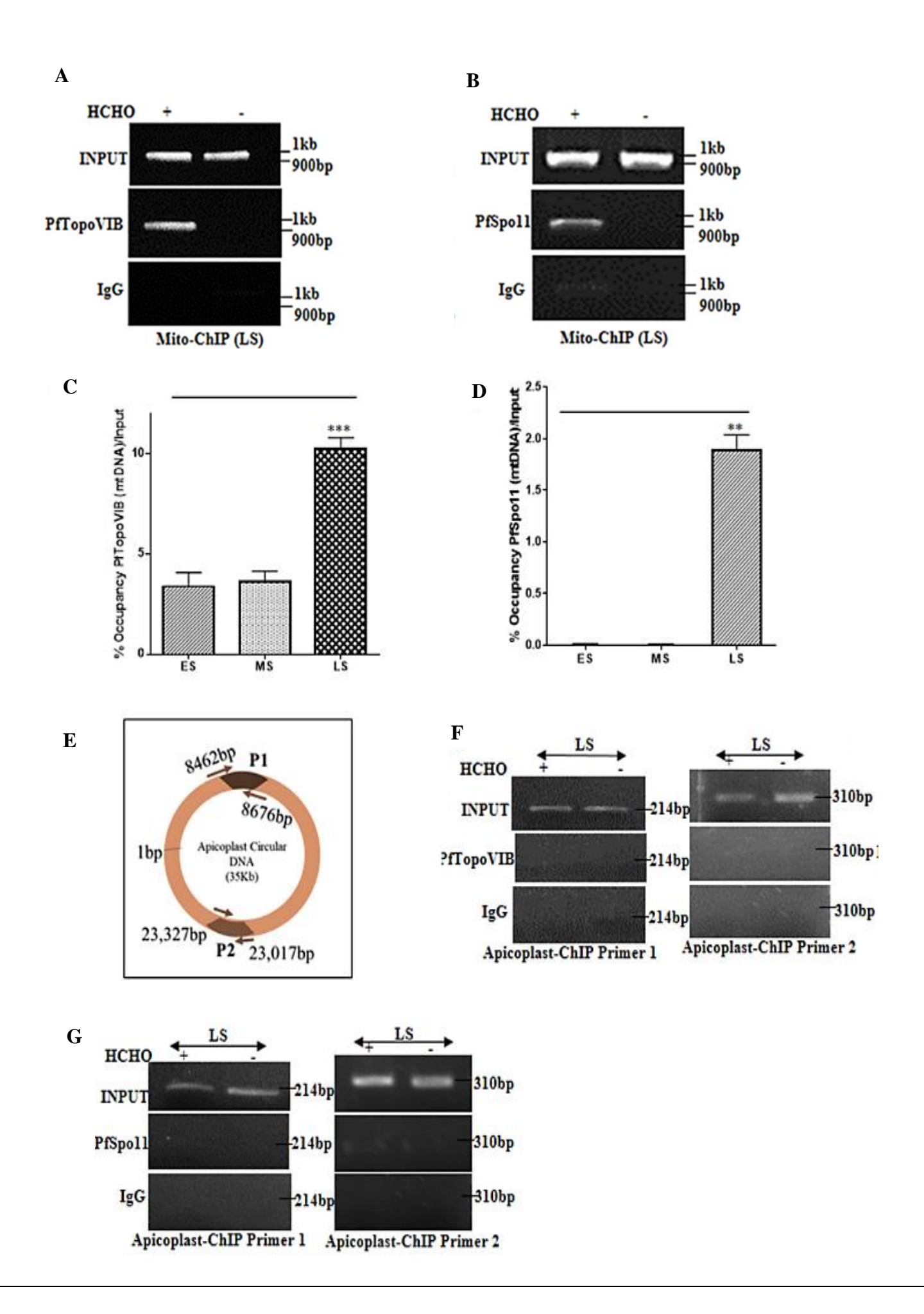
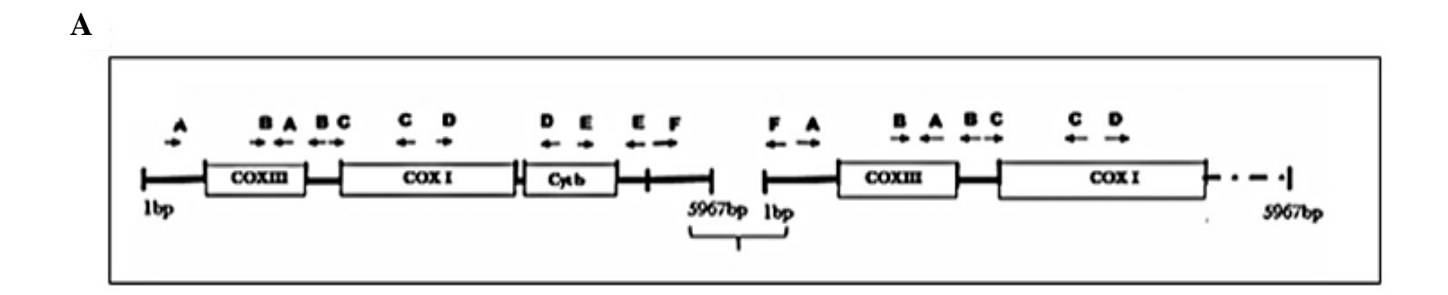


Figure 15: PfTopoVIB and PfSpo11 are recruited specifically to the mitochondrial genome but not to the apicoplast genome. (A) The recruitment of PfTopoVIB to the mitochondrial genome during the LS stage was examined using chromatin immunoprecipitation (ChIP). Negative control samples, treated without formaldehyde, were utilized to validate the specificity of recruitment. (B) Chromatin immunoprecipitation (ChIP) was performed to investigate the recruitment of PfSpo11 to the mitochondrial genome during the LS stage. Negative control samples, untreated with formaldehyde, were included to confirm specific recruitment. (C and D) The occupancy of PfTopoVIB and PfSpo11 on the mitochondrial genome was quantified by qPCR and presented graphically. The analysis was conducted on parasites at different developmental stages: ES (35 to 36 hpi), MS (39 to 40 hpi), and LS (44 to 45 hpi). The experiment was replicated with three independent batches of parasites, and the mean values (±) standard deviation (SD) were plotted. Statistical significance was determined using a two-tailed Student's t-test (\*\*\*, P < 0.001; \*\*, P < 0.01; N.S., not significant). The data were normalized to the respective IgG immunoprecipitation (IP) values. (D) Schematic representation of the primer positions (P1 and P2) used in the apicoplast ChIP assay, covering regions of 214 bp and 310 bp, respectively, in the apicoplast genome. (E) ChIP analysis was performed to examine the recruitment of PfTopoVIB to the apicoplast genome (P1 and P2) during the LS stage. The results indicated no significant recruitment of PfTopoVIB to the apicoplast genome. (F) ChIP analysis was conducted to investigate the recruitment of PfSpo11 to the apicoplast genome (P1 and P2) during the LS stage. The results revealed no significant recruitment of PfSpo11 to the apicoplast genome

### 3.4.2. PfTopoVI recruits uniformly throughout the mt-genome of Plasmodium falciparum

To evaluate the specificity of the recruitment towards any specific parts of mt-DNA, we used a set of six primers (A to F), each amplifying around 1 kb long mt-genome, thereby, covering the whole 6 kb of the mitochondrial genome. While A to E primer sets were used to amplify the intra-mitochondrial DNA, the F primer amplifies the junctional sequence and produces amplicon when two monomeric mt-DNA units form concatemers (**Figure 16A**). The quantitative PCR analysis was performed to calculate % occupancy of PfTopoVIB and PfSpo11 on mtDNA with respect to input. Our data showed no significant difference towards the occupancy of PfTopoVIB and PfSpo11 to any specific regions mt-genome (**Figure 16B and C**).



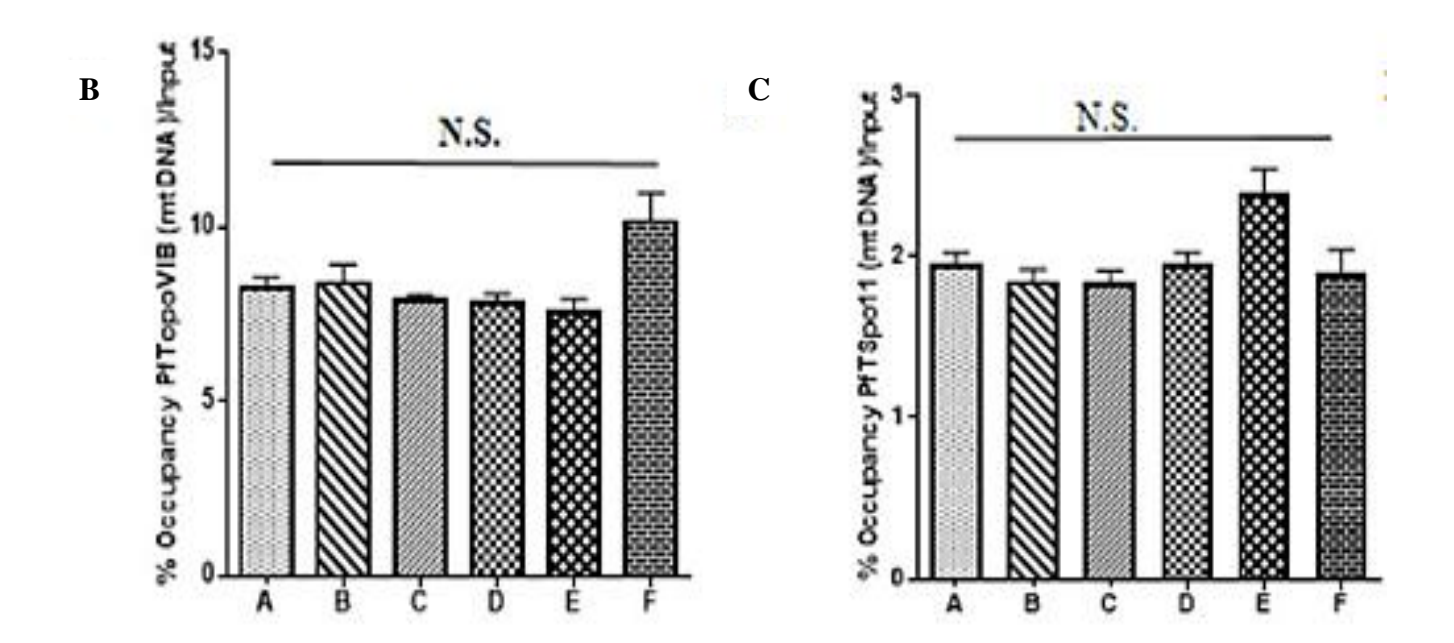


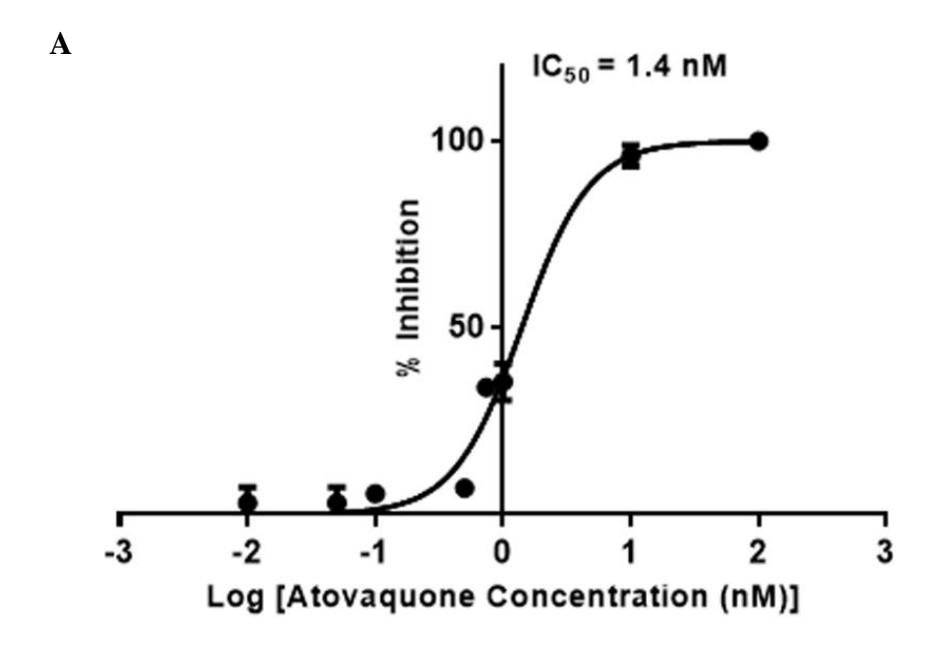
Figure 16: PfTopoVIB and PfSpo11 are evenly distributed to the mitochondrial genome. (A) A schematic representation is provided to illustrate the primer positions used in the chromatin immunoprecipitation (ChIP) assay. These primers, designated as A to F, were designed to target specific 1-kilobase regions within the mitochondrial genome. (B) The occupancy of PfTopoVIB at different segments (A to F) of the mitochondrial genome was assessed during the late schizont (LS) stage. The results indicated a consistent percentage of occupancy for PfTopoVIB across all the segments examined. (C) Similarly, the occupancy of PfSpo11 at various segments (A to F) of the mitochondrial genome was examined during the LS stage. The findings revealed a consistent percentage of occupancy for PfSpo11 across all the segments analysed. The relative occupancy was quantified using quantitative polymerase chain reaction (qPCR), and the mean values (±) standard deviation (SD) were plotted. Statistical significance was determined using a two-tailed Student's t-test, and non-significant results were indicated as "N.S." The data were normalized to the corresponding IgG immunoprecipitation (IP) values.

### 3.4.3. PfTopoVIB inhibitor Radicicol and Atovaquone potentiate each other

It is established that Atovaquone collapses the mitochondrial membrane potential of the parasite. We hypothesised that treatment of Atovaquone would reduce the import of PfTopoVI subunits into the mitochondria. On the other hand, because PfTopoVI is crucial in maintaining the mitochondrial genome, inhibition of this enzyme complex with Radicicol, should affect the mitochondrial genome replication. Indeed, our earlier experimental data showed that Radicicol treatment reduces the mitochondrial genome content of the parasite significantly, without having any effect on nuclear and/or Apicoplast genome content (59). Thus, we hypothesise that Atovaquone and Radicicol should potentiate one another's effects. To prove that, first we determined the IC<sub>50</sub> values for Atovaquone and Radicicol to 3D7 parasite and determined that to be 1.4 nM and 8.05 μM respectively (**Table 1**, **Figure 17A and B**). We noticed that there is a substantial decrease in the IC<sub>50</sub> of Atovaquone from 1.4 nM to 0.12 nM when identical experiment was carried out in the presence of IC<sub>50</sub> concentration of Radicicol (8.05 μM) (**Table 3**). Radicicol offered Atovaquone an 11.7-fold potentiation (**Table 1**). Similarly, we found that the Atovaquone potentiated the action of Radicicol and shifted the IC<sub>50</sub> concentration of Radicicol from 8.05 μM to 1.7μM, thus potentiating Radicicol by 4.7-fold (**Table 1**).

### 3.4.4. The PfTopoVIB inhibitor Radicicol interacts with Atovaquone in a synergistic manner

We further investigated whether the interaction between the PfTopoVI inhibitor Radicicol and the Atovaquone is additive or synergistic. We determined the fractional inhibitory concentration (FIC) by running a fixed ratio drug combination experiment and plotting the dose-response curves. The dose-response curves for each drug combination were plotted (data not shown), and the fractional inhibitory concentration (FIC) was calculated. The sum of the FIC values were then determined (Table 2). These values were used to construct an isobologram (Figure 18A).



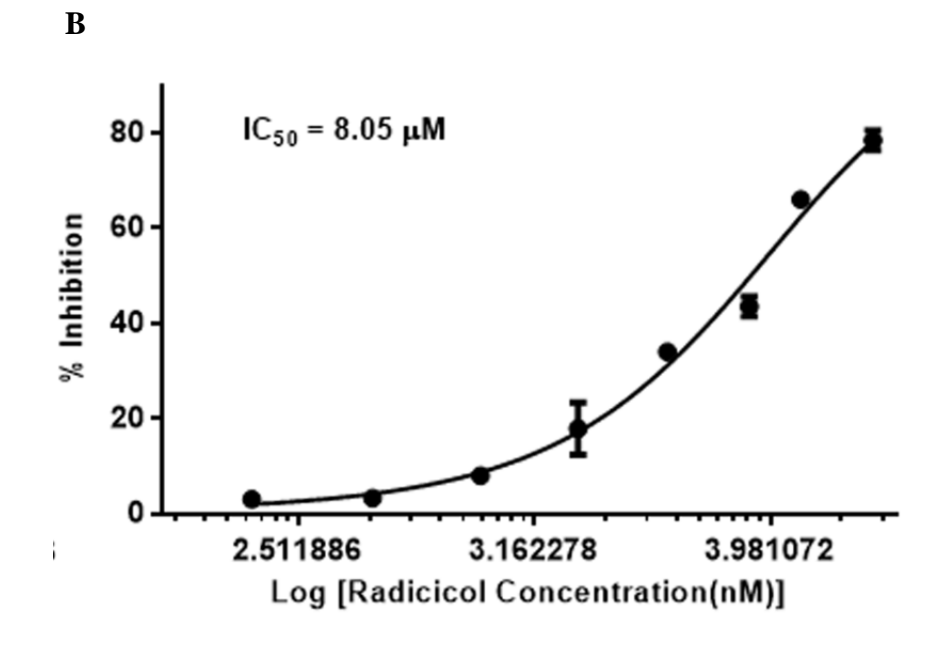


Figure 17: IC<sub>50</sub> determination of Atovaquone and Radicicol in 3D7 parasite. A) Tightly synchronized trophozoite stage (3D7) specific parasites were grown in the presence of different concentration (0.01 nM, 0.05 nM, 0.1 nM, 0.5 nM, 0.75 nM, 1 nM, 10 nM, and 100 nM) of Atovaquone for 48h and the parasitemia was determined by SYBR green-I based fluorescent measurement. Percent inhibition of the parasite growth was plotted for all the drug concentrations to obtain the IC<sub>50</sub> value of the drug. B) Tightly synchronized mid-Schizont stage (3D7) parasites were grown in presence of different concentration of (0.25  $\mu$ M, 0.5  $\mu$ M,1  $\mu$ M, 2  $\mu$ M, 8  $\mu$ M, 12  $\mu$ M, 25  $\mu$ M) Radicicol for 48h and parasitemia was determined by SYBR green-I based fluorescent measurement. Percent inhibition of the parasite growth was plotted for all the drug concentrations to obtain the IC<sub>50</sub> value of the drug. Each experiment was repeated three times and mean ( $\pm$ SD) was plotted.

TABLE 1. Representing the  $IC_{50}$  values of Radicicol and Atovaquone in combination and *vice versa* in strain 3D7

Drug or drug combination	IC <sub>50</sub>	Potentiation factor
Radicicol alone	8 μM	1
Radicicol $+$ atovaquone <sup>a</sup>	1.7 $\mu$ M	4.7
Atovaquone alone	1.4 nM	1
Atovaquone + radicicol <sup>b</sup>	0.12 nM	11.67

 $<sup>^{\</sup>alpha} The \, IC_{50}$  of atova quone in strain 3D7 was used.

TABLE 2. Representing the FIC values for the combinations of Atovaquone and Radicicol/Radicicol and Chloroquine in 3D7 strain

	FIC of:		
Drug ratio	Atovaquone or radicicol	Radicicol or chloroquine	ΣFIC
Atovaquone/radicicol	Atovaquone	Radicicol	
5:0	1	0	1
4:1	0.41	0.106	0.5
3:2	0.425	0.291	0.716
2:3	0.29	0.460	0.75
1:4	0.175	0.724	0.899
0:5	0	1	1
Radicicol/chloroquine	Radicicol	Chloroquine	
5:0	1	0	1
4:1	0.702	0.347	1.049
3:2	0.38	0.497	0.877
2:3	0.33	0.967	1.297
1:4	0.11	0.877	0.987
0:5	0	1	1

<sup>&</sup>lt;sup>b</sup>The IC<sub>so</sub> of radicicol in strain 3D7 was used.

The isobologram demonstrated that the sum of FIC values (ΣFIC) was less than 1 for all combinations of Radicicol and Atovaquone (5:0, 4:1, 3:2, 2:3, 1:4, and 0:5), indicating a synergistic interaction between the two drugs. To assess the specificity of the Radicicol-Atovaquone interaction, we also examined the interaction between Radicicol and an unrelated drug, Chloroquine. The Isobologram analysis revealed an ΣFIC≥1 indicating additive interaction between Chloroquine and Radicicol (Figure 18B). Thus, the synergistic interaction between PfTopoVI inhibitor and Atovaquone, chemical that collapses mitochondrial membrane potential provides supporting evidence that PfTopoVI is a mitochondrial topoisomerase.

### 3.4.5. Atovaquone reduces mitochondrial import of PfTopoVIB and PfSpo11 in a dosedependent manner

To support our conclusion further, we wanted to determine whether Atovaquone treatment really affects the mitochondrial import of PfTopoVI. To accomplish this objective, a specific parasite culture at the synchronous mid-trophozoite stage was treated with increasing concentrations of Atovaquone. The treated parasites were allowed to progress until they reached the late-schizont stage (Figure 19A). Subsequently, the cultures were collected, and an immunofluorescence assay (IFA) was performed to assess the mitochondrial localizations of PfTopoVIB and PfSpo11. The results were compared with those of the untreated parasites. To ensure that the observed effects were not due to a reduction in the overall expression of Cytc or PfTopoVI caused by Atovaquone treatment, western blot analysis was conducted using a sublethal dose of Atovaquone (0.5 nM). The results were compared to those obtained from the atovaquone untreated sample (Figure 19B). The experiment was replicated with two separate batches of cells, and the band intensity of each PfTopoVI subunit and Cyt c in the western blots was quantified using ImageJ and plotted (Figure 19C). No significant differences in the expression of PfTopoVIB, PfSpo11, and PfCytc were observed under the treated condition. Subsequently, an Immunofluorescence assay was conducted to investigate the effect of Atovaquone on the localization of PfTopoVIB and PfSpo11 within the mitochondria of the malaria

parasite. Late-schizont stage specific parasites treated with Atovaquone were subjected to immunofluorescence analysis, using the same methodology as described earlier. To visualize the red fluorescence associated with PfTopoVIB and PfSpo11, Alexa Red 594-conjugated secondary antibody was employed. The green fluorescence of the mitochondrial protein Cytc was visualized using an anti-cytochrome c (anti-Cytc) antibody, with the secondary antibody conjugated with Alexa Fluorophore 488. To evaluate the extent of colocalization, the average Pearson's correlation coefficient (PCC) values were calculated from 25 individual cells treated with 0.5 nM Atovaquone and compared with those of the untreated parasites. The results showed a significant decrease in colocalization between the subunits of PfTopoVI and Cyt c in the Atovaquone-treated parasites. Specifically, the average PCC values were shifted from 0.835 to 0.66 for PfTopoVIB (Figure 19D), and from 0.871 to 0.69 for PfSpo11 (Figure 19E). These findings indicate a notable reduction in the degree of colocalization between PfTopoVI subunits and Cyt c in the Atovaquone-treated parasites.

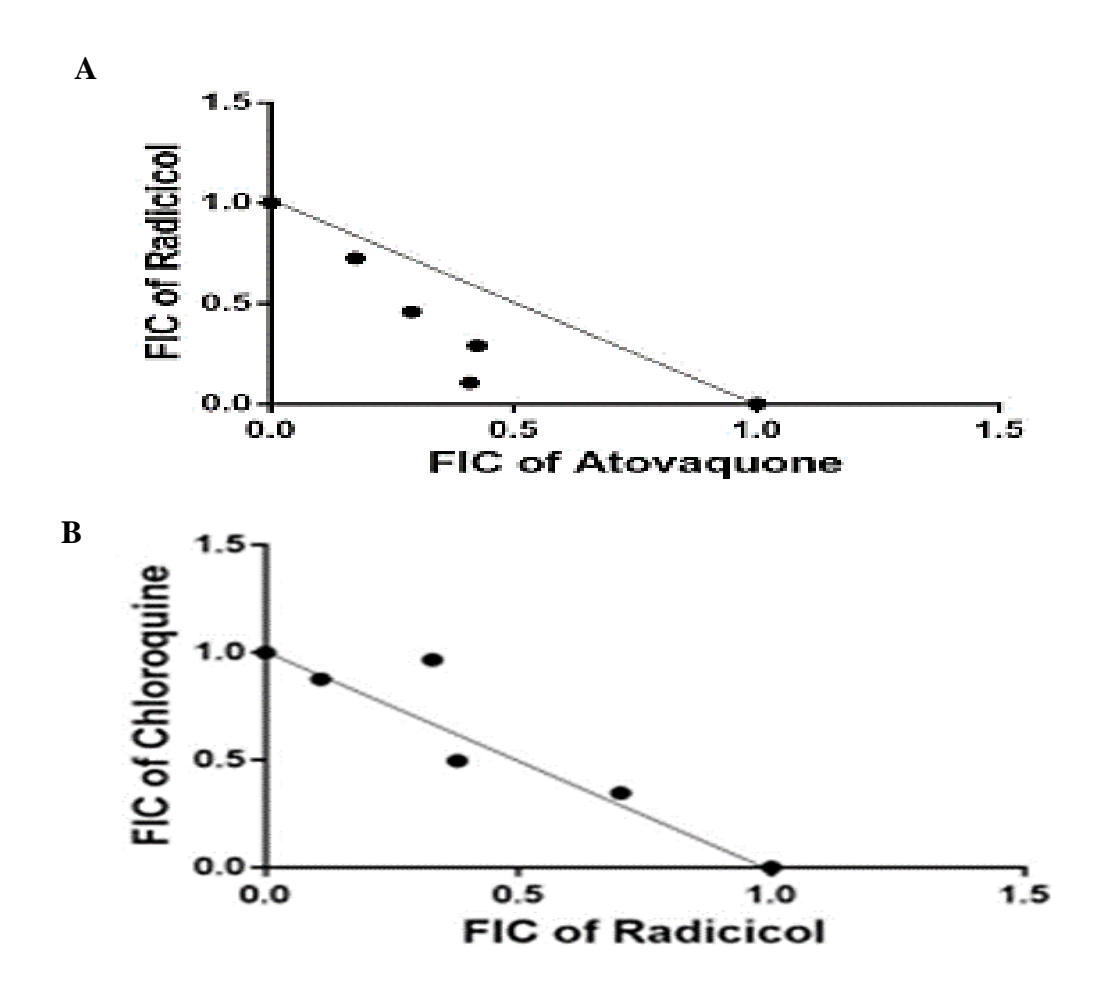


Figure 18. PfTopoVIB inhibitor Radicicol and Atovaquone show synergism with each other. (A) The combined effect of the PfTopoVIB inhibitor radicicol and atovaquone was evaluated by plotting an isobologram to assess their interaction in the 3D7 strain of the parasite. The isobologram displayed data points representing the average half-maximal inhibitory concentration ( $IC_{50}$ ) of the drug combination, obtained from three independent experiments. A solid line was drawn connecting the  $IC_{50}$  values of radicicol and atovaquone when used individually. The fractional inhibitory concentration (FIC) was calculated to determine the level of synergy between the two drugs. (B) Similarly, an isobologram was constructed to analyse the interaction between radicicol and chloroquine in the 3D7 strain. Each data point on the isobologram represented the average  $IC_{50}$  value of the drug combination, derived from two independent experiments. A solid line connected the  $IC_{50}$  values of radicicol and chloroquine when administered alone.

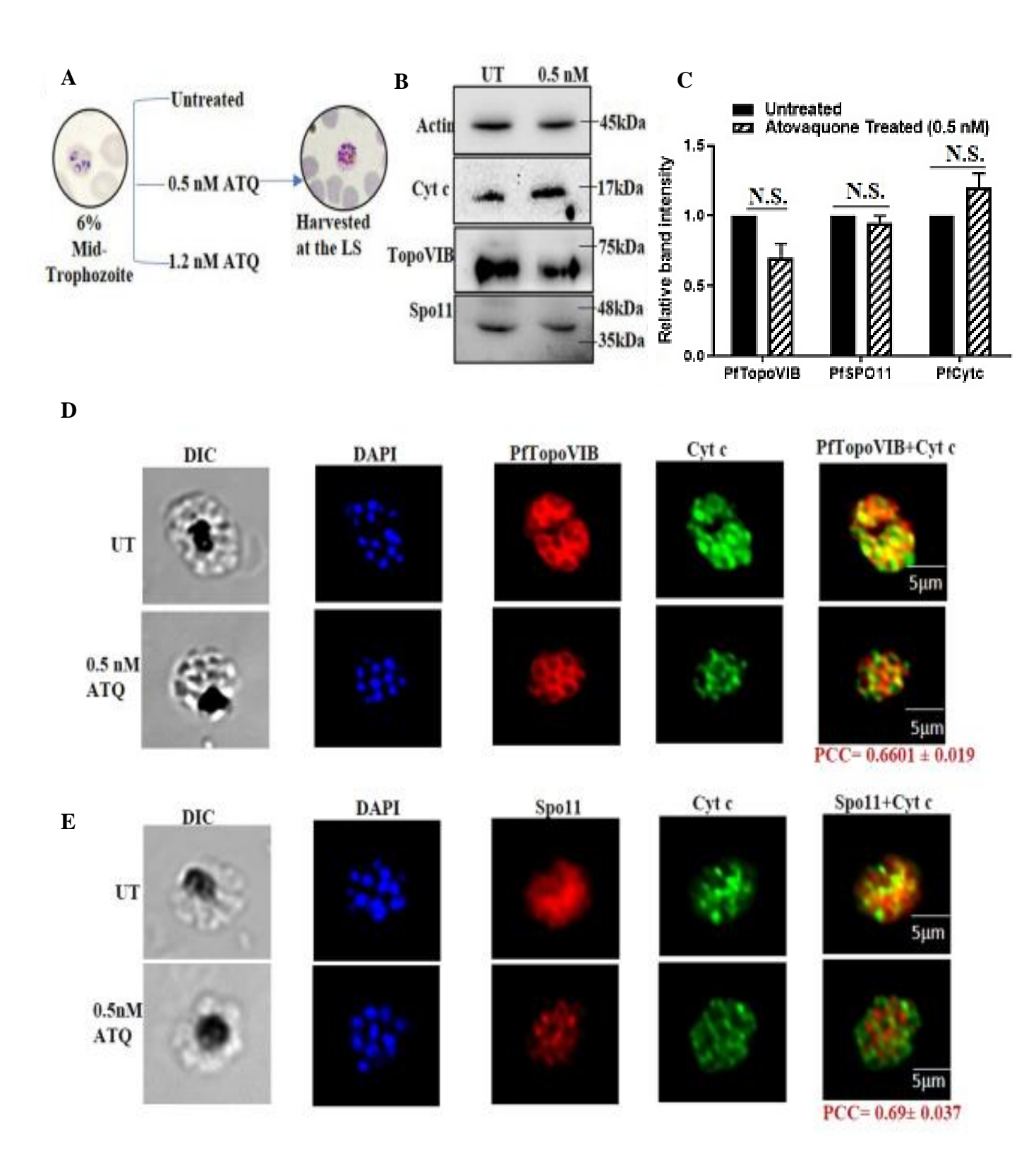


Figure 19. Atovaquone reduces mitochondrial import of PfTopoVIB and PfSpo11 in a dosedependent manner. (A) The experimental setup involved dividing synchronized mid-trophozoitespecific parasite cultures (6% parasitaemia) into three groups: one un-treated control parasites and two groups treated with different concentrations of Atovaquone. Subsequently, the parasites were harvested at the late schizont (LS) stage (44 to 45 hours post-invasion) after the treatment with atovaquone. Parasites treated with 0.5 nM Atovaquone underwent immunofluorescence assay (IFA), while the ChIP assay was performed on parasites treated with 0.5 and 1.2 nM Atovaquone, as well as the untreated control. (B) Western blot analysis was conducted to evaluate the endogenous levels of PfSpo11, PfTopoVIB, and PfCytc in the Atovaquone-treated culture compared to the untreated condition. The results indicated no significant difference in the protein expression levels. (C) The intensities of the Western blot bands corresponding to PfTopoVIB, PfSpo11, and PfCytc were quantified using ImageJ software. The graph represents the relative band intensities obtained from two independent protein preparations. (D and E) The immunofluorescence assay demonstrated a significant reduction in the colocalization (depicted as yellow colour) of Cytc (green) with PfTopoVIB and PfSpo11 (red) in the parasites treated with 0.5 nM Atovaquone compared to the untreated parasites. The Pearson correlation coefficient (PCC) values were determined from 25 individual cells in each IFA, and the average value is displayed at the bottom of the merged image.

### 3.4.6. Atovaquone reduces mtDNA recruitment of PfTopoVIB and PfSpo11 in a dose-dependent manner

To further confirm our findings, we examined the recruitment of these two subunits to the mitochondrial genome in the presence of Atovaquone. We conducted a Chromatin Immunoprecipitation (ChIP) assay using a PfTopoVIB antibody, and the assay was performed with increasing concentrations of Atovaquone at 0.5 nM and 1.2 nM. To ensure accuracy, we normalized the input sample for both the Atovaquone-treated and untreated samples (Figure 20A & C, first lane from the top). Immuno-precipitation with Rabbit immunoglobulin G, acted as a negative control in our ChIP experiment (Figure 20A & C, third lane from the top). A gradual decrease in the recruitment of PfTopoVIB to the mitochondrial genome was observed (Figure 20A, second lane from the top). To quantify the occupancy of PfTopoVIB in relation to the input DNA, real-time qPCR analysis was conducted, with IgG values subtracted in each case (Figure 20B). In the presence of sublethal doses (0.5 nM) of Atovaquone, there was an approximately 30% reduction in the occupancy of PfTopoVIB on the mitochondrial genome, and this reduction became more prominent at higher concentrations of Atovaquone. Similarly, the recruitment of PfSpo11 to the mitochondrial genome was examined at the two above mentioned doses of Atovaquone. A similar trend was observed in the association of PfSpo11 to the mitochondrial genome (Figure 20C, second lane from the top), and real-time quantification analysis indicated a dose-dependent decrease in the recruitment of PfSpo11 to the mitochondrial genome (Figure 20D).

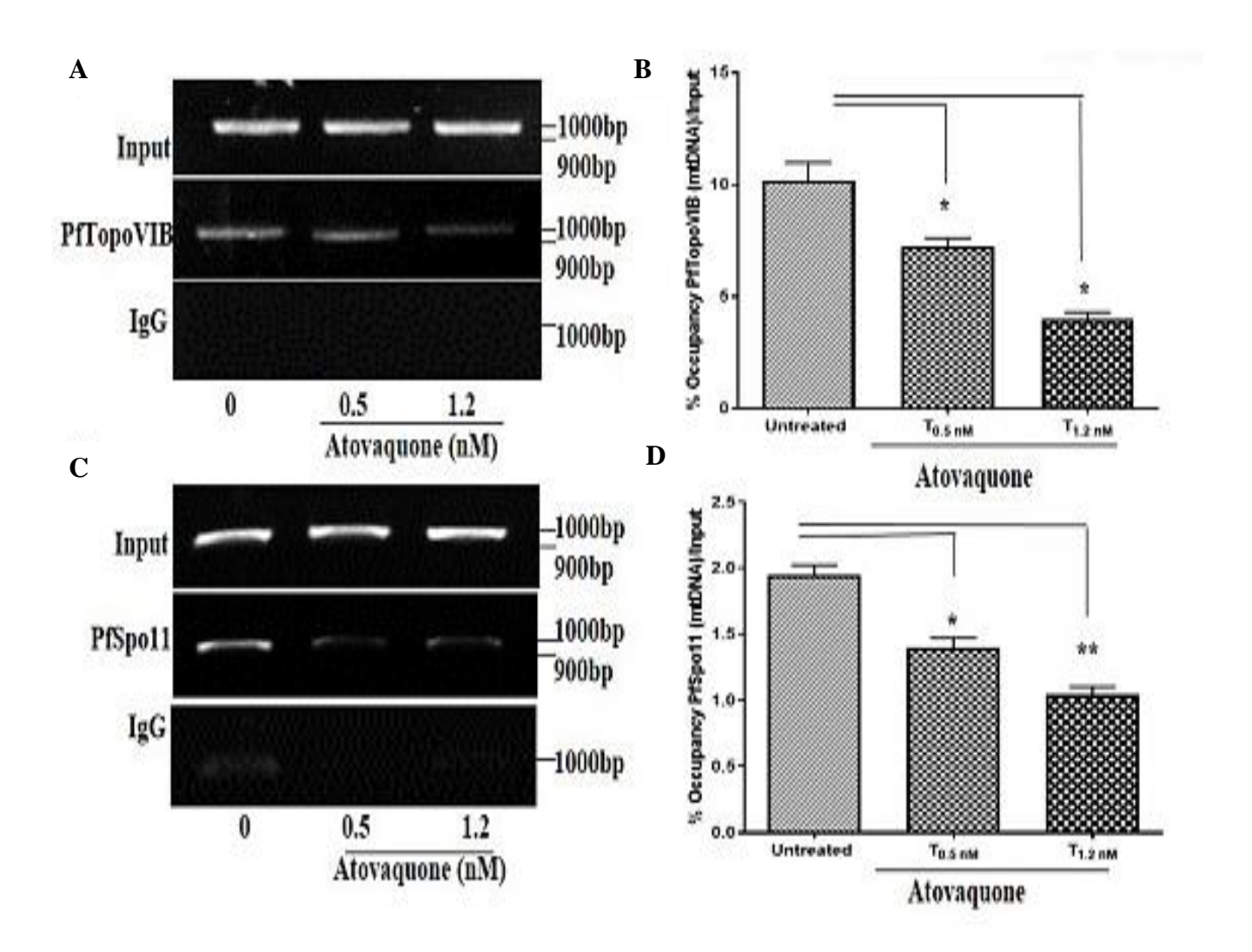


Figure 20. Atovaquone reduces mtDNA recruitment of PfTopoVIB and PfSpo11 in a dose-dependent manner. (A) The presence of Atovaquone resulted in a dose-dependent reduction in the recruitment of PfTopoVIB to the mitochondrial genome. (B) The level of PfTopoVIB recruitment on the mitochondrial genome was quantified through real-time PCR analysis in two independent experiments, and the findings were presented. (C) Similarly, the recruitment of PfSpo11 on the mitochondrial genome decreased with increasing concentrations of Atovaquone. (D) Real-time PCR analysis was conducted to measure the recruitment of PfSpo11 on the mitochondrial genome, using data from two independent experiments. The statistical significance was determined using a two-tailed Student's t-test (\*\*, P < 0.01; \*, P < 0.05; N.S., not significant).

# 3.5. Computational analysis predicts structural differences between PfTopoVIB and HsTopoVIBL

In human, Topoisomerase VIBL (VIB Like protein) has been identified. To explore potential structural similarities between *Plasmodium* TopoVIB and its orthologs in other species, we performed a multiple sequence alignment using ClustalV. Specifically, we focused on the Bergerat fold region of the protein. The aligned sequences include those from various species, namely S. shibatae (Ss) with accession number O05207, P. falciparum (Pf) with accession number Q8ID53, P. berghei (Pb) with accession number A0A509AMZ8, M. musculus (Mm) with accession number J3QMY9, and H. sapiens (Hs) with accession number Q8N6T0. The alignment results can be observed in (Figure 21). The Bergerat fold of *Plasmodium falciparum* TopoVIB spans from amino acids 22 to 166, which constitutes four core motifs, i.e., N-box, G1, G2 and G3 motifs. The N box within Sulfolobus shibatae and *Plasmodium* species shows conserved residues, but there is limited conservation between human/mouse and *Plasmodium* in the N, G1, and G2 motifs of the signature box, except for conserved glycines (**Figure 21**). However, the glycines in the third core motif i.e., G3 motif are not conserved. To assess the structural dissimilarities, the structures of PfTopoVIB and HsTopoVIBL were obtained from the Alpha Fold database (76), and structure alignment was performed using VMD (Visual Molecular Dynamics) (80) (Figure 22). The analysis indicated significant differences in the Bergerat fold between these two proteins. Specifically, the core motifs (N, G1, and G2) of the Bergerat fold did not align with the corresponding fold observed in the human VIBL protein, suggesting distinct spatial orientations of these core elements (Figure 22). Consequently, it can be inferred that there are likely notable variations in the catalytic activity between these two proteins.

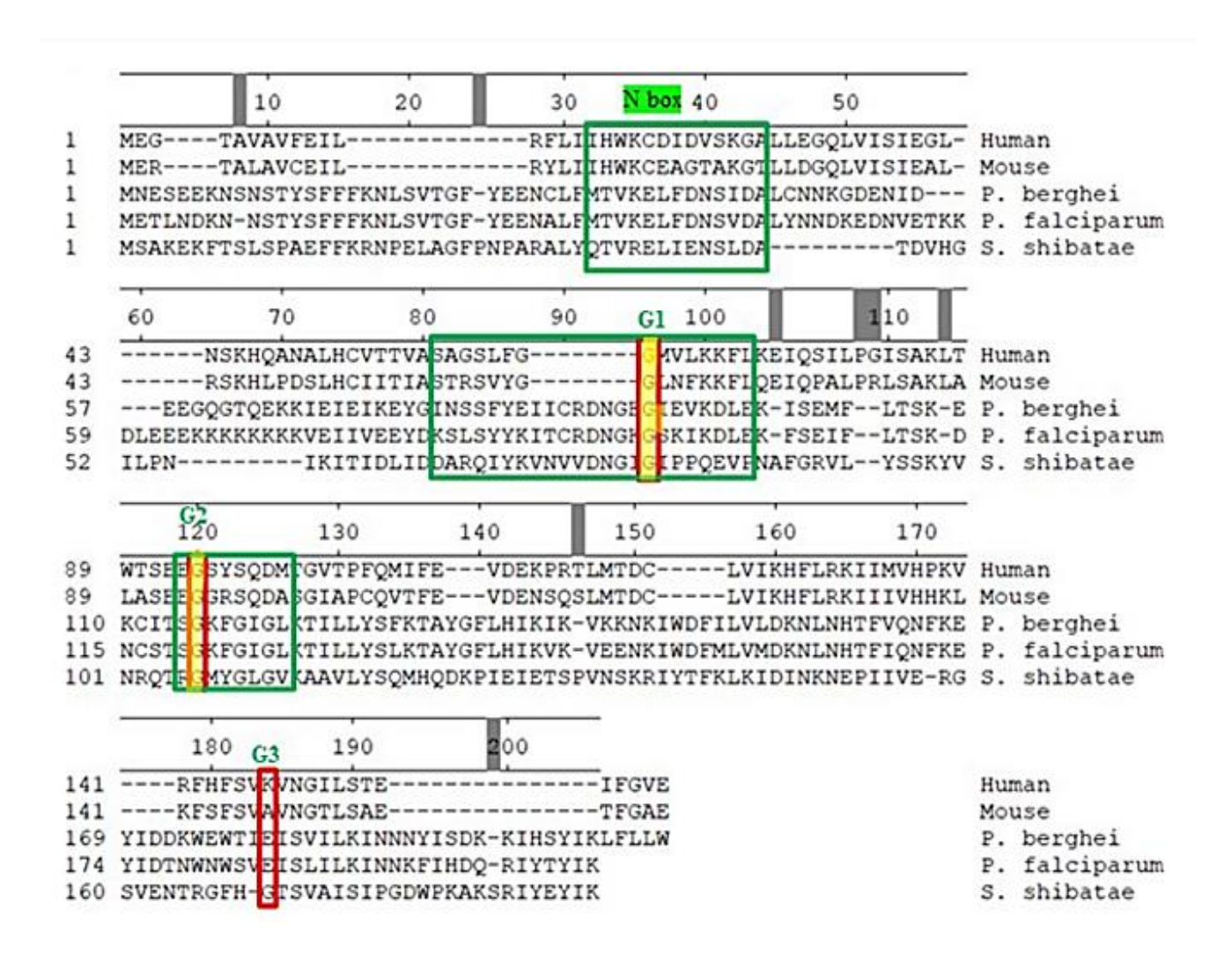
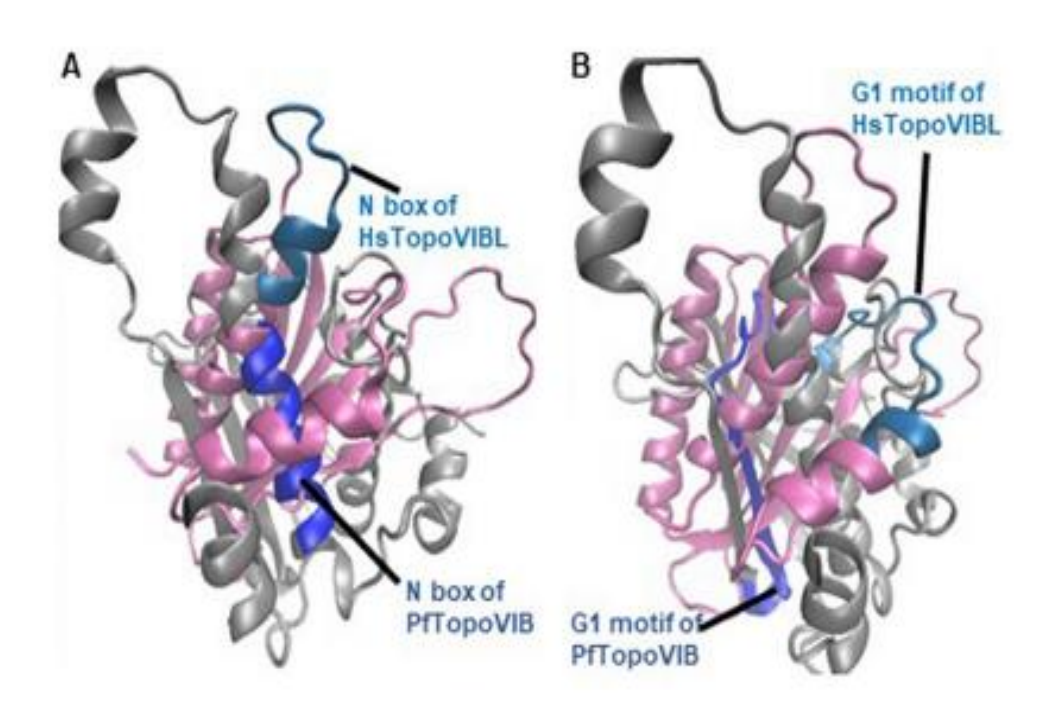


Figure 21. Multiple-sequence alignment of TopoVIB/TopoVIBL proteins from S. shibatae (Ss) O05207, P. falciparum (Pf) Q8ID53, P. berghei (Pb) A0A509AMZ8, M. musculus (Mm) J3QMY9, and H. sapiens (Hs)Q8N6T0, and their UniProt ID. The glycines conserved between the species are shown in red boxes, and the four core elements of the Bergerat fold are marked in green colour: N-box, G1, G2 and G3 motifs.



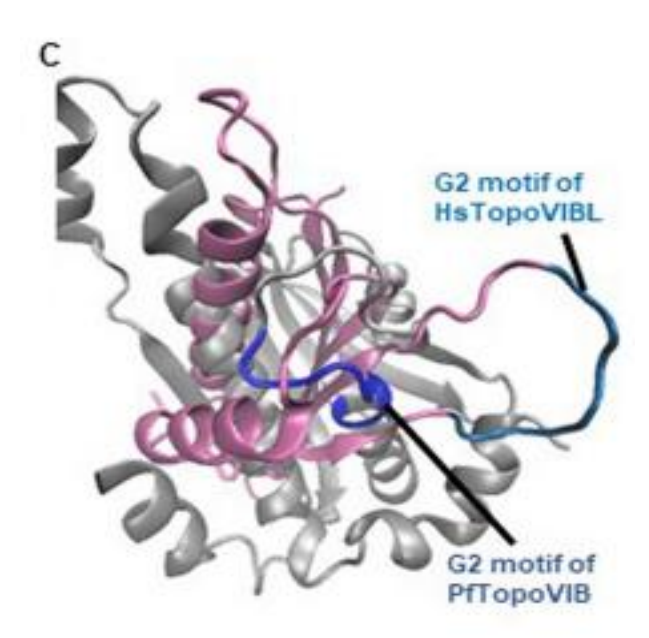


Figure 22. Structural alignment of the Bergerat fold region of PfTopoVIB and HsTopoVIBL from different angles. The key structural components of the Bergerat fold, represented by the blue elements, can be observed in the figure. The figure highlights the variation in the spatial orientation of these core elements. (A) N box; (B) G1 motif; (C) G2 motif.

#### **DISCUSSION**

*Plasmodium* is the parasite responsible for malaria, a prevalent and devastating disease. Our primary focus in this study was to investigate the role of Topoisomerase VI in mitochondrial maintenance of Plasmodium falciparum. Topoisomerase VI is a type IIB topoisomerase that regulates the topological state of DNA, influencing crucial processes such as DNA replication, transcription, and recombination. However, the specific mechanisms and functions of TopoVI in *Plasmodium*, particularly its involvement in mitochondrial DNA segregation, have yet to be fully elucidated. We employed a combination of cellular, biochemical, and genetic techniques to decipher the role of Plasmodium Topoisomerase VI. Earlier study has shown in plants and algae that this enzyme is composed of two subunits TOPOVIA (SPO11) and TOPOVIB. We have conclusively demonstrated through various independent approaches that the expression of PfTOPOVI in Plasmodium falciparum is tightly regulated. Specifically, both subunits of *PfTOPOVI* are specifically upregulated during the late schizont stage of the parasite, occurring at approximately 44 to 45 hours post-infection. This upregulation precedes the onset of mitochondrial genome segregation and strongly suggests that the main role of PfTopoVI is associated with genome segregation rather than genome replication. In contrast, we observed the presence of transcripts for other Type II topoisomerases such as *PfTOPOII*, PfGYRA, and PfGYRB in the early schizont (ES), mid-schizont (MS), and late schizont (LS) stages of the parasite. The detection of these transcripts during the LS stage indicates their potential involvement in various cellular processes. Alternatively, it is plausible that the transcripts of these topoisomerases exhibit greater stability with longer half-lives, allowing their detection even at the LS stage.

In our investigation, we have demonstrated the presence of a *Plasmodium* topoisomerase VI holoenzyme complex in the parasite lysate during the late schizont (LS) stage. Through various experimental approaches, we have established the physical interaction between the two subunits of

PfTopoVI (PfTopoVIB and PfSpo11) and confirmed the existence of the holoenzyme at the LS stage. Additionally, using fluorescence microscopy analysis, we have observed the localization of both subunits within the mitochondria of the parasite. This localization strongly supports the notion that topoisomerase VI functions as a mitochondrial topoisomerase in *Plasmodium*. Furthermore, our findings indicate that both subunits remain associated with the entire mitochondrial genome, which is consistent with their expression pattern. Moreover, we have discovered that the disruption of mitochondrial membrane potential by Atovaquone leads to the inhibition of mitochondrial import and the recruitment of PfTopoVI subunits to the mitochondria, and this inhibition is dose dependent. Notably, we have found that Atovaquone and the PfTopoVIB inhibitor Radicicol exhibit a synergistic interaction, enhancing each other's actions. Lastly, we have provided a summarized overview of our results in (Figure 23).

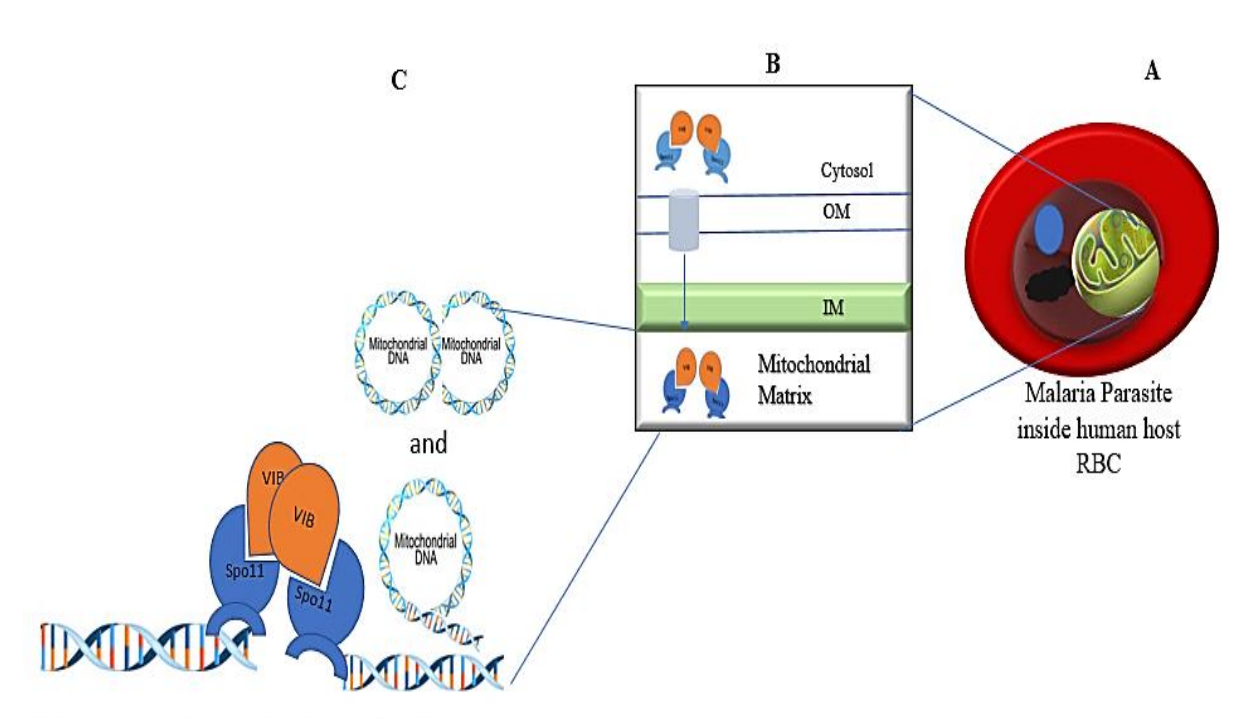
Earlier studies have put forth the hypothesis that the replication of the *Plasmodium* mitochondrion follows a rolling circle mechanism. During replication, homologous recombination occurs between circular and linear molecules, resulting in the formation of complex lariat-like structures. To ensure proper segregation of the replicated mitochondrial genome during endoreduplication, the involvement of a type II topoisomerase is necessary to decatenate the DNA. Previous reports have indicated that PfGyrase, a type II topoisomerase in the malaria parasite, is exclusively associated with the apicoplast genome and not found in mitochondria. Our findings align with this observation, as we have determined that PfTopoVI does not localize to the apicoplast genome. Based on these findings, we propose that PfTopoVI functions as a mitochondrial type II topoisomerase, specifically involved in the segregation of the mitochondrial genome.

The association of PfTopoVI subunits with the mitochondrial genome corresponds to their expression levels in the parasite. Inhibition of PfTopoVI is likely to impede the process of endoreduplication by interfering with the segregation of the mitochondrial genome.

This notion is supported by our previous observations, wherein the use of Radicicol, an inhibitor of PfTopoVIB, resulted in the arrest of parasites at the late schizont stage and disrupted the transition from schizont to ring stage. While we do not exclude the possibility of PfTopoVI having additional nuclear functions, our experimental data revealed a moderate correlation between PfTopoVIB/PfSpo11 and DAPI staining, implying a potential relationship. Nevertheless, the nuclear role of PfTopoVI was not specifically investigated in the present study.

Plasmodium topoisomerase VI, classified as a type IIB topoisomerase, presents a potential target for novel antimalarial interventions due to its absence in humans. Our experimental results indicate that the human Spo11 antibody exhibits cross-reactivity with PfSpo11, suggesting a level of structural conservation between human and Plasmodium Spo11 proteins. However, the sequence identity between PfTopoVIB and the TopoVIBL protein in mice and humans is significantly lower (10%). Structural analysis reveals that the ATP binding pocket, known as the Bergerat fold, of PfTopoVIB does not overlap with the corresponding region in the human TopoVIBL protein. Consequently, targeting the ATP binding pocket of PfTopoVIB with a specific inhibitor is less likely to hinder the function of the human TopoVIBL protein. Previous research in our laboratory demonstrated the inhibitory effect of Radicicol on PfTopoVI's decatenation activity. Although Radicicol is a paninhibitor of the heat shock protein Hsp90 and can bind to the Bergerat fold of human Hsp90, it is important to note that TopoVIB and Hsp90 are distinct molecules that share the Bergerat fold. Therefore, it is possible to identify selective inhibitors of PfTopoVIB that do not impact human Hsp90. Future investigations should focus on screening small molecule inhibitors that specifically target PfTopoVIB without affecting human Hsp90.

We speculate that any inhibitor that specifically targets the PfTopoVIB ATP binding pocket will prevent the PfSpo11-TopoVIB enzyme complex from functioning and will halt the parasite's endoreduplication.



Topoisomerase decatenating/segregating the mitochondrial genome of malaria parasite

Figure 23. The figure demonstrates the interaction between Plasmodium Topoisomerase VIB and Spo11, forming a functional type IIB topoisomerase complex in the malaria parasite. It is anticipated that this complex plays a role in the segregation of mitochondrial DNA within the parasite. The complex is depicted as a dimer consisting of Topoisomerase VIB (colored blue) and Spo11 (colored orange), with their catalytic domains indicated in Spo11. The complex as shown in the figure, is imported into the mitochondrial matrix. This topoisomerase VI associates with the mitochondrial DNA (represented by the circular structure), indicating its potential involvement in DNA segregation.

# Chapter 4

Results
Specific Aim-2

## 4. Specific Aim 2

To decipher whether PfTopoIII participates in the mitochondrial DNA segregation of the malaria parasite

Our second specific aim was to understand whether PfTopoIII, the Type I topoisomerase, is required for mitochondrial DNA maintenance in malaria parasite TopoIIIa is vital for maintaining mtDNA in humans. Depletion of TopoIIIa in cells results in a significant decrease in monomeric mtDNA and the formation of extensive catenated networks (35). Electron microscopy and two-dimensional gel electrophoresis was done to establish that the mitochondrial genome of malaria parasite undergoes rolling circle mode of DNA replication (81) and during that process, recombination happens between the multiple copy of genomes. As a result, single-stranded concatemers were observed in the mitochondrial genome during the microscopic analysis (82). These single-stranded catenated genomes need Type I topoisomerases for their proper segregation. However, till now it was not being identified that which Type I topoisomerase is involved in mitochondrial DNA replication/segregation of malaria parasite.

Previous work in our lab established that PfTopoIII is localized in both nuclear and mitochondria of the parasite. To enhance our understanding of the role of PfTopoIII in maintaining the mitochondrial genome, our aim is to examine whether its expression correlates with the replicating stage of the parasite and/or specifically during the late-schizont (LS) stage when mitochondrial segregation occurs. We also wanted to monitor whether it is a part of the mitochondrial replisome. It was earlier identified that the mitochondrial DNA polymerase of malaria parasite showed interaction with the PfRad51 and PfBlm (83), however whether PfTopoIII is also associated with the mtDNA polymerase of the malaria parasite was not evaluated. Also, it was never addressed whether it is recruited to the mitochondrial genome in a stage specific manner. Our study has allowed us to establish the probable function of PfTopoIII during mtDNA replication/ segregation of the parasite.

# 4.1. To study the stage specific expression of *PfTOPOIII* at different replicative stages of *Plasmodium*

We monitored the stage specific expression of *PfTOPOIII* at three tightly synchronized schizont developmental stages of the malaria parasite, Early (ES), Mid (MS) and Late-Schizont (LS) stage. The semi-quantitative PCR analysis demonstrated that *PfTOPOIII* expression was detected in all schizont stages, with the lowest expression observed at the early-schizont (ES) stage and the highest expression at the late-schizont stage of the parasite (1st Row, Figure 24A). The constitutively expressed gene ARP was used as a loading control throughout all stages of the parasite (2<sup>nd</sup> Row, Figure 24A). To eliminate the possibility of genomic DNA contamination in the cDNA samples, we performed PfTopoIII amplification using stage-specific mRNAs that were treated with DNase but not reverse transcriptase (-RT samples). No amplification was observed in these PCR samples, confirming the absence of genomic DNA in the cDNA samples (3<sup>rd</sup> Row, Figure 24A). However, PCR amplification was successful when genomic DNA was used as a template, serving as a control for the PCR reaction (3<sup>rd</sup> Row, Figure 24A). We further validated the expression by performing western blot analysis at three schizont stages of the parasite. A peptide antibody was raised against the residues spanning 281–300 amino-acids of PfTopoIII (DSNNYSDETDDYYGDEKK) in rabbit (39). Blot was probed using the PfTopoIII specific antibody and the protein loading was normalized by constitutively expressing Actin protein. We observed that PfTopoIII protein-expression is similar to that of the transcript data and there was a moderate expression at the MS stages of the parasite, and highest expression at the LS of the parasite (Figure 24B). Our data indicates that this enzyme is important for the replication as well as the genome segregation of the parasite.

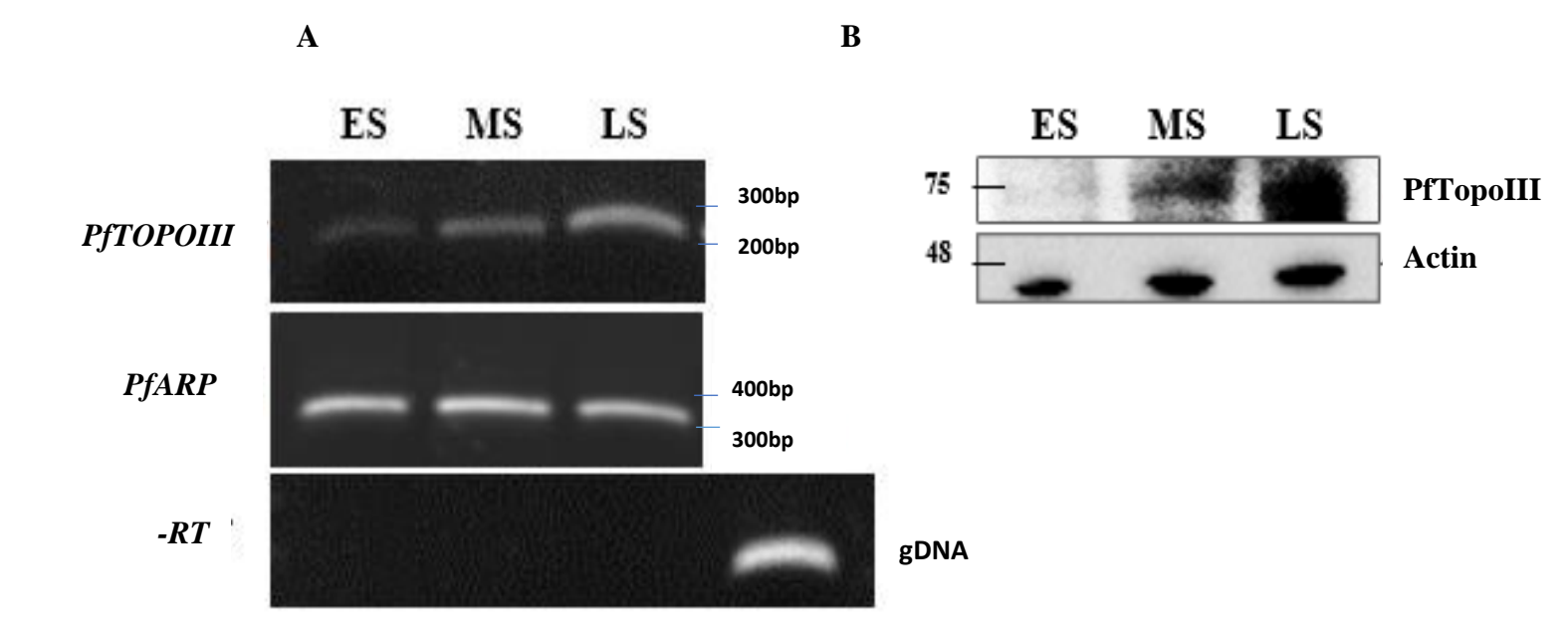


Figure 24: Expression analysis of PfTopoIII at different Schizont stages of the malaria parasite. A) RT-PCR analysis was carried out using RNA samples extracted from the early-schizont (ES), mid-schizont (MS), and late-schizont (LS) stages. Specific primers for PfTOPOIII and ARP were used for PCR amplification. The absence of a PfTOPOIII band was observed in the absence of reverse transcriptase (-RT), while genomic DNA (gDNA) served as a positive control. (B) Western blotting analyses were performed on parasite cell extracts obtained from the (ES), (MS), and (LS) stages, using PfTopoIII antibody. Actin was used as a loading control (bottom panel). The molecular weight marker is indicated on the right side of the blot.

### 4.2. To study whether PfTopoIII is a part of the mitochondrial replisome

To validate whether PfTopoIII is a part of mitochondrial replisome, we investigated its interaction with the mitochondrial DNA polymerase of the malaria parasite. Empty pGADC1 (Yeast two-hybrid ""prey"" vector containing a LEU2 marker) and pGBDUC1 (Yeast two-hybrid "bait" vector with a URA3 marker) to generate a control yeast strain PSY5, the vectors were transformed into the PJ694a parental strain. This control strain was established to investigate the interaction between PfmtDNApolymerase with PfTopoIII protein. PSY8, PSY7 and PSY6 were created by transforming pGADC1-PfmtDNApolymerase + pGBDUC1-PfTopoIII, pGADC1 + pGBDUC1-PfTopoIII and pGADC1-PfmtDNApolymerase + pGBDUC1 constructs into PJ694a strain, respectively. These strains were grown on the double dropout media SC-Ura-Leu as presented in Figure 25A. We performed yeast two hybrid analysis using these strains to monitor the interaction between PfTopoIII with the mitochondrial DNA polymerase. To that end, we first monitored the HIS3 reported gene activity. We observed that the strain expressing both the PfmtDNApolymerase, fused to Gal4 activation domain (GAD) and PfTopoIII, fused to GAL4 DNA binding domain (GBD) can activate the reporter gene activity as seen by their growth on the triple drop out plate, SC-Lue-Ura-His (Figure 25B). However, individually they could not activate the reporter gene activity (Figure 25B). We tested whether their interaction is strong or not, by probing whether they can activate ADE2 reporter gene activity or not. We did not find any growth on the triple drop out plate SC-Lue-Ura-Ade. Thus, our finding indicates that PfTopoIII interacts weakly with PfmtDNApolymerase (Figure 25C).

# 4.3. To study whether PfTopoIII is associated with the mitochondrial genome of the malaria parasite

To investigate the potential association between PfTopoIII and the mitochondrial genome, we performed chromatin immunoprecipitation (ChIP) assays using four tightly synchronized developmental stages of the parasite: ring (R), trophozoite (T), early schizont (ES), and late schizont (LS). The ChIP assay procedure was conducted following the methods described earlier in this

section. PfTopoIII specific antibody was used in the ChIP analysis and the immuno-precipitated samples were amplified using six-set of primers (A-F), each primer amplifying 1 kb amplicon, spanning the whole 6 kb of mitochondrial genome, as illustrated in (Figure 26A). A control antibody, rabbit immunoglobulin G (IgG), was utilized for Chromatin Immunoprecipitation (ChIP) as a negative control. Prior to plotting the data, the PfTopoIII ChIP recruitment values were adjusted by subtracting the corresponding IgG values. The calculation of relative occupancy involved assessing the PfTopoIII recruitment on the mitochondrial genome in relation to the input value. It was observed that PfTopoIII primarily associates with the terminal end of the mtDNA (F-set primer) during the late schizont stage of the parasite. Minimal recruitment of PfTopoIII was observed during the R, T, and ES stages, while an increase was noted during the LS stage, indicating its potential role in mtDNA decatenation during segregation (Figure 26B).

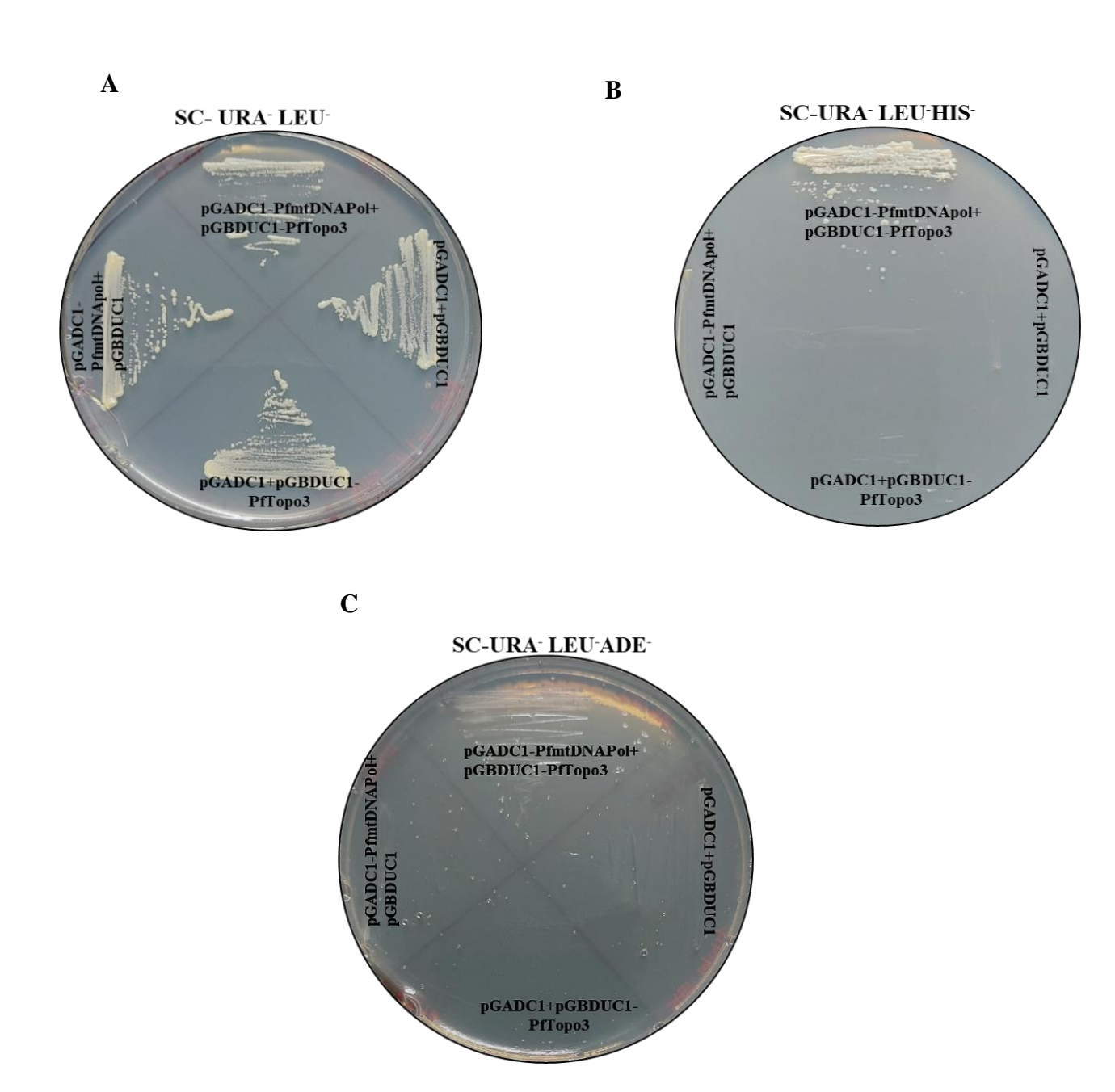
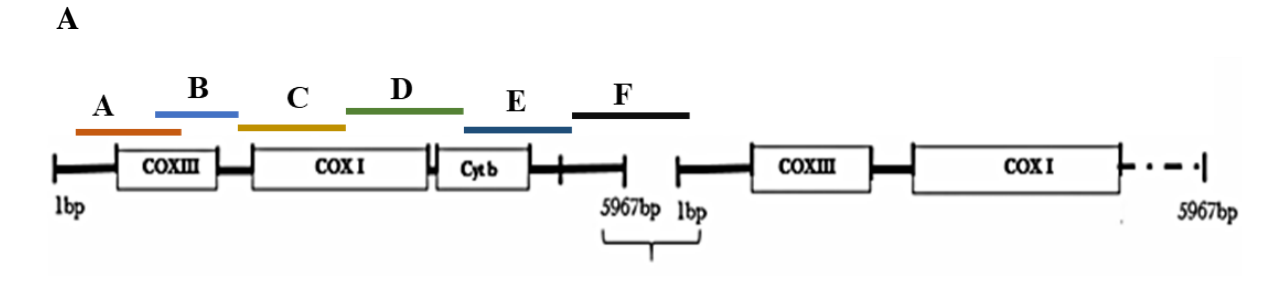


Figure 25. PfTopoIII interacts with PfmtDNApolymerase. To investigate this interaction, yeast two-hybrid assay was performed using the PJ69-4A strain, with HIS3 serving as the reporter gene. The yeast two-hybrid analysis revealed the interaction between PfTopoIII and PfmtDNApolymerase. Different strains harbouring bait and prey vectors were utilized and cells from each strain were patched onto distinct selection plates. The protein interaction was monitored by patching the cells onto medium lacking LEU and URA (A), medium lacking LEU, URA, and HIS (B), and finally, medium lacking LEU, URA, and ADE (C)



B

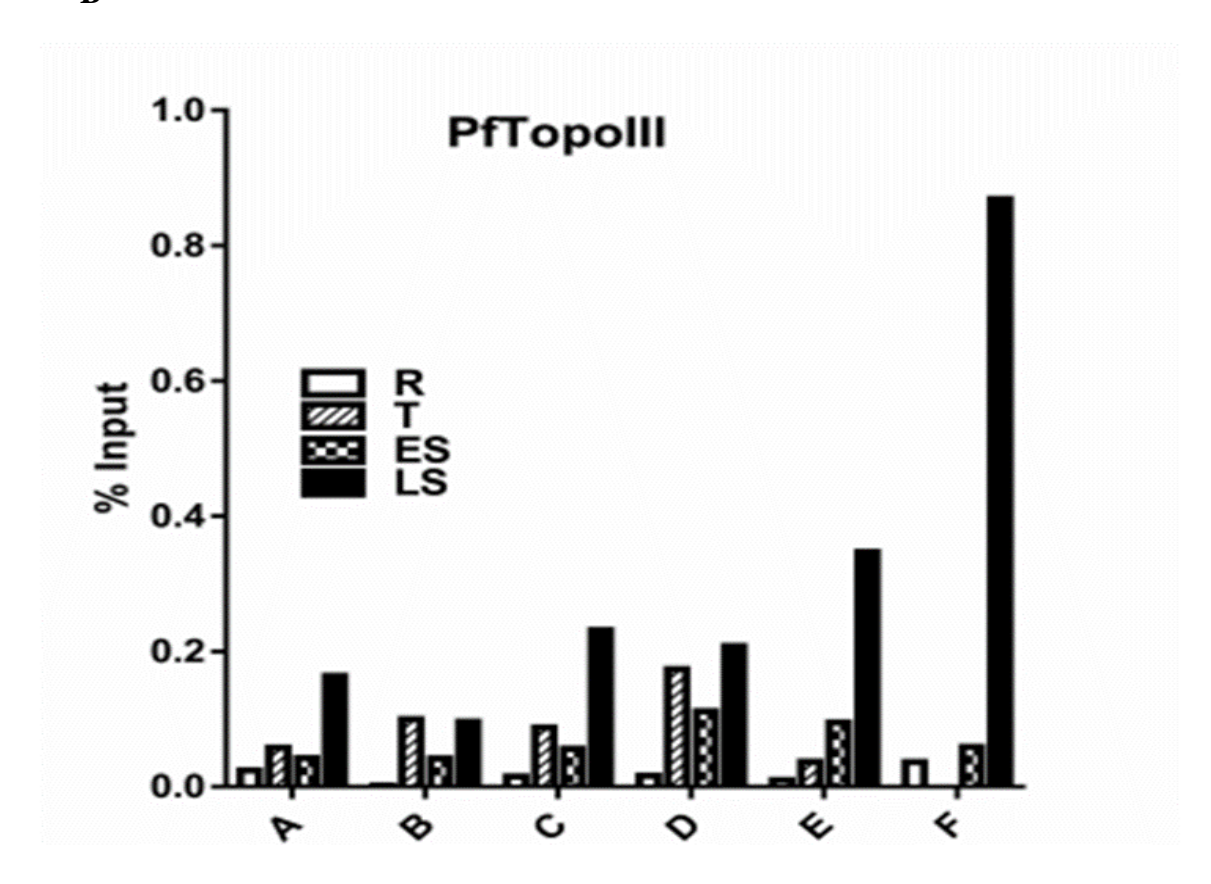
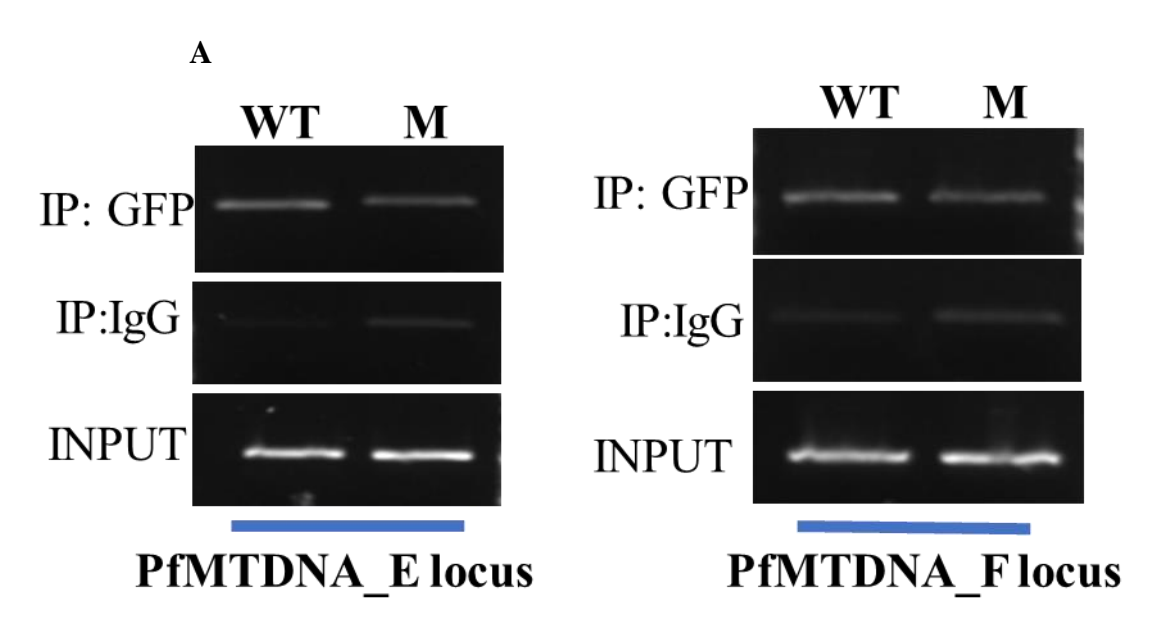


Figure 26. PfTopoIII interacts with mitochondrial genome. (A) The mitochondrial DNA (mtDNA) of P. falciparum is characterized by a linear tandem array spanning 6 kb, with adjacent ends joined together. A schematic representation illustrates the positions of primer sets (A to F) that collectively cover the entire mtDNA. Furthermore, the diagram indicates the presence of three distinct genes—COXIII, CYT b, and COXI—encoded within the Plasmodium mitochondrial genome. (B) The graph presents the percentage of PfTopoIII occupancy on mtDNA relative to the input, plotted on the Y-axis, while the X-axis represents different sections (A-F) of the mitochondrial genome, that encompass the whole mtDNA.

We wanted to identify the domains in PfTopoIII that are responsible for its binding to the mt-genome. In a previous investigation, it was demonstrated that the charged loop in bacterial Topoisomerase III from Escherichia coli is indispensable for DNA binding during the decatenation process of intertwined DNA (38, 84). Consequently, our objective was to determine whether the charged linker region of PfTopoIII also plays a crucial role in efficient DNA binding. To achieve this, our laboratory performed molecular dynamic simulations involving the PfTopoIII structure and a single-stranded DNA octamer with the sequence (5' CGCAACTT 3'). The simulations revealed a shift the conformational of enzyme upon DNA binding, with the charged domain of PfTopoIII interacting with the DNA, thereby stabilizing the DNA-bound conformation of the enzyme (39).

To investigate the functional significance of the charged domain of PfTopoIII, we generated two transgenic parasite lines in our laboratory. One line expressed the wild-type PfTopoIII fused to GFP, while the other line expressed a mutant form of PftopoIII-GFP with a deletion of the charged domain (259-337). We conducted Western blotting analyses to evaluate the stability of both the mutant and wild-type proteins in the mutant parasites. The results revealed comparable expression levels of the mutant PftopoIII( $\Delta$ 259–337)-GFP protein and the wild-type PfTopoIII-GFP protein in the transgenic parasites (data not shown) (39). With these two transgenic parasites, we performed ChIP assay, where we immunoprecipitated their respective genomes using anti-GFP antibody (Allied Scientific Products) using the tightly synchronized schizont stages and monitored their respective recruitment by amplifying the *E* and *F* loci of mitochondrial genome (**Figure 26A**). After normalizing the input values (3<sup>rd</sup> Row-Figure 27A) for both wild type and mutant parasites, we compared the recruitment between the mutant PftopoIII and the wild-type PfTopoIII (1<sup>st</sup> Row-Figure 27A). In a control experiment immunoprecipitation was performed in each strain, using the IgG antibody but the same did not show any PCR amplification of either *E* or *F* loci (2<sup>nd</sup> Row-Figure 27A). The experiment was conducted twice, and the measurement of mutant PftopoIII( $\Delta$ 259–337) and wild type-PfTopoIII

recruitment to the E and F regions of mtDNA was assessed using qRT-PCR analysis. The inputs were normalized, as depicted (**Figure 27B**). Before plotting the data, the PfTopoIII ChIP value was adjusted by subtracting the corresponding IgG recruitment values. Our study showed that the mutant PftopoIII(259-337) protein displayed a considerably reduced interaction with the mtDNA.



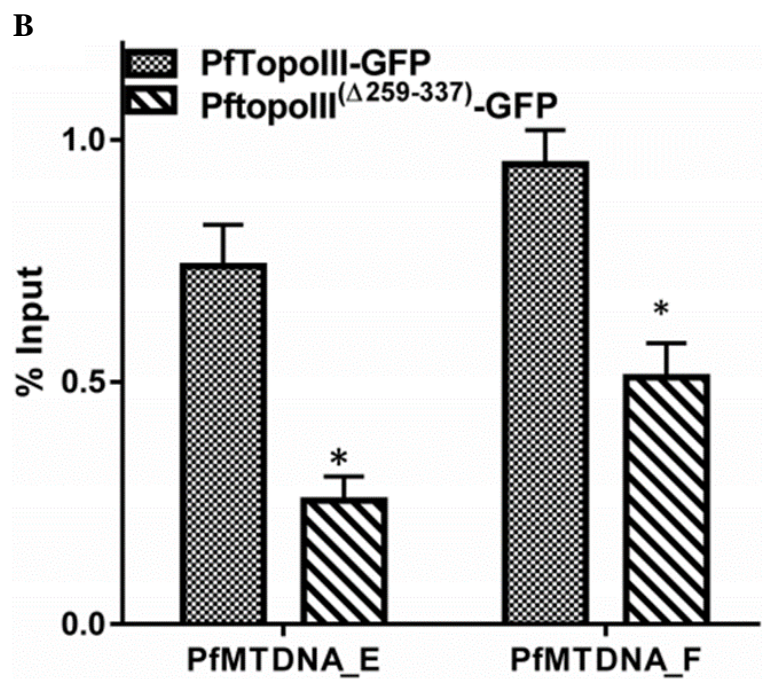


Figure 27. PftopoIII( $\Delta 259$ –337) shows poor association with mtDNA. (A) Semiquantitative PCR was used to compare the recruitment of wild-type and mutant PfTopoIII(259-337)-GFP at two loci (E and F) in the mitochondrial genome. IgG immunoprecipitation served as a check against both the mutant and wild-type proteins. (B) The ChIP studies demonstrate enhanced recruitment of PfTopoIII-GFP to two distinct loci (E and F) of the mitochondrial genome as compared to PftopoIII(259-337)-GFP. Error bars show mean and standard deviation; n = 2; and \*P < 0.05.

#### **DISCUSSION**

In the specific aim 2, we explored the role of Topoisomerase III, a Type IA, topoisomerase in the malaria parasite. The spatiotemporal expression pattern of this enzyme during the actively replicating stage indicated that *PfTOPOIII* expression is present at all the schizont stages, , and the Late-schizont stage of the parasite exhibits the highest level of expression. This suggests its probable function in the replication as well as in the segregation of the genome. TopoIII-depleted cells had a considerable loss of monomeric mtDNA and formed extensive catenated networks, supporting earlier studies that demonstrated human TopoIII is necessary for the maintenance of mtDNA (35). Our findings from mitochondrial immunoprecipitation demonstrate that the malaria parasite PfTopoIII is a mitochondrial topoisomerase. Further evidence for PfTopoIII's participation in decatenating catenated mtDNA and assisting in the segregation of mtDNA came from its particular interaction with the terminal end of mtDNA (F-region of mtDNA) during the last stage of parasite replication. Yeast two-hybrid interaction between PfTopoIII and PfmtDNAPolymerase indicates the existence of a "replisome" complex within the parasite, where these proteins likely work together to facilitate efficient DNA replication. An understanding of the molecular mechanisms underlying the interaction between PfTopoIII and DNA is provided by earlier discoveries made in our laboratory as part of the MDS investigation. In order to properly facilitate DNA replication and segregation, the charged domain of PfTopoIII is proven to stabilize the protein's effective interaction with DNA (39). Our ChIP research lends additional support to this observation. Comparing transgenic parasites to the parasites in the wild type, we found that the removal of the charged region in PftopoIII(259-337) results in a reduced interaction of the protein with mtDNA. This suggests that the charged domain of PfTopoIII plays a crucial role in mediating the interaction between PfTopoIII and mtDNA, emphasizing its significance in the overall function of the protein. Together, these findings offer

strong support for PfTopoIII's role in the parasite's mtDNA replication and segregation, suggesting potential targets for future therapeutic approaches.

#### References

- 1. Nosten F, Richard-Lenoble D, Danis M. A brief history of malaria. La Presse Médicale. 2022;51(3):104130.
- 2. Carter R, Mendis KN. Evolutionary and historical aspects of the burden of malaria. Clinical microbiology reviews. 2002;15(4):564-94.
- 3. Monroe A, Williams NA, Ogoma S, Karema C, Okumu F. Reflections on the 2021 World Malaria Report and the future of malaria control. BioMed Central; 2022.
- 4. Anderson RM, May RM. Infectious diseases of humans: dynamics and control: Oxford university press; 1991.
- 5. Tuteja R. Malaria an overview. The FEBS journal. 2007;274(18):4670-9.
- 6. da Silva AFC, Benchimol JL. Malaria and quinine resistance: a medical and scientific issue between Brazil and Germany (1907–19). Medical history. 2014;58(1):1-26.
- 7. Kirkman LA, Deitsch KW. Antigenic variation and the generation of diversity in malaria parasites. Current opinion in microbiology. 2012;15(4):456-62.
- 8. Recker M, Buckee CO, Serazin A, Kyes S, Pinches R, Christodoulou Z, et al. Antigenic variation in Plasmodium falciparum malaria involves a highly structured switching pattern. PLoS Pathogens. 2011;7(3):e1001306.
- 9. McDonald J, Merrick CJ. DNA replication dynamics during erythrocytic schizogony in the malaria parasites Plasmodium falciparum and Plasmodium knowlesi. PLoS Pathogens. 2022;18(6):e1010595.
- 10. Matthews H, Duffy CW, Merrick CJ. Checks and balances? DNA replication and the cell cycle in Plasmodium. Parasites & vectors. 2018;11:1-13.
- 11. Waldecker M, Dasanna AK, Lansche C, Linke M, Srismith S, Cyrklaff M, et al. Differential time-dependent volumetric and surface area changes and delayed induction of new permeation pathways in P. falciparum-infected hemoglobinopathic erythrocytes. Cellular microbiology. 2017;19(2):e12650.
- 12. Machado M, Steinke S, Ganter M. Plasmodium Reproduction, Cell Size, and Transcription: How to Cope With Increasing DNA Content? Frontiers in Cellular and Infection Microbiology. 2021;11:660679.
- 13. Leete T, Rubin H. Malaria and the cell cycle. Parasitology today. 1996;12(11):442-4.
- 14. Zeeshan M, Pandey R, Ferguson DJ, Tromer EC, Markus R, Abel S, et al. Real-time dynamics of Plasmodium NDC80 reveals unusual modes of chromosome segregation during parasite proliferation. Journal of cell science. 2021;134(5):jcs245753.
- 15. Bhatnagar S, Sawhney V. Endosperm—Its Morphology, infrastructure, and Histochemistry. International Review of Cytology. 73: Elsevier; 1981. p. 55-102.
- 16. Kowles RV, Phillips RL. Endosperm development in maize. International Review of Cytology. 1988;112:97-136.
- 17. van Dooren GG, Marti M, Tonkin CJ, Stimmler LM, Cowman AF, McFadden GI. Development of the endoplasmic reticulum, mitochondrion and apicoplast during the asexual life cycle of Plasmodium falciparum. Molecular microbiology. 2005;57(2):405-19.
- 18. Painter HJ, Morrisey JM, Vaidya AB. Mitochondrial electron transport inhibition and viability of intraerythrocytic Plasmodium falciparum. Antimicrobial agents and chemotherapy. 2010;54(12):5281-7.
- 19. Vaidya AB, Mather MW. Mitochondrial evolution and functions in malaria parasites. Annual review of microbiology. 2009;63:249-67.
- 20. Srivastava IK, Vaidya AB. A mechanism for the synergistic antimalarial action of atovaquone and proguanil. Antimicrobial agents and chemotherapy. 1999;43(6):1334-9.
- 21. Ke H, Ganesan SM, Dass S, Morrisey JM, Pou S, Nilsen A, et al. Mitochondrial type II NADH dehydrogenase of Plasmodium falciparum (PfNDH2) is dispensable in the asexual blood stages. PLoS One. 2019;14(4):e0214023.

- 22. Singh P, Rani K, Gotmare A, Bhattacharyya S. A tale of topoisomerases and the knotty genetic material in the backdrop of Plasmodium biology. Bioscience Reports. 2022;42(6):BSR20212847.
- 23. Slesarev AI, Stetter KO, Lake JA, Gellert M, Krah R, Kozyavkin SA. DNA topoisomerase V is a relative of eukaryotic topoisomerase I from a hyperthermophilic prokaryote. Nature. 1993;364(6439):735-7.
- 24. Taneja B, Patel A, Slesarev A, Mondragón A. Structure of the N-terminal fragment of topoisomerase V reveals a new family of topoisomerases. The EMBO Journal. 2006;25(2):398-408.
- 25. Wang JC. Cellular roles of DNA topoisomerases: a molecular perspective. Nature reviews Molecular cell biology. 2002;3(6):430-40.
- 26. Taneja B, Schnurr B, Slesarev A, Marko JF, Mondragón A. Topoisomerase V relaxes supercoiled DNA by a constrained swiveling mechanism. Proceedings of the National Academy of Sciences. 2007;104(37):14670-5.
- 27. Rajan R, Osterman A, Mondragon A. Methanopyrus kandleri topoisomerase V contains three distinct AP lyase active sites in addition to the topoisomerase active site. Nucleic acids research. 2016;44(7):3464-74.
- 28. Rajan R, Prasad R, Taneja B, Wilson SH, Mondragon A. Identification of one of the apurinic/apyrimidinic lyase active sites of topoisomerase V by structural and functional studies. Nucleic acids research. 2013;41(1):657-66.
- 29. Belova GI, Prasad R, Kozyavkin SA, Lake JA, Wilson SH, Slesarev AI. A type IB topoisomerase with DNA repair activities. Proceedings of the National Academy of Sciences. 2001;98(11):6015-20.
- 30. Wallis JW, Chrebet G, Brodsky G, Rolfe M, Rothstein R. A hyper-recombination mutation in S. cerevisiae identifies a novel eukaryotic topoisomerase. Cell. 1989;58(2):409-19.
- 31. Arthur WL. Characterization of a novel eukaryotic topoisomerase (TOP3) in Saccharomyces cerevisiae that affects recombination and gene expression: Columbia University; 1991.
- 32. Gangloff S, Zou H, Rothstein R. Gene conversion plays the major role in controlling the stability of large tandem repeats in yeast. The EMBO journal. 1996;15(7):1715-25.
- 33. Li W, Wang JC. Mammalian DNA topoisomerase III $\alpha$  is essential in early embryogenesis. Proceedings of the National Academy of Sciences. 1998;95(3):1010-3.
- 34. Cejka P, Plank JL, Dombrowski CC, Kowalczykowski SC. Decatenation of DNA by the S. cerevisiae Sgs1-Top3-Rmi1 and RPA complex: a mechanism for disentangling chromosomes. Molecular cell. 2012;47(6):886-96.
- 35. Nicholls TJ, Nadalutti CA, Motori E, Sommerville EW, Gorman GS, Basu S, et al. Topoisomerase  $3\alpha$  is required for decatenation and segregation of human mtDNA. Molecular cell. 2018;69(1):9-23. e6.
- 36. Ahmad M, Shen W, Li W, Xue Y, Zou S, Xu D, et al. Topoisomerase  $3\beta$  is the major topoisomerase for mRNAs and linked to neurodevelopment and mental dysfunction. Nucleic Acids Research. 2017;45(5):2704-13.
- 37. Aravind L, Leipe DD, Koonin EV. Toprim—a conserved catalytic domain in type IA and II topoisomerases, DnaG-type primases, OLD family nucleases and RecR proteins. Nucleic acids research. 1998;26(18):4205-13.
- 38. Li Z, Mondragón A, Hiasa H, Marians KJ, DiGate RJ. Identification of a unique domain essential for Escherichia coli DNA topoisomerase III-catalysed decatenation of replication intermediates. Molecular microbiology. 2000;35(4):888-95.
- 39. Bansod S, Bung N, Singh P, Suthram N, Choudhury H, Roy A, et al. Elucidation of an essential function of the unique charged domain of Plasmodium topoisomerase III. Biochemical Journal. 2020;477(24):4745-67.
- 40. Maric C, Bénard M. Replication forks reverse at high frequency upon replication stress in Physarum polycephalum. Chromosoma. 2014;123:577-85.
- 41. Nitiss JL. DNA topoisomerase II and its growing repertoire of biological functions. Nature Reviews Cancer. 2009;9(5):327-37.
- 42. Champoux JJ. DNA topoisomerases: structure, function, and mechanism. Annual review of biochemistry. 2001;70(1):369-413.
- 43. Lee I, Dong KC, Berger JM. The role of DNA bending in type IIA topoisomerase function. Nucleic acids research. 2013;41(10):5444-56.

- 44. Pearl LH, Prodromou C. Structure and mechanism of the Hsp90 molecular chaperone machinery. Annu Rev Biochem. 2006;75:271-94.
- 45. Takahashi DT, Da Cunha V, Krupovic M, Mayer C, Forterre P, Gadelle D. Expanding the type IIB DNA topoisomerase family: identification of new topoisomerase and topoisomerase-like proteins in mobile genetic elements. NAR Genomics and Bioinformatics. 2020;2(1):lqz021.
- 46. Cao L, Alani E, Kleckner N. A pathway for generation and processing of double-strand breaks during meiotic recombination in S. cerevisiae. Cell. 1990;61(6):1089-101.
- 47. Diaz RL, Alcid AD, Berger JM, Keeney S. Identification of residues in yeast Spo11p critical for meiotic DNA double-strand break formation. Molecular and cellular biology. 2002;22(4):1106-15.
- 48. Bergerat A, De Massy B, Gadelle D, Varoutas P-C, Nicolas A, Forterre P. An atypical topoisomerase II from Archaea with implications for meiotic recombination. Nature. 1997;386(6623):414-7.
- 49. Klapholz S, Waddell CS, Esposito RE. The role of the SPO11 gene in meiotic recombination in yeast. Genetics. 1985;110(2):187-216.
- 50. Romanienko PJ, Camerini-Otero RD. The mouse Spo11 gene is required for meiotic chromosome synapsis. Molecular cell. 2000;6(5):975-87.
- 51. Keeney S. Spo11 and the formation of DNA double-strand breaks in meiosis. Recombination and meiosis: crossing-over and disjunction: Springer; 2007. p. 81-123.
- 52. Hartung F, Puchta H. Molecular characterisation of two paralogous SPO11 homologues in Arabidopsis thaliana. Nucleic acids research. 2000;28(7):1548-54.
- 53. Breuer C, Stacey NJ, West CE, Zhao Y, Chory J, Tsukaya H, et al. BIN4, a novel component of the plant DNA topoisomerase VI complex, is required for endoreduplication in Arabidopsis. The Plant Cell. 2007;19(11):3655-68.
- 54. Fu M, Wang C, Xue F, Higgins J, Chen M, Zhang D, et al. The DNA Topoisomerase VI–B Subunit OsMTOPVIB is Essential for Meiotic Recombination Initiation in Rice. Molecular Plant. 2016;9(11):1539-41.
- 55. An XJ, Deng ZY, Wang T. OsSpo11-4, a rice homologue of the archaeal TopVIA protein, mediates double-strand DNA cleavage and interacts with OsTopVIB. PloS one. 2011;6(5):e20327.
- 56. Romanienko PJ, Camerini-Otero RD. Cloning, characterization, and localization of mouse and human SPO11. Genomics. 1999;61(2):156-69.
- 57. Robert T, Nore A, Brun C, Maffre C, Crimi B, Guichard V, et al. The TopoVIB-Like protein family is required for meiotic DNA double-strand break formation. Science. 2016;351(6276):943-9.
- 58. Tran TN, Schimenti JC. A segregating human allele of SPO11 modeled in mice disrupts timing and amounts of meiotic recombination, causing oligospermia and a decreased ovarian reserve. Biology of Reproduction. 2019;101(2):347-59.
- 59. Chalapareddy S, Bhattacharyya MK, Mishra S, Bhattacharyya S. Radicicol confers mid-schizont arrest by inhibiting mitochondrial replication in Plasmodium falciparum. Antimicrobial agents and chemotherapy. 2014;58(8):4341-52.
- 60. Chalapareddy S, Chakrabarty S, Bhattacharyya MK, Bhattacharyya S. Radicicol-mediated inhibition of topoisomerase VIB-VIA activity of the human malaria parasite Plasmodium falciparum. Msphere. 2016;1(1):e00025-15.
- 61. Hasinoff BB, Abram ME, Barnabé N, Khélifa T, Allan WP, Yalowich JC. The catalytic DNA topoisomerase II inhibitor dexrazoxane (ICRF-187) induces differentiation and apoptosis in human leukemia K562 cells. Molecular Pharmacology. 2001;59(3):453-61.
- 62. Classen S, Olland S, Berger JM. Structure of the topoisomerase II ATPase region and its mechanism of inhibition by the chemotherapeutic agent ICRF-187. Proceedings of the National Academy of Sciences. 2003;100(19):10629-34.
- 63. Chavalitshewinkoon P, Wilairat P, Gamage S, Denny W, Figgitt D, Ralph R. Structure-activity relationships and modes of action of 9-anilinoacridines against chloroquine-resistant Plasmodium falciparum in vitro. Antimicrobial agents and chemotherapy. 1993;37(3):403-6.
- 64. Gobert C, Bracco L, Rossi F, Olivier M, Tazi J, Lavelle F, et al. Modulation of DNA topoisomerase I activity by p53. Biochemistry. 1996;35(18):5778-86.

- 65. Gellert M, O'Dea MH, Itoh T, Tomizawa J-I. Novobiocin and coumermycin inhibit DNA supercoiling catalyzed by DNA gyrase. Proceedings of the National Academy of Sciences. 1976;73(12):4474-8.
- 66. Sugino A, Peebles CL, Kreuzer KN, Cozzarelli NR. Mechanism of action of nalidixic acid: purification of Escherichia coli nalA gene product and its relationship to DNA gyrase and a novel nicking-closing enzyme. Proceedings of the National Academy of Sciences. 1977;74(11):4767-71.
- 67. Gadelle D, Bocs C, Graille M, Forterre P. Inhibition of archaeal growth and DNA topoisomerase VI activities by the Hsp90 inhibitor radicicol. Nucleic acids research. 2005;33(7):2310-7.
- 68. Corbett KD, Berger JM. Structural basis for topoisomerase VI inhibition by the anti-Hsp90 drug radicicol. Nucleic acids research. 2006;34(15):4269-77.
- 69. Bansod S, Raj N, Nair AS, Bhattacharyya S. Molecular docking and molecular dynamics simulation identify a novel Radicicol derivative that predicts exclusive binding to Plasmodium falciparum Topoisomerase VIB. Journal of Biomolecular Structure and Dynamics. 2022;40(15):6939-51.
- 70. Laskar S, Bhattacharyya MK, Shankar R, Bhattacharyya S. HSP90 controls SIR2 mediated gene silencing. Plos one. 2011;6(8):e23406.
- 71. Tabassum W, Bhattacharyya S, Varunan SM, Bhattacharyya MK. Febrile temperature causes transcriptional downregulation of Plasmodium falciparum Sirtuins through Hsp90-dependent epigenetic modification. Molecular Microbiology. 2021;115(5):1025-38.
- 72. Roy N, Bhattacharyya S, Chakrabarty S, Laskar S, Babu SM, Bhattacharyya MK. Dominant negative mutant of P lasmodium R ad51 causes reduced parasite burden in host by abrogating DNA double-strand break repair. Molecular microbiology. 2014;94(2):353-66.
- 73. Moll K, Kaneko A, Scherf A, Wahlgren M. Methods in Malaria Research.: EviMalaR. Glasgow, UK & MR4/ATCC, Manassas, VA, USA. 2013.
- 74. Suthram N, Padhi S, Jha P, Bhattacharyya S, Bulusu G, Roy A, et al. Elucidation of DNA repair function of PfBlm and potentiation of artemisinin action by a small-molecule inhibitor of RecQ helicase. Msphere. 2020;5(6):e00956-20.
- 75. McGarvey PB, Nightingale A, Luo J, Huang H, Martin MJ, Wu C, et al. UniProt genomic mapping for deciphering functional effects of missense variants. Human mutation. 2019;40(6):694-705.
- 76. Jumper J, Evans R, Pritzel A, Green T, Figurnov M, Ronneberger O, et al. Highly accurate protein structure prediction with AlphaFold. Nature. 2021;596(7873):583-9.
- 77. Humphrey W, Dalke A, Schulten K. J. I\/lolec. J Mol Graphics. 1996;14:33-8.
- 78. Neiman AM. Sporulation in the budding yeast Saccharomyces cerevisiae. Genetics. 2011;189(3):737-65.
- 79. Keeney S, Giroux CN, Kleckner N. Meiosis-specific DNA double-strand breaks are catalyzed by Spo11, a member of a widely conserved protein family. Cell. 1997;88(3):375-84.
- 80. Humphrey W, Dalke A, Schulten K. VMD: visual molecular dynamics. Journal of molecular graphics. 1996;14(1):33-8.
- 81. Preiser P, Wilson R, Moore P, McCready S, Hajibagheri M, Blight K, et al. Recombination associated with replication of malarial mitochondrial DNA. The EMBO journal. 1996;15(3):684-93.
- 82. Kyes SA, Christodoulou Z, Raza A, Horrocks P, Pinches R, Rowe JA, et al. A well-conserved Plasmodium falciparum var gene shows an unusual stage-specific transcript pattern. Molecular microbiology. 2003;48(5):1339-48.
- 83. Jha P, Gahlawat A, Bhattacharyya S, Dey S, Kumar KA, Bhattacharyya MK. Bloom helicase along with recombinase Rad51 repairs the mitochondrial genome of the malaria parasite. Msphere. 2021;6(6):e00718-21.
- 84. Lee CM, Wang G, Pertsinidis A, Marians KJ. Topoisomerase III acts at the replication fork to remove precatenanes. Journal of Bacteriology. 2019;201(7):e00563-18.

# **Appendix**

A1: Cloning of *PfSPO11* in yeast expression vector: The position of the promoter within the vector and the position of *SalI* site within the insert are schematically represented (**Figure 28A**). The full-length *PfSPO11* was PCR amplified using the primer pairs OSB 645 and OSB 646, each having a *BamHI* restriction site and 3D7 cDNA as a template (**Figure 28B**). Further it was digested with *BamHI* restriction enzyme and cloned in the *pHCA* vector by nondirectional cloning. *SalI* restriction site is present in the sequence of *PfSPO11* at 43 bp and one *SalI* site is present in the vector as well. If it is cloned in right orientation inside *pHCA* vector (**as indicated in Figure 28A**), the digestion of the recombinant clone using *SalI* restriction enzyme, will release the insert of size 990 bp and 5.49 kb respectively, as depicted (**Figure 28C**). Further DNA sequencing of the recombinant clone was performed to confirm the cloning.

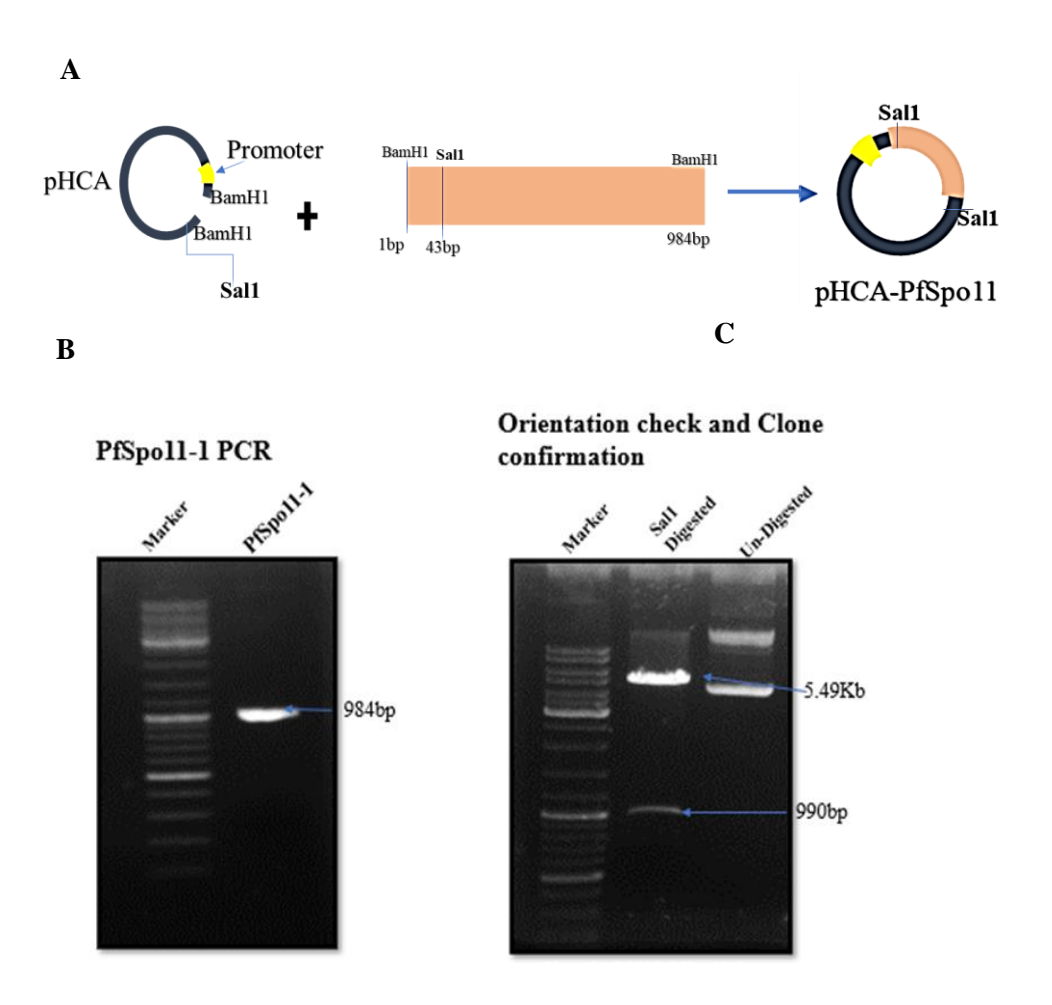


Figure 28: Cloning of PfSPO11, into pHCA vector: (A) Diagrammatic representation of the cloning strategy. (B) Agarose gel image depicting the PCR amplified product of PfSpo11 of 984 bp length. (C) Clone confirmation and orientation check of pHCA-PfSPO11 was done by the release of insert of size 990 bp and 5.49 kb respectively upon digestion of the plasmid using Sall enzyme.

## A2: Cloning of *PfSPO11Y65F* in yeast expression vector

The *PfSpo11Y65F* mutant was generated by Splice Overlap Extension (SOE) PCR, using three successive PCR steps as depicted above (**Figure 29A**) and subsequently cloned in the *pHCA* vector at the *BamHI* site, using the same cloning strategy as described above. First, product A and B were amplified using OSB645/OSB 652 and OSB653/OSB646 (**Figure 29B**) respectively each having the mutation as shown in the figure. Product A primers displayed in blue and red colour were used as shown in the schematics (**Figure 29A**). Similarly, for Product B, primers displayed in Black and yellow colour were used. Further, the full-length *PfSPO11* containing the mutation at 65<sup>th</sup> position of tyrosine was amplified using the product A and B mentioned above, as a template using primer pair OSB (645 and 646) (**Figure 29 B**) (**Table 4**), shown in blue and yellow colour (**Figure 29A**). The final mutated insert was cloned into the *pHCA* vector using the same strategy as used above (**Figure 29A**). The correct orientation of the insert *Pfspo11Y65F* within the vector was checked using *Sall* restriction enzyme as mentioned above, by the release of insert of size 990 bp and 5.49 kb vector respectively (**Figure 29 C**). Further DNA sequencing of the recombinant clone was performed to confirm the cloning.

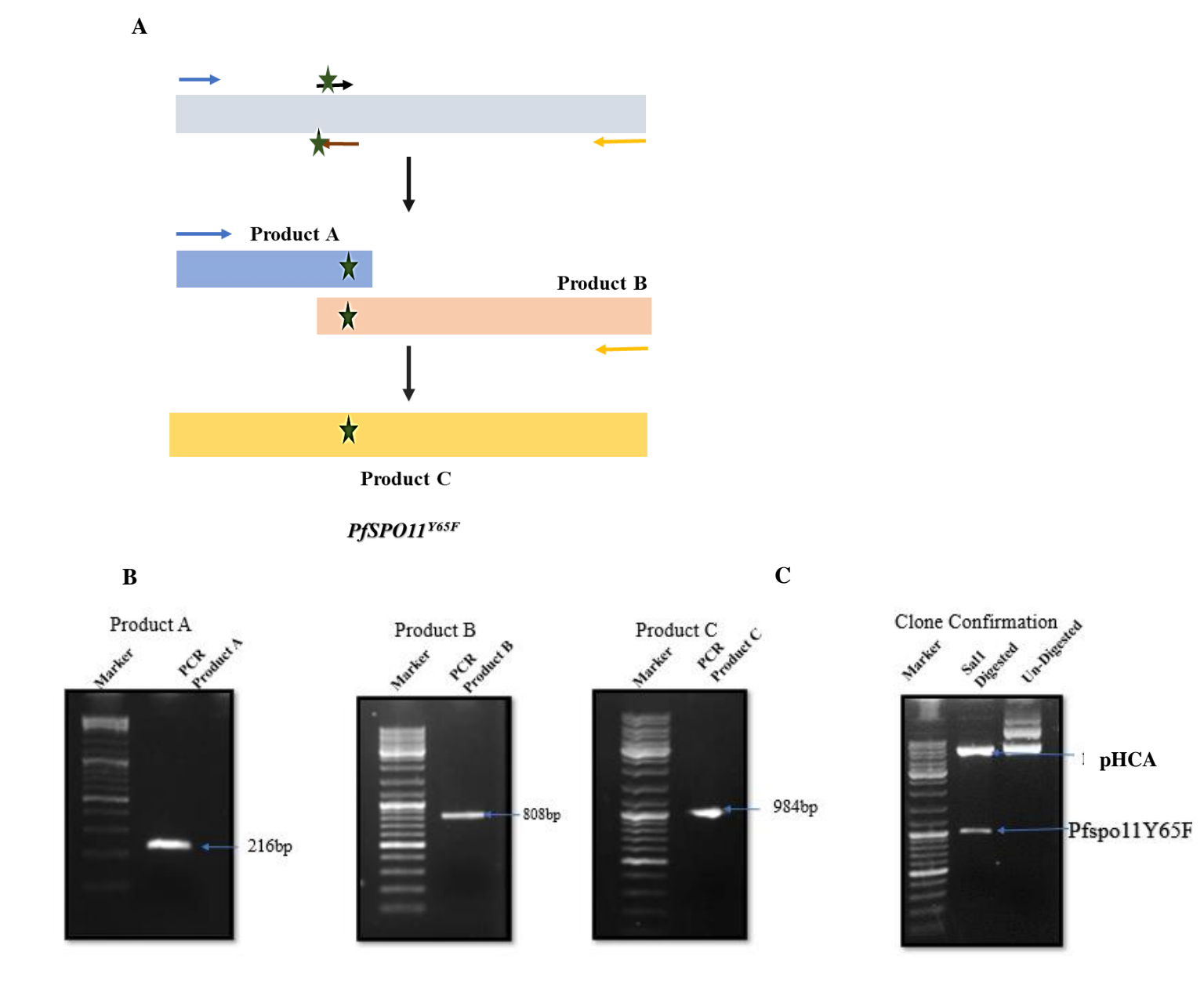


Figure 29. Cloning of PfSPO11<sup>Y65F</sup>, into pHCA vector: (A) Diagrammatic representation of the generation of Pfspo11Y65F by employing Splice Overall Extension (SOE) PCR. (B) Agarose gel image depicting the PCR amplified product A, B, and final mutant Product C of Pfspo11Y65F of 984 bp length. (C) Clone confirmation and of pHCA-PfSPO11<sup>Y65F</sup> was done by the release of insert by Sall restriction digestion of size 990 bp and 5.49 kb respectively upon digestion of the plasmid using Sall enzyme.

### A3: Cloning of *ScSPO11* in yeast expression vector

ScSPO11 (Full-length) was cloned in the yeast centromeric expression vector pHCA via PCR amplifying ScSPO11 using yeast genomic DNA (Figure 30A) using the forward primer OSB 643 with a BamHI site and the reverse primer OSB 644 with a SalI restriction site (Table 4). Clone confirmation of pHCA-ScSPO11 was done using BamHI and SalI restriction enzyme, by the release of insert of size 1197 bp and 5.5 kb pHCA plasmid respectively, as depicted (Figure 30B). Further DNA sequencing of the recombinant clone was performed to confirm the cloning.

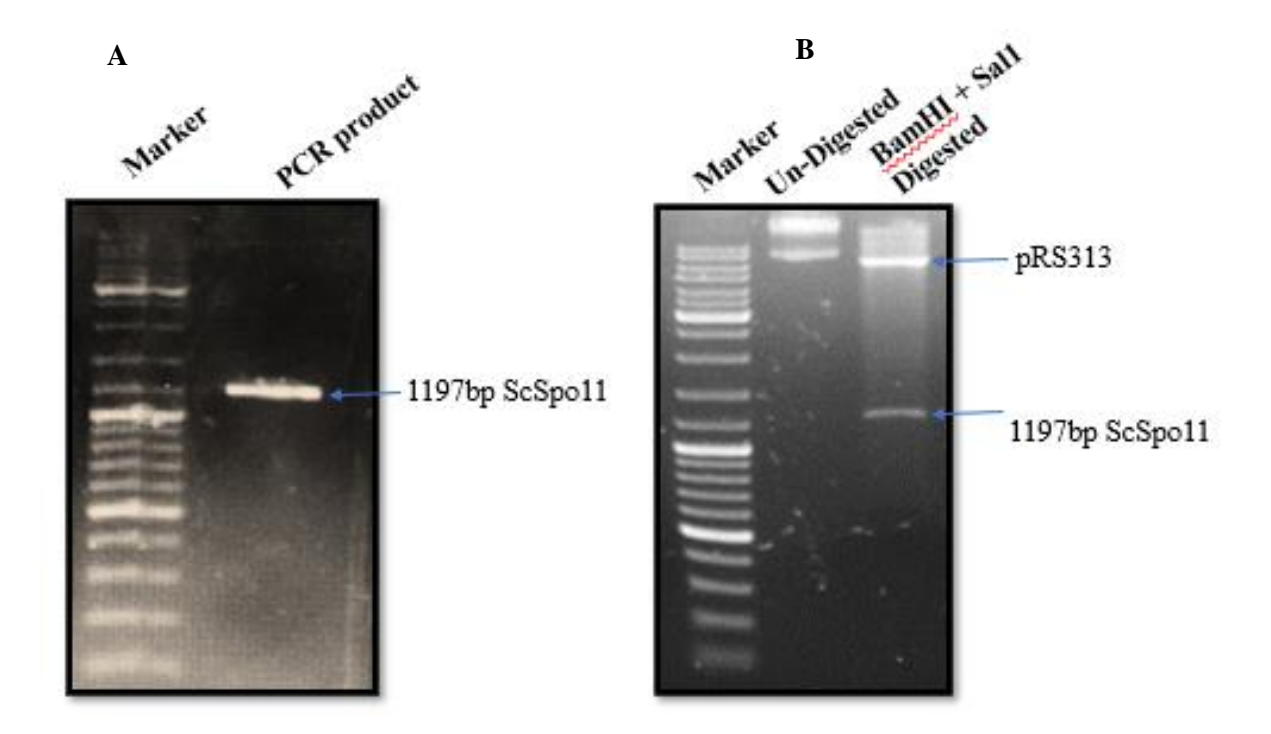


Figure 30. Cloning of ScSPO11, into pHCA vector: (A) Agarose gel image depicting the PCR amplified product of ScSPO11 of 1197bp length. (B) Clone confirmation of pHCA-ScSPO11 was done by the release of insert of size 1197 bp and 5.5 kb pHCA plasmid, respectively upon digestion of the plasmid using BamHI and SalI enzyme.

### A4: Cloning of Full Length *PfmtDNAPolymerase* in *pGADC1* Yeast two-hybrid Vector

PfmtDNAPolymerase was PCR amplified (**Figure 31B**) from cDNA as template using the primers OSB 502 and OSB 503 (**Table 4**). The PCR amplified product was BamHI and SalI double digested and was subsequently ligated with pGADC1 vector using T4 DNA ligase. As the size of PfmtDNApolymerase and pGADC1 were almost equal, the clone was confirmed by digesting the cloned plasmid with EcoRI restriction digestion. The position of the EcoRI site within the insert and in the vector are depicted in the figure. Performing EcoRI digestion, we achieved bands of sizes 2316 bp and 8686 bp (**Figure 31C**) in the confirmed clone as depicted in the schematics (**Figure 31A**). Further DNA sequencing of the recombinant clone was performed to confirm the cloning.

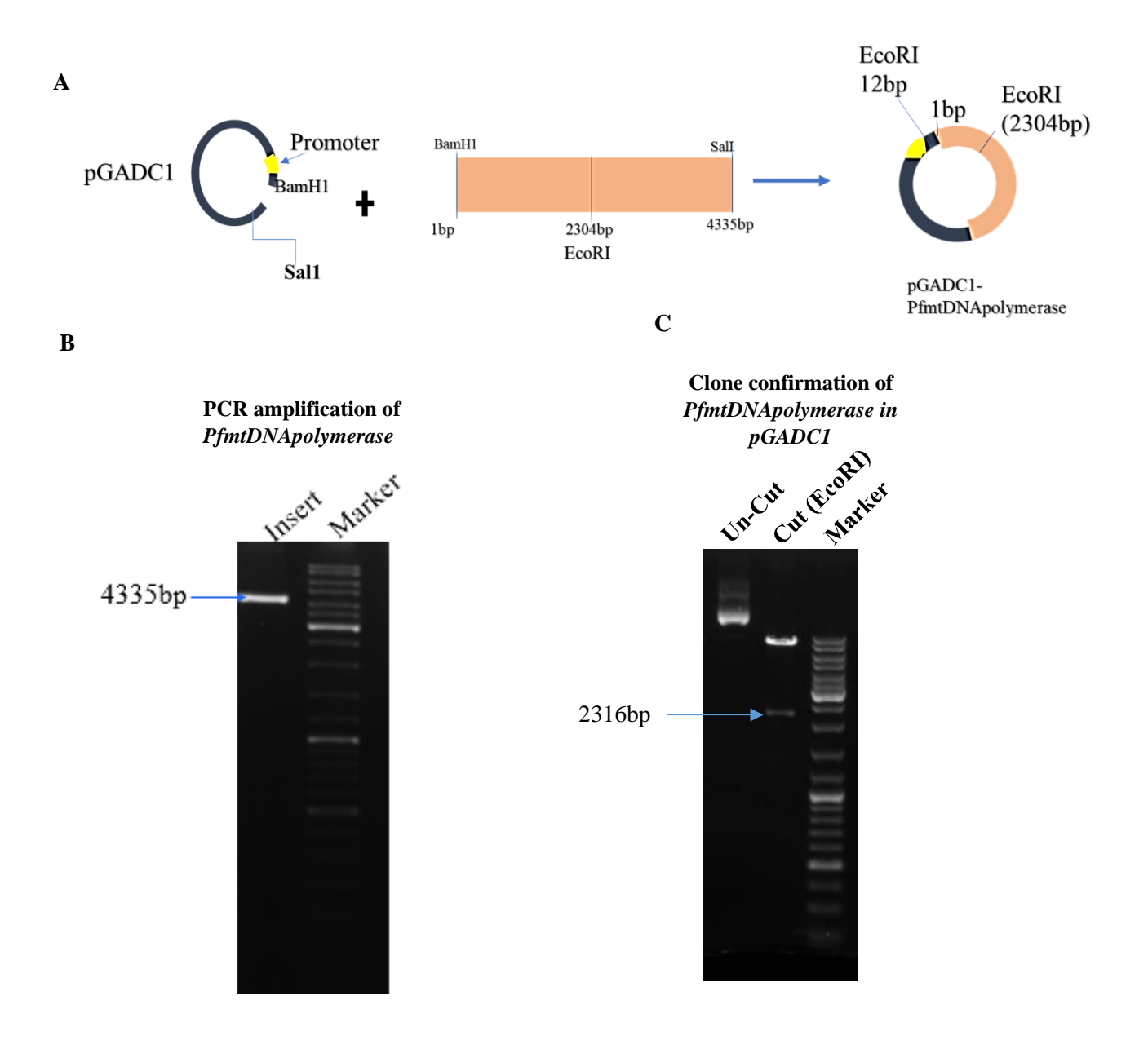


Figure 31: Cloning of PfmtDNAPolymerase in pGADC1 vector: (A) Diagrammatic representation of the cloning strategy. (B) PCR amplification of PfmtDNApolymerase. (C) Clone confirmation of pGADC1-PfmtDNApolymerase was done by the release of insert of size 2316 bp and 8698 bp pGADC1 plasmid, respectively upon digestion of the plasmid using EcoRI enzyme.

Table 3. Yeast strains used in this study

Strains	Genotype			
spo114 BY4743	MATa/MATa			
	$his 3\Delta 1/his 3\Delta 1$ $leu 2\Delta 0/leu 2\Delta 0$ $LYS2/lys 2\Delta 0$ $met 15\Delta 0/MET 15$ $ura 3\Delta 0/ura 3\Delta 0$			
	YHL022c/YHL022c::kanMX4)			
PSY1	MATa/MATa			
	$his 3\varDelta 1/his 3\varDelta 1  leu 2\varDelta 0/leu 2\varDelta 0  LYS2/lys 2\varDelta 0  met 15\varDelta 0/MET 15  ura 3\varDelta 0/ura 3\varDelta 0$			
	YHL022c/YHL022c::kanMX4) pHCA-PfSPO11			
PSY2	MATa/MATa			
	$his 3\varDelta 1/his 3\varDelta 1  leu 2\varDelta 0/leu 2\varDelta 0  LYS2/lys 2\varDelta 0  met 15\varDelta 0/MET 15  ura 3\varDelta 0/ura 3\varDelta 0$			
	YHL022c/YHL022c::kanMX4) pHCA-Pfspo11Y65F			
PSY3	MATa/MATa			
	$his 3\varDelta 1/his 3\varDelta 1  leu 2\varDelta 0/leu 2\varDelta 0  LYS2/lys 2\varDelta 0  met 15\varDelta 0/MET 15  ura 3\varDelta 0/ura 3\varDelta 0$			
	YHL022c/YHL022c::kanMX4) pHCA-ScSPO11			
PSY4	MATa/MATa			
	$his 3\varDelta 1/his 3\varDelta 1  leu 2\varDelta 0/leu 2\varDelta 0  LYS2/lys 2\varDelta 0  met 15\varDelta 0/MET 15  ura 3\varDelta 0/ura 3\varDelta 0$			
	YHL022c/YHL022c::kanMX4) pHCA-Empty			
PJ69-4A	MATα trpl-901 leu 2-3, 112 ura3-52 his3-200 gal 4Δ gal80Δ LYS2::GALi-HIS3			
	GAL2-ADE2 met2::GAL7-lacZ			
PSY5	PJ69-4A+ epGADC1+ epGBDU			
PSY6	PJ69-4A+pGADC1/PfmtDNAPolymerase +epGBDU			
PSY7	PJ69-4A+epGADC1+pGBDU/PfTopoIII			
PSY8	PJ69-4A+pGADC1/PfmtDNAPolymerase + pGBDU/PfTopoIII			

Table 4. Primers used in this study

No.	Name	Sequence	Purpose
1	OSB 94	5' CTGTAACACATAATAGATCCGAC 3'	Forward primer for the amplification of 300-bp amplicon of PfARP gene
2	OSB95	5' TTAACCATCGTTATCATCATTATTTC 3'	Reverse primer for the amplification of 300-bp amplicon of PfARP gene
3	OSB 548	5'GGTGTTCAGTTAGCATCTTC 3'	Forward primer to amplify 332bp fragment of PfTopoVIB C-terminal
4	OSB549	5'CATTCATCTTCACCTTCACC 3'	Reverse primer to amplify 332bp fragment of PfTopoVIB C-terminal
5	OSB 578	5'AAACCAAGATTAACCTTATCTG 3'	Forward primer to amplify 222bp fragment of PfTopoII C-terminal
6	OSB579	5'TTAAATGTTGTATGAACTATCAC 3'	Reverse primer to amplify 222bp fragment of PfTopoII C-terminal
7	OSB 580	5'GGAAAAGGACATAGAATCATG 3'	Forward primer to amplify 357bp fragment of PfGyrA C-terminal
8	OSB 581	5'TCAGATTATGTCAAAATAAACC 3'	Reverse primer to amplify 357bp fragment of PfGyrA C-terminal
9	OSB 582	5'GTGAATGAAGAGGGTTCGAC 3'	Forward primer to amplify 268bp fragment of PfGyrB C-terminal
10	OSB 583	5'CTGATAATGAATTTGTATTTTCC3'	Reverse primer to amplify 268bp long fragment of PfGyrB C-terminal
11	OSB589	5'TGATATGTCCATCGAGAATCTTC 3'	Forward primer to amplify 278bp fragment of PfSpo11 C-terminal
12		5'CCTTAATGCGATTATTTATATGTTC 3'	Reverse primer to amplify 278bp fragment of PfSpo11 C-terminal
13		5'AGCGGTACCGTGGCACCTTGTATGTTTAC 3'	Forward primer to amplify upstream 620bp of PfTopoVIB
14		5'AGCATGCATTATTATACACAACAT AAATATATATA 3'	Reverse primer to amplify upstream 620bp of PfTopoVIB
15		77 5'GCTTCTGATATTATGATAGATAAC 3'	Forward primer to amplify upstream 252bp of PfCox
16		18 5'TTACGGCACATTATCTCACCG 3'	Reverse primer to amplify upstream 252bp of PfCox
17		5'TTCCCCTAGTGTTACATTTGG 3'	Forward primer to amplify upstream 310bp of PfSpo11
18		5'TAGGAAATCATATTTCATTTTAC 3'	Reverse primer to amplify upstream 310bp of PfSpo11
19		5'GACGGATCCATGGCTTTGGAGGGATTGCG 3'	Forward primer for amplification of ScSpo11 for cloning in <i>pHCA</i>
20		5'GACGTCGACTCATTTGTATTCAAAAATTCTGGC 3'	Reverse primer for amplification of ScSpo11 for cloning in pHCA
21		5'GACGGATCCATGCCTCGTCTGGATATC 3'	Forward primer for amplification of PfSpo11 for cloning in pHCA
22		5'GACGGATCCTTATAAAAGCTCCTTAATGCG 3'	Reverse primer for amplification of PfSpo11 for cloning in <i>pHCA</i>
23		5'TATAAATAATTTTGGATTGGTAAAAAATATTTGTC 3'	Reverse primer for making PfSpo11Y65F point mutant
24			Forward primer for making PfSpo11Y65F point mutant
25		5'CAACTTTAAGACAAATATTTTTTACCAATCC 3' 40 5'GAGTGGATTAAATGCCCAGCC 3'	Forward primer for making Pisport Four point mutant  Forward primer for amplification of fragment A
26		5'GCATCTCTACAAACTACAGAG 3'	Reverse primer for amplification of fragment A
27		5'CATTGGAATGAGAGTTCACCG 3'	Reverse primer for amplification of fragment A for Real-Time analysis
28		5' TACTCTGTAGTTTGTAGAGATGC 3'	Forward primer for amplification of fragment B
29 30		5' CCTCACAGCTTTATTCGGTCC 3' 5' TGTATTTTCATCTTTAACTTCTGG 3'	Reverse primer for amplification of fragment B Reverse primer for amplification of fragment B for Real-time analysis
31		15 5' CTGGCCTACACTATAAGAACG 3' 5' CATCCCATAGCAAGTATCATAG 3'	Forward primer for amplification of fragment C
		5' TGAAGAATATAATTCAGTACGTAG 3'	Reverse primer for amplification of fragment C
33			Reverse primer for amplification of fragment C for Real-Time analysis
34		16 5'CTACTGGTTTAGAAGTTGATAC3'	Forward primer for amplification of fragment D
35		17 5'TACTGGAATAGAGGATAACAAG 3'	Reverse primer for amplification of fragment D
36	OSB 599	5'TACTGGTTTAGAAGTTGATACTAG 3'	Forward primer for amplification of fragment D for Real-time analysis
37	OSB 600	5'ATCTTGAAATGCACTTACAGTTG 3'	Reverse primer for amplification of fragment D for Real-Time analysis
38		18 5' GTTATCCTCTATTCCAGTAGC 3'	Forward primer for amplification of fragment E
39		19 5' CATACATCCTAACATTAATAACG 3'	Reverse primer for amplification of fragment E
40	OSB 601	5'TTATCCTCTATTCCAGTAGCAC 3'	Forward primer for amplification of fragment E for Real-Time analysis
41	OSB 602	5'ACGATAGCATTATCAGGATGTG 3'	Reverse primer for amplification of fragment E for Real-Time analysis
42		20 5' CGCTGACTTCCTGGCTAAAC 3'	Forward primer for amplification of fragment F
43		41 5'ATTGTTCTACATTACGAGATACC 3'	Reverse primer for amplification of fragment F
44	OSB 603	5' GAATTGAAGTGTGGAGAGAATC 3'	Reverse primer for amplification of fragment F for Real-Time analysis
45	OSB 502	5' ATCGGATCCATGAAATTGTTTGATTCATTTTTTAAA	1 1
46	OSB 503	5' ATCGTCGACTTATGA AGACTCCTTGTAGACTCC 3	
47	OSB 619	5' GTACTATAGGGCATGTAGATC3'	Forward primer for amplification of Apicoplast genome for ChIP
48	OSB620	5' TCGGAATGTCCTGGACAATC 3'	Reverse primer for amplification of Apicoplast genome for ChIP
49	OSB621	5' ATAGTAGAAGGGTATTTCCATG 3'	Forward primer for amplification of Apicoplast genome for ChIP
50	OSB622	5' CTGATTTTGCACAATTTGAACG 3'	Reverse primer for amplification of Apicoplast genome for ChIP
51	OSB 336	5' TGCGTCGACTGTATATGAGAGCTGATCGGG 3'	Reverse primer to amplify PfTopoIII
52	OSB 337	5'TAGGTATAGCCTTAGTACAATC3'	Forward primer to amplify 3' end of PfTopoIII

# **Synopsis**

School of Life Sciences, Checklist for submission of Ph.D. synopsis

1. Candidate Name: Priyanka Singh

2. Department: Department of Biotechnology and Bioinformatics

3. Ph.D. Registration Number: 17LTPH05

4. Date of the Ph.D. Registration: 08-08-2017

5. Date of Pre Ph.D.-Seminar: 18-05-2023

**8.** Information related to the presentation of research work in conferences:

**6.** Has the candidate completed Ph.D. course work: **Yes** 

7. Marks/Grade obtained in the course work: Pass

1. Poster presentation entitled, 'Study of mitochondrial import and mt-DNA recruitment of

Plasmodium falciparum topoisomerase VI' in Molecular parasitology meeting, MPM XXXII 2021,

Marine Biological Laboratory, Woods Hole, Massachusetts, United States, October 5-9, 2021.

2. **Lightning talk** entitled "Plasmodium Topoisomerase VIB and Spo11 constitute functional type IIB

topoisomerase in the malaria parasite, Future of Malaria Research Symposium, 2022, Johns

Hopkins Bloomberg School of Public Health, Baltimore, Maryland, United States, October

28<sup>th</sup>, 2022.

3. **Oral presentation** entitled, 'Topoisomerase VI: a functional type II mitochondrial topoisomerase

in the malaria parasite Plasmodium falciparum' in BioAnveshna, Symposium on frontiers in

Biotechnology and Bioinformatics, Department of Biotechnology and Bioinformatics,

University of Hyderabad, November 7-8, 2022.

**9.** Details of the research paper published in peer-reviewed journals:

1) Priyanka Singh, Wahida Tabassum, Nupur Fangaria, Sandeep Dey, Siladitya Padhi, Mrinal K.

Bhattacharyya, Kota Arun Kumar, Arijit Roy, and Sunanda Bhattacharyya\*, Plasmodium

- Topoisomerase VIB and Spo11 Constitute Functional Type IIB Topoisomerase in Malaria Parasite: Its Possible Role in Mitochondrial DNA Segregation (2023), **Microbiology Spectrum**, <u>doi:</u> <a href="https://doi.org/10.1128/spectrum.04980-22">https://doi.org/10.1128/spectrum.04980-22</a>
- 2) Nupur Fangaria, Khushboo Rani, Priyanka Singh, Sandeep Dey, Kota Arun Kumar, and Sunanda Bhattacharyya\*, DNA damage-induced nuclear import of HSP90α is promoted by Aha1 (2022), Molecular Biology of the Cell, doi:10.1091/mbc. E21-11-0554
- 3) Priyanka Singh, Khushboo Rani, Akanksha Gotmare, Sunanda Bhattacharyya\*, A tale of topoisomerases and the knotty genetic material in the backdrop of *Plasmodium* biology (2022), Bioscience Reports, doi: 10.1042/BSR20212847
- 4) Wahida Tabassum, **Priyanka Singh**, Niranjan Suthram, **Sunanda Bhattacharyya\***, Mrinal Kanti Bhattacharyya\*, Synergistic action between PfHsp90 inhibitor and PfRad51 inhibitor induces elevated DNA damage sensitivity in the malaria parasite (2021), **Antimicrobial Agents and Chemotherapy**, doi:10.1128/AAC.00457-21
- 5) Shephali Bansod, Navneet Bung, Priyanka Singh, Niranjan Suthram, Himashree Choudhury, Arijit Roy, Gopalkrishnan Balusu, Sunanda Bhattacharyya\*, Elucidation of an essential function of the unique charged domain of *Plasmodium* topoisomerase III (2020), Biochemical Journal, doi: 10.1042/BCJ20200318
- 10. Has the candidate enclosed a soft copy of the synopsis: Yes
- 11. List of six examiners with their designations, web links, email, and numbers: Enclosed
- **12.** Synopsis and references (Only abstract and summary of the work not more than 10% of the thesis):

Malaria is a life-threatening disease caused by the unicellular eukaryotic parasite of genus *Plasmodium*. The disease affects millions of people every year and poses a significant public health challenge worldwide. The World Malaria Report 2022 published by the World Health Organization (WHO), estimated 247 million cases of malaria worldwide and 619 000 malaria-related deaths. Approximately 80% of malaria deaths were among children under the age of five [1]. Malaria control and eradication attempts are significantly hampered by antimalarial drug resistance, especially in regions where the disease is endemic. Resistance occurs when malaria parasites develop mutations in their genes that allow them to survive and reproduce in the presence of the drug [2]. To counteract this resistance, new medications and drug combinations have been designed, and current research is aimed at deciphering the causes of resistance and creating novel targets and target proteins for the treatment of malaria.

Malaria parasite undergoes a non-canonical method of cell division during its development which is known as endoreduplication. Endoreduplication is a process in which cells undergo multiple rounds of genome replication without the cell division resulting in the production of multiple nuclear and organelle genome within a single cell which further get distributed to the daughter merozoites after proper segregation [3-5]. In malaria parasites, endoreduplication plays an essential role in the development of the parasite within the host's red blood cells. This endoreduplication process occurs twice in the human host (liver stage and blood stage) and once inside the midgut of mosquito host. This process enables the enhanced rate of infectivity of the parasite within the host.

Mitochondrion of the malaria parasite is now being explored as an antimalarial target due to its divergence from human host mitochondria [6]. *Plasmodium* mt-DNA is a 6 kb long linear dsDNA that is associated with each other (about twenty copies) in the form of linear concatemers [7]. Electron microscopy and two-dimensional gel electrophoresis showed that parasite mitochondrial genome undergoes rolling circle mode of DNA replication [8] and during that process, recombination happens between the multiple copy of genomes. As a result, a long and highly branched DNA structure, arranged in the form of single-strand and double-strand concatemers, are being generated [9]. These catenated genomes need to be properly segregated into the newly formed rings. However, the Type I/II topoisomerases involved in mitochondrial DNA replication/segregation of malaria parasite have not been identified yet.

Topoisomerases are now being considered as a novel target to conquer malaria due to their essential role in DNA replication and repair. They play a crucial role in the biology of *Plasmodium* by regulating DNA topology and few of these unique topoisomerases are absent from the human genome [10]. Topoisomerases help to relieve the tension caused by the formation of knots and tangles in DNA that can lead to cell death. In this study, we aimed to understand the role of topoisomerases in the mitochondrial genome maintenance of the malaria parasite and their potential as targets for new antimalarial therapies.

Topoisomerases are categorized as type I and type II topoisomerases. Type I topoisomerases are classified into two subtypes, IA and IB, based on their mechanism of action. Type I topoisomerases are monomeric enzymes, cut a single strand of DNA and perform their activity independent of ATP and remain transiently associated with either 3' or 5' phosphoryl group [11]. Type IA topoisomerases join and cleave ssDNA before permitting a second single strand to pass through the transient break. It has long been considered that a protein-mediated DNA gate is involved in this strand transit mechanism [12].

Type II topoisomerases are dimeric proteins, that are divided into two subtypes, IIA and IIB based on their domain organization. Type IIA topoisomerases use the N-gate, DNA-gate, and C-gate protein interphases to perform their function. The N-gate (entry gate) is the point at which the DNA segment that needs to be cut, enters the enzyme making enzyme bound DNA duplex (G-Segment). When ATP is bound, the amino-terminal domain begins to dimerize, closing the entry N-gate, transiently cleaving the G segment, and releasing the second DNA duplex (T segment) through the third gate, known as the C-gate. After that, the G section is ligated [13]. Type IIB topoisomerases, on contrary, carry out their action through two protein gates and do not possess C-gate. After cleaving the G segment, they immediately release the T segment through the G gate. This type of topoisomerases has two subunits, A and B; while the DNA binding and cleavage domains are found in the A subunit, the ATPase domain is found in the B subunit.

Nuclear genome of the malaria parasite encodes both type I and Type II topoisomerases. The *Plasmodium* genome comprises of Topoisomerase III (PfTopoIII) and Topoisomerase IB (PfTopoI)

from the Type I family. Type IIA, topoisomerases encoded by *Plasmodium falciparum* genome are, Topoisomerase II (PfTopoII) and Gyrase (PfGyrase). Topoisomerase VI (PfTopoVI) belongs to the Type IIB topoisomerases in malaria parasite [10].

Our first specific aim was to understand the function of PfTopoVI in the biology of the malaria parasite. Genetic studies of TopoVI in *Arabidopsis thaliana* revealed that Topoisomerase VI is essential for decatenation of replicated chromosome during endoreduplication [14]. Topoisomerase VI knock out plants showed dwarf phenotype; it was observed that the mutant-plants display only 8C nuclei, unlike the 32C nuclei seen in the wild-type plant. This result suggested that Topo VI is required for the proper progression of endoreduplication in Arabidopsis. Earlier research in our lab demonstrates that PfTopoVIB and PfSpo11 (TopoVIA) together can reverse the lethal phenotype of yeast *topoII* mutants [15]. Also, the yeast cell extract harboring PfTopoVIB and PfSpo11 can relax supercoiled plasmid DNA and decatenate kDNA in an ATP and magnesium-dependent manner [15]. However, their specific function in *Plasmodium* biology remains unknown.

Topoisomerase VI was first discovered in *Sulpholobus shibatae* [16], and later in the plants. TopoVIA and TopoVIB are the two subunits of the functioning enzyme found in plants and algae. TopoVIB has the GHKL domain, which is important for ATP binding and ATP hydrolysis, whereas TopoVIA contains the DNA binding and DNA cleavage domain. It has been established that ATP binding to the TopoVIB is essential for providing the energy required during DNA cleavage. Spo11 is the eukaryotic orthologue of TopoV1A. The PfTopoVI subunits, PfSpo11 (ID: PF3D7\_1217100) and PfTopoVIB (ID: PF3D7\_1365600), are both present in *Plasmodium*. Using the yeast two hybrid assay, it has been demonstrated previously that PfTopoVIA and PfTopoVIB subunits associate with each other. Furthermore, it was demonstrated that Radicicol inhibits the decatenation activity of the enzyme [15]. Treatment of Radicicol lowered the parasite's mitochondrial genome content at sub-lethal levels, however the mechanism behind that was not determined.

In this study, we hypothesise that PfTopoVI (PfSpo11 and PfTopoVIB) plays a role in the decatenation of replicated chromosomes *i.e.*, segregation of chromosomes during the endoreduplication process. We designed the following objectives:

1. To investigate whether PfSpo11 is the catalytic subunit of TopoVI enzyme

- 2. To determine whether PfTopoVI is expressed at the stage where mitochondrial genome segregation occurs
- 3. Whether PfSpo11 and PfTopoVIB constitute the functional holoenzyme within the parasite
- 4. Whether PfTopoVI is a mitochondrial topoisomerase of the malaria parasite

We attempted to express the recombinant PfSpo11 protein in several bacterial systems to assess the function of PfSpo11; however, we were not successful, so we used yeast as a surrogate system. It is established that, diploid budding yeast undergoes meiosis in response to nitrogen deprivation and produce haploid nuclei during meiosis which are further packaged into spores [17]. Spo11 is established protein in yeast that triggers the meiosis, by catalysing the breakage of double strand DNA which is then repaired by recombination between the paternal chromosomes. In plants, Spo11 and TopoVIB form a functional complex, whereas in yeast, Spo11 catalyses the double strand breaks (DSBs) by interacting with several other proteins without TopoVIB. Sequence analysis revealed that the active site tyrosine yeast Spo11 is essential for its DSB induction activity [18]. We did the pairwise alignment of PfSpo11 along with ScSpo11 and observed that the catalytic tyrosine residue (the 65th amino acid) is conserved in *Plasmodium* Spo11. We created a point mutation (Y to F) to the catalytic tyrosine residue of *PfSPO11* using site-directed mutagenesis and cloned it in a yeast centromeric expression plasmid. We used diploid \$\Delta spo11\$ yeast strain and generated four isogenic strains by transforming the following 4 centromeric vectors as: empty vector (negative control), PfSPO11, PfSPO11<sup>Y65F</sup>, and ScSPO11 (positive control). The four strains were then allowed to sporulate by growing individually in the sporulation medium and we measured the spore forming ability in each one of them. We stained the nucleus of each strain with DAPI and, the spore development was observed using a fluorescence microscope. It was discovered that the strain expressing PfSPO11 can overcome the sporulation deficiency of the \( \Delta spo11 \) strain like that of the strain expressing ScSpo11. Our study showed that PfSpo11 or ScSpo11-expressing strains formed 4 distinct nuclei, however the catalytic mutant of PfSpo11 was unable to sporulate. We measured the sporulation efficiency of each strain and observed that while the \( \Delta spo 11 \) strain showed 1.1% efficiency, the ScSPO11- harbouring strain's sporulation efficiency (6.6%) was comparable to that of the PfSPO11- harbouring strain's (8.3%), but the catalytic mutant PfY65Fspo11 had a severe sporulation defect and showed 1.7% frequency, which is same as that of the \( \Delta spo 11 \) strain. Thus, our study establishes that PfSpo11 is the functional ortholog of ScSpo11 and its nuclease activity is essential for the enzyme activity.

Malaria parasite undergoes various morphological changes during its complex multi-stage life cycle. Live-cell imaging identified three distinct schizont stages during the asexual development of the parasite namely, Early (ES), Mid (MS) and Late-schizonts (LS). It was identified that the nuclear and apicoplast genome segregation of the malaria parasite take place in the early and mid-schizont stages, respectively, whereas the mitochondrial genome segregation takes place just before the cell division *i.e.*, at the late-schizont stage of the *Plasmodium falciparum* [19].

To understand the potential role of PfTopoVI, at the stage where mitochondrial genome segregation occurs, we assessed the expression of the all-Type II topoisomerase subunits at three different developmental stages of schizont. We employed tightly synchronised early schizont (ES) stage-specific parasites at 35–36 hpi (hours-post-invasion), mid-schizont (MS) at 39-40 hpi, and late-schizont (LS) at 44-45 hpi for all our assays and performed semi-quantitative RT-PCR analysis. Our result showed that PfTOPOVIB and PfSPO11 had a distinct expression pattern in contrast to other Type II topoisomerases and were not expressed in the ES and MS stages. Expression of Plasmodium TOPOVI subunits were induced only at the LS of the parasite which marks the cease of nuclear division. Realtime RT-PCR and western blotting further confirmed the induced expression of both the subunits of PfTopoVI at the LS of the parasite. The result showed that PfSpo11 and PfTopoVIB expressions were upregulated 5-times and 10-times respectively at the LS stage compared to the ES/MS stage of the parasite. Indirect immunofluorescence assay was performed to monitor the expression of PfTopoVI subunit at the three different schizont phases of the parasite. The Alexa Red 594 conjugated secondary antibody was utilised to observe the red fluorescence for both PfTopoVIB and PfSpo11. The nucleus was stained with DAPI. We studied hundreds of cells and discovered that both subunits have their highest expression in the parasite's late schizont stage, indicating the likely role of PfTopoVI in mitochondrial genome segregation but not in replication.

To validate the unique expression pattern of PfTopoVI, we looked at the chromatin compaction of the promoter regions of *PfTOPOVIB* and *PfSPO11* at various phases of the parasite's growth. To accomplish this, we have employed FAIRE (Formaldehyde-Assisted Isolation of Regulatory Elements) assay, which

enables one to ascertain whether a particular region of chromatin is in the nucleosome free state, or the nucleosome bound state. By performing FAIRE at three tightly synchronized schizont stages of the parasite, we found that the promoter of PfTOPOVIB remained in hetero-chromatinized state at the ES and the MS stages, whereas it is shifted to the nucleosome-free state at the LS stage of the parasite. The promoter of PfSPO11 showed the similar trend to that of UAS PfTOPOVIB. Quantification of gel images revealed 25-fold and 4-fold relaxation in the chromatin compaction of the PfTOPOVIB and the PfSPO11 promoter respectively at the LS stage of the parasite compared to the MS stage respectively. We also assessed the occupancy of two well-established epigenetic marks, namely the activation mark H3K4me3 and the repression mark H3K9me3, to the promoter-proximal regions of PfTOPOVIB and PfSPO11 at three schizont stages of the parasite. To do this, we used anti-H3K4me3, anti-H3K9me3, or IgG antibodies in chromatin immunoprecipitation analysis. At the promoter-proximal region of PfTOPOVIB and PfSPO11, respectively, we discovered 6-fold and 2-fold enrichments of H3K4me3, at the LS stage compared to the MS stage. On the other hand, we observed that the recruitment of H3K9me3 at the PfTOPOVIB UAS and PfSPO11-1 UAS, were gradually decreased from ES to LS stage. Thus, our findings conclude that the promoter-proximal sequences of PfTOPOVIB and PfSPO11 undergo active transcription only at the LS stage.

We determined the localization of PfTopoVI subunits inside the malaria parasite. We used anti-Cytc antibody to visualize the green fluorescence of mitochondrial protein Cytc. We determined the average Pearson Correlation Coefficient (PCC) for 20-25 images to evaluate whether red-signals specific to PfTopoVIB or PfSpo11 colocalise with the green fluorescence of Cytc. We also calculated the average Pearson Correlation Coefficient (PCC) to evaluate the localisation of PfTopoVIB or PfSpo11 with the nuclear stain DAPI. We infer that both the subunits are predominantly present in mitochondria of the malaria parasite with a stronger correlation with Cytc (PCC > 0.8) and moderate correlation with DAPI (PCC < 0.5).

To establish that PfSpo11 and PfTopoVIB forms a holoenzyme complex inside malaria parasite, we determined the physical association between PfTopoVIB and PfSpo11 within the parasite by employing co-immunoprecipitation assay. The LS stage specific parasites were immunoprecipitated with PfSpo11 specific antibody and the pellet fraction was probed with PfTopoVIB antibody. We found that

PfTopoVIB was co-precipitated with PfSpo11, thus establishing a physical association between the two subunits. Immunoprecipitation with IgG was used as a negative control, and we didn't detect any PfTopoVIB protein in the IgG pull-down pellet fraction.

To establish the possible function of PfTopoVI in the mitochondrial genome segregation, we performed chromatin immunoprecipitation (ChIP) assay to detect the recruitment of PfTopoVIB and PfSpo11 to the mitochondrial genome in the presence or absence of formaldehyde cross-linking. We found specific binding of PfTopoVIB and PfSpo11 to the mt-genome at the LS-stage specific parasites. We monitored the recruitment at synchronous ES, MS and LS stage specific parasites and quantified the percent occupancy of PfTopoVIB to mitochondrial DNA with respect to the input by employing quantitative PCR (qPCR). We observed that PfTopoVIB recruitment to the mt-DNA is positively correlated with its expression and is significantly enriched at the LS stage of the parasites compared to the other stages. To evaluate the specificity of the recruitment towards any specific parts of mt-DNA, we used a set of six primers (A to F), each amplifying around 1 kb long mt-genome, thereby, covering the whole 6 kb of the mitochondrial genome. While A to E primer sets were used to amplify the intra-mitochondrial DNA, the F primer amplifies the junctional sequence and produces amplicon when two monomeric mt-DNA units form concatemers. The quantitative PCR analysis showed no significant difference towards the occupancy of PfTopoVIB and PfSpo11 to any specific regions mt-genome. Additionally, we observed that the association of both subunits is specific only to mitochondrial genome but not to the apicoplast genome. Together, our data suggest that PfTopoVI may have a role in mitochondrial genome segregation during the late schizont stage of the parasite.

It is established that Atovaquone collapses the parasite's mitochondrial membrane potential. We hypothesised that treatment of Atovaquone would reduce the import of PfTopoVI subunits into the mitochondria. On the other hand, because PfTopoVI is crucial in maintaining the mitochondrial genome, inhibition of this enzyme complex with Radicicol should affect the mitochondrial genome replication. Indeed, our earlier experimental data showed that Radicicol treatment reduces the mitochondrial genome content of the parasite significantly, without having any effect on nuclear and/or Apicoplast genome content [20]. Thus, we hypothesise that Atovaquone and Radicicol should potentiate one another's effects. To prove that, first we determined the IC<sub>50</sub> values for Atovaquone and Radicicol

to 3D7 parasite and determined that to be 1.4 nM and 8.05  $\mu$ M respectively. We noticed that there is a substantial decrease in the IC<sub>50</sub> of Atovaquone from 1.4 nM to 0.12 nM when identical experiment was carried out in the presence of IC<sub>50</sub> concentration of Radicicol (8.05  $\mu$ M). Radicicol offered Atovaquone an 11.7-fold potentiation. Similarly, we found that the Atovaquone potentiated the action of Radicicol and shifted the IC<sub>50</sub> concentration of Radicicol from 8.05  $\mu$ M to 1.7 $\mu$ M, thus potentiating Radicicol by 4.7-fold. We further investigated whether the interaction between the PfTopoVI inhibitor Radicicol and the Atovaquone is additive or synergistic. We determined the fractional inhibitory concentration (FIC) by running a fixed ratio drug combination experiment and plotting the dose-response curves. The sum FIC was then plotted in the isobologram. The isobologram analysis demonstrates synergistic interaction between Radicicol and Atovaquone. We employed an unrelated drug Chloroquine and checked its interaction with Radicicol to examine the specificity of the Radicicol-Atovaquone interaction. Isobologram analysis revealed an  $\Sigma$ FIC $\ge$ 1 indicating additive interaction between Chloroquine and Radicicol.

To support our conclusion further, we wanted to determine whether Atovaquone treatment really affects the mitochondrial import and the mitochondrial DNA recruitment of PfTopoVI. To that end, the synchronous mid-trophozoite specific parasite culture was treated with increasing doses of Atovaquone and the treated parasites were allowed to grow until they reached the late-schizont stage. We calculated the average PCC values from 25 individual cells that were treated with 0.5 nM Atovaquone and compared with that of the untreated parasites. We observed that in Atovaquone (0.5 nM) treated parasite, the average PCC values were shifted from 0.835 to 0.66 in case of PfTopoVIB and the same was shifted from 0.871 to 0.69 in case of PfSpo11. We conclude that the degree of colocalization between PfTopoVI with Cytc has decreased in Atovaquone treated parasites. To validate this further, we determined the recruitment of these two subunits to the mitochondrial genome in Atovaquone treated condition. We observed about 30% reduction in the occupancy of PfTopoVIB to the mito-genome in the presence of the sublethal doses (0.5 nM) of Atovaquone, which further showed reduction at higher concentration of Atovaquone. We noticed similar result when we looked at the mitochondrial genome recruitment of PfSpo11 at each of the three Atovaquone treated conditions. Real-time quantification analysis revealed

a dose dependant reduction in the recruitment of both PfTopoVIB and PfSpo11 to the mitochondrial genome.

To end with, we conclude that due to its absence in humans, *Plasmodium* Topoisomerase VI, can be used as a potential anti-malarial target. Although human and Plasmodium Spo11 share some structural similarities, however, there is only 10% sequence identity between the mouse/human TopoVIBL (TopoVIB like protein) and PfTopoVIB. PfTopoVIB and HsTopoVIBL structures were retrieved from the Alpha Fold database [21] and structure alignment was performed using VMD (Visual molecular dynamics) [22]. It was predicted that structures of these two proteins differ significantly in the Bergerat fold, which is the ATP binding pocket of PfTopoVIB, and the core motifs (N, G1 and G2) of the B-fold do not superimpose with the similar fold found in human VIBL protein and difference in spatial orientation of these core elements was detected. As a result, a particular inhibitor that binds to the ATP binding site of PfTopoVIB is less likely to prevent the human TopoVIBL protein from performing its function. Radicicol used in our study is a pan-inhibitor of Hsp90 and can bind to the Bergerat fold region present in the human Hsp90, However, aside from this Bergerat fold, TopoVIB and Hsp90 are quite distinct molecules. Any inhibitor that precisely targets the PfTopoVIB subunit will limit the activity of the complete PfSpo11-TopoVIB enzyme complex and stop the parasite's endoreduplication. Our second specific aim was to understand whether PfTopoIII is the Type I topoisomerase that is required for mitochondrial DNA maintenance in malaria parasite. Previous work in our lab established that PfTopoIII is localized in both nuclear and mitochondria of the parasite. The mitochondrial DNA polymerase of malaria parasite showed interaction with the PfRad51 and PfBlm [23], however if PfTopoIII is a mitochondrial topoisomerase, it should interact with mtDNA polymerase of the malaria parasite. In human, TopoIIIα is essential for maintenance of the mtDNA, and cells depleted with TopoIIIα showed significant loss of monomeric mtDNA and form large catenated networks [24]. To understand whether PfTopoIII has any role in mtDNA replication/ segregation of the parasite, we developed the following objectives, which provided the framework for the investigation:

- 1. To study the stage specific expression of *PfTOPOIII* at different replicative stages of *Plasmodium*
- 2. To study whether PfTopoIII is part of the mitochondrial replisome
- 3. To study whether PfTopoIII is associated with the mitochondrial genome of the malaria parasite

We monitored the stage specific expression of *PfTOPOIII* at three tightly synchronized schizont developmental stages of the malaria parasite, Early (ES), Mid (MS) and Late-Schizont (LS) stage. The semi-quantitative PCR analysis showed that *PfTOPOIII* expression was present at all the schizont stages, and it is maximum at the late-schizont stage of the parasite. We further validated the expression by performing western blot analysis at three schizont stages of the parasite by using PfTopoIII specific antibody and after normalizing the loading control Actin, we observed that PfTopoIII expression is visible at all the schizont stages of the parasite, being maximum at the LS of the parasite, indicating its likely role in mitochondrial genome segregation that is reported to occur at LS stage.

To validate whether PfTopoIII is a part of mitochondrial replisome, we investigated its interaction with the mitochondrial DNA polymerase of the malaria parasite. We performed yeast two hybrid analysis to monitor the interaction of PfTopoIII with the mitochondrial DNA polymerase. Yeast two hybrid analysis showed that PfTopoIII interacted with PfmtDNA polymerase. Together our results indicate that PfTopoIII is a mitochondrial topoisomerase of malaria parasite *Plasmodium falciparum*.

To investigate whether PfTopoIII is associated with the mt-genome, we used four tightly synchronised developmental phases of the parasite—the ring (R), trophozoite (T), early schizont (ES), and late schizont (LS) and performed chromatin immunoprecipitation (ChIP) assay. PfTopoIII specific antibody was used in ChIP analysis and the immuno-precipitated samples were amplified using six-set of primers (A-F) as described above. We found that PfTopo III is primarily recruited to the terminal end of the mtDNA (F-set primer) during the late schizont stage. PfTopoIII recruitment was also minimal in the R, T, and ES stages but increased in the LS stage, indicating its possible role of in the decatenation of mtDNA during segregation. We wanted to identify the domains in PfTopoIII that are responsible for its binding to the mt-genome. Topoisomerase III of malaria parasite (Gene ID: PF3D7\_1347100) encodes a 710 amino acid long protein. The full-length enzyme shares 39% sequence identity with its human orthologue, and there are few variations between the amino acid sequences of PfTopoIII and hTopIII. PfTopoIII has a distinct charged 85-amino-acid long stretch (ranging amino acids 259-337) in domain II, which is absent in hTopoIII, although, the TOPRIM domain and catalytic tyrosine residue in the GYISYPRTET motif are preserved. All eukaryotic Topo III lacks the charged amino acids) in length.

To understand the structure-function relation of this domain, we performed molecular dynamic simulations of PfTopoIII structure along with a single-stranded DNA octamer (5' CGCAACTT 3'). It was observed that the enzyme undergoes a conformational shift upon DNA-binding, and the charged domain makes contact with the DNA, thereby stabilizes the DNA bound form of the enzyme [25]. It has been suggested that in case of E. coli TopoIII, the charged domain is crucial for the enzyme's efficient binding to DNA [26]. To examine the functional importance of the charged domain of PfTopoIII, two transgenic parasite lines were created in lab; one that expressed the wild-type PfTopoIII fused to GFP and the mutant PftopoIII-GFP with a deletion of charged domain. We immunoprecipitated the genome of two aforementioned transgenic parasites using anti-GFP antibody from the synchronous schizont stages of the parasites. We measured the recruitment of mutant PftopoIII(259-337) towards the mtDNA and compared with that of wild-type PfTopoIII. Our study showed that the mutant PftopoIII<sup>(259-</sup> <sup>337)</sup> protein displayed a considerably reduced interaction with the mtDNA [25]. Together, we conclude that PfTopoIII expression coincides with its recruitment to the mt-genomes of the malaria parasite. Further its association with the mitochondrial polymerases indicates its function as a mitochondrial replisome of the parasite. Specific association with the terminal region of the mtDNA indicate the involvement of PfTopoIII in the decatenation of the catenated mtDNA to aid in mtDNA segregation at the late schizont stage of the parasite; and also established that the charged amino-acid region of PfTopoIII is essential for its effective association with the mtDNA.

In conclusion, through our research we have discovered and characterized *Plasmodium* topoisomerase VIB and Spo11 as functional Type IIB topoisomerase and Topoisomerase III as a Type I topoisomerase in the malaria parasite. We established a possible role for these proteins in the segregation of mitochondrial DNA, that occurs at the late-schizont stage of the parasite. This could have implications for better understanding the parasite biology and treatment of malaria as the maintenance and proper distribution of genome during the parasite's life cycle is essential for its infectivity.

### References

- 1. Organization, W.H., World malaria report 2022. 2022: World Health Organization.
- 2. Goodman, C.D., H.D. Buchanan, and G.I. McFadden, *Is the mitochondrion a good malaria drug target?* Trends in parasitology, 2017. **33**(3): p. 185-193.
- 3. Matthews, H., C.W. Duffy, and C.J. Merrick, *Checks and balances? DNA replication and the cell cycle in Plasmodium.* Parasites & vectors, 2018. **11**: p. 1-13.
- 4. Reilly, H.B., et al., *Quantitative dissection of clone-specific growth rates in cultured malaria parasites.* International journal for parasitology, 2007. **37**(14): p. 1599-1607.
- 5. Murray, L., et al., *Multiplication rate variation in the human malaria parasite Plasmodium falciparum.* Scientific reports, 2017. **7**(1): p. 6436.
- 6. Hikosaka, K., et al., *Mitochondria of malaria parasites as a drug target*. An Overview of Tropical Diseases, 2015.
- 7. Wilson, R. and D.H. Williamson, *Extrachromosomal DNA in the Apicomplexa*. Microbiology and Molecular Biology Reviews, 1997. **61**(1): p. 1-16.
- 8. Preiser, P., et al., *Recombination associated with replication of malarial mitochondrial DNA*. The EMBO journal, 1996. **15**(3): p. 684-693.
- 9. Kyes, S.A., et al., *A well-conserved Plasmodium falciparum var gene shows an unusual stage-specific transcript pattern.* Molecular microbiology, 2003. **48**(5): p. 1339-1348.
- 10. Singh, P., et al., A tale of topoisomerases and the knotty genetic material in the backdrop of *Plasmodium biology.* Bioscience Reports, 2022. **42**(6): p. BSR20212847.
- 11. Slesarev, A.I., et al., *DNA topoisomerase V is a relative of eukaryotic topoisomerase I from a hyperthermophilic prokaryote*. Nature, 1993. **364**(6439): p. 735-737.
- 12. Dekker, N., et al., *The mechanism of type IA topoisomerases*. Proceedings of the National Academy of Sciences, 2002. **99**(19): p. 12126-12131.
- 13. Lee, I., K.C. Dong, and J.M. Berger, *The role of DNA bending in type IIA topoisomerase function.* Nucleic acids research, 2013. **41**(10): p. 5444-5456.
- 14. Sugimoto-Shirasu, K., et al., *DNA topoisomerase VI is essential for endoreduplication in Arabidopsis*. Current Biology, 2002. **12**(20): p. 1782-1786.
- 15. Chalapareddy, S., et al., *Radicicol-mediated inhibition of topoisomerase VIB-VIA activity of the human malaria parasite Plasmodium falciparum*. Msphere, 2016. **1**(1): p. e00025-15.
- 16. Bergerat, A., D. Gadelle, and P. Forterre, *Purification of a DNA topoisomerase II from the hyperthermophilic archaeon Sulfolobus shibatae. A thermostable enzyme with both bacterial and eucaryal features.* Journal of Biological Chemistry, 1994. **269**(44): p. 27663-27669.
- 17. Neiman, A.M., *Sporulation in the budding yeast Saccharomyces cerevisiae*. Genetics, 2011. **189**(3): p. 737-765.
- 18. Keeney, S., C.N. Giroux, and N. Kleckner, *Meiosis-specific DNA double-strand breaks are catalyzed by Spo11, a member of a widely conserved protein family.* Cell, 1997. **88**(3): p. 375-384.
- 19. van Dooren, G.G., et al., *Development of the endoplasmic reticulum, mitochondrion and apicoplast during the asexual life cycle of Plasmodium falciparum.* Molecular microbiology, 2005. **57**(2): p. 405-419.
- 20. Chalapareddy, S., et al., *Radicicol confers mid-schizont arrest by inhibiting mitochondrial replication in Plasmodium falciparum*. Antimicrobial agents and chemotherapy, 2014. **58**(8): p. 4341-4352.
- 21. Jumper, J., et al., *Highly accurate protein structure prediction with AlphaFold.* Nature, 2021. **596**(7873): p. 583-589.
- 22. Humphrey, W., A. Dalke, and K. Schulten, *VMD: visual molecular dynamics.* Journal of molecular graphics, 1996. **14**(1): p. 33-38.
- 23. Jha, P., et al., Bloom helicase along with recombinase Rad51 repairs the mitochondrial genome of the malaria parasite. Msphere, 2021. **6**(6): p. e00718-21.

- 24. Nicholls, T.J., et al., *Topoisomerase*  $3\alpha$  *is required for decatenation and segregation of human mtDNA*. Molecular cell, 2018. **69**(1): p. 9-23. e6.
- 25. Bansod, S., et al., *Elucidation of an essential function of the unique charged domain of Plasmodium topoisomerase III.* Biochemical Journal, 2020. **477**(24): p. 4745-4767.
- 26. Li, Z., et al., *Identification of a unique domain essential for Escherichia coli DNA topoisomerase III-catalysed decatenation of replication intermediates.* Molecular microbiology, 2000. **35**(4): p. 888-895.

# PORTLAND PRESS

# Research Article

# Elucidation of an essential function of the unique charged domain of *Plasmodium* topoisomerase III

Shephali Bansod<sup>1</sup>, Navneet Bung<sup>2</sup>, Priyanka Singh<sup>1</sup>, Niranjan Suthram<sup>3</sup>, Himashree Choudhury<sup>1</sup>, Arijit Roy<sup>2</sup>, Gopalakrishnan Bulusu<sup>2</sup> and <sup>©</sup> Sunanda Bhattacharyya<sup>1</sup>

Correspondence: Sunanda Bhattacharyya (sdeb70@gmail.com)

Topoisomerase III (TopoIII) along with RecQ helicases are required for the resolution of abnormal DNA structures that result from the stalling of replication forks. Sequence analyses have identified a putative Topolll in the *Plasmodium falciparum* genome (PfTopolll). PfTopoIII shows dual nuclear and mitochondrial localization. The expression and association of PfTopoIII with mtDNA are tightly linked to the asexual replication of the parasite. In this study, we observed that PfTopoIII physically interacts with PfBIm and PfWrn. Sequence alignment and domain analyses have revealed that it contains a unique positively charged region, spanning 85 amino acids, within domain II. A molecular dynamics simulation study revealed that this unstructured domain communicates with DNA and attains a thermodynamically stable state upon DNA binding. Here, we found that the association between PfTopolII and the mitochondrial genome is negatively affected by the absence of the charged domain. Our study shows that PfTOPOIII can completely rescue the slow growth phenotype of the ∆topolll strain in Saccharomyces cerevisiae, but neither PfY421FtopoIII (catalytic-active site mutant) nor Pf(Δ259-337)topoIII (charged region deletion mutant) can functionally complement ScTOPOIII. Hydroxyurea (HU) led to stalling of the replication fork during the S phase, caused moderate toxicity to the growth of P. falciparum, and was associated with concomitant transcriptional up-regulation of PfTOPOIII. In addition, ectopic expression of PfTOPOIII reversed HU-induced toxicity. Interestingly, the expression of Pf(\( \Delta 259 - 337 \)) topollI failed to reverse HU-mediated toxicity. Taken together, our results establish the importance of TopolII during Plasmodium replication and emphasize the essential requirement of the charged domain in PfTopoIII function.

# Introduction

Malaria is a life-threatening disease caused by *Plasmodium* parasites. According to the latest report of the World Health Organization, there were 228 million cases of malaria worldwide in 2018 (https://www.who.int/news-room/feature-stories/detail/world-malaria-report-2019). Because the parasite has begun to develop resistance to antimalarial medicines [1–3], it is necessary to identify novel targets that are essential to the parasite's biology. Topoisomerases are attractive targets because they are required for cellular function; indeed they are currently being used to successfully treat bacterial infection [4] and cancer [5]. This group of enzymes is essential for DNA metabolism and plays a crucial role during DNA replication, transcription, recombination, and repair. There are two subgroups of topoisomerases, categorized based on their mode of action: Type I and Type II [6]. PfTopoII [7], PfGyrase [8–10], and PfTopoVI [11,12] are Type II topoisomerases, which have been characterized in detail.

Received: 24 April 2020 Revised: 27 September 2020 Accepted: 26 November 2020

Accepted Manuscript online: 26 November 2020 Version of Record published: 24 December 2020

<sup>&</sup>lt;sup>1</sup>Department of Biotechnology and Bioinformatics, School of Life Sciences, University of Hyderabad, Hyderabad, India; <sup>2</sup>Tata Consultancy Services Limited, Hyderabad, India; <sup>3</sup>Department of Biochemistry, School of Life Sciences, University of Hyderabad, Hyderabad, India



P. falciparum possesses a putative DNA topoisomerase III (TopoIII) as the sole member of the type IA family of topoisomerases, which transiently cleaves single-stranded DNA through the formation of a covalent 5' phosphotyrosine intermediate, releasing a free 3'-OH end. The parasite has another subclass of topoisomerase I, type IB, which belongs to an evolutionarily distinct class than type IA. A previous study revealed that PfTOPOIB mRNA is transcribed at the trophozoite stage but not at the schizont stage [13]. The TopoIB enzyme relaxes both positive and negative supercoils in DNA, cleaves the single-stranded DNA through formation of 3' phosphotyrosine intermediate, and allows the 5'-OH strand to undergo a restrained rotation around the non-scissile strand [14]. The TopoIB enzyme plays a major role in removing DNA supercoiling during DNA transcription and replication. However, topoisomerase IA performs additional roles besides working as a swivel during DNA replication. Owing to the difference in strand passage activity, Type IA enzymes play an important role in chromosome segregation during DNA replication and also perform regulatory roles in the formation or resolution of recombination intermediates along with the RecQ helicases [15].

Bacteria possess two Type IA topoisomerases, TopoI and TopoIII, which share a high degree of protein sequence similarity except that TopoIII contains a unique 17 amino acid (aa) charged loop present in the central hole of the enzyme. This gives TopoIII a distinct cleavage pattern compared with TopoI [16] and serves as a potent decatenase of replication intermediates [17] but inefficient relaxation of supercoiled DNA [18]. A recent study showed that bacterial TopoIII remains physically associated with the actively replicating fork and unlinks the catenated and precatenated DNA rings that result during DNA replication [19].

Budding yeast cells that lack topoisomerase III are viable; however, their growth rate is reduced by two-fold due to the accumulation of cells in the late S/G2 phase of the cell cycle and show hyper-recombination between repetitive sequences [20]. In addition, yeast homozygous null diploid *topoIII*/*topoIII* cells are unable to sporulate [20]. There are two homologous genes for TopoIII in vertebrates (TopoIIIα and TopoIIIβ). Inactivation of TopoIIIα leads to embryonic lethality in mice [21].

Yeast TopoIII and human TopoIII $\alpha$  physically interact with Sgs1 and Blm, respectively, and resolve the double Holliday junctions that are generated within the replicating sister chromosomes during sudden stalling of the replication fork; this subsequently suppresses genetic crossover [22]. TopoIII $\alpha$  is also required for the decatenation and segregation of human mitochondrial DNA (mtDNA) following replication [23].

Plasmodium mitochondrial and nuclear replication initiates in the late trophozoite stage [24]. It has been demonstrated that mtDNA of Plasmodium follows the rolling circle mode of replication like that of Saccharomyces cerevisiae [25]. During this process, inter-molecular homologous recombination results in the formation of a circular as well as a lariat-like complex network, which is eventually processed to form linear concatamers of DNA [26]. This suggests the possible involvement of Type I and/or Type II topoisomerases in mtDNA replication, which are essential for proper segregation of mtDNA in newly formed rings; however, to date, there is no report of this.

We investigated the function of TopoIII in *Plasmodium* biology. Our results establish that it plays an important role during the replication of the parasite. We found that the enzyme is expressed specifically during the onset of replication and its dual presence in the nucleus and mitochondria suggests its involvement during the replication of both genomes. Additionally, the stronger association between PfTopoIII and mtDNA during the late schizont stage of the parasite development indicates that it might play a role in mtDNA segregation. Our study also demonstrates a physical association between PfTopoIII and PfRecQ helicases.

Our study points out an important feature toward structure-function relation of PfTopoIII. We have identified a unique highly charged low complexity region (residues 253–336) in PfTopoIII, which is rich in aspartic acid and lysine rich repetitive sequences. It is noteworthy that about half of the ORFs of parasite genome are having repetitive sequences [27] although their role in protein function remains unclear. Using several genetic studies we have concluded that, deletion of this region completely abolishes the function of PfTopoIII. The presence of this unique 85 amino acid region affirms the enzyme as an attractive target for the design of antimalarial agents.

# Materials and methods Plasmids

The sequences of all primers used in this study are tabulated in Supplementary Table S3. *PfTOPOIII*, PfY421FtopoIII, and  $Pf(\Delta 259-337)topoIII$  were cloned in 2  $\mu$  yeast expression vector pTA [28] between the BamH1 and SalI restriction sites using the primer pairs OSB 334 and OSB 335. *ScTOPOIII* was cloned in pTA



vector using primer pairs OSB 346 and OSB 455. Full-length PfTOPOIII and  $Pf(\Delta 259-337)topoIII$  were cloned in centromeric Plasmodium expression vector pPfCENv3 (a gift from Dr. Puran Singh Sijwali, CCMB, Hyderabad) [29] under the promoter of PfCAM using forward primer OSB 334 and the reverse primer OSB 497. PfTOPOIII and its mutant were expressed as a C-terminal GFP fusion product. PfTOPOIII, and  $Pf(\Delta 259-337)topoIII$  were individually subcloned into bait vector pGBDUC1 between BamHI and SalI restriction sites to create the pGBDUC1PfTOPOIII and  $pGBDUC1Pf(\Delta 259-337)topoIII$  plasmids. We received the prey plasmids pGADC1PfBLM and pGADC1PfWRN as a gift from Professor Mrinal K. Bhattacharyya of the University of Hyderabad.

# Site-directed mutagenesis

Point mutations and deletion mutations were introduced in PfTopoIII using the splice overlap extension (SOE) PCR technique. Primer sets with the required mutations were designed to incorporate mutations in PfTOPOIII at the desired locations. Plasmodium 3D7 genomic DNA was used as a template and a full-length gene was amplified in two segments to insert a point mutation. To amplify the first and second segments to generate the PfY421FtopoIII mutation, the OSB 334/OSB 452 and OSB 453/OSB 335 primer sets were used, respectively. Then full-length PftopoIII containing the Y421F mutation was amplified using the first two segments along with primer set OSB 334 and OSB 335. Finally PfY421FtopoIII mutant was cloned into pTA 2  $\mu$  yeast expression vector between the BamH1 and Sall sites. After successful cloning, the PfY421FtopoIII construct was sequenced to confirm the desired mutation. To generate a Y-to-F mutation at the 421st aa residue, we changed the codons TAC to TTT. Similarly, to generate the  $Pf(\Delta 259-337)topoIII$  mutation, the OSB 334/OSB 450 and OSB 451/OSB 335 primer sets were used, respectively, for amplification, as mentioned earlier. Then full-length PftopoIII with the deletion of the abovementioned segment was amplified using the first two segments along with the primer set OSB 334/OSB 335. Finally, a  $Pf(\Delta 259-337)topoIII$  deletion mutant was cloned into pTA 2  $\mu$  yeast expression vector between the BamH1 and Sall sites. After successful cloning, the  $Pf(\Delta 259-337)topoIII$  construct was sequenced to confirm the desired deletion.

#### Yeast strains

The strains used in this study are listed in Table 1. The ΔSctopoIII strain was generated by homologous recombination-mediated gene knockout. To that end, a deletion cassette [30] with an HIS3 gene flanked by 40 bp upstream and 40 bp of the 3' terminal end of ScTOPOIII ORF was amplified using the primer set OSB 348/OSB 385. Then the cassette was transformed in the wild-type strain and the transformed colonies were selected using histidine drop-out plates. Individual colonies were screened for SctopoIII knockout clone by PCR-mediated confirmation using primer pairs OSB 350 and OSB 385. For a functional complementation study in yeast, we transformed the empty vector (pTA), pTAScTOPOIII, pTAPfTOPOIII, pTAPfY421FtopoIII, and pTAPf(Δ259-337)topoIII individually into the ΔtopoIII strain to generate SBY2, SBY3, SBY4, SBY5, and SBY6, respectively. To perform yeast two-hybrid analyses, we used a PMY3 strain that harbors empty pGADC1 and pGBDUC1 vectors [31]. To study the interaction between PfTopoIII and PfBlm as well as PfWrn, the HCY1 and HCY2 strains were created by transforming Prey-PfBLM + Bait-PfTOPOIII and Prey-PfWRN + Bait PfTOPOIII constructs into the PJ69-4A strain, respectively. Similarly, to study the interaction between PftopoIII $^{(\Delta259-337)}$  and PfBlm as well as PfWrn, strains HCY3 and HCY4 were generated by transforming the Prey-PfBLM + Bait- $Pf(\Delta 259-337)topoIII$  and Prey-PfWRN + Bait- $Pf(\Delta 259-337)topoIII$  constructs, respectively into the PJ69-4A strain. The strains HCY7, HCY8, HCY9, and HCY10 were used as controls. These strains were generated by transforming empty Prey + Bait-PfTOPOIII, Prey-PfBLM + empty Bait, Prey-PfWRN + empty Bait, and empty Prey + Bait- $Pf(\Delta 259-337)$ topoIII vectors respectively into the PJ69-4A strain.

# Synchronization of P. falciparum in vitro culture

Synchronization was done following a previously published protocol [32]. Briefly, 10 ml ring-stage parasites were centrifuged at 2500 rpm for 10 min at room temperature. The supernatant was removed using a Pasteur pipette and the pellet was carefully re-suspended in two bed volumes of pre-warmed 5% sorbitol (Sigma) solution at 37°C. The sample was incubated at 37°C for 10 min with intermittent tapping. After that, pre-warmed incomplete medium was added to a volume of 10 ml, and the sample was centrifuged at 3000 rpm for 10 min. The supernatant was removed and the pellet was washed three times with pre-warmed incomplete medium. Then the parasites were allowed to grow normally until the early ring stage, and sorbitol synchronization was



**Table 1 Yeast strains** 

Strain	Genotype	Source
SBY1	MATα leu2-3,112 trp1-1 can1-100 ura3-1 ade2-1 his3-11,15 [phi + ] TOPOIII::HIS3	This study
SBY2	MATα leu2-3,112 trp1-1 can1-100 ura3-1 ade2-1 his3-11,15 [phi+] TOPOIII::HIS3 Pta	This study
SBY3	MATα leu2-3,112 trp1-1 can1-100 ura3-1 ade2-1 his3-11,15 [phi+] TOPOIII::HIS3 pTAScTOPOIII	This study
SBY4	MATα leu2-3,112 trp1-1 can1-100 ura3-1 ade2-1 his3-11,15 [phi+] TopoIII::HIS3 pTAPfTOPOIII	This study
SBY5	MATα leu2-3,112 trp1-1 can1-100 ura3-1 ade2-1 his3-11,15 [phi+] TopoIII::HIS3 pTAPfY421FtopoIII	This study
SBY6	MATα leu2-3,112 trp1-1 can1-100 ura3-1 ade2-1 his3-11,15 [phi + ] TOPOIII::HIS3 pTAPf(Δ259–337)topoIII	This study
PJ694a	MATa trpl-901 leu2-3,112 ura3-52 his3-200 ga14∆ ga180∆ LYS2 :: GALI-HIS3 GAL2-ADE2, met2::GAL7-lacZ	[31]
PMY3	MATa trpl-901 leu2-3,112 ura3-52 his3-200 ga14∆ ga180∆ LYS2 :: GALI-HIS3 GAL2-ADE2, met2::GAL7-lacZ pGADC1,pGBDUC1	[31]
HCY1	MATa trpl-901 leu2-3,112 ura3-52 his3-200 ga14Δ ga180Δ LYS2 :: GALI-HIS3 GAL2-ADE2, met2::GAL7-lacZ pGADC1/PfBLM, pGBDUC1/PfTOPOIII	This study
HCY2	MATa trpl-901 leu2-3,112 ura3-52 his3-200 ga14Δ ga180Δ LYS2 :: GALI-HIS3 GAL2-ADE2, met2::GAL7-lacZ pGADC1/PfWRN, pGBDUC1/PfTOPOIII	This study
HCY3	MATa trpl-901 leu2-3,112 ura3-52 his3-200 ga14Δ ga180Δ LYS2 :: GALI-HIS3 GAL2-ADE2, met2::GAL7-lacZ pGADC1/PfBLM, pGBDUC1/Pf(Δ259–337)topolll	This study
HCY4	MATa trpl-901 leu2-3,112 ura3-52 his3-200 ga14Δ ga180Δ LYS2 :: GALI-HIS3 GAL2-ADE2, met2::GAL7-lacZ pGADC1/PfWRN, pGBDUC1/Pf(Δ259–337)topolll	This study
HCY7	MATa trpl-901 leu2-3,112 ura3-52 his3-200 ga14Δ ga180Δ LYS2 :: GALI-HIS3 GAL2-ADE2, met2::GAL7-lacZ pGADC1, pGBDUC1/PfTOPOIII	This study
HCY8	MATa trpl-901 leu2-3,112 ura3-52 his3-200 ga14Δ ga180Δ LYS2 :: GALI-HIS3 GAL2-ADE2, met2::GAL7-lacZ pGADC1/PfBLM, pGBDUC1	This study
HCY9	MATa trpl-901 leu2-3,112 ura3-52 his3-200 ga14Δ ga180Δ LYS2 :: GALI-HIS3 GAL2-ADE2, met2::GAL7-lacZ pGADC1/PfWRN, pGBDUC1	This study
HCY10	MATa trpl-901 leu2-3,112 ura3-52 his3-200 ga14Δ ga180Δ LYS2 :: GALI-HIS3 GAL2-ADE2, met2::GAL7-lacZ pGADC1, pGBDUC1/Pf(Δ259–337)topolll	This study

performed again to obtain close to 100% synchronized ring-stage parasites. These synchronized parasites were grown further to obtain synchronized trophozoite-stage and synchronized schizont-stage parasites.

### Generation of transgenic parasites

For transfection, plasmid DNA was purified using Maxi kit (Qiagen) and was re-suspended in 50  $\mu$ l cytomix solution (10 mM K<sub>2</sub>HPO<sub>4</sub> pH 7.6, 120 mM KCl, 0.15 mM CaCl<sub>2</sub>, 25 mM HEPES pH 7.6, 2 mM EGTA pH 7.6, 5 mM MgCl<sub>2</sub>) and kept at 4°C for overnight before transfection. Tightly synchronized ring-stage *P. falciparum* culture (6% parasitemia) was electroporated (Bio-Rad Gene Pulser) with 80–100  $\mu$ g plasmids. Transfected cells were initially allowed to grow in the absence of drug (normal RPMI media) until the parasitemia reached 4%. Later cells were maintained in media containing Blasticidin (2.4  $\mu$ g/ml) until transfectants appeared. Transgenic parasites were confirmed by checking the expression of GFP-tagged protein via Western blotting analyses.

# Yeast two-hybrid analyses

Yeast two-hybrid analyses were performed as described previously [31]. The strains PMY3, HCY1, HCY2, HCY3, HCY4, HCY7, HCY8, HCY9, and HCY10 were grown in SC-Ura-Leu medium until the logarithmic



phase. Then they were diluted serially and spotted in SC-Ura-Leu and SC-Ura-Leu-His media. The plates were kept at 30°C for 3–4 days. The strain PMY3 was used as the negative control in our study.

# **Chromatin immunoprecipitation assay**

We followed a previously described method [32]. Briefly, synchronized asexual erythrocytic stages (R, T, ES, and LS) of *P. falciparum* 3D7 parasite were cultured in RPMI1640 media. Formaldehyde (37%) was added to the parasite culture to a final concentration of 1% and the sample was incubated at 37°C for 10 min. The sample was sonicated six times (Elma; model-S-60H) at a frequency of 37 kHz for 10 s, followed by 5 min incubation on ice to generate an average DNA fragment size of 1 kb. Then protein–DNA complexes were selectively immunoprecipitated using antiPfTopoIII antibody. Reverse cross-linking was performed using 5 M NaCl. Finally, DNA was extracted using proteinase K-phenol chloroform. We quantified PfTopoIII recruitment to mtDNA using specific primers pairs for different regions of the *P. falciparum* mitochondrial genome, i.e. for A set-OMKB 540, OSB 251; for B set-OSB 493, OSB 495; for C set-OMKB 615, OSB 176; for D set-OMKB 616, OMKB 617; for E set-OMKB 618, OMKB 619; and for F set-OMKB 620, OMKB 541 as shown in Figure 4A. Control antibody used for ChIP was rabbit immunoglobulin G, which acted as a negative control. The IgG values were 0 or negligible. The IgG values were subtracted from the PfTopoIII ChIP value before plotting. To compare the recruitment of wild-type PfTopoIII and mutant PftopoIII ChIP value before plotting. To compare the recruitment of wild-type PfTopoIII and mutant PftopoIII ChIP value before plotting. To compare the recruitment of wild-type PfTopoIII and mutant PftopoIII ChIP value before plotting. To compare the recruitment of wild-type PfTopoIII and mutant PftopoIII chiP value before plotting. To compare the recruitment of wild-type PfTopoIII and mutant PftopoIII chiP value and used anti-GFP antibody to precipitate PfTopoIII-bound DNA.

# Real-time PCR analyses

Equal amounts of RNA (10 µg) from ring-, trophozoite- and schizont-stage parasites were first subjected to DNase I (Fermentas) digestion for 15 min at room temperature. Then, DNase I was inactivated by incubation with 25 mM EDTA at 65°C for 10 min. The absence of genomic DNA was verified by amplification with genespecific primers before the reverse-transcriptase step. Next, each RNA sample was reverse-transcribed with oligo dT primer (Sigma-Aldrich) using reverse transcriptase (Omni Script; Qiagen, Hilden, Germany) [12]. The resulting cDNA was subjected to semi-quantitative reverse transcription (RT)-PCR to detect the transcript level of P. falciparum TopoIII in all of the asexual stages. Similarly, the expression of PfBLM was measured by amplifying 149 bp gene-specific regions using the primer pairs OMKB 332 and OMKB 333. In addition, PfWRN expression was measured by amplifying 225 bp gene-specific regions using the primer pairs OMKB 334 and OMKB335. For real-time PCR, cDNA from each stage was diluted (1:50) and used for PCR using an RT-PCR kit (Roche). Real-time analyses were conducted using the Applied Biosystems 7500 Fast Real-Time PCR system. The threshold cycle  $(C_T)$  value of the ARP transcript of each sample was used to normalize the corresponding  $C_T$  values of the PfTopoIII transcripts. The normalized  $C_T$  values of PfTOPOIII from different samples were compared with obtain  $\Delta C_T$  values. The relative levels of mRNA were deduced from the formula: change in mRNA level =  $2^{\Delta CT}$ . The primers OSB 337 and OSB 335 were designed to amplify a 254 bp genespecific region of PfTOPOIII, and OSB 94 and OSB 95 were used to amplify a 300 bp gene-specific region of P. falciparum aspartate-rich protein (PfARP) [12]. To further investigate the mRNA levels of PfTOPOIII under HU conditions, RNA was isolated under treated and untreated conditions. The same procedure was followed to check the expression of PfTOPOIII. The primers OMKB 198 and OMKB 17 were used to amplify 314 bp genespecific regions of PfRAD51.

## Immunofluorescence assay

Plasmodium culture (6% parasitemia in the late-schizont stage) harboring PfTopoIII-GFP expression vector and that harboring PftopoIII<sup>( $\Delta 259-337$ )</sup>-GFP expression vector was stained with DAPI and separately with Mitotracker for 30 min at 37°C prior to imaging. Subsequently, fluorescence levels as assessed via DAPI, Mitotracker, and GFP were observed and captured from live cells using a fluorescence microscope (Axio Observer Z1 with Apotome, Carl Zeiss).

# PfTopolII structure modeling and molecular dynamics

The PfTopoIII structure was modeled using the I-TASSER server [33], employing the 4CGY (PDB ID) structure as a template [34]. For residues with no matching template, I-TASSER performs *ab initio* modeling. To check the stability of the modeled structure, explicit solvent MD simulation was performed using Gromacs 4.5.5 [35] and CHARMM36 force field [36]. The apo-structure was solvated in an octahedron box with a



TIP3P water model [37]. The charges on the protein were neutralized by adding chloride ions. NVT- and NPT-position restrained equilibrations were done for 200 ps and 1 ns, respectively. The modeled apo structure was used for 50 ns molecular dynamics (MD) simulations.

A clustering calculation was performed on the last 10 ns of the trajectory from the 50 ns simulation of the PfTopoIII apo-structure. The structure at the center of the largest cluster was chosen as the starting structure for the subsequent simulations. To study the binding of single-stranded DNA in the PfTopoIII structure, the *E. coli* structure was used. The 117D (PDB ID) [38] structure was aligned to the PfTopoIII to generate a holo structure with a single-stranded DNA octamer. The holo structure of PfTopoIII was simulated for 100 ns using a similar procedure as mentioned above. VMD 1.9.2 [39] and Gromacs 4.5.5 [35] were used to analyze the trajectories. The root-mean-square fluctuations (RMSFs) of the  $C\alpha$  atoms of the entire protein were calculated by using the g\_rmsf module of Gromacs.

# Phylogenetic analyses

The TopoIII sequences of various organisms (*P. falciparum*, *S. cerevisiae*, human, mouse, *E. coli*, *V. cholerae*, *V. nereis*, *E. lignolyticus* and *S. enterica*) were obtained from Uniprot [40] and PlasmoDB [41]. Then multiple sequence alignment (MSA) was performed using ClustalW [42]. A phylogenetic tree was constructed using fasttree [43] as implemented in Genomenet (http://www.genome.jp) [44].

## **Subcellular fractionation**

Samples (60 ml) of 8% parasitized erythrocytes specific to the late-schizont stage were harvested and treated with 0.15% saponin to free parasites from red blood cells (RBCs). The standard protocol for subcellular fractionation was followed [12].

# MMS sensitivity assay

SBY2, SBY3, SBY4, SBY5, and SBY6 were tested for DNA damage sensitivity. All strains were grown overnight in tryptophan dropout synthetic medium at 30°C. The next day, secondary culture was grown until 0.5  $\rm OD_{600}$  at 30°C. After  $\rm OD_{600}$  reached to 0.5, the culture was divided into three sets. One set of cells was treated with 0.01% (vol/vol) methyl methanesulfonate (MMS) (Sigma–Aldrich), and the second set of cells was treated with 0.04% MMS and grown at 30°C for 2 h. The third set was continuously grown at 30°C for 2 h without MMS. After this process, approximately 1000 untreated and 1000 treated cells were spread on selective media and incubated at 30°C for 2–3 days.

# **HU** sensitivity assay

In survivability assays, HU (Sigma) was added to the highly synchronized late-trophozoite stage of *P. falcip-arum* culture (~1% parasitaemia) at a concentration of 2.5 mM for 30 h at 37°C. Parasitemia was determined via Giemsa staining (Sigma) at every 10 h by counting at least 2000 RBCs. For each strain, 3–4 independent assays were conducted. In return-to-growth assays, 1% synchronized parasites were treated with 2.5 mM HU for 6 h. After 6 h treatment with HU, cells were washed twice and allowed to grow for 26 h in complete media. Then 6 h and 26 h slides were prepared for both HU-treated and untreated samples and parasitemia was measured. This experiment was repeated three times in 3D7 and in strains over-expressing *PftopoIII* (\$\text{\

#### Western blotting

Parasite proteins were extracted from the ring, trophozoite, and schizont stages of the parasite and were loaded on SDS polyacrylamide gels. A polyvinylidene difluoride (PVDF) membrane was used for transfer, as described previously [28]. The primary antibodies used were mouse antihAct1 antibody (Abcam) and rabbit antiPfTopoIII antibody (KR Instruments and Chemicals) at 1:5000 dilutions. For subcellular fractionation, we used rabbit antiHistone H3 antibody (Imperial Life Sciences) and mouse antiCytochrome C antibody (Allied Scientific) at 1:5000 and 1:3000 dilutions, respectively. For secondary antibodies, horseradish peroxide-conjugated antirabbit antibody (Promega) and antimouse antibody (Santa Cruz Biotechnology Inc. CA, U.S.A.) were used at 1:10 000 dilution. To check the expression of the PfTopoIII in the yeast surrogate system, proteins were isolated from the SBY3, SBY4, and SBY5 strains. The primary antibody against antiScActin (Abcam) was used at a concentration of 1:10 000 dilutions. The western blots were developed using a chemiluminescent detection system (Pierce). Every experiment was repeated at least three times and band intensities were



quantified using Image J software. Mean relative densities were plotted using GraphPad prism. To detect the transgenic parasite, we used rabbit anti-GFP antibody (Allied Scientific Products) at 1:5000 dilutions. To further study the effects of HU on protein levels of PfTopoIII, western blotting analyses were performed on 20 ml *Plasmodium* cultures. The culture was divided equally into two groups: samples treated with 10 mM HU and kept for 20 h at 37°C and an untreated group. After 20 h, parasitized erythrocytes specific to the late-schizont stage were harvested, treated with 0.15% saponin, and washed three times with 1× PBS; then protein was isolated by using standard procedures.

# **Results**

# A unique charged domain in PfTopolII

The *P. falciparum* genome database (http://www.plasmoDB.org) shows the presence of a putative PfTopoIII (Gene ID: PF3D7\_1347100) gene. It has no intron and it is predicted to code a 710 aa protein. Multiple sequence alignment of PfTopoIII showed significant homology in the catalytic TOPRIM domain (aa 5 to 150) across various TopoIII sequences (Figure 1) with two conserved aspartates at positions 118 and 120 and one conserved glutamate at position 122 (red box in the figure). The catalytic tyrosine residue of the enzyme is located at position 421 (blue star) within a highly conserved GYISYPRTET sequence (green box). PfTopoIII lacks a stretch of 30 aa residues at the N-terminal end and an extended 362 aa at the C-terminal domain that are present in human and mouse TopoIIIα. These extended N-terminal and C-terminal regions are also absent from ScTopoIII. However, there is a unique charged aa containing region spanning residues 253 to 336, which is absent from other eukaryotic TopoIII. It showed 75% sequence identity with *Plasmodium berghei* TopoIII and 35–39% sequence identity with other orthologs of TopoIII (Supplementary Table S1). The UniProt IDs for TopoIII orthologs are presented in Supplementary Table S2.

TopoIII protein sequences obtained from both eukaryotic and prokaryotic organisms were aligned using ClustalW (see Methods). In our phylogenetic analyses, prokaryotic and eukaryotic sequences formed two distinct branches from the root. The TopoIII sequence from *P. falciparum* was close to ScTopoIII and human TopoIIIα (Supplementary Figure S1A), while the TopoIII sequences from *E. coli*, *V. cholerae*, *V. nereis*, *E. lignolyticus* and *S. enterica* were clustered together. *PfTOPOIII* with 2133 base pairs was PCR amplified using 3D7 *P. falciparum* genomic DNA as a template (Supplementary Figure S1B) and was subsequently cloned into pET28a bacterial expression vector and was sequenced.

# PfTopolII expression is tightly linked with the replication of the parasite

We isolated RNA from various synchronized asexual stages of the parasite (ring, trophozoite, and schizont) and performed semi-quantitative RT-PCR and real-time RT-PCR. Our semi-quantitative results indicated that *PfTOPOIII* transcript is expressed in the schizont stage of the parasite (Figure 2A). Aspartate-rich protein (ARP), which is constitutively expressed at all stages of the parasite, was used as a loading control. Real-time RT-PCR analyses showed that the schizont stage of the parasite expressed more than 30-fold greater *PfTOPOIII* transcript compared with the ring and trophozoite stages, indicating its direct role during the replication of the parasite (Figure 2B).

To investigate the expression of PfTopoIII at the protein level, we raised antibody against the enzyme. *PfTOPOIII* was cloned in a bacterial expression vector using histidine tag. However, it could not be expressed under various conditions. Hence, we designed a peptide spanning residues 281–300 of PfTopoIII (DSNNYSDETDDYYGDEKK) and raised antibodies against the peptide. Immune sera analyses showed a specific band near 75 kDa (Figure 2C, right blot), which was absent when probed with pre-immune sera (Figure 2C, left blot). Using this specific antibody, we performed western blotting to investigate the stage-specific expression of the protein. We found that PfTopoIII is expressed specifically in the schizont stage (Figure 2D). Actin was used as a loading control. Thus, the expression profiles at the transcript level and protein level corroborated each other.

# Subcellular localization of PfTopolII

To examine the localization of PfTopoIII in the parasite, the distribution of endogenous PfTopoIII was studied by subcellular fractionation as well as by fluorescence microscopy. We conducted three independent subcellular fractionations of the parasite culture, and one representative image is presented in Figure 3A. We found that PfTopoIII was present both in the nuclear as well as in the organelle fraction. Histone H3 and cytochrome C





Figure 1. Sequence analysis results shows the identification of a unique charged domain in PfTopoIII.

Multiple sequence alignment of PfTopolII (*P. falciparum*), PbTopolII (*Plasmodium berghei*), HsTopolIIα (*Homo sapiens*), MmTopolIIα (*Mus musculus*) and ScTopolII (*Saccharomyces cerevisiae*) shows the presence of two conserved aspartate residues and one glutamate residue in the toprim domain (red box). Moreover, one conserved tyrosine residue (represented by a blue star) is present in the catalytic domain (green box).

were used as nuclear and mitochondrial protein markers, respectively. We generated a transgenic parasite line expressing PfTopoIII-GFP. Western blotting analyses of synchronous parasites in the schizont stage confirmed the expression of PfTopoIII-GFP (Figure 3B) in the parasite. The localization of the GFP-tagged protein was studied by live-cell imaging using a fluorescence microscope (Carl Zeiss). We found that PfTopoIII-GFP showed distinct nuclear foci and was co-localized with DAPI (Figure 3C). PfTopoIII-GFP was also co-localized with MitoTracker dyes (Figure 3D). These results correlate with the subcellular fractionation analyses and confirm its presence in both the nucleus and mitochondria of the parasite.

### PfTopoIII interacts with the mitochondrial genome

To determine whether PfTopoIII is associated with mtDNA, we conducted mtDNA immunoprecipitation (mtDNA-IP) assays on four synchronized developmental stages of the parasite, namely, the ring (R), trophozoite (T), early schizont (ES), and late schizont (LS) stages. We designed six sets of primers (A–F) in such a way that PCR amplification of immune-precipitated samples with each set of primers gave rise to fragments of similar length (1 kb). The position of each primer set is presented in Figure 4A and their sequences are listed



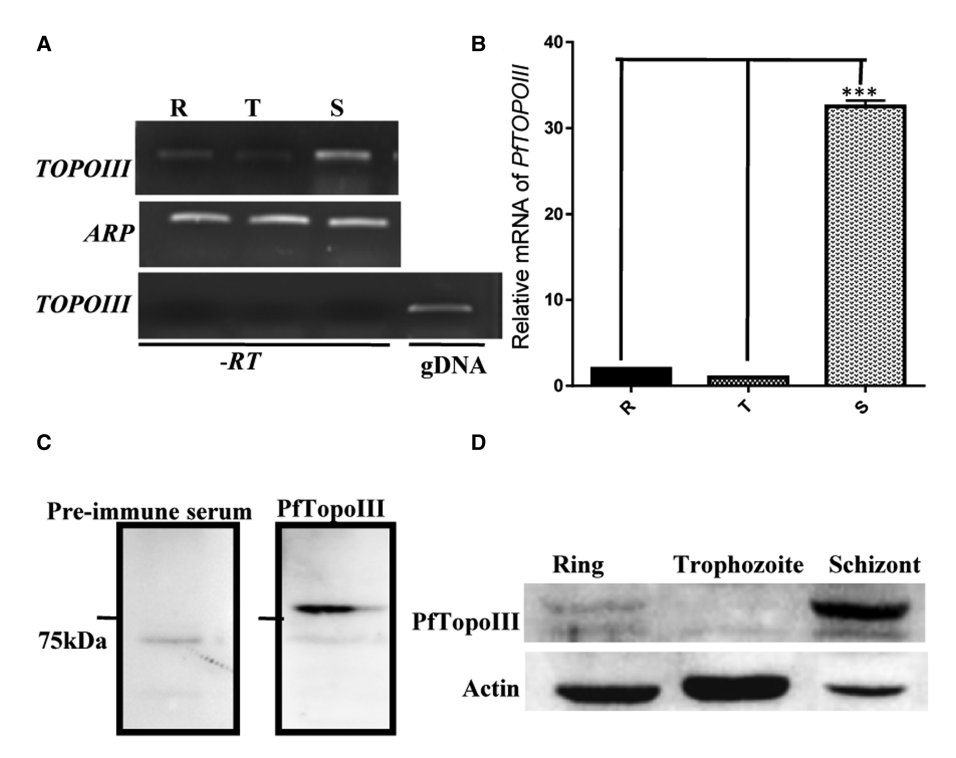


Figure 2. PfTopoIII expression is tightly linked with the replication of the parasite.

(A) RT-PCR analysis with RNA isolated from the rings (R), trophozoites (T) and schizonts (S) stages. PCR amplification was done using PfTOPOIII and ARP (Aspartate rich protein) specific primers which amplify 254 bp and 300 bp specific to the 3' end of the transcript, respectively. The bottom panel shows the lack of a PfTOPOIII band in the absence of reverse transcriptase (-RT). Genomic DNA (gDNA) served as a positive control. (B) Real-time RT-PCR shows the relative abundance of PfTOPOIII at various stages of the parasites. Error bars indicate mean  $\pm$  SD; n = 3; P = 0.0003. (C) Western blotting analyses of parasite cell extracts with pre-immune serum (left blot) and with an antibody raised against PfTopoIII (right blot). The molecular weight marker is indicated on the left. (D) Stage dependent expression of PfTopoIII in P. falciparum lysate has been shown: R, middle rings; T, early/mid trophozoite; S, mid/late schizont. Actin served as a loading control.

in Supplementary Table S3. Considering that, in *P. falciparum*, linear mtDNA of 6 kb unit length forms multimers in a head-to-tail fashion [26], the primer sets corresponding to A–E were used to amplify the internal DNA sequence within each monomer of linear mtDNA. On the other hand, the primer set F was used to amplify the junctional sequence spanning two monomeric mtDNAs. We found that the relative occupancy of PfTopoIII to the F site of mtDNA was much higher compared with the other sites. In addition, PfTopoIII recruitment was negligible in the R, T and ES stages but enhanced in the LS stage (Figure 4B). Together, these results suggest that PfTopoIII might be involved in the segregation of mtDNA of the parasite in the late-schizont stage.

# Molecular dynamic simulations indicate that the flexible charged domain of PfTopolII stabilizes upon DNA binding

We modeled PfTopoIII using the I-TASSER server by selecting human TopoIII $\alpha$  as a template (PDB ID: 4CGY) (Figure 5A). Domain analyses of PfTopoIII indicated the presence of an extra charged region within domain II that was disordered and away from the DNA binding region. The stability of the structure was evaluated via MDS for 50 ns. During the simulations, the PfTopoIII structure was stable but the charged region showed large fluctuations (data not shown). In a 50 ns apo-PfTopoIII simulation, the charged domain remained away from the DNA binding region (Supplementary Figure S2).

To understand whether the charged domain had any role in DNA binding, we compared it to the structure of *E. coli* TopoIII, which has a charged loop similar to that of PfTopoIII [17]. To that end, the structure of *E.* 



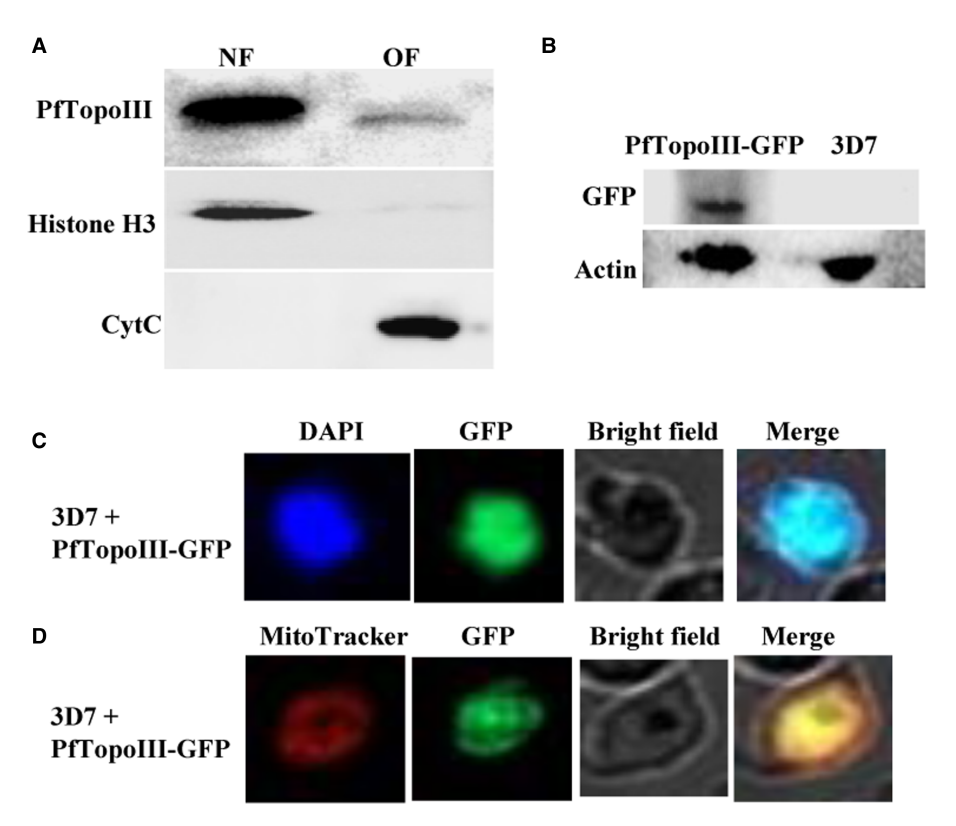


Figure 3. Subcellular localization of PfTopoIII.

(A) Western blotting analyses of the nuclear (NF) and organelle fractions (OF) of 3D7 parasite infected RBC were done using anti-PfTopolll antibody. Histone H3 and Cytochrome C were used as the nuclear and mitochondrial markers, respectively. (B) Western blotting analyses of the total protein extracted from 3D7 and a transgenic parasite strain harboring PfTopolll-GFP expression vector were performed using anti-GFP antibody. Actin served as a loading control. (C and D) Fluorescence microscopy shows the expression of PfTopolll-GFP at the late schizont stage. Parasite nucleus was stained with DAPI (blue) while parasite mitochondria were stained with MitoTracker Red (red).

coli TopoIII (PDB ID: 117D) with a single-stranded DNA octamer (5'-CGCAACTT 3') was aligned to the PfTopoIII and the single-stranded DNA octamer was placed in the binding site to generate a structure of PfTopoIII bound with DNA. The holo structure of PfTopoIII was simulated for 100 ns using a similar procedure as mentioned above. RMSFs of the PfTopoIII-DNA complex were computed for the Cα atoms of complete protein to capture the dynamics of individual amino acids. From the RMSF plot, the maximum fluctuations were observed in parts of the charged domain, the Toprim domain, and domain III (Supplementary Figure S3A). Other fluctuations were also observed in the amino and carboxyl-terminal of the protein (Supplementary Figure S3A). In principal component analyses (PCA), used to identify the dominant motions during the simulations [45], both, PC1 and PC2 showed major fluctuations in the charged domain with similar direction, towards the bindings site of single-stranded DNA (Supplementary Figure S3B). PC1 also showed fluctuations in parts of Toprim and domain III, which are in the opposite direction, indicating the opening of a central hole of the PfTopoIII protein (Supplementary Figure S3B). From these observations, it can be inferred that there are two major conformational changes in the protein. First, domain III and Toprim domain open up to accommodate the oligonucleotide, and then the charged domain comes closer to and interacts with the oligonucleotide.

The distance between the centers of mass of domain III (residues 380–511) and parts of Toprim domain (residues 12–26 and 152–163) were computed to quantify the movement between these two domains (Figure 5B). The domains moved by a distance of 7 Å compared with the PfTopoIII modeled structure (Figure 5B).

In the RMSF and PCA analyses, the charged domain showed high flexibility during MDS. The conformations of the charged domain could largely be clustered into four bins, as can be seen in the free energy



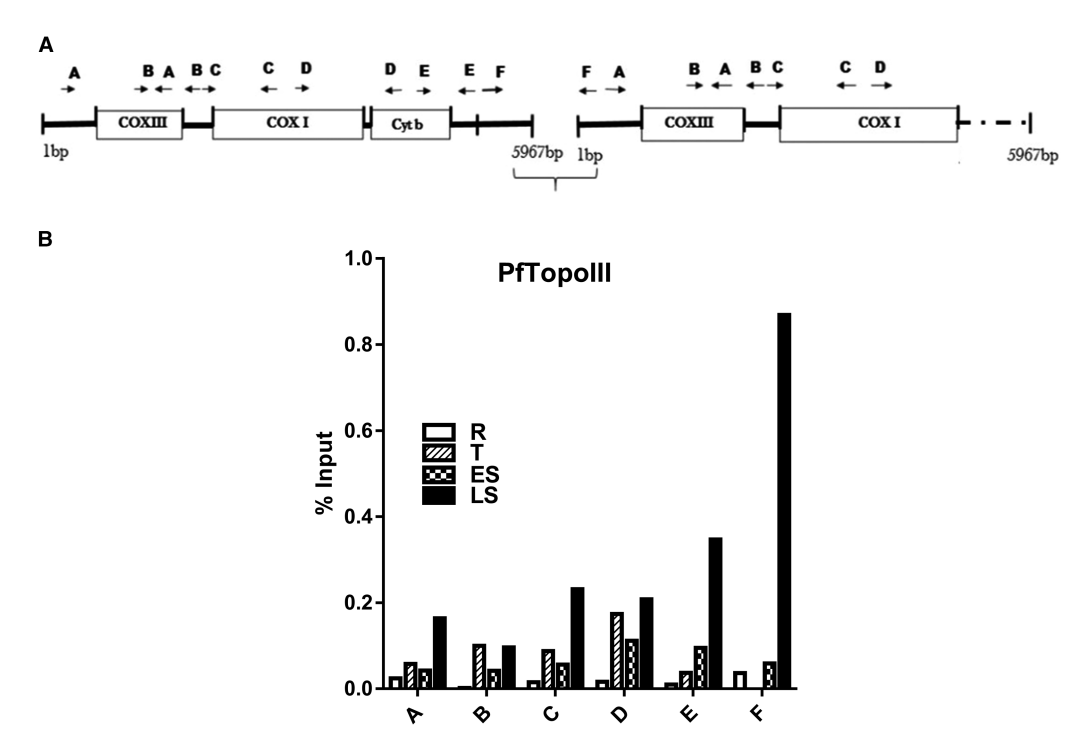


Figure 4. PfTopolII interacts with mitochondrial genome.

(A) The 6-kb long mitochondrial DNA (mtDNA) of *P. falciparum* exists as a linear tandem array joining in a head to tail manner as shown. The map displays three different genes encoded by *Plasmodium* mitochondrial genome *COXIII*, *CYTb* and *COXI* and the position of different primer sets from A to F; each set of primers covers ~1 kb length and together cover the whole mtDNA.
(B) The graph displays the occupancy of PfTopoIII on mtDNA as % input on the Y-axis with respect to the different regions of the mitochondrial genome on the X-axis [A–F] covering the entire mtDNA.

landscape (FEL) plot (Figure 5C). During the start of the simulation, the charged domain interacted with parts of domain III, similar to the apo-structure simulation (Figure 5D, red). Around 34 ns, the domain adopted an open conformation to interact with the DNA octamer (Figure 5D, black). At ~46 ns, residues D296, E297, K302, and K304 started interacting with the oligonucleotide (Figure 5D,E). During the latter part of the simulation, the charged domain was in a closed conformation. The charged and aromatic residues in the charged domain interacted with and stabilized the DNA octamer (Figure 5D,E). The residues from this domain (K302, K301, K299 and others) formed hydrogen bonds and stacked interactions with the nitrogenous bases of the DNA octamer (Figure 5E). These interactions helped to stabilize and place the DNA octamer in the cavity for further processing (Supplementary video S1 and S2). Thus, the MDS and the structural data established that the charged domain of PfTopoIII stabilizes the binding of single-stranded DNA.

# Pftopolll $^{(\Delta 259-337)}$ shows a poor association with mtDNA

To determine the functional significance of the charged domain of PfTopoIII, we generated a transgenic parasite that expressed mutant PftopoIII-GFP with a deletion of 259–337 charged aa residues from PfTopoIII. We conducted immunoprecipitations of mtDNA from the synchronous schizont stage of the parasite harboring the mutant PftopoIII<sup>( $\Delta 259-337$ )</sup>-GFP protein and that harboring the wild-type PfTopoIII-GFP protein. The experiment were repeated twice; the recruitment of mutant PftopoIII<sup>( $\Delta 259-337$ )</sup> towards E and F regions of mtDNA were measured and compared with that with the wild-type PfTopoIII (Figure 6A). The mutant PftopoIII<sup>( $\Delta 259-337$ )</sup> protein showed a significantly decreased association with the mtDNA compared with the wild-type protein. Western blotting analyses confirmed the expression of mutant PftopoIII<sup>( $\Delta 259-337$ )</sup>-GFP protein in the parasite (Figure 6B). To rule out the possibility that the decreased association was due to defective mitochondrial trafficking of the mutant PftopoIII, we performed live cell imaging of the mutant parasite-infected cells and



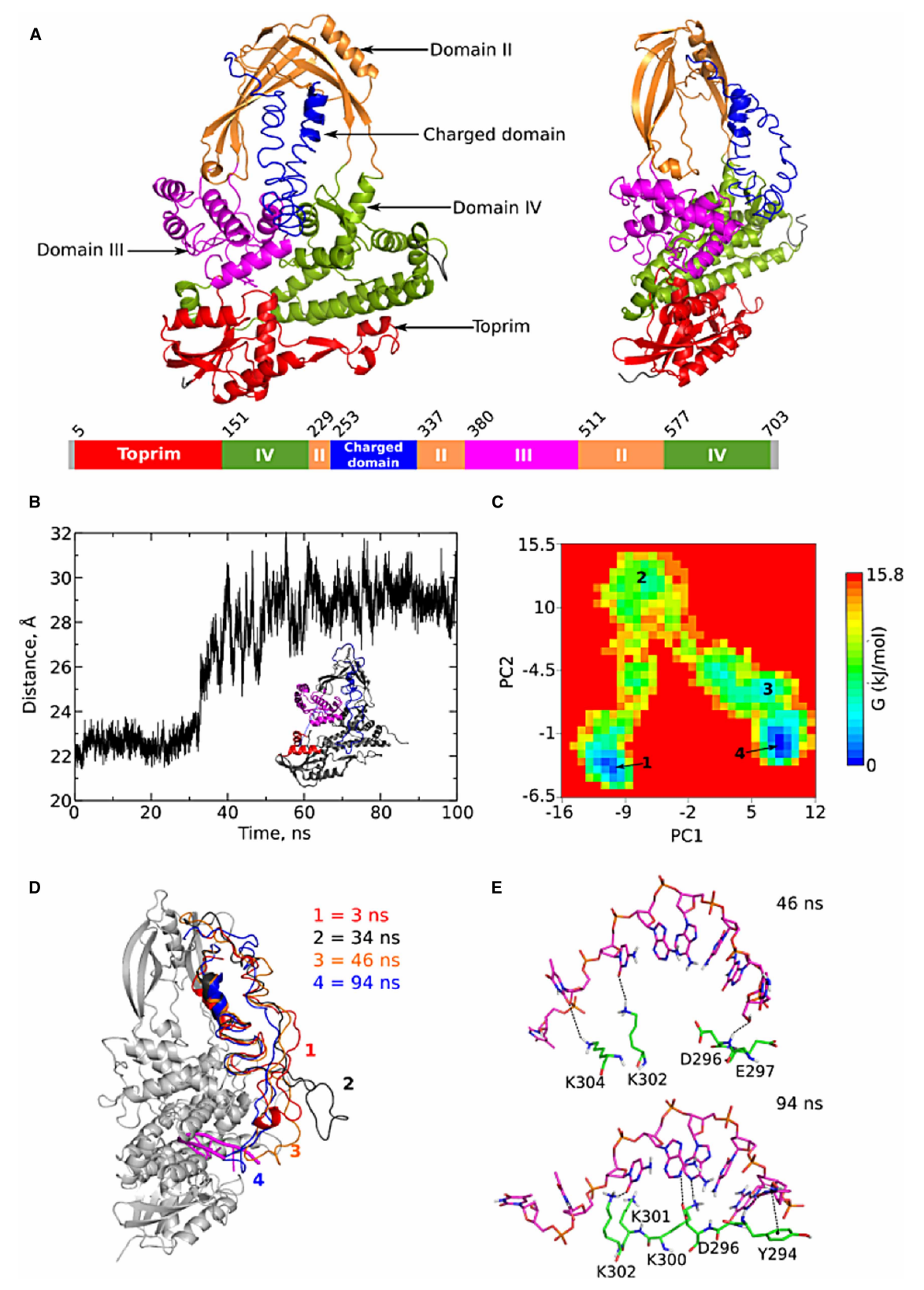


Figure 5. Molecular dynamic simulations indicate that the charged domain of PfTopolII remains flexible and stabilizes upon DNA binding.

Part 1 of 2

(A) Structure of PfTopoIII modeled using the I-TASSER. The toprim domain and domain III are colored in red and magenta,



Figure 5. Molecular dynamic simulations indicate that the charged domain of PfTopolII remains flexible and stabilizes upon DNA binding.

Part 2 of 2

respectively. The domains II and IV are colored in orange and green, respectively. The charged domain which is a part of domain II is shown in blue. (**B**) Graph showing the distance between the centers of mass of parts of toprim (residues 12–26 and 152–163 shown in red) and domain III (residues 380–511 shown in magenta) during the simulation of PfTopolII holo structure. (**C**) Free energy landscape (FEL) with respect to principal components 1 and 2. (**D**) Major conformations of charged domain (residues 251–337) sampled during 100 ns simulation obtained from FEL have been shown in red, black, orange and blue color, respectively. E. Interactions of charged domain (green) with the DNA octamer (magenta) have been shown.

observed that the mutant protein was co-localized with DAPI as well as with MitoTracker, like that of the wild-type protein (Figure 6C,D).

# PfTOPOIII complements the function of ScTOPOIII but Pf(∆259–337)topoIII does not

To decipher the *in vivo* role of PfTopoIII, we used *S. cerevisiae* as a surrogate model system. To determine whether full-length PfTopoIII can reverse the slow-growth phenotype of  $\Delta topoIII$  yeast strain, we deleted *TOPOIII* from the *S. cerevisiae* genome and transformed *ScTOPOIII* expressing vector (pTA-ScTOPOIII) into the knock-out strain. This strain served as a positive control in our study. We cloned *PfTOPOIII* in yeast expression vector (pTA-PfTOPOIII) and transformed it into  $\Delta topoIII$  to generate an isogenic strain. We grew each strain in fresh liquid media from overnight culture and monitored their growth for 15 h at regular intervals. We found that full-length PfTopoIII fully rescued the slow-growth phenotype of the  $\Delta topoIII$  strain to the same extent as that of ScTopoIII (Figure 7A). To confirm that the growth recovery was not due to any compensatory mechanism, we created an isogenic strain where the putative active tyrosine of PfTopoIII (at the 421st position) was mutated to phenylalanine. The mutant was unable to suppress the slow-growth phenotype of  $\Delta topoIII$  strain, confirming the role of this active tyrosine inside this yeast strain (Figure 7A). To rule out the possibility that loss of complementation is not due to loss of expression of PftopoIII  $^{Y421F}$ , we checked the expression of wild-type PfTOPOIII and PftopoIIIY421F both at the RNA level (Figure 7B) and at the protein level (Figure 7C). Both proteins were stably maintained in the  $\Delta topoIII$  strain.

Next, we investigated whether the charged domain present in PfTopoIII is essential for its function. To that end, we made a charged domain deletion mutant of PftopoIII by deleting 259–337 aa and transformed  $pTA-PftopoIII^{(\Delta 259-337)}$  into the  $\Delta topoIII$  strain to check whether it would show PfTopoIII-like activity. This mutant failed to rescue the slow-growth phenotype of the  $\Delta topoIII$  strain in liquid medium, suggesting that the charged domain was essential for functional complementation (Figure 7A). To rule out the possibility that loss of function of the mutant protein was due to the loss of expression of the mutant protein, we studied the mRNA expression of  $pTA-PftopoIII^{(\Delta 259-337)}$ ; it was detected at the same level as that of other test strains (Figure 7B). However, we could not check its expression at the protein level as the peptide antibody was raised against the charged region of PfTopoIII. This experiment emphasizes the importance of the charged region in PfTopoIII function.

# PfTopolII interacts with PfBlm and PfWrn

We have a used yeast two-hybrid assay to monitor the interaction between PfTopoIII and the RecQ helicases of *Plasmodium*. We subcloned *PfTOPOIII* in bait vector as a fusion to the Gal4 DNA binding domain and *PfBLM/PfWRN* individually to the prey vector as a fusion to the Gal4 activation domain (Figure 8A). The recombinant bait and prey vectors were transformed in PJ69-4A and the interaction between PfTopoIII and RecQ helicases were scored by monitoring both *HIS3* and *ADE2* reporter gene activity. We found that PfTopoIII, PfBlm, and PfWrn individually did not self-activate the reporter gene activity, as they failed to grow in medium lacking histidine (Figure 8B, rows 2–4). However, PfTopoIII interacted with PfBlm as well as with PfWrn as they grew in such medium (Figure 8B, rows 5 and 6). No growth was observed in adenine dropout medium indicating that their interaction was not strong enough to induce the expression of sufficient adenine (data not shown). We also addressed whether the presence of the charged domain in PfTopoIII is essential for mediating the interaction with RecQ helicases. We found that the mutant PftopoIII<sup>(Δ259–337)</sup> interacted with both PfBlm and PfWrn with the same efficiency as that of the full-length protein (Figure 8B, rows 8 and 9), indicating that the charged domain is dispensable for the interaction with RecQ helicases. Next, we checked



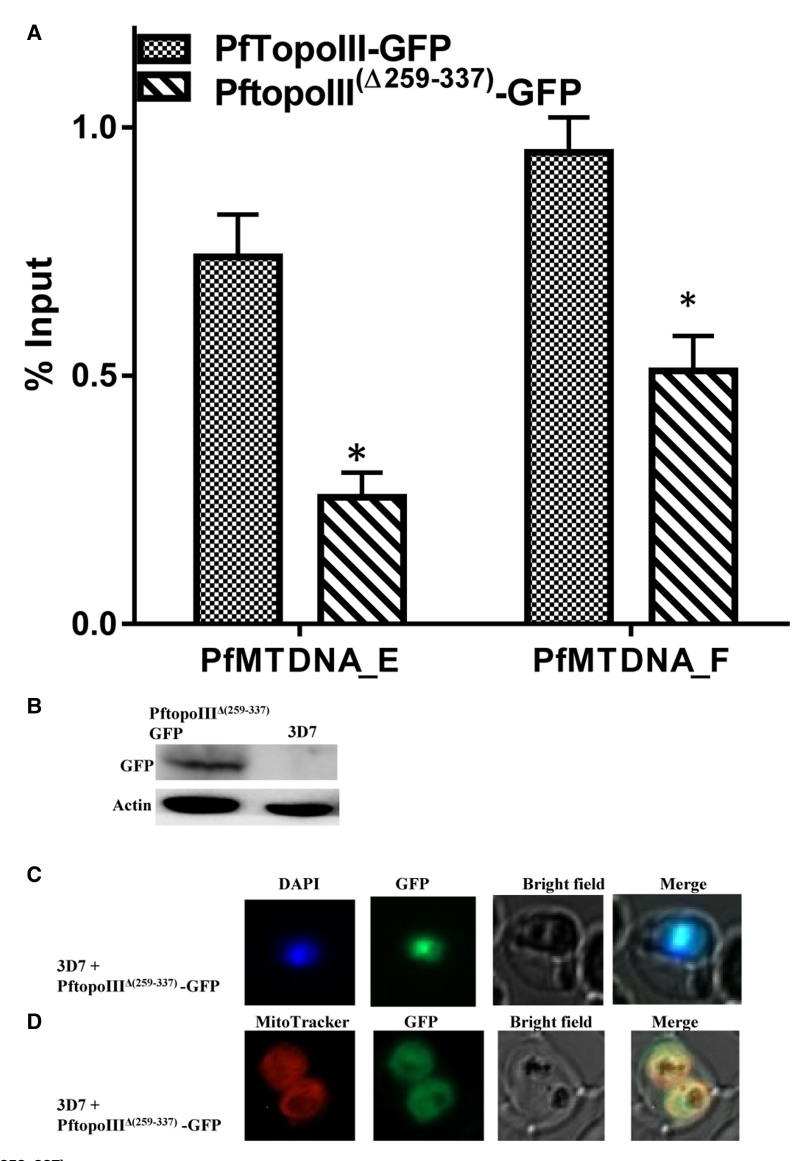


Figure 6. PftopollI $^{(\Delta 259-337)}$  shows poor association with mtDNA.

(A) The mtChIP analyses show the recruitment of PfTopoIII-GFP in comparison with PftopoIII( $^{\Delta259-337}$ )-GFP to two different loci (E and F) of the mitochondrial genome. Error bars indicate mean  $\pm$  SD; n = 2; \* P < 0.05. (B) Immunoblot shows the expression of mutant PftopoIII( $^{\Delta259-337}$ )-GFP protein in the transgenic parasite line. (C and D) Fluorescence microscopic images show the localization of PftopoIII( $^{\Delta259-337}$ )-GFP. Parasite nucleus was stained with DAPI (blue) and parasite mitochondria were stained with MitoTracker Red (red).

whether *PfBLM* and *PfWRN* were expressed in the schizont stage of the parasite along with *PfTopoIII*. Semi-quantitative RTPCR indicated that both RecQ helicases were abundantly expressed along with *PfTOPOIII* at the asexual replicative stage of the parasite (Figure 8C).

# Replication block-induced sensitivity in $\Delta topolll$ is rescued by ectopic expression of full-length PfTopolll but not by the charged domain mutant protein

MMS modifies the DNA by adding methyl groups and the methylated DNA subsequently physically blocks replication forks [46]. It has been earlier reported that TopoIII along with Sgs1 can eliminate the obstacle



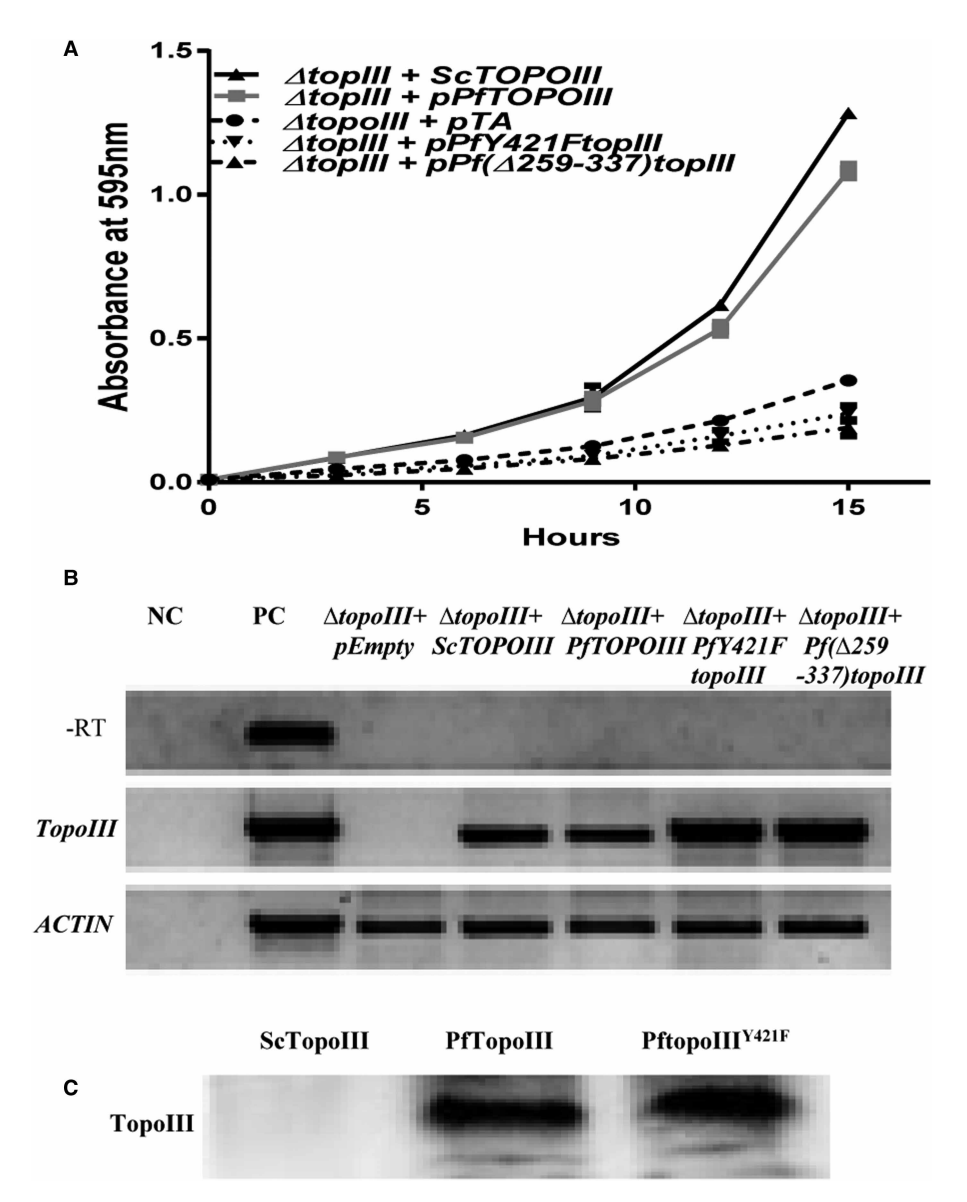


Figure 7. PfTOPOIII can complement the function of ScTOPOIII, but Pf(\( \Delta 259-337 \)) topoIII cannot.

(A) S. cerevisiae  $\Delta topolll$  strain was individually transformed with empty vector, vector expressing ScTOPOlll, PfTOPOlll, PfY421Ftopolll and  $Pf(\Delta 259-337)topolll$ . Growth rate of all the strains were measured in liquid synthetic medium lacking tryptophan and the  $OD_{595}$  was plotted against time. The results shown represent the mean of three independent experiments. (B) The expression of TOPOlll from the above mentioned strains was monitored using gene specific primers; Actin served as positive control. NC denotes negative control, i.e. ScTOPOlll PCR amplification without genomic DNA and PC denotes positive control i.e. ScTOPOlll PCR amplification with genomic DNA as a template. (C) Total protein was isolated from the strains as indicated at the top and probed with PfTopolll specific antibody.

during replication fork progression and that deletion of *TOPOIII* causes MMS sensitivity in a dose-dependent manner [47]. We assessed whether PfTopoIII could suppress the cytotoxic effects of DNA alkylating agent in a yeast model system. To that end, we exposed the test strains to different concentrations of MMS (0.01% and 0.04%) for 2 h, and then returned them to normal media. The percent survivability of each strain at each concentration of MMS is plotted in Figure 9. Full-length PfTopoIII completely rescued the MMS sensitivity of the  $\Delta topoIII$  strain to the same as that of ScTopoIII, whereas PftopoIII<sup>Y421F</sup> and PftopoIII ( $\Delta topoIII$ ) did not. Hence the Y421 residue of the catalytic domain and the charged aa-rich region of PfTopoIII are indispensable for its function.



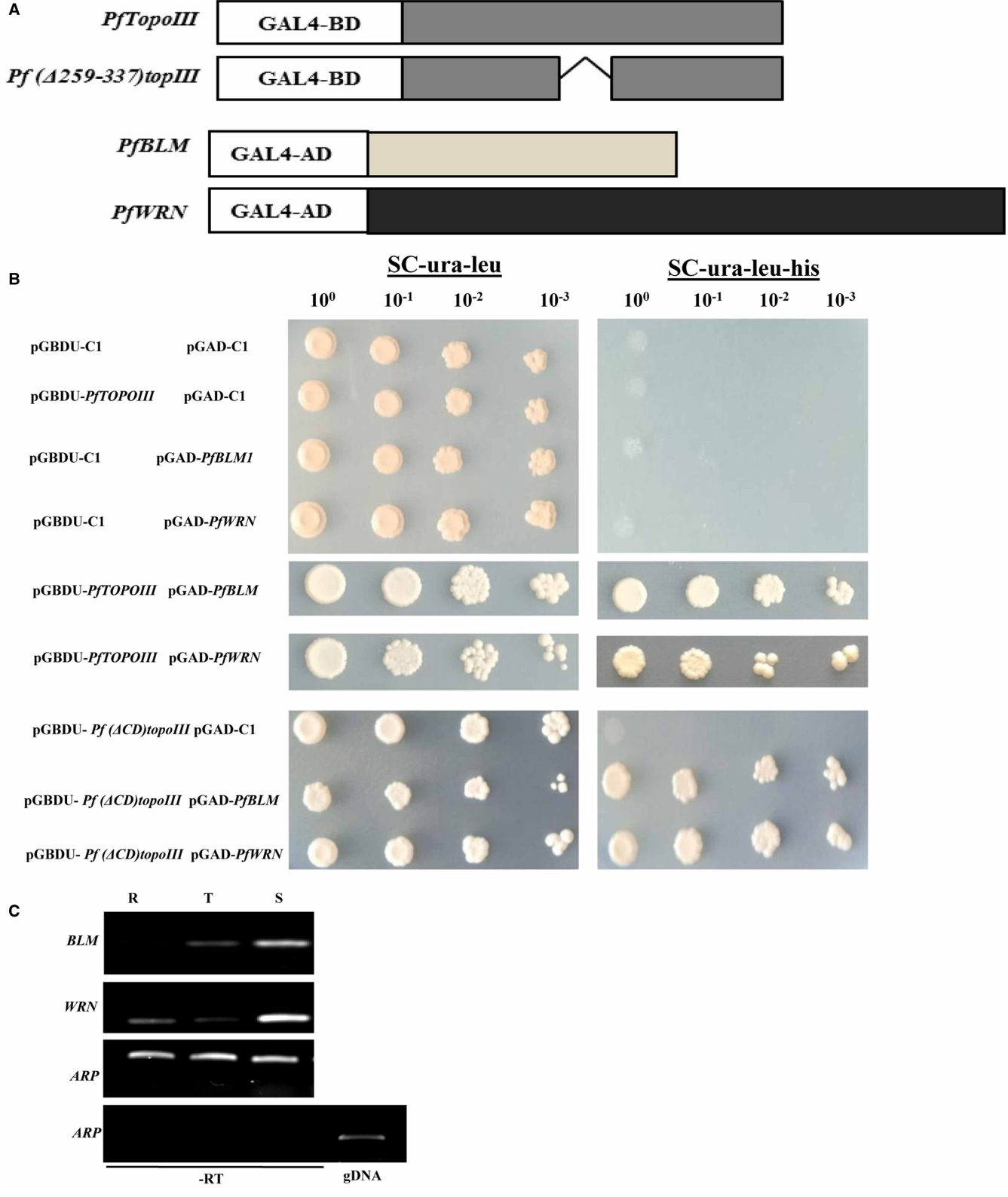


Figure 8. PfTopolII interacts with PfBlm and PfWrn.

Part 1 of 2

(A) The schematic representation showing that full length PfTopoIII and PftopoIII $^{(\Delta 259-337)}$  were fused to the Gal4 DNA binding domain generating chimeric constructs in *pGBDUC1* bait vector. Similarly, PfBIm and PfWrn were fused to Gal4 activation domain to generate chimeric constructs in *pGADC1* prey vector. (B) Yeast two-hybrid assays were performed in PJ69-4A strain using *HIS3* as a reporter gene. The left panel represents the

#### Figure 8. PfTopolII interacts with PfBlm and PfWrn.

Part 2 of 2

spotting of equal number of cells with serial dilution in the medium lacking leucine and uracil while the right panel scores the interaction between respective pairs. (**C**) Semi quantitative RT-PCR shows the expression of *PfBLM* and *PfWRN* at the ring (R), trophozoite (T) and schizont (S) stage of the parasite. Aspartate-Rich Protein (ARP) was used as a loading control. PCR without reverse transcriptase (–RT) does not show any amplification except for the positive control i.e. genomic DNA (gDNA).

# Replication stress-induced expression of PfTOPOIII

HU inhibits ribonucleotide reductase, an enzyme that is required for the generation of deoxyribonucleotide triphosphates during the S-phase of the cell cycle. We studied the effects of prolonged HU-mediated replication stress on malaria parasites. We used synchronized 2% trophozoite-stage parasites exposed to 2.5 mM HU to induce replication stress, as established in a previous study [48]. The growth of the parasites was measured in 10 h time intervals (post HU treatment) and compared with that of untreated parasites. The experiment was repeated three times and the survivability at each time point was plotted (Figure 10A). We found a three-fold increase in parasitemia in untreated parasites at the end of the 30th hour, however, the HU-treated parasites showed severe sensitivity and their survivability was significantly reduced in a time-dependent manner. We also studied the morphology and development in each group at three different time intervals (Supplementary Figure S4). Untreated parasites mostly form mature schizonts (segmenters) at the end of 20th hour eventually ruptured and produced rings at the end of the 30th hour, which caused an increase in parasitemia (Supplementary Figure S4). However, HU treatment caused an arrest in the development of the parasite; mature schizonts could not develop and eventually died. Next, we studied the effects of short-term exposure to HU on parasite survivability. We used synchronized 1% trophozoite-stage parasites and exposed them to 2.5 mM HU for 6 h. Subsequently, HU was extensively washed and the parasites were returned to normal media and allowed to grow for 26 h. We found a 5-fold increase in parasitemia in untreated parasites (Figure 10B). However, treated parasites did not show a decrease in survivability; rather their growth was arrested and they remained at the same developmental stage as that at which they started (Figure 10B). It was reported that ΔtopoIII condition in Saccharomyces cerevisiae displays severe sensitivity towards HU [47], which indicates that TopoIII plays an important role in resolving the aberrant structure generated from the arrest of the replication fork. To explore the direct role of PfTopoIII during replication stress, we evaluated the level of PfTopoIII after HU treatment. We exposed synchronous trophozoite-stage parasites to two different doses of HU (2.5 mM and 10 mM) for 6 h. Subsequently, HU was extensively washed, the parasites were returned to the normal media for 26 h and then extracted proteins both groups. We found that PfTopoIII was moderately induced in a dose-dependent manner upon HU treatment, supporting its direct role in mitigating replication stress (Figure 10C). We repeated the experiment twice and quantified the band intensity using Image J software. We found that there was a 3.5-fold induction in PfTopoIII expression in parasites treated with 10 mM

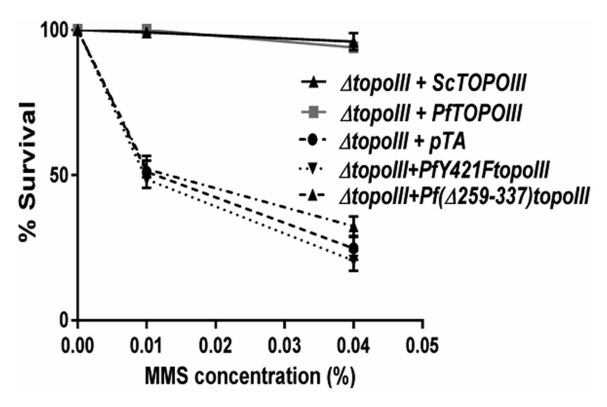


Figure 9. Replication block induced DNA damage sensitivity in \( \triangle topolli \) yeast cells is rescued by expression of full length \( PfTOPOIII \) but not by the expression of mutant protein with deletion in its charged domain.

Isogenic strains, as indicated, were grown to early log phase and exposed to 0.01% MMS and 0.04% MMS treatment. The percent survival of each strain was determined. Error bars indicate mean  $\pm$  SD; n = 3.



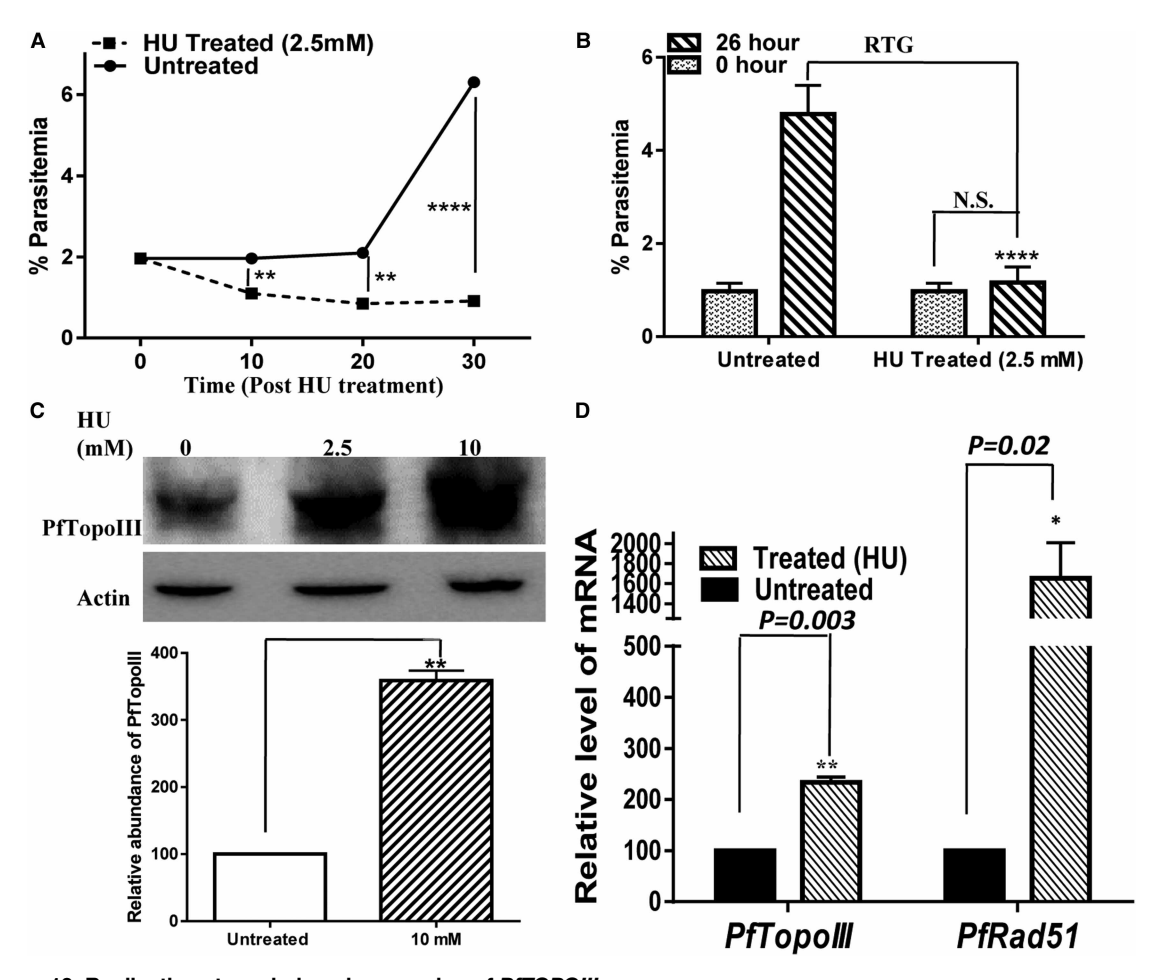


Figure 10. Replication stress induced expression of PfTOPOIII.

(A) Synchronous trophozoite stage specific 3D7 parasites were exposed to 2.5 mM HU for 30 h and parasitemia was measured for untreated and treated batch at every 10 h intervals. Error bars indicate mean  $\pm$  SD; n = 3; \*\*\*\*\* P < 0.0001; \*\*\* P < 0.01. (B) Synchronous trophozoite stage specific 3D7 parasites were exposed to 2.5 mM HU for 6 h, after which HU was extensively washed out and the parasites were subsequently returned to grow (RTG) in normal media. The parasitemia was measured at the end of 26 h for the untreated and treated batch. Error bars indicate SD; n = 3; \*\*\*\*\* P < 0.0001; N.S. not significant. (C) Untreated and treated parasites (at 2.5 mM and 10 mM HU treatment) were processed in the same way as that described in (B) and were harvested. The total protein was extracted and probed with anti-PfTopolll antibody. Actin served as a loading control. Quantification of Western blots from three independent experiments was done using Image J software. The band intensities in each lane were normalized against Actin and mean densities were plotted. Error bars indicate mean  $\pm$  SD; n = 3; \*\*\* P < 0.01. (D) Synchronized trophozoite stage specific 3D7 parasites were treated with HU and the total RNA was extracted from untreated and treated parasites. Relative abundance of *PfTOPOIII* transcripts by real time RT-PCR revealed significant induction of *PfTOPOIII* upon HU treatment. *PfRad51* expression was measured as a positive control. The *P*-value was calculated as 0.003 and 0.02 for *PfTOPOIII* and *PfRAD51* induction respectively using the two-tailed Student's *t*-test.

HU (Figure 10C). To understand whether the increase in expression occurred due to the stabilization of proteins or at the transcript level, we extracted RNA from untreated and HU-treated parasites and quantified the *PfTOPOIII* cDNA by real-time RT-PCR. There was a 2.5-fold induction in the expression of *PfTOPOIII* upon HU treatment. Rad51 plays an essential role in replication fork stability and regression [49]. Rad51 expression was used as a positive control in our experiment (Figure 10D). The transcriptional induction of *PfTOPOIII* in response to HU treatment indicates that the increased level of endogenous *PfTopoIII* is required to promote recovery from replication stress. This finding reveals that *PfTopoIII* plays a key role in the response to replication stress in the parasite.



# PfTopolII but not PftopolII $^{(\Delta 259-337)}$ expression rescues the growth defect induced by replication stress

Because we found that PfTopoIII expression is induced in response to replication stress, probably to counteract the stress, we wanted to determine whether the ectopic expression of PfTopoIII, through a centromeric plasmid, would promote survival in HU-treated parasites. To this end, we compared the growth of three different strains of parasites: 3D7, 3D7 with PfTopoIII expression, and 3D7 with PftopoIII(\$\tilde{\Delta}259-337\$) expression. In the first assay, we treated synchronous trophozoite-stage parasites with 2.5 mM HU continuously for 30 h and have measured parasitemia in intervals of 10 h. We repeated the experiment three times and observed that PfTopoIII expression considerably reduced dose-dependent death of the parasites at the 20th and 30th hours (Figure 11A). Interestingly, the transgenic parasites harboring PftopoIII(\(\hat{\Delta}259-337\)) expression plasmid did not show a reversed growth defect and behaved similar to that of the 3D7 parasites (Figure 11B). In the second assay, we exposed the parasites to 2.5 mM HU for 6 h, subsequently, it was extensively washed out and they were returned to normal growth media for 26 h. We found that the 3D7 parasites were severely affected even with 6 h treatment of HU and their growth remained arrested compared with the untreated parasites. The PfTopoIII transgenic parasite line showed fully rescued survivability and there was no significant difference between the survivability of treated versus untreated parasites (Figure 11C). However, the PftopoIII (A259-337) parasite line showed a similar trend as that of 3D7 parasites and displayed a significant difference in survivability compared with untreated parasites (Figure 11C). Hence, the charged domain of PfTopoIII is essential for in vivo function of the enzyme.

# **Discussion**

This is the first study to identify functionally active TopoIII from a malaria parasite. We demonstrated that the spatiotemporal expression of PfTopoIII occurs in the nucleus and in the mitochondria during the actively replicating stage of the parasite. It is noteworthy that in humans, mice, and Drosophila, there is a mitochondrial localization signal at the amino terminal end of TopoIII $\alpha$  [50] and a nuclear localization signal at the carboxyl terminal end [51]. Although Plasmodium TopoIII is devoid of any such signal sequences, our subcellular fractionation data, immunofluorescence data, and mitochondrial immunoprecipitation results collectively establish that PfTopoIII is a mitochondrial topoisomerase. This finding again reinforces the notion that the mechanism behind mitochondrial import is poorly understood in malaria parasites.

Human TopoIIIα is required for the maintenance of mtDNA, and TopoIIIα-depleted cells show a significant loss of monomeric mtDNA and form large catenated networks [23]. *Plasmodium* mitochondria undergo a rolling circle mode of replication to form a complex network of linear concatamers during active replication of the parasite [26]. Consistent with this notion, the specific association between PfTopoIII at the terminal end of mtDNA during the final stage of parasite replication indicates its likely involvement in the decatenation of the catenated mtDNA to aid in mtDNA segregation.

HU treatment depletes the cellular pool of deoxyribonucleotides and subsequently causes stalling of the replication fork [52]. Eventually, there occurs accumulation of joint DNA molecules in the direction opposite to the replication fork, and this results in the formation of so-called chicken foot structures [53] that have serious implications on cell survivability. As these structures resemble Holliday junctions [54], we speculate that if such a condition is generated in P. falciparum, PfTopoIII along with its cognate helicases might play an important role in resolving the structures and converting them back into the replication forks. Our study demonstrated the direct role of PfTopoIII in mitigating HU-mediated replication stress. First, PfTopoIII expression is induced in a dose-dependent manner in response to HU treatment. Second, expression of PfTopoIII can completely bypass the HU-induced growth defect in the parasites. It is noteworthy that the HU-mediated aberrant structure is resolved by the dual action of TopoIII and RecQ helicases. There are two members of the RecQ family of DNA helicases in Plasmodium, namely, PfBlm and PfWrn. The absence of either of these enhances the rate of formation of stalled replication forks, indicating that both the members are required for efficient Plasmodium DNA replication [55]. E. coli RecQ helicases interact with TopoIII and help resolve converging replication forks [56]. In humans, TopoIIIα can dissolve Holliday structures jointly with Blm but not with Wrn [57]. In this study, we found that PfTopoIII interacts with PfBlm and PfWrn with equal efficiency and that both helicases are expressed at the active replication stage of the parasite. However, it is necessary to investigate further whether both helicases mobilize a double Holliday junction and the resulting catenated DNA is resolved by PfTopoIII in malaria parasites.



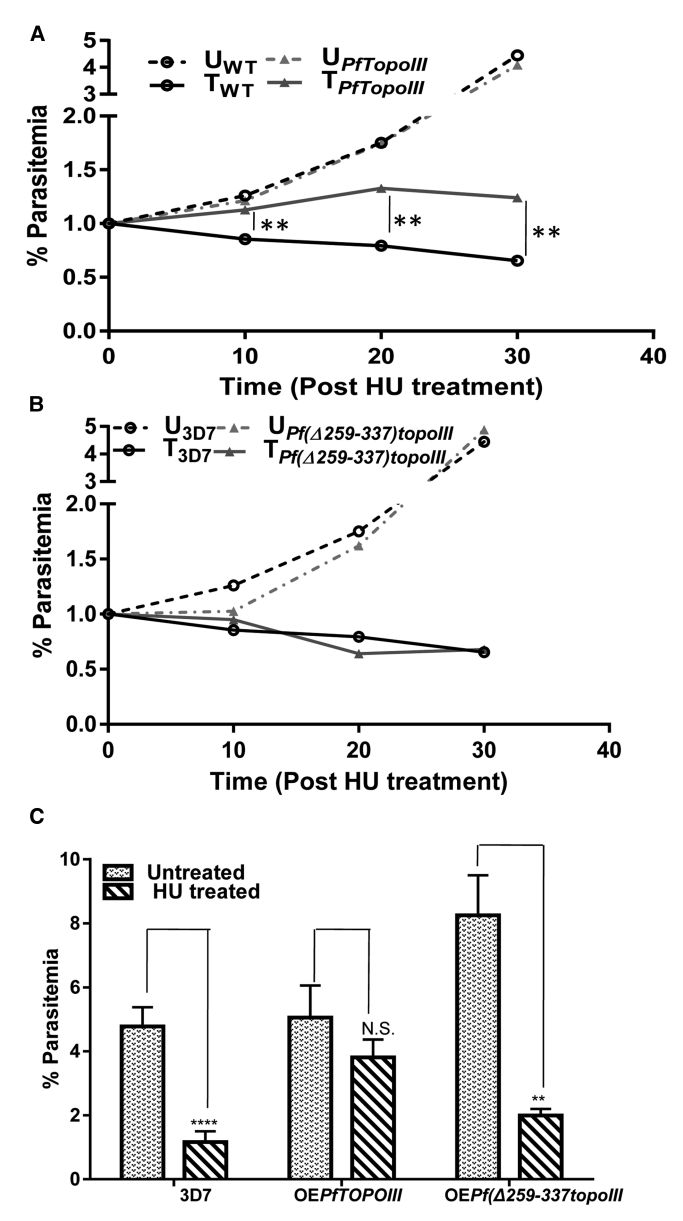


Figure 11. PfTopolII but not PftopolII ( $^{\Delta259-337}$ ) expression reverses the replication stress induced growth defect. (A) 3D7 and  $^{P}$  PfToPolII over-expressing parasites, synchronized at trophozoite stage, were treated with 2.5 mM HU for 30 h. The parasitemia of each treated and untreated strain was measured after 10 h, 20 h and 30 h time intervals. At each time point, approximately 2000 RBC were counted and the mean parasitemia was plotted. Error bars indicate mean  $\pm$  SD; n = 3; \*\*  $^{P}$  < 0.01. (B) A similar experiment was performed with 3D7 and  $^{P}$  ( $^{\Delta259-337}$ )topolII over-expressing strain with HU treatment for 30 h. More than three independent experiments were conducted and the mean parasitemia (%) was plotted. (C) 3D7,  $^{P}$  PfTopolII over-expressing strain and  $^{P}$  ( $^{\Delta259-337}$ )topolII over-expressing strain were synchronized at the trophozoite stage and treated with 2.5 mM HU for 6 h. Afterwards, HU was extensively washed and treated parasite strains were subsequently grown in normal media for 26 h following which, parasitemia was measured. For each strain, minimum three batches of experiments were done and mean values of parasitemia for untreated and treated condition for each of the three strains were plotted. Error bars indicate SD; n = 3; \*\*\*\*  $^{P}$  < 0.001;  $^{P}$  N.S. not significant.

Our study identified a charged domain within PfTopoIII that is indispensable for its *in vivo* function. MDS of PfTopoIII with DNA octamer showed that the enzyme undergoes a conformational change upon DNA binding. At the start of the DNA protein interaction, PfTopoIII-ssDNA adopts a closed conformation similar



to that of the apo enzyme (PfTopoIII alone). However, gradually a central cavity is created by the movement of domain III and the Toprim domain so that the DNA can be accommodated. This movement of domains is often referred to as protein-mediated gate dynamics [58] and has an important implication in their biochemical activities. The DNA octamer is stabilized by the hydrogen bonding and stacking interactions between bases and the positively charged residues present in the charged domain of PfTopoIII. Hence, it can be concluded that the charged domain stabilizes the effective binding of PfTopoIII with DNA and thus may play an important role in the catalytic mechanism of PfTopoIII protein. This is supported by our study, which reveals that the removal of the charged region, as in PftopoIII (\$\tilde{\text{\Delta}}259-337)\$ shows lesser association with mtDNA in the transgenic parasites. Our genetic study emphasized the essential requirement of this domain for PfTopoIII function. First, the expression of wild-type PfTopoIII fully rescued the slow-growth phenotype and MMS-induced toxicity in yeast, but the expression of mutant PftopoIII  $(\Delta 259-337)$  failed to do the same and mimicked the phenotype of the topoisomerase-inactive mutant PftopoIIIY421F. We found that the loss of activity in the mutant PftopoIII $^{(\Delta 259-337)}$  strain was not due to poor heterologous expression of *Plasmodium* protein in *S. cerevisiae*. Although the expression of PftopoIII $^{(\Delta 259-337)}$  could not be demonstrated by western blotting analyses, the interaction between PftopoIII(\(\Delta 25\hat{9}-337\)) and PfBlm/PfWrn in yeast two-hybrid studies indirectly demonstrated the expression of the mutant protein in yeast. Second, the transgenic mutant parasite line (PftopoIII $^{(\Delta 259-337)}$ -GFP) failed to rescue itself from short-term exposure to replication stress, like the transgenic parasite line PfTopoIII-GFP. Together, our results emphasize the importance of the charged domain in PfTopoIII function. Although this type of charged domain is absent from other eukaryotic TopoIII, a similar kind of multiple positively charged insertions, albeit shorter stretches have been observed in E. coli and many other prokaryotic TopoIII sequences [17]. A previous experimental study showed that the charged loop present in bacterial TopoIII is essential for decatenation of replication intermediates [17]. To date, no inhibitors of TopoIII have been identified. However, identification of the unique and indispensable charged domain of PfTopoIII qualifies itself as a target against malaria.

## **Competing Interests**

The authors declare that there are no competing interests associated with the manuscript.

#### **Funding**

The work is supported by grants from the Department of Science and Engineering Research Board (DST-SERB), India [EMR/2017/001173].

#### **Author Contributions**

S.B. conceived the idea, designed the experiments, guided and wrote the paper. S.Ba., P.S., N.S. and H.C. have conducted all the experiments. N.B. has done all the computational work. A.R. and G.B. have planned and guided the computational work. A.R. has written a part of the paper related to computational study.

#### **Acknowledgements**

The work was supported by the Department of Science and Engineering Research Board (DST-SERB), India [EMR/2017/001173] to S.B. S.Ba. was supported by the Senior Research Fellowships from Council for Scientific and Industrial Research (CSIR), India. P.S. was supported by the Junior Research Fellowships from Council for Scientific and Industrial Research (CSIR), India. N.S. was supported by the Senior Research Fellowships from University Grants Commission (UGC). H.C. was supported by the MSc. thesis grant, Department of Biotechnology, India. We acknowledge UGC-SAP for funding the Department of Biotechnology and Bioinformatics, University of Hyderabad to procure Fluorescence microscope, which was used in the present study. We thank Professor Mrinal K Bhattacharyya for helpful discussions and for critical reading of the manuscript.

#### **Abbreviations**

ARP, Aspartate-rich protein; ES, early schizont; FEL, free energy landscape; HU, Hydroxyurea; LS, late schizont; MD, molecular dynamics; MMS, methyl methanesulfonate; PCA, principal component analyses; RBCs, red blood cells; RMSFs, root-mean-square fluctuations; RT, reverse transcription.



#### References

- 1 Rathod, P.K., McErlean, T. and Lee, P.C. (1997) Variations in frequencies of drug resistance in *Plasmodium falciparum. Proc. Natl Acad. Sci. U.S.A.* **94**, 9389–9393 https://doi.org/10.1073/pnas.94.17.9389
- 2 Ariey, F., Witkowski, B., Amaratunga, C., Beghain, J., Langlois, A.C., Kim, S. et al. (2014) A molecular marker of artemisinin-resistant *Plasmodium falciparum* malaria. *Nature* **505**, 50–55 https://doi.org/10.1038/nature12876
- 3 Miller, L.H., Ackerman, H.C., Su, X.Z. and Wellems, T.E. (2013) Malaria biology and disease pathogenesis: insights for new treatments. *Nat. Med.* **19**, 156–167 https://doi.org/10.1038/nm.3073
- Widdowson, K. and Hennessy, A. (2010) Advances in structure-based drug design of novel bacterial topoisomerase inhibitors. Future Med. Chem. 2, 1619–1622 https://doi.org/10.4155/fmc.10.250
- 5 Nitiss, J.L. (2009) Targeting DNA topoisomerase II in cancer chemotherapy. Nat. Rev. Cancer 9, 338–350 https://doi.org/10.1038/nrc2607
- 6 Wang, J.C. (1996) DNA topoisomerases. Annu. Rev. Biochem. 65, 635-692 https://doi.org/10.1146/annurev.bi.65.070196.003223
- Mudeppa, D.G., Kumar, S., Kokkonda, S., White, J. and Rathod, P.K. (2015) Topoisomerase II from human malaria parasites. Expression, purification and selective inhibition. *J. Biol. Chem.* 290, 20313–20324 https://doi.org/10.1074/jbc.M115.639039
- 8 Raghu Ram, E.S.V., Kumar, A., Biswas, S., Kumar, A., Chaubey, S., Siddiqi, M.I. et al. (2007) Nuclear gyrB encodes a functional subunit of the Plasmodium falciparum gyrase that is involved in apicoplast DNA replication. Mol. Biochem Parasitol. 154, 30–39 https://doi.org/10.1016/j.molbiopara. 2007.04.001
- 9 Dar, M.A., Sharma, A., Mondal, N. and Dhar, S.K. (2007) Molecular cloning of apicoplast-targeted *Plasmodium falciparum* DNA gyrase genes: unique intrinsic ATPase activity and ATP-independent dimerization of *Pl*GyrB subunit. *Eukaryot. Cell* **6**, 398–412 https://doi.org/10.1128/EC.00357-06
- Gupta, A., Mehra, P., Deshmukh, A., Dar, A., Mitra, P., Roy, N. et al. (2009) Functional dissection of the catalytic carboxyl-terminal domain of origin recognition complex subunit 1 (*Pf*ORC1) of the human malaria parasite *Plasmodium falciparum*. *Eukaryot*. *Cell* 8, 1341–1351 https://doi.org/10.1128/FC.00170-09
- 11 Chalapareddy, S.K., Chakrabarty, S., Bhattacharyya, M. and Bhattacharyya, S. (2016) Radicicol-mediated inhibition of topoisomerase VIB-VIA activity of the human malaria parasite *Plasmodium falciparum*. mSphere 1, e00025-15 https://doi.org/10.1128/mSphere.00025-15
- 12 Chalapareddy, S.K., Bhattacharyya, M.K., Mishra, S. and Bhattacharyya, S. (2014) Radicicol confers mid-schizont arrest by inhibiting mitochondrial replication in *Plasmodium falciparum*. *Antimicrob. Agents Chemother.* 58, 4341–4352 https://doi.org/10.1128/AAC.02519-13
- 13 Tosh, K., Chessman, S., Horrocks, P. and Kilbey, B. (1999) Plasmodium falciparum: stage related expression of topoisomerase I. Exp. parasitol. 91, 126–132 https://doi.org/10.1006/expr.1998.4362
- 14 Stewart, L., Redinbo, M.R., Qiu, X., Hol, W.G.J. and Champoux, J.J. (1998) A model for the mechanism of human topoisomerase I. Science 279, 1534–1541 https://doi.org/10.1126/science.279.5356.1534
- Plank, J. and Hsieh, T.S. (2009) Helicase-appended topoisomerases: new insight into the mechanism of directional strand transfer. J. Biol. Chem. 284, 30737–30741 https://doi.org/10.1074/jbc.R109.051268
- Dean, F., Krasnow, M., Otter, R., Matzuk, M., Spengler, S. and Cozzarelli, N. (1983) *Escherichia coli* type-1 topoisomerases: identification, mechanism, and role in recombination. *Cold Spring Harb. Symp. Quant. Biol.* **49**, 769–777 https://doi.org/10.1101/SQB.1983.047.01.088
- 17 Zhiyu, L., Mondragón, A., Hiasa, H., Marians, K. and DiGate, R.J. (2002) Identification of a unique domain essential for *Escherichia coli* DNA topoisomerase III -catalysed decatenation of replication intermediates. *Mol. Microbiol.* 35, 888–895 https://doi.org/10.1046/j.1365-2958.2000.01763.x
- 18 DiGate, R.J. and Marians, K.J. (1988) Identification of a potent decatenating enzyme from *Escherichia coli. J. Biol. Chem.* **263**, 13366–13373 PMID:2843517
- 19 Lee, C.M., Wang, G., Pertsinidis, A. and Marians, K.J. (2019) Topoisomerase III acts at the replication fork to remove precatenanes. J. Bacteriol. 201, e00563-18 https://doi.org/10.1128/JB.00563-18
- 20 Wallis, J., Chrebet, G., Brodsky, G., Rolfe, M. and Rothstein, R. (1989) A hyper-recombination mutation in S.cerevisiae identifies a novel eukaryotic topoisomerase. Cell 58, 409–419 https://doi.org/10.1016/0092-8674(89)90855-6
- 21 Hanai, R., Caron, P.R. and Wang, J.C. (1996) Human TOP3: A single-copy gene encoding DNA topoisomerase III. Proc. Natl Acad. Sci. U.S.A. 93, 3653–3657 https://doi.org/10.1073/pnas.93.8.3653
- 22 Oakley, T.J. and Hickson, I.D. (2002) Defending genome integrity during S-phase: putative roles for RecQ helicases and topoisomerase III. *DNA Repair* 1, 175–207 https://doi.org/10.1016/S1568-7864(02)00002-2
- 23 Nicholls, T.J., Nadalutti, C.A., Motori, E., Sommerville, E., Gorman, G., Basu, S. et al. (2018) Topoisomerase 3α is required for decatenation and segregation of human mtDNA. *Mol. Cell* **69**, 9–23.e6 https://doi.org/10.1016/j.molcel.2017.11.033
- Preiser, P., Wilson, R., Moore, P., McCready, S., Hajibagheri, M., Blight, K. et al. (1996) Recombination associated with replication of malarial mitochondrial DNA. EMBO J. 15, 684–693 https://doi.org/10.1002/j.1460-2075.1996.tb00401.x
- 25 Maleszka, R., Skelly, P.K. and Clark- walker, G.D. (1991) Rolling circle replication of DNA in yeast mitochondria. EMBO J. 10, 3923–3929 https://doi.org/10.1002/j.1460-2075.1991.tb04962.x
- Wilson, R.J. and Williamson, D.H. (1997) Extrachromosomal DNA in the apicomplexa. *Microbil. Mol. Biol. Rev.* **61**, 1–16 https://doi.org/10.1128/.61.1.
- 27 Mendes, T.A., Lobo, F.P., Rodrigues, T.S., Rodrigues-Luiz, G.F., da Rocha, W.D., Fujiwara, R.T. et al. (2013) Repeat-enriched proteins are related to host cell invasion and immune evasion in parasitic protozoa. *Mol. Biol. Evol.* **30**, 951–963 https://doi.org/10.1093/molbev/mst001
- 28 Laskar, S., Bhattacharyya, M., Shankar, R. and Bhattacharyya, S. (2011) HSP90 controls SIR2 mediated gene silencing. PLoS ONE 8, e23406 https://doi.org/10.1371/journal.pone.0023406
- 29 Govindarajalu, G., Rizvi, Z., Kumar, D. and Sijwali, P.S. (2019) Lyse-reseal erythrocytes for transfection of *Plasmodium falciparum*. Sci. Rep. 9, 19952 https://doi.org/10.1038/s41598-019-56513-9
- 30 Longtine, M.S., Mc kenzie, III, A., Demarini, D.J., Shah, N., Wach, A., Brachat, A. et al. (1998) Additional modules for versatile and economical PCR-based gene deletion and modification in Saccharomyces cerevisiae. Yeast 14, 953–961 https://doi.org/10.1002/(SICI)1097-0061(199807) 14:10<953::AID-YEA293>3.0.CO;2-U
- 31 Suhane, T., Bindumadhavan, V., Fangaria, N., Nair, A., Tabassum, W., Muley, P. et al. (2019) Glu-108 in *Saccharomyces cerevisiae* Rad51 is critical for DNA damage-induced nuclear function. *mSphere* **4**, e00082-19 https://doi.org/10.1128/mSphere.00082-19



- 32 Moll, K., Ljungstrom, I., Perlmann, H., Scherf, A. and Wahlgren, M. (2008) *Methods in Malaria Research*, Malaria Research and Reference Reagent Resource Center/ATCC. Manassas. VA
- 33 Yang, J. and Zhang, Y. (2015) Protein structure and function prediction using I-TASSER. *Curr. Protoc. Bioinformatics* **52**, 5–8 https://doi.org/10.1002/0471250953.bi0508s52
- 34 Bocquet, N., Bizard, A.H., Abdulrahman, W., Larsen, N.B., Faty, M., Cavadini, S. et al. (2014) Structural and mechanistic insight into Holliday-junction dissolution by topoisomerase Illa and RMI1. *Nat. Struct. Mol. Biol.* **21**, 261–268 https://doi.org/10.1038/nsmb.2775
- Hess, B., Kutzner, C., Spoel, D.V. and Lindahl, E. (2008) GROMACS 4: Algorithms for highly efficient, load-balanced, and scalable molecular simulation. *J. Chem. Theory Comput.* **4**, 435–447 https://doi.org/10.1021/ct700301g
- Huang, J. and MacKerell, Jr, A.D. (2013) CHARMM36 all-atom additive protein force field: Validation based on comparison to NMR data. *J. Comput. Chem.* **34**, 2135–2145 https://doi.org/10.1002/jcc.23354
- 37 Jorgensen, W.L., Chandrasekhar, J., Madura, J.D., Impey, R.W. and Klein, M.L. (1983) Comparison of simple potential functions for simulating liquid water. *J. Chem. Phys.* **79**, 926–935 https://doi.org/10.1063/1.445869
- 38 Changela, A., DiGate, R.J. and Mondragon, A. (2001) Crystal structure of a complex of a type IA DNA topoisomerase with a single-stranded DNA molecule. *Nature* **441**, 1077–1081 https://doi.org/10.1038/35082615
- 39 Humphrey, W., Dalke, A. and Schulten, K. (1996) VMD: visual molecular dynamics. *J. Mol. Graph.* **14**, 33–38 https://doi.org/10.1016/0263-7855(96) 00018-5
- 40 The UniProt Consortium. (2017) Uniprot: the universal protein knowledgebase. *Nucleic Acids Res.* **45**, D158–D169 https://doi.org/10.1093/nar/gkw1099
- 41 Aurrecoechea, C., Brestelli, J., Brunk, B.P., Dommer, J., Fischer, S., Gajria, B. et al. (2009) PlasmoDB: a functional genomic database for malaria parasites. *Nucleic Acids Res.* **37**, D539–D543 https://doi.org/10.1093/nar/gkn814
- 42 Thompson, J.D., Higgins, D.G. and Gibson, T.J. (1994) CLUSTAL w: improving the sensitivity of progressive multiple sequence alignment through sequence weighting, position-specific gap penalties and weight matrix choice. *Nucleic Acids Res.* **22**, 4673–4680 https://doi.org/10.1093/nar/22.22.4673
- 43 Price, M.N., Dehal, P.S. and Arkin, A.P. (2009) Fasttree: computing large minimum evolution trees with profiles instead of a distance matrix. Mol. Biol. Evol. 26, 1641–1650 https://doi.org/10.1093/molbev/msp077
- 44 Kanehisa, M., Goto, S., Kawashima, S. and Nakaya, A. (2002) The KEGG databases at genomeNet. *Nucleic Acids Res.* **30**, 42–46 https://doi.org/10.1093/nar/30.1.42
- 45 Harte, W.E., Swaminathan, S., Mansuri, M.M., Martin, J.C., Rosenberg, I.E. and Beveridge, D.L. (1990) Domain communication in the dynamical structure of human immunodeficiency virus 1 protease. *Proc. Natl Acad. Sci. U.S.A.* **87**, 8864–8868 https://doi.org/10.1073/pnas.87.22.8864
- 46 Groth, P., Ausländer, S., Majumder, M.M., Schultz, N., Johansson, F., Petermann, E. et al. (2010) Methylated DNA causes a physical block to replication forks independently of damage signalling, O(6)-methylguanine or DNA single-strand breaks and results in DNA damage. *J. Biol. Chem.* **402**, 70–82 https://doi.org/10.1016/j.jmb.2010.07.010
- 47 Chakraverty, R.K., Kearsey, J.M., Oakley, T., Grenon, J., Ruiz, M., Lowndes, M.A.T. et al. (2001) Topoisomerase III acts upstream of Rad53p in the S-Phase DNA damage checkpoint. *Mol. Cell. Biol.* **21**, 7150–7162 https://doi.org/10.1128/MCB.21.21.7150-7162.2001
- 48 Mitra, P., Banu, K., Deshmukh, A.S., Subbarao, N. and Dhar, S.K. (2015) Functional dissection of proliferating-cell nuclear antigen (1 and 2) in human malarial parasite *Plasmodium falciparum*: possible involvement in DNA replication and DNA damage response. *Biochem. J.* **470**, 115–129 https://doi.org/10.1042/BJ20150452
- 49 Zellweger, R., Dalcher, D., Mutreja, K., Berti, M., Schmid, J.A., Herrador, R. et al. (2015) Rad51-mediated replication fork reversal is a global response to genotoxic treatments in human cells. J. Cell Biol. 208, 563–579 https://doi.org/10.1083/jcb.201406099
- 50 Wang, Y., Lyu, Y.L. and Wang, J.C. (2002) Dual localization of human DNA topoisomerase Illα to mitochondria and nucleus. *Proc. Natl Acad. Sci. U.S.A.* **99**, 12114–12119 https://doi.org/10.1073/pnas.192449499
- 51 Wu, J., Feng, L. and Hsieh, T. (2010) Drosophila topo Illα is required for the maintenance of mitochondrial genome and male germ-line stem cells. *Proc. Natl Acad. Sci. U.S.A.* **107**, 6228–6233 https://doi.org/10.1073/pnas.1001855107
- 52 Bianchi, V., Pontis, E. and Reichard, P. (1986) Changes of deoxyribonucleoside triphosphate pools induced by hydroxyurea and their relation to DNA synthesis. *J. Biol. Chem.* **261**, 16037–16042 PMID:3536919
- 53 Chrystelle, M. and Bénard, M. (2014) Replication forks reverse at high frequency upon replication stress in *Physarum polycephalum*. *Chromosoma* **123**, 577–585 https://doi.org/10.1007/s00412-014-0471-z
- Liu, Y. (2016) EEPD1: breaking and rescuing the replication fork. PLoS Genet. 12, e1005742 https://doi.org/10.1371/journal.pgen.1005742
- Claessens, A., Harris, L.M., Stanojcic, S., Chappell, L., Stanton, A., Kuk, N. et al. (2018) Recq helicases in the malaria parasite *Plasmodium falciparum* affect genome stability, gene expression patterns and DNA replication dynamics. *PLoS Genet.* **14**, e1007490 https://doi.org/10.1371/journal.pgen.
- 56 Suski, C. and Marians, K. (2008) Resolution of converging replication forks by RecQ and topoisomerase III. *Mol. Cell* **30**, 779–789 https://doi.org/10.1016/i.molcel.2008.04.020
- 57 Wu, L., Chan, K.L., Ralf, C., Bernstein, D.A., Garcia, P.L., Bohr, V.A. et al. (2005) The HRDC domain of BLM is required for the dissolution of double Holliday junctions. *EMBO J.* **24**, 2679–2687 https://doi.org/10.1038/sj.emboj.7600740
- 58 Mills, M., Tse-Dinh, Y. and Neuman, K.C. (2018) Direct observation of topoisomerase IA gate dynamics. *Nat. Struct. Mol. Biol.* **25**, 1111–1118 https://doi.org/10.1038/s41594-018-0158-x





### Plasmodium Topoisomerase VIB and Spo11 Constitute Functional Type IIB Topoisomerase in Malaria Parasite: Its Possible Role in Mitochondrial DNA Segregation

Priyanka Singh,<sup>a</sup> Wahida Tabassum,<sup>b</sup> Nupur Fangaria,<sup>a</sup> Sandeep Dey,<sup>c</sup> Siladitya Padhi,<sup>d</sup> Mrinal K. Bhattacharyya,<sup>b</sup> Kota Arun Kumar,<sup>c</sup> Arijit Roy,<sup>d</sup> Sunanda Bhattacharyya

<sup>a</sup>Department of Biotechnology and Bioinformatics, School of Life Sciences, University of Hyderabad, Hyderabad, India

**ABSTRACT** The human malaria parasite undergoes a noncanonical cell division, namely, endoreduplication, where several rounds of nuclear, mitochondrial, and apicoplast replication occur without cytoplasmic division. Despite its importance in Plasmodium biology, the topoisomerases essential for decatenation of replicated chromosome during endoreduplication remain elusive. We hypothesize that the topoisomerase VI complex, containing *Plasmodium* falciparum topiosomerase VIB (PfTopoVIB) and catalytic P. falciparum Spo11 (PfSpo11), might be involved in the segregation of the Plasmodium mitochondrial genome. Here, we demonstrate that the putative PfSpo11 is the functional ortholog of yeast Spo11 that can complement the sporulation defects of the yeast  $\Delta spo11$  strain, and the catalytic mutant Pfspo11Y65F cannot complement such defects. PfTopoVIB and PfSpo11 display a distinct expression pattern compared to the other type II topoisomerases of Plasmodium and are induced specifically at the late schizont stage of the parasite, when the mitochondrial genome segregation occurs. Furthermore, PfTopoVIB and PfSpo11 are physically associated with each other at the late schizont stage, and both subunits are localized in the mitochondria. Using PfTopoVIB- and PfSpo11-specific antibodies, we immunoprecipitated the chromatin of tightly synchronous early, mid-, and late schizont stage-specific parasites and found that both the subunits are associated with the mitochondrial genome during the late schizont stage of the parasite. Furthermore, PfTopoVIB inhibitor radicicol and atovaquone show synergistic interaction. Accordingly, atovaquone-mediated disruption of mitochondrial membrane potential reduces the import and recruitment of both subunits of PfTopoVI to mitochondrial DNA (mtDNA) in a dose-dependent manner. The structural differences between PfTopoVIB and human TopoVIB-like protein could be exploited for development of a novel antimalarial agent.

**IMPORTANCE** This study demonstrates a likely role of topoisomerase VI in the mitochondrial genome segregation of *Plasmodium falciparum* during endoreduplication. We show that PfTopoVIB and PfSpo11 remain associated and form the functional holoenzyme within the parasite. The spatiotemporal expression of both subunits of PfTopoVI correlates well with their recruitment to the mitochondrial DNA at the late schizont stage of the parasite. Additionally, the synergistic interaction between PfTopoVI inhibitor and the disruptor of mitochondrial membrane potential, atovaquone, supports that topoisomerase VI is the mitochondrial topoisomerase of the malaria parasite. We propose that topoisomerase VI may act as a novel target against malaria.

**KEYWORDS** *Plasmodium* mitochondria, *Plasmodium* topoisomerase VI, apicomplexan topoisomerase

**Editor** Anat Florentin, Hebrew University of

Copyright © 2023 Singh et al. This is an openaccess article distributed under the terms of the Creative Commons Attribution 4.0

Address correspondence to Sunanda Bhattacharyya, sdeb70@gmail.com, or sbtsl@uohvd.ac.in.

The authors declare no conflict of interest.

**Received** 3 December 2022 **Accepted** 7 May 2023

<sup>&</sup>lt;sup>b</sup>Department of Biochemistry, School of Life Sciences, University of Hyderabad, Hyderabad, India

<sup>&</sup>lt;sup>c</sup>Department of Animal Biology, School of Life Sciences, University of Hyderabad, Hyderabad, India

dTCS Research-Hyderabad (Life Sciences Division), Tata Consultancy Services Limited, Hyderabad, India

10.1128/spectrum.04980-22

alaria is a serious concern to public health. According to the latest WHO report (1), there were an estimated 241 million malaria cases in 2020 and 95% of these cases were reported in Africa. Alarmingly, 80% of malaria-related deaths in Africa occur in children under the age of 5 years. This necessitates the importance of basic research with malaria parasites to identify novel proteins that can act as an antimalarial target. Topoisomerases pose an attractive antimalarial target due to the absence of some of the unique topoisomerases from the human genome (2).

The malaria parasite undergoes a noncanonical cell division known as endoreduplication: twice in the human host and once in the mosquito midgut. During this cell cycle, multiple rounds of genome replication occur without cytokinesis. An earlier study has shown that in *Arabidopsis thaliana*, topoisomerase VI (TopoVI) is essential for decatenation of the replicated chromosome during endoreduplication (3). It was reported that TopoVI deletion mutants can complete only first two endocycles and stall at 8C, compared to the wild-type cells that complete four rounds of endoreduplication and display 32C (3). *Plasmodium* possesses topoisomerase VI, but whether it is involved in the segregation of the parasite genome during endoreduplication remains elusive. Live-cell imaging of *Plasmodium falciparum* revealed that while the nuclear and apicoplast division occur in the early and mid-schizont stages, respectively, the mitochondrial division happens shortly before the cell division (4). It can be speculated that the mitochondrial genome segregation is initiated in the late schizont stage of the parasite.

Earlier we have shown that *Plasmodium* topoisomerase VI can genetically complement topoisomerase II function in *Saccharomyces cerevisiae*. Ectopic expression of *P. falciparum* TopoVI (PfTopoVI) was found to rescue a  $\Delta topoII$  lethal mutant strain (5). Using the cell extract of  $\Delta topoII$  yeast harboring PfTopoVI, we have shown that it can decatenate the kinetoplast DNA. Although PfTopoVI has a type II topoisomerase activity, direct demonstration of its precise function in the malaria parasite has not been done so far.

Topoisomerase VI was first characterized in Sulfolobus shibatae (6) and then in plants (3). In plants and algae, TopoVI has two subunits, TopoVIA and TopoVIB, which together form the functional enzyme. While TopoVIA harbors the DNA binding and DNA cleavage domain, TopoVIB harbors the GHKL domain responsible for ATP binding and ATP hydrolysis. It was demonstrated that ATP binding to the TopoVIB is essential for stabilization of TopoVI enzyme, which is required for DNA cleavage (7). The eukaryotic orthologue of TopoV1A is known as Spo11 (8). Plasmodium harbors both subunits of PfTopoVI, namely, PfSpo11 (new ID, PF3D7\_1217100) and PfTopoVIB. In our earlier study, PfSpo11 was referred to as PfTopoVIA (old ID, PF3D7 1217100.1) (5). Here, we have referred to this protein as PfSpo11. Using a yeast two-hybrid assay, it was shown earlier that PfTopoVIA and PfTopoVIB associate with each other. Furthermore, using yeast cell extract harboring PfTopoVI, it was shown that the decatenation activity of the enzyme is inhibited by radicicol; this was observed at sublethal doses, Radicicol reduces the mitochondrial genome content of the parasite (9), but the mechanism of such an effect was not investigated. Furthermore, whether PfSpo11 and PfTopoVIB form the functional holoenzyme within the parasite mitochondria remains elusive. In addition, whether PfSpo11 is the catalytic subunit of TopoVI enzyme was not investigated.

In this study, we have established for the first time that PfSpo11 is the functional ortholog of yeast Spo11. We provide evidence for the existence of PfTopoVI holoenzyme within the mitochondria of malaria parasite and its probable function in mitochondrial genome segregation. Our study was further supported by the result that the PfTopoVIB inhibitor radicicol synergizes with atovaquone, an antimalarial drug that collapses mitochondrial membrane potential, within the malaria parasite.

In humans, TopoVIB orthologs are not found, albeit human TopoVIB-like protein (TopoVIBL) has been identified, which shows 10% identity with *Plasmodium* TopoVIB. The ATPase domain of PfTopoVIB is distinct from the canonical ATP binding fold (Walker ATPases) and known as the Bergerat fold, which is characterized by four signature boxes: N, G1, G2, and G3. We found that there is no similarity between the predicted structures of the Bergerat folds of human TopoVIBL and *Plasmodium* VIB protein.

### **RESULTS**

PfSpo11 complements the sporulation defect of a diploid  $\Delta$ spo11 strain. To evaluate the function of PfSpo11, we tried to express the recombinant PfSpo11 protein in various bacterial systems (5); however, we were not successful, and hence we used yeast as a surrogate system. Diploid budding yeast undergoes meiosis in response to nitrogen starvation, and the haploid nuclei generated during meiosis are packaged in spores. The meiosis is initiated by Spo11, which catalyzes the cleavage of double-stranded DNA, which is subsequently repaired by recombination between the parental chromosomes. In plants, Spo11 along with TopoVIB forms the functional complex; however, in yeast, TopoVIB being absent, yeast Spo11 (ySpo11) can catalyze the double-strand break (DSB) formation by interacting with several other proteins (10). It was reported earlier that diploid cells with Spo11 deleted display reduced efficiency of sporulation due to the defect in meiotic recombination (11). We examined whether putative PfSpo11 can complement the function of S. cerevisiae Spo11 (ScSpo11). PfSpo11 harbors the conserved DNA binding CAP (catabolite activating protein) domain and metal binding TOPRIM domain, which share 42.7% and 59.5% sequence similarity, respectively, with the corresponding domains of ScSpo11 (5). We cloned PfSPO11 and ScSPO11 in the centromeric yeast expression vectors. Using site-directed mutagenesis, we generated a point mutation (Y to F) to the catalytic tyrosine residue of PfSPO11 at the 65th position with phenylalanine. For our assay, we used the diploid  $\Delta spo11$  strain (BY4741), which is of S228C origin and was earlier reported to show 5 to 15% sporulation efficiency (12). We generated four isogenic strains, each harboring empty vector (negative control), PfSPO11, Pfspo11Y65F, and ScSPO11 (positive control), as presented schematically in Fig. 1A. The sporulation was induced in these strains by growing them in presporulation liquid medium for 18 h at 30°C, and we subsequently allowed them to grow for another 48 h in sporulation medium at 18°C. The spore formation was visualized under a fluorescence microscope after staining with DAPI (4',6-diamidino-2-phenylindole) (Fig. 1B). It was observed that PfSPO11-expressing strain can bypass the sporulation defect of the  $\Delta Scspo11$  strain and produces a comparable number of spores to that of the strain expressing ScSPO11. PfSPO11- or ScSPO11-expressing strains formed 4 distinct nuclei, as represented in the figure; however, the catalytic mutant failed to sporulate. In order to rule out the possibility that the loss of sporulation in the PfSpo11Y65F strain is due to loss of expression of the mutant protein in yeast, we performed a Western blot analysis with the proteins extracted from each of the strains. Our study confirmed the expression of PfSpo11 and the mutant in the respective strains (Fig. 1C). We measured the sporulation efficiencies with three independent batches of cells in each strain and counted more than 1,000 cells in each case; the data are presented in Fig. 1D. We observed that PfSpo11 can complement the sporulation defect of the  $\Delta spo11$ strain (1.1%) to the same extent as ScSpo11. Our analysis showed that the PfSPO11-harboring strain showed a sporulation efficiency (8.3%) similar to that obtained by the ScSPO11-harboring strain (6.6%); however, the catalytic mutant Pfspo11Y65F strain showed a severe defect in sporulation as there was a drastic reduction in its efficiency (1.7%), which was comparable to that of the  $\Delta spo11$  strain. Thus, our study shows for the first time that PfSpo11 is the functional ortholog of ySpo11 and its activity is dependent on the catalytic tyrosine residue.

PfTopoVIB and PfSpo11 display a unique expression compared to the other type II topoisomerases of *P. falciparum*. Parasite genome replication is initiated at the late trophozoite/early schizont stage of the parasite, and hence the type II topoisomerases that remove the topological strains for the progression of the replication fork need to be expressed during the initiation of DNA replication. Earlier we found that the two subunits of PfTopoVI were predominantly expressed in the schizont-specific stages compared to the ring and trophozoite stages, respectively (9). In order to have a better understanding of the function of PfTopoVI, we measured the transcripts of other type II topoisomerase subunits identified in the parasite (2) at three distinct developmental stages within the schizont. We used tightly synchronized parasites 35 to 36 h postinvasion (hpi) as early schizont (ES) stage-specific, 39 to 40 hpi as mid-schizont (MS) stage-specific, and 44 to 45 hpi as late schizont (LS) stage-specific parasites for all of our experiments (Fig. 2A). These stages were carefully chosen by examining the relative size of the nucleus under a microscope as shown in the representative pictures. The semiquantitative reverse transcription-PCR (semi-qRT-PCR) data

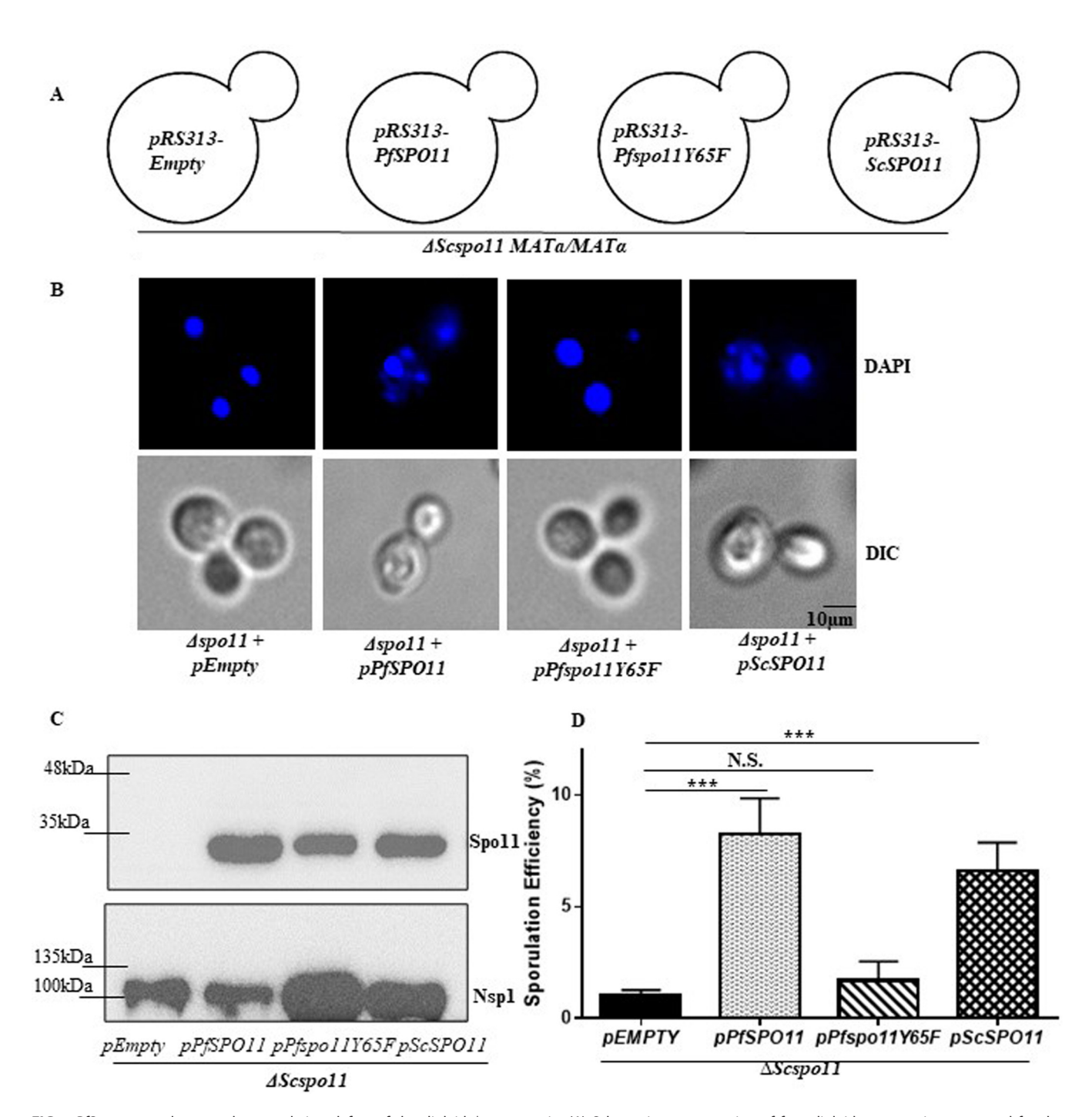


**FIG 1** PfSpo11 complements the sporulation defect of the diploid  $\Delta spo11$  strain. (A) Schematic representation of four diploid yeast strains generated for the sporulation assay:  $\Delta Scspo11$  MATa/MATα-Empty pRS313,  $\Delta Scspo11$  MATa/MATα-PRS313-PfSPO11,  $\Delta Scspo11$  MATa/MATα-PRS313-Pfspo11Y65F, and  $\Delta Scspo11$  MATa/MATα-PRS313-ScSPO11; (B) fluorescence imaging of the respective diploid strains that were subjected to sporulation. The cells were stained with DAPI to visualize the nuclei. The strain expressing PfSPO11 can complement the sporulation defect of  $\Delta Scspo11$  strains; however, the strain expressing Pfspo11Y65F cannot. DIC, differential inference contrast. (C) Western blot showing the expression of Spo11 in the respective strains. Nsp1 was used as a loading control. (D) For each strain, we counted the number of cells that can form mature asci (3 or 4 spores), and the percentage of sporulation was calculated. The experiment was repeated with three independent batches of cells for each strain (n = 1,000 cells). The mean values  $\pm$  SD were plotted for each strain using GraphPad Prism 6. P values were calculated using two-tailed Student's t test (\*\*\*\*, P < 0.001; N.S., not significant).

showed that *PfTOPOVIB* and *PfSPO11* displayed a unique expression pattern, unlike other type II topoisomerase genes, and were not expressed in the ES and MS stages (Fig. 2B). The expression of *PfTOPOVIB* and *PfSPO11* was induced at the late schizont stage of the parasite, when the nuclear replication is reported to have ceased (13). To rule out the possibility that the cDNA preparation is not contaminated with the genomic DNA, we did the

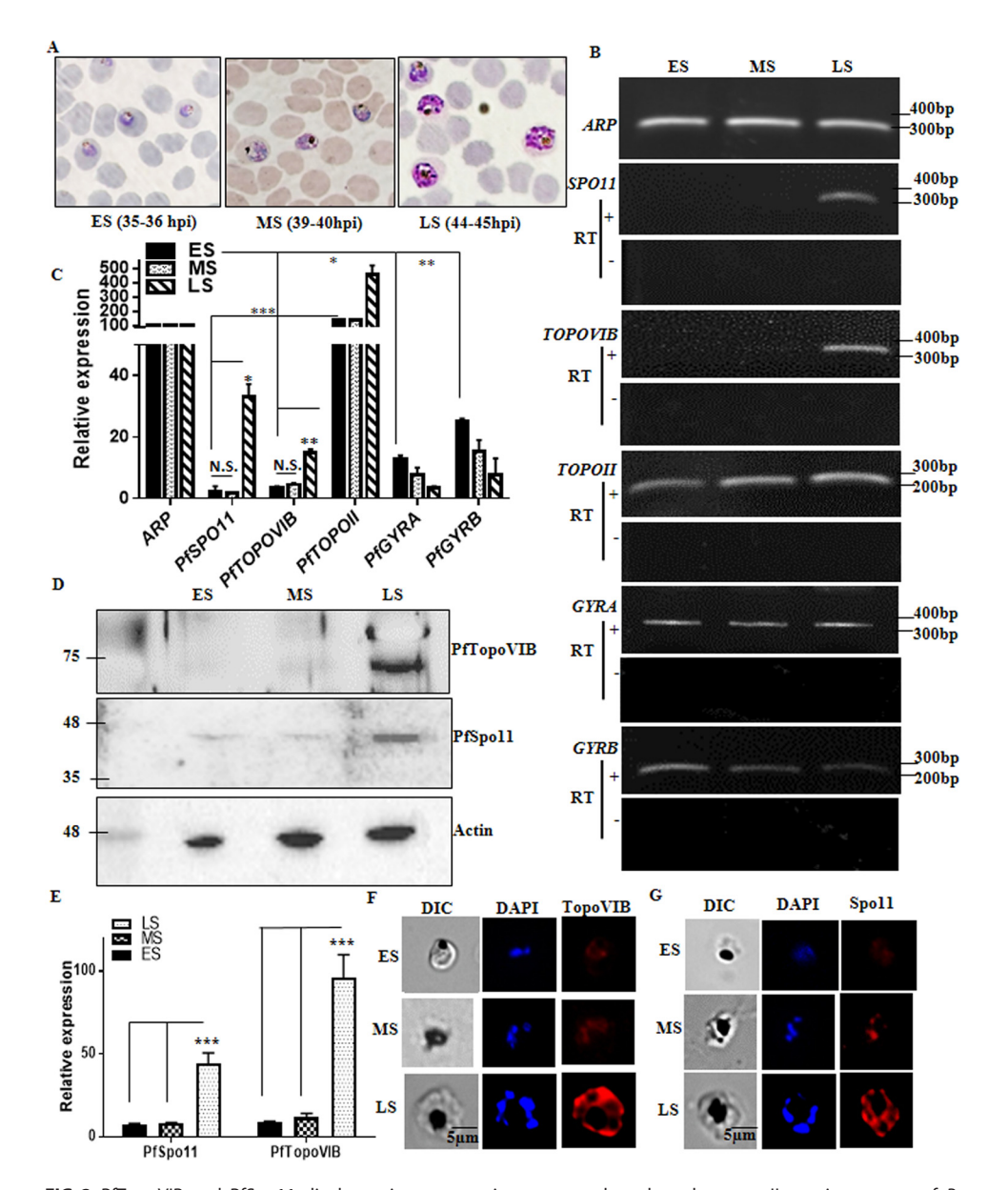


**FIG 2** PfTopoVIB and PfSpo11 display unique expression compared to the other type II topoisomerases of *P. falciparum*. (A) Giemsa-stained representative images of the synchronized ES (early schizont [35 to 36 hpi]), MS (mid-schizont [39 to 40 hpi]), and LS (late schizont [44 to 45 hpi])-specific 3D7 parasites; (B) semi-qRT-PCR analysis was done from the cDNA prepared from the ES, MS, and LS stages of the parasites to visualize the expression of all type II topoisomerases (*PfTOPOII*, *PfGYRA*, *PfGYRB*, *PfTOPOVIB*, and *PfSPO11*). Agarose gel images for both positive and negative reverse transcriptase (+ RT and – RT, respectively) samples are presented. (C) Real-time RT-PCR analysis was done to quantify the relative expression of all of the type II topoisomerases in comparison to those constitutively expressing *ARP* at the ES, MS, and LS stages. The experiment was repeated with two independent batches of parasites. *P* values were calculated using two-tailed Student's *t* test (\*\*\*, P < 0.001; \*\*, P < 0.05; N.S., not significant). (D) Western blot analysis shows that PfTopoVIB and PfSpo11 are expressed predominantly at the LS stage-specific parasite; actin was used as a normalizing control. (E) Relative levels of protein expression of PfTopoVIB and PfSpo11 were calculated using ImageJ from three independent batches of synchronized ES, MS, and LS stage-specific parasite proteins, and the mean values  $\pm$  SD were plotted. *P* values were calculated using the two-tailed Student's *t* test (\*\*\*, P < 0.001). (F and G) Indirect immunofluorescence images showing the expression of PfTopoVIB and PfSpo11 predominantly at the LS stages. DAPI was used to stain the nucleus.

amplification of topoisomerases with each of the stage-specific mRNAs, which were pretreated with DNase but not with reverse transcriptase. We found no amplicons in PCR samples not pretreated with reverse transcriptase, confirming that the cDNA samples were devoid of genomic DNA. We did the qRT-PCR analysis with two independent batches of parasites and found that PfTOPOVIB and PfSPO11 expression remained significantly lower than PfTOPOVIB and PfSYRASE expression at the ES stage (Fig. 2C). To confirm the expression pattern at the

protein level, we isolated total parasite proteins from the ES, MS, and LS stages and probed them with PfTopoVIB or PfSpo11 antibodies. Western blot analysis showed the presence of the PfTopoVI subunits exclusively at the LS stage of the parasites (Fig. 2D). We isolated the proteins from three independent batches of synchronous ES, MS, and LS stage-specific parasites and performed Western blot analysis for each set; eventually, the band intensity of each blot was analyzed using ImageJ analysis. We normalized the band intensity of PfTopoVIB and PfSpo11 with the loading control actin and plotted the intensity (Fig. 2E). The result showed that the levels of PfSpo11 and PfTopoVIB expression were upregulated 5-fold and 10-fold, respectively, at the LS stage compared to the ES/MS stage. We also performed the indirect immunofluorescence assay to visualize the expression of PfTopoVI subunits in three distinct schizont stages of the parasite. Alexa Red 594-conjugated secondary antibody was used to visualize the red fluorescence for both PfTopoVIB and PfSpo11 by using Nicon Eclipse NiE AR fluorescence microscope. DAPI was used to stain the nucleus. We scanned hundreds of cells and found that both the subunits are predominantly expressed at the late schizont stage of the parasite. Hence, our study indicates that PfTopoVI may not have any function during genome replication; rather, it may play a role in genome segregation.

Stage-specific promoter activity of PfTopoVI subunits. To further validate the unique expression pattern of PfTopoVI subunits, we wanted to investigate the chromatin compaction of the promoter regions of PFTOPOVIB and PFSPO11 at different developmental stages of the parasite. To this end, we used formaldehyde-assisted isolation of regulatory elements (FAIRE), which allows one to determine whether a specific region of chromatin is in nucleosome-free state or a nucleosome-bound state. Our assay was aimed at identifying whether the promoter regions of PfTOPOVIB and PfSPO11 were indeed active specifically at the LS stage. We used 620-bp and 311-bp upstream activator sequences (UASs) from the translation start sites (ATG) of PfTOPOVIB and PfSPO11, respectively, for our analysis, as shown in Fig. 3A. As mitochondrial DNA (mtDNA) is not associated with the nucleosome, we used the COX3 promoter sequence as the normalizing control. We found that the promoter of PFTOPOVIB remains in a nucleosome-bound state at the ES and the MS stages, whereas it is shifted to the nucleosome-free state at the LS stage of the parasite (Fig. 3B). The promoter of PfSPO11 shows a similar pattern to UAS\_PFTOPONB; however, it shows slightly loose chromatin compaction even in the mid-schizont stage. We repeated this experiment, and quantification of gel images revealed 25-fold and 4-fold relaxation in the chromatin compaction of the PfTOPOVIB and the PfSPO11 promoters, respectively, at the LS stage of the parasite (Fig. 3C) compared to the MS stage. We determined the occupancy of two established epigenetic marks (14), namely, the activation mark H3K4me3 and the repression mark H3K9me3 to the promoter-proximal regions of PfTOPOVIB and PfSPO11 at various schizont stages. For that, we performed chromatin immunoprecipitation (ChIP) analysis with the synchronous cultures of the ES, MS, and LS stages of the parasites using anti-H3K4me3, anti-H3K9me3, or anti-IgG antibodies. We found 6-fold and 2-fold enrichment of H3K4me3 at the promoter-proximal region of both PFTOPOVIB (Fig. 3D and E) and PfSPO11-1 (Fig. 3G and H), respectively, especially at the LS stage. On the contrary, we found negligible recruitment of H3K9me3 at the PfTOPOVIB<sub>UAS</sub> and PfSPO11-1<sub>UAS</sub> at the ES stage, which was further decreased at the LS stage. To ascertain the specificity of the recruitment of H3K4me3 or H3K9me3 at the promoter-proximal region of PfTOPOVIB/PfSPO11, we performed the ChIP experiment with probes located within the 3' end of the ORF of the aforementioned genes (C-terminal end [CTE] probes), as shown in Fig. 3A. However, the levels of recruitment of H3K4me3 at the CTE regions of PfTOPOVIB or PfSPO11 were found be negligible, with no further increase at the LS stage (Fig. 3E and F and Fig. 3H and I). Similarly, the recruitment of H3K9me3 remained unchanged at the CTE region of PfTOPOVIB or PfSPO11 within the different stages of schizont. Together, we conclude that the promoter-proximal sequences of PfTOPOVIB remain as heterochromatin during the ES/MS stage and undergo active transcription only at the LS stage. In case of PfSPO11<sub>UAS</sub>, we observe that the promoter-proximal region shows little activity in the MS stage and shows highest activity in the LS stage.

**PfTopoVIB and PfSpo11 form the functional holoenzyme in the parasite.** We determined the localization of PfTopoVI subunits within the parasite. For that, we harvested LS

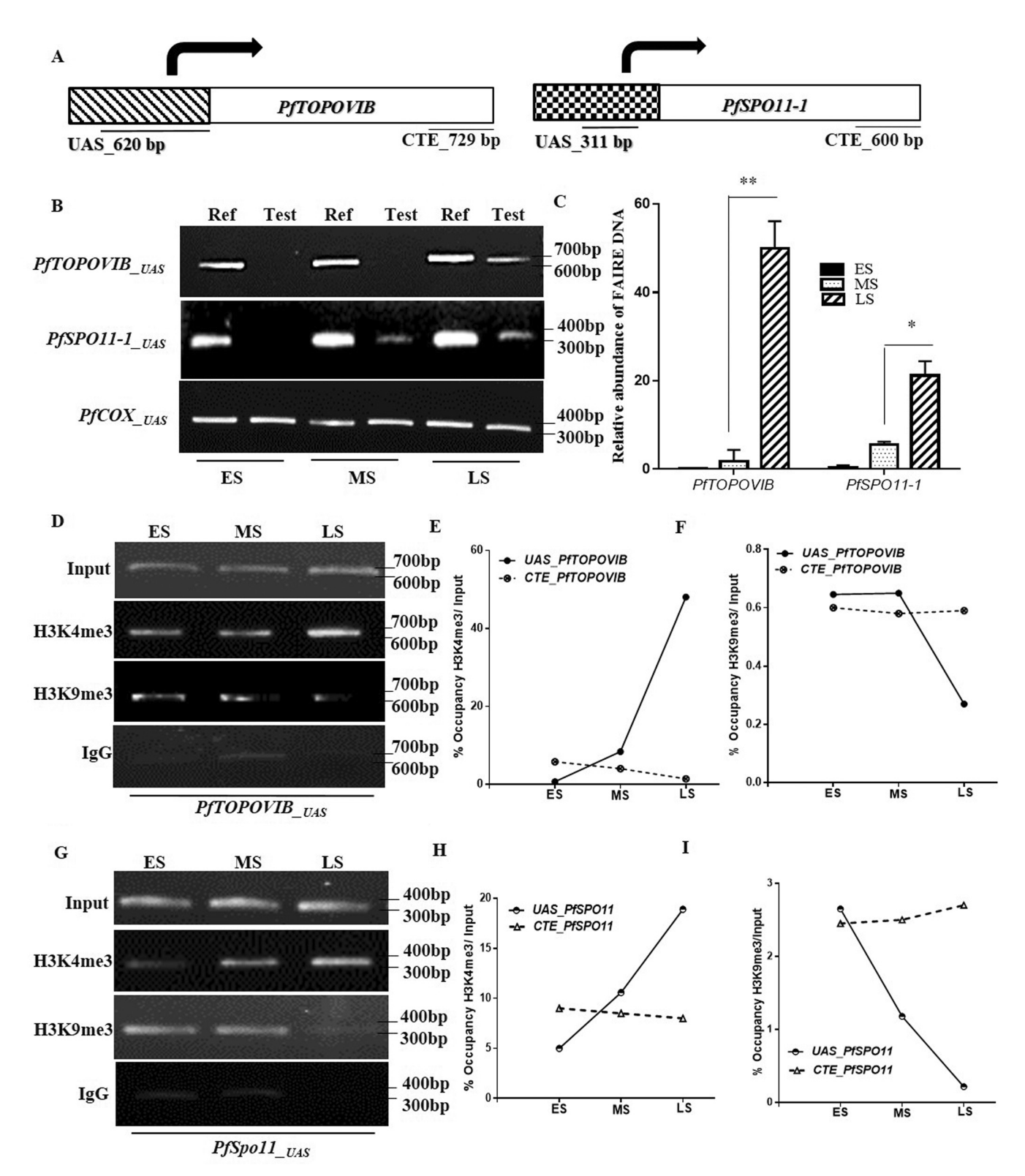
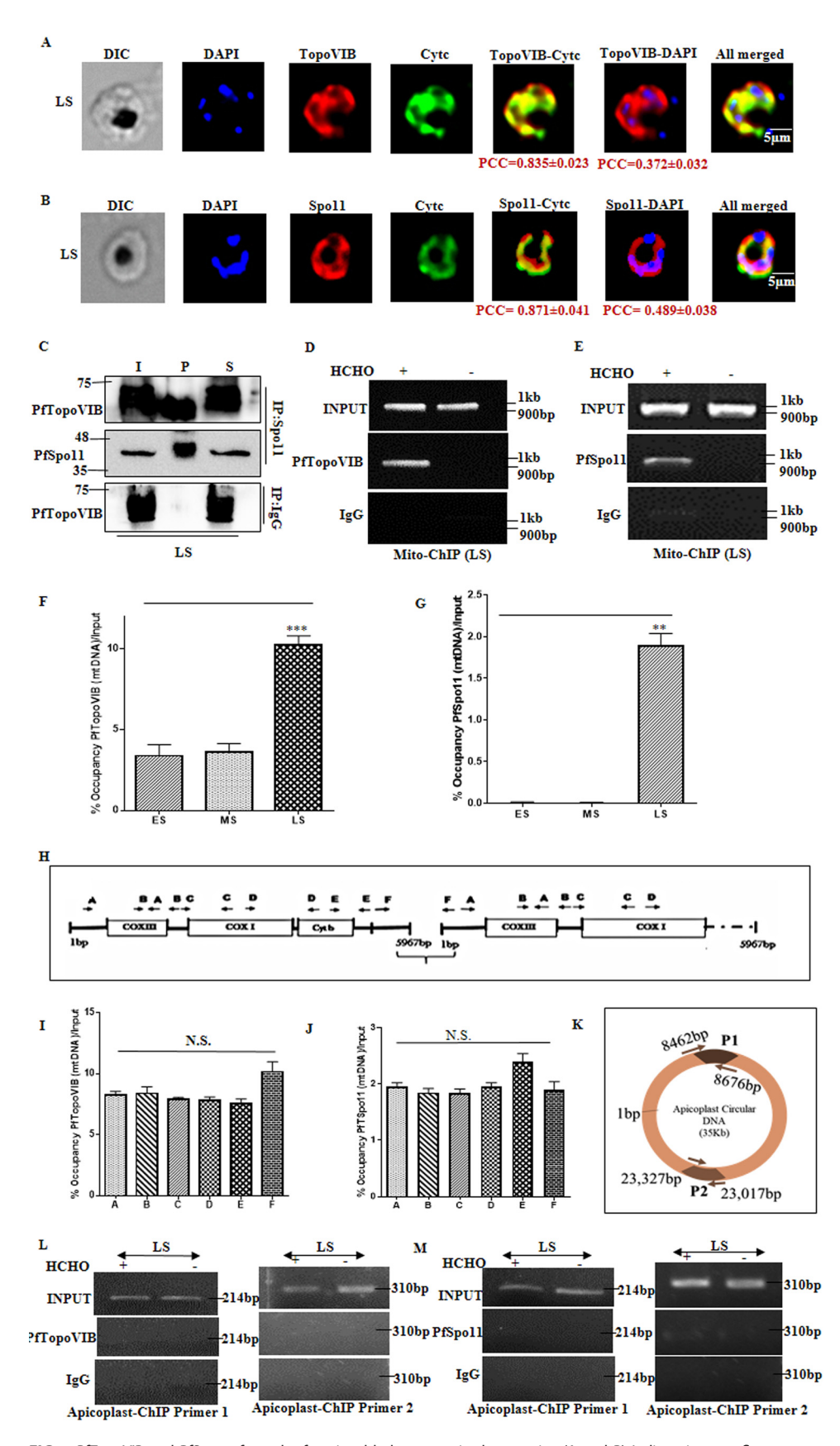


FIG 3 Stage-specific promoter activity of PfTopoVI subunits. (A) The positions of the upstream activator sequence (620\_UASPITOPOVIB) and C-terminal end (729\_CTE) of PfTOPOVIB used in ChIP analysis are presented in the left panel. Similarly, the position of the UAS and CTE of PfSPO11 (i.e., 311\_UASPISpO11 and 600\_CTE) used in ChIP analysis are presented in the right panel. (B) FAIRE was performed with tightly synchronized ES, MS, and LS stages of the parasite to find that the PfTOPOVIB\_UAS and PfSPO11\_UAS chromatin remained loosely packed at the LS stage. COX3 was used as a normalizing control. Lane 1, reference at ES; lane 2, test at ES; lane 3, reference at MS; lane 4, test at MS; lane 5, reference at LS; lane 6, test at LS. (C) The experiment described above was done with two independent sets of experiments, and the mean values ± SD were plotted, P values were calculated using two-tailed Student's t test (\*\*, P < 0.01; \*, P < 0.05). Both PfTOPOVIB\_UAS are present as the nucleosome-free DNA at the LS stage. (D) ChIP assay was performed with the ES, MS, and LS stage-specific parasites using anti-H3K4me3 (Continued on next page)

stage-specific parasites and performed indirect immunofluorescence to visualize PfTopoVIB and PfSpo11 as red fluorescence, as shown in Fig. 2F and G, respectively. We determined the average Pearson correlation coefficient (PCC) for 20 to 25 images to evaluate the localization of PfTopoVIB or PfSpo11 with the nuclear stain DAPI, as shown in Fig. 4A and B; the values are presented underneath the images in panels A and B. We used anti-cytochrome c (anti-Cytc) antibody to visualize the green fluorescence of mitochondrial protein Cytc, where the secondary antibody was conjugated with Alexa Fluor 488. We determined the average PCC to evaluate whether red signals specific to PfTopoVIB or PfSpo11 colocalize with the green fluorescence of Cytc; the average values are presented underneath the figure panels. We conclude that both the subunits are predominantly present in mitochondria as the average PCC values of each subunit show stronger correlation with Cytc (PCC > 0.8) and moderate correlation with DAPI (PCC < 0.5). We have provided additional cell images to show the localization of PfTopoVIB and PfSpo11 in the supplemental material (see Fig. S1C and D, respectively). Next, we determined the physical association between PfTopoVIB and PfSpo11 within the parasite by employing a coimmunoprecipitation assay. The LS stage-specific parasites were immunoprecipitated with PfSpo11-specific antibody, and the pellet fraction was probed with PfTopoVIB antibody. We found that PfTopoVIB was coprecipitated with PfSpo11, thus establishing a physical association between the two subunits (Fig. 4C). In a parallel experiment, immunoprecipitation was done with IgG, and when probed, no PfTopoVIB protein was detected in the pellet fraction. Thus, our study confirmed the presence of PfTopoVI holoenzyme at the late schizont stage of the parasite. As the holoenzyme expression does not correlate with the onset of replication of the parasite genome, we predict that it might function in mitochondrial genome segregation, which was earlier reported to occur at the late schizont stage of the parasite (4). In order to evaluate their possible function in the mitochondrial genome segregation, we determined whether the two subunits of PfTopoVI interact with the mitochondrial DNA. We employed the chromatin immunoprecipitation (ChIP) assay to detect the recruitment of PfTopoVIB and PfSpo11 to the mitochondrial genome in the presence or absence of formaldehyde cross-linking. We found the specific binding of PfTopoVIB (Fig. 4D) and PfSpo11 (Fig. 4E) to the mitochondrial genome in the LS stage-specific parasites and found that the mtDNA was only amplified in the presence of formaldehyde. We isolated synchronous ES (35 to 36 hpi), MS (39 to 40 hpi), and LS (44 to 45 hpi) stage-specific parasites and quantified the percentage of occupancy of PfTopoVIB of mtDNA with respect to the input by employing quantitative PCR (qPCR). We found that PfTopoVIB recruitment to the mtDNA is positively correlated with its expression and is significantly enriched at the LS stage of the parasites compared to the other stages (Fig. 4F). Similarly, ChIP was done with PfSpo11-specific antibody for the stage-specific parasites mentioned above. The qPCR showed that the percentage of occupancy of PfSpo11 in mtDNA was highest in the LS stage-specific parasites (Fig. 4G). To evaluate whether the enzyme shows any preference in the association toward any specific parts of mtDNA, we used a set of six primers (A to F), as presented schematically in Fig. 4H. Each primer pair results in 1-kb amplified fragments, and together A to E encompass the entire mitochondrial genome; additionally, the primer pair F has been designed such that it amplifies the junctional sequence and produces the amplicon from circular mtDNA or when two monomeric mtDNA units form concatemers. With the LS stage-specific PfTopoVIB-mtDNA as well as PfSpo11-mtDNA IP sample, we monitored the percentage of occupancy of the subunits in various parts (A to F) of mtDNA. The qPCR analysis showed no significant difference between

### FIG 3 Legend (Continued)

and anti-H3K9me3 antibodies to find their recruitment at the PFTOPOVIB\_UAS' IgG was used as a negative control. (E) qPCRs from two independent sets of ChIP assays were performed, and mean values ± SD were plotted. The recruitment of H3K4me3 to UAS\_PFTOPOVIB was found to increase by 6-fold at the LS stage compared to that of the MS stage, although recruitment of H3K4me3 to CTE\_PFTOPOVIB at the same stage was negligible. (F) The recruitment of H3K9me3 to UAS\_PFTOPOVIB was found to decrease by 2-fold at the LS stage compared to that of the MS stage; however, recruitment of CTE\_PFTOPOVIB under the same conditions remains unaltered. (G) The ChIP assay was performed with the ES, MS, and LS stage-specific parasites using anti-H3K4me3/anti-H3K9me3-specific antibodies to determine their recruitment at the PfSPO11\_UAS' IgG was used as a negative control. (H) qPCR using two independent sets of ChIP assays was performed, and mean values ± SD were plotted. The recruitment of the activation mark to UAS\_PfSPO11 was increased by 2-fold at the LS stage compared to that of the MS stage; however, recruitment under the same conditions at CTE\_PfSPO11 was not altered within the different stages. (I) The recruitment of the repressor mark showed a downward trend in UAS\_PfSPO11 and was almost negligible at the LS stage; however, the repressor mark remained bound at CTE\_PfSPO11 at all schizont stages.



**FIG 4** PfTopoVIB and PfSpo11 form the functional holoenzyme in the parasite. (A and B) Indirect immunofluorescence of LS stage-specific parasites shows the distribution of both PfTopoVIB (red) and PfSpo11 (red) in the parasite nucleus (Continued on next page)

TABLE 1 IC<sub>50</sub> for strain 3D7 of radicicol in combination with atovaquone and vice versa

Drug or drug combination	IC <sub>50</sub>	Potentiation factor	
Radicicol alone	$8\mu{ m M}$	1	
Radicicol + atovaquone <sup>a</sup>	1.7 $\mu$ M	4.7	
Atovaquone alone	1.4 nM	1	
Atovaquone $+$ radicicol $^b$	0.12 nM	11.67	

<sup>&</sup>lt;sup>a</sup>The IC<sub>50</sub> of atovaquone in strain 3D7 was used.

the occupancies of PfTopoVIB (Fig. 4I) and PfSpo11 (Fig. 4J) of any specific regions of mtDNA. Furthermore, to evaluate whether the recruitment of the enzyme is specific to the mitochondrial genome or not, we monitored the association of both the subunits across the apicoplast genome by using two primer sets, P1 and P2, which cover 214 bp and 310 bp, respectively, as shown in Fig. 4K. In the LS stage-specific PfTopoVIB and PfSpo11 IP samples, we didn't find any occupancy in the apicoplast genome (Fig. 4L and M). Together, these studies indicate a probable functional association of PfTopoVI during mitochondrial genome segregation at the late schizont stage of the parasite.

PfTopoVIB inhibitor radicicol and atovaquone potentiate each other. Since atovaguone collapses the mitochondrial membrane potential of the parasite (15), we speculated that treatment with it should reduce the mitochondrial import of PfTopoVI subunits. On the other hand, since PfTopoVI is involved in mitochondrial genome maintenance, inhibition of this enzyme complex by radicicol (5) should affect the effective replication of mitochondrial genome. In our earlier work, it was observed that radicicol treatment indeed reduced the mitochondrial genome content of the parasite (9); hence, we speculate that the total amount of transcripts of mitochondrial genes, including cytochrome b and subunit I of cytochrome c oxidase (Cox I), which are the targets of atoyaquone (bc, complex), will be decreased. Hence, we hypothesize that atovaquone and radicicol should potentiate each other's action. We treated the synchronous trophozoite stage-specific 3D7 parasites with various doses of atovaquone for 48 h and measured the parasite survivability by the SYBR green method. The 50% inhibitory concentration (IC<sub>50</sub>) value obtained was 1.4 nM under our experimental condition (Table 1; Fig. S1A). When a similar experiment was performed in the presence of an IC $_{50}$  of radicicol of 8.05  $\mu$ M (Fig. S1B) (9), we observed a significant shift in the IC<sub>50</sub> of atovaquone, and it was reduced to 0.12 nM (Table 1). Thus, radicicol imparted 11.7-fold potentiation to atovaquone (Table 1). Similarly, we observed that the presence of

### FIG 4 Legend (Continued)

and mitochondria. After calculating the average (mean  $\pm$  standard error of the mean [SEM]) PCC values (n = 25) in each case, PfTopoVIB and PfSpo11 fluorescence showed a moderate correlation (PCC < 0.5) with nuclear stain DAPI (blue) but strong correlation (PCC > 0.8) with Cytc (green). The average MOC for the fraction of red fluorescence of PfTopoVIB overlapping green Cytc was 0.964, and that for the fraction of PfSpo11 fluorescence overlapping green Cytc was 0.938. (C) Western blot analysis showing the coimmunoprecipitation of PfTopoVIB with PfSpo11 from the synchronized LS stage of the parasite lysate. Pulldown was done with anti-PfSpo11 and IgG antibodies. I, input; P, immunoprecipitation (IP) pellet fraction; S, supernatant. (D) Chromatin immunoprecipitation showing recruitment of PfTopoVIB on the mitochondrial genome at the LS stage. Samples without formaldehyde treatment were used as a negative control to confirm the specific recruitment. (E) Chromatin immunoprecipitation showing recruitment of PfSpo11 on the mitochondrial genome at the LS stage. Samples without formaldehyde treatment were used as a negative control to confirm the specific recruitment. (F and G) Graphical representation of relative occupancy (percentage of input) of PfTopoVIB and PfSpo11, respectively, on the mitochondrial genome in parasites at different developmental stages as quantified by qPCR: ES (35 to 36 hpi), MS (39 to 40 hpi), and LS (44 to 45 hpi). The experiment was done with three independent batches of parasites, and the mean values  $\pm$  SD were plotted. *P* values were calculated using two-tailed Student's *t* test (\*\*\*, *P* < 0.001; \*\*, *P* < 0.01; N.S., not significant); the data were normalized using the respective IgG IP values. (H) Schematic representation of all the primers used in the ChIP assay, represented as A to F, each covering a 1-kb region of the mitochondrial genome. (I) PfTopoVIB shows uniform percentage of occupancy at different segments of mitochondrial genome (A to F) at the LS stage. (J) PfSpo11 also shows uniform percentage of occupancy at different segments of mitochondrial genome (A to F) at the LS stage. In both the cases in panels I and J, the relative occupancy was quantified by qPCR and the mean values  $\pm$  SD were plotted. P values were calculated using two-tailed Student's t test (N.S., not significant); the data were normalized using respective IgG-IP values. (K) Schematic representation of the primers used in the apicoplast ChIP assay, represented as P1 and P2, each covering 214 bp and 310 bp, respectively, of the apicoplast genome; (L) chromatin immunoprecipitation showing no recruitment of PfTopoVIB on apicoplast genome (P1 and P2) at the LS stage; (M) chromatin immunoprecipitation showing no recruitment of PfSpo11 on apicoplast genome (P1 and P2) at the LS stage.

<sup>&</sup>lt;sup>b</sup>The IC<sub>50</sub> of radicicol in strain 3D7 was used.

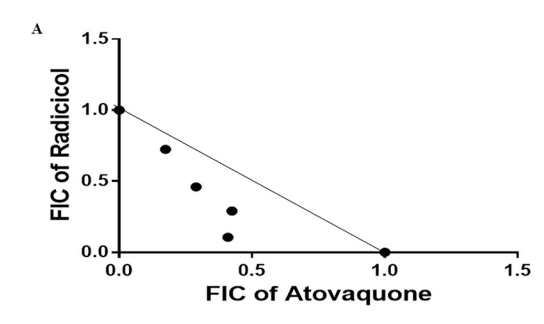
**TABLE 2** FIC values for strain 3D7 for the combinations of atovaquone and radicicol and radicicol and chloroquine

	FIC of:		
Drug ratio	Atovaquone or radicicol	Radicicol or chloroquine	$\Sigma$ FIC
Atovaquone/radicicol	Atovaquone	Radicicol	
5:0	1	0	1
4:1	0.41	0.106	0.5
3:2	0.425	0.291	0.716
2:3	0.29	0.460	0.75
1:4	0.175	0.724	0.899
0:5	0	1	1
Radicicol/chloroquine	Radicicol	Chloroquine	
5:0	1	0	1
4:1	0.702	0.347	1.049
3:2	0.38	0.497	0.877
2:3	0.33	0.967	1.297
1:4	0.11	0.877	0.987
0:5	0	1	1

an IC<sub>50</sub> of atovaquone reduces the IC<sub>50</sub> of radicicol to 1.7  $\mu$ M. Thus, atovaquone was also found to potentiate radicicol by 4.7-fold (Table 1).

The PfTopoVIB inhibitor radicicol interacts with atovaquone in a synergistic manner. We studied whether the interactions between the PfTopoVI inhibitor radicicol and atovaquone are synergistic or additive. For that, we performed a fixed-ratio drug combination assay. For each combination of the drugs, the dose-response curves were plotted (data not shown) and the fractional inhibitory concentration (FIC) was calculated and tabulated (Table 2). Subsequently, the sum of FIC values was calculated (Table 2) and plotted in an isobologram (Fig. 5A). The isobologram shows that the interaction between radicicol and atovaquone is synergistic in nature. In order to investigate the specificity of radicicol-atovaquone interaction, we used an unrelated drug, chloroquine, and determined its interaction with radicicol. We calculated the FIC and  $\Sigma$ FIC (Table 2), and the isobologram (Fig. 5B) was plotted. We found that a  $\Sigma$ FIC of  $\geq$ 1 represents no interaction between radicicol and chloroquine. Thus, the synergistic interaction between PfTopoVI inhibitor and chemical that collapses mitochondrial membrane potential provides supporting evidence that PfTopoVI is a mitochondrial topoisomerase.

Atovaquone reduces mitochondrial import and mtDNA recruitment of PfTopoVIB and PfSpo11 in a dose-dependent manner. In order to support our conclusion further, we sought to determine whether atovaquone treatment really affects the mitochondrial import and the mitochondrial DNA recruitment of PfTopoVI. To that end, the synchronous mid-trophozoite-specific parasite culture was treated with increasing doses



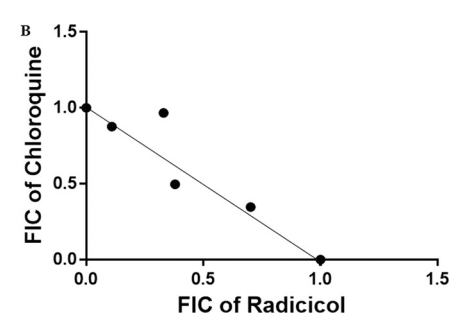


**FIG 5** PfTopoVIB inhibitor radicicol and atovaquone show synergism with each other. (A) Synergistic interaction between the PfTopoVIB inhibitor radicicol and atovaquone was determined by plotting an isobologram of radicicol and atovaquone interaction in the 3D7 strain. Each point represents the mean half-maximal inhibitory concentration ( $IC_{50}$ ) of the drug combination from three independent experiments. A solid line was drawn between the  $IC_{50}$  values of each of the drugs radicicol and atovaquone when used alone. FIC, fractional inhibitory concentration. (B) In a similar way, an isobologram of radicicol and chloroquine interaction in the 3D7 strain was plotted. Each point represents the mean  $IC_{50}$  of the drug combination experiment from two independent experiments. A solid line was drawn between the  $IC_{50}$  values of each drug when used alone.

of atovaquone and allowed to grow until the parasites reached the late schizont stage. The plan of the experiment is schematically presented in Fig. 6A. Subsequently, the cultures were harvested and the mitochondrial localizations of PfTopoVIB and PfSpo11 were measured using an immunofluorescence assay (IFA) and compared with those of the untreated parasites. In order to rule out the possibility that atovaquone treatment reduces the overall expression of Cytc or PfTopoVI, we performed Western blot analysis under the treatment condition using 0.5 nM atovaquone and compared the result with that from the untreated sample (Fig. 6B). The experiment was repeated with two independent batches of cells, and we calculated the band intensity of each of the PfTopoVI subunits in the Western blots using ImageJ and plotted the intensities (Fig. 6C). We found no significant difference in the levels of expression of PfTopoVIB, PfSpo11, and PfCytc under the treated condition. We calculated the average PCC values from 25 individual cells that were treated with 0.5 nM atovaquone and compared them with those of the untreated parasites. We observed that in the parasites treated with 0.5 nM atovaquone, the average PCC values were shifted from 0.835 to 0.66 in the case of PfTopoVIB (Fig. 6D), and the same values were shifted from 0.871 to 0.69 in the case of PfSpo11 (Fig. 6E). We conclude that the degree of colocalization between PfTopoVI with Cytc decreased in atovaquone-treated parasites. To validate this further, we determined the recruitment of these two subunits to the mtDNA under the atovaquone-treated condition. The ChIP assay with PfTopoVIB antibody was done with atovaquone concentrations of 0.5 nM and 1.2 nM, and there was a gradual decrease in recruitment of PfTopoVIB to the mitochondrial genome (Fig. 6F). The occupancy of PfTopoVIB with respect to the input DNA was quantified by realtime qPCR and is presented graphically in Fig. 6G. We observed about 30% reduction in the occupancy of PfTopoVIB in the mitochondrial genome in the presence of the sublethal doses (0.5 nM) of atovaquone, which showed a further reduction at a higher concentration of atovaquone. Similarly, we investigated the mitochondrial recruitment of PfSpo11 at three doses of atovaquone as described above. We observed a similar effect (Fig. 6H), and real-time quantification analysis revealed a dose-dependent reduction of recruitment of PfSpo11 to the mitochondrial genome (Fig. 6I).

**PfTopoVIB and HsTopoVIBL differ in their Bergerat folds.** There is only 10% identity in the amino acid sequences between *Plasmodium* TopoVIB and human TopoVIBL protein (2). A multiple-sequence alignment of the Bergerat fold region from different species is shown in Fig. 7. Although there are a number conserved residues in the N box within *Sulfolobus shibatae* and *Plasmodium* species, there is a low degree of conservation between human/mouse and *Plasmodium* within the signature box N, G1, and G2 motifs, apart from the conserved glycines. The glycines in the G3 motif are not conserved though. A structural alignment of the Bergerat fold region from PfTopoVIB and HsTopoVIBL is shown in Fig. 8. The structures of the two proteins differ significantly in the Bergerat fold region. This suggests that there could be major differences in the catalytic activity of the two proteins.

### **DISCUSSION**

This study demonstrates the existence of *Plasmodium* topoisomerase VI holoenzyme complex in the parasite lysate at the LS stage of the parasite. Furthermore, in this article we have established topoisomerase VI as a mitochondrial topoisomerase of the parasite. First, we have shown the localization of a topoisomerase holoenzyme (PfTopoVIB and PfSpo11) within the mitochondria. Second, both subunits remain associated with the whole mitochondrial genome in accordance with their expression. Third, the disrupter of mitochondrial membrane potential atovaquone inhibits the mitochondrial import and the recruitment of PfTopoVI subunits to the mitochondria in a dose-dependent manner. Finally, atovaquone and the PfTopoVIB inhibitor radicicol potentiate each other's action and display synergistic interaction with each other.

It was proposed earlier that the *Plasmodium* mitochondrion undergoes a rolling circle mode of replication, and during replication there is homologous recombination between circles and the termini of the linear molecules, which generates complex lariat-like structures (16, 17). This necessitates the involvement of a type II topoisomerase, which should decatenate

Month YYYY Volume XX Issue XX 10.1128/spectrum.04980-22

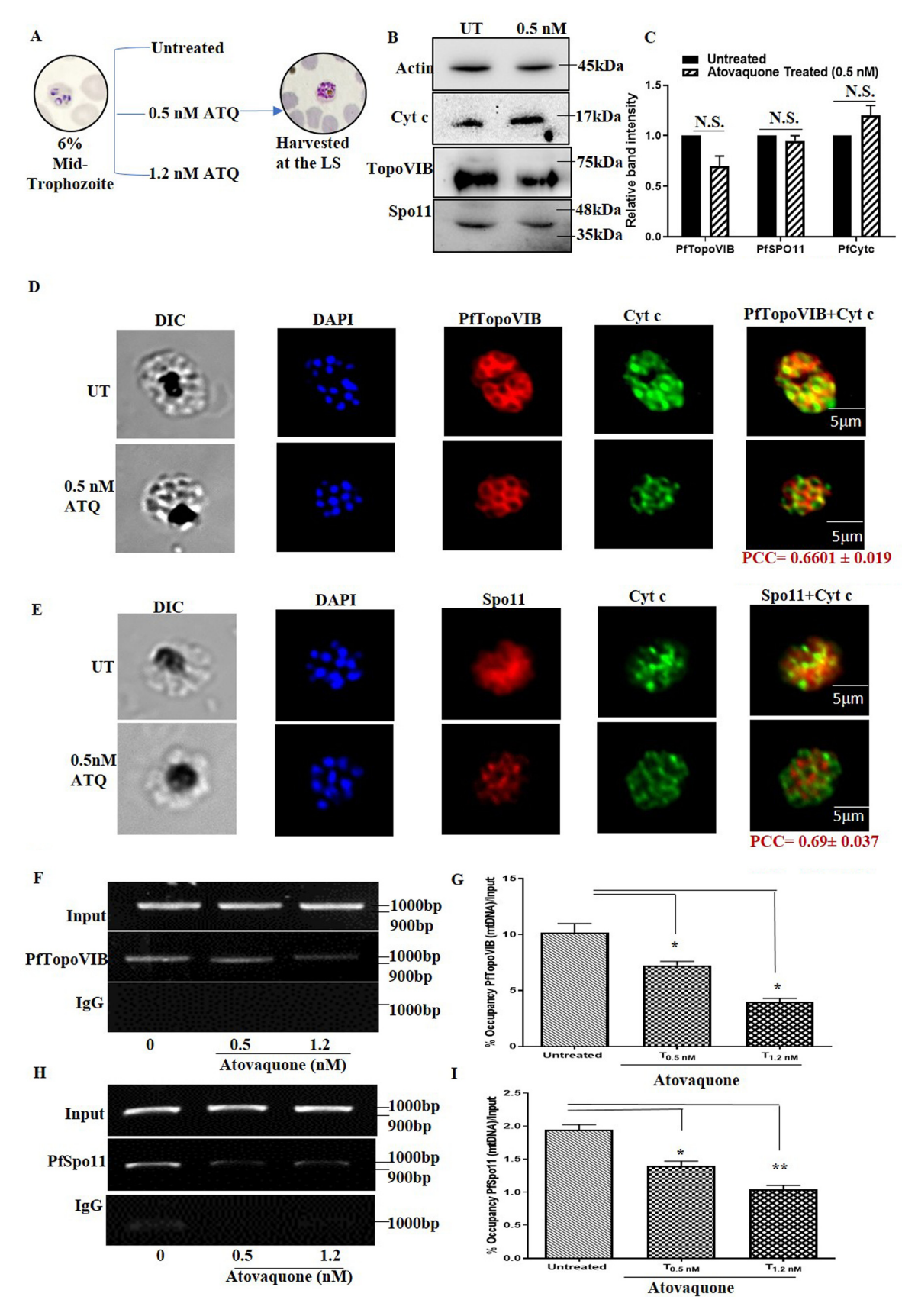


**FIG 6** Atovaquone reduces mitochondrial import and mtDNA recruitment of PfTopoVIB and PfSpo11 in a dose-dependent manner. (A) Schematic presentation of the assay in the presence of atovaquone. Synchronized mid-trophozoite-specific parasite cultures (6% parasitemia) (Continued on next page)

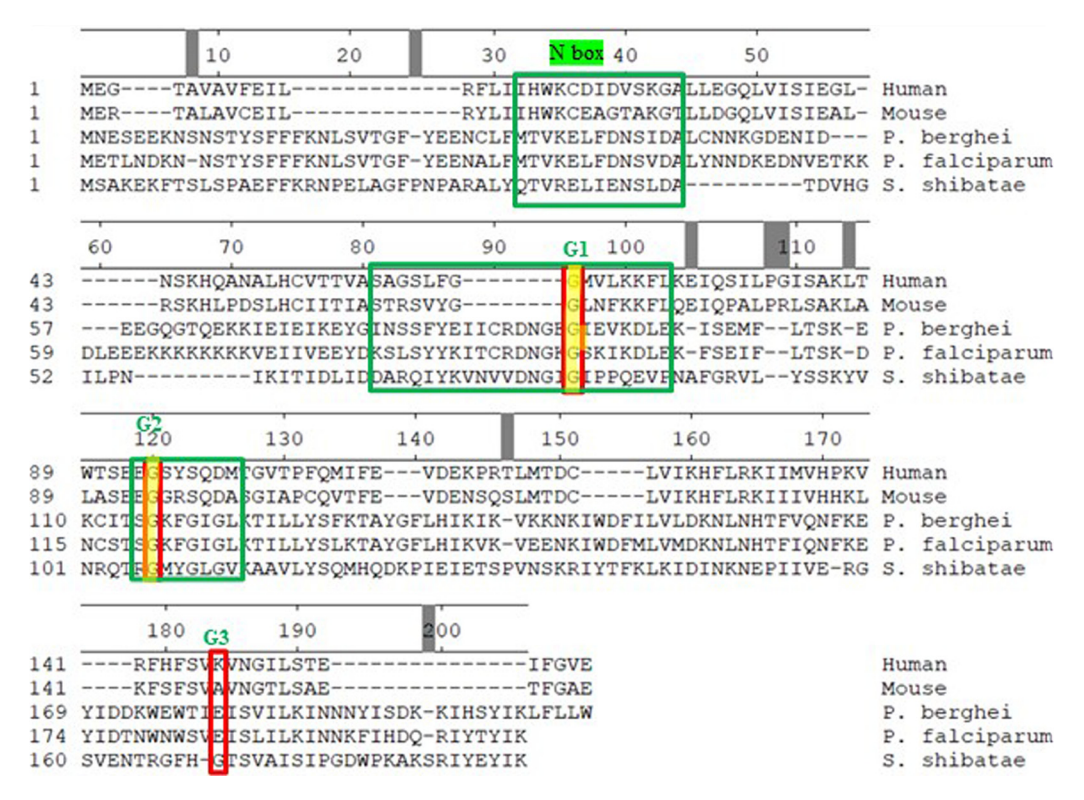


**FIG 7** Multiple-sequence alignment of TopoVIB/TopoVIBL proteins from *S. shibatae* (Ss), *P. falciparum* (Pf), *P. berghei* (Pb), *M. musculus* (Mm), and *H. sapiens* (Hs). The UniProt ID numbers and the residue numbers considered in the alignment are given next to the species. The conserved glycines are shown in red boxes, and the four core elements of the Bergerat fold are shown in blue boxes.

the replicated mitochondrial genome before endoreduplication so that it can be segregated to the progeny. It was reported earlier that PfGyrase, another type II topoisomerase of the malaria parasite, was a bona fide apicoplast-specific topoisomerase (18) and was not detected in mitochondria. Our study suggests a likely role of PfTopoVI in the segregation of the mitochondrial genome. We found that the expression of PfTopoVI is very tightly regulated, and both the subunits are induced during the late schizont (44 to 45 hpi) stage of the parasite, before the initiation of genome segregation. Furthermore, the subunits' recruitment to mitochondrial genome correlates well with their expression in the parasite. It can be speculated that inhibition of PfTopoVI might impair the endoreduplication due to the inhibition of mitochondrial genome segregation. Indeed, this notion is supported by our earlier observations that radicicol (PfTopoVIB inhibitor) treatment arrests the parasites at the late schizont stage and inhibits the transition from schizont to ring stage (9).

We do not rule out the possibility that PfTopoVI has an additional nuclear function as the PCC values determined through our experiments indicate a moderate correlation between

### FIG 6 Legend (Continued)

were divided into 3 parts: one set was untreated, and the other two sets were treated with different doses of atovaquone. Subsequently parasites were harvested at the LS stage (44 to 45 hpi); parasites treated with 0.5 nM atovaquone were subjected to IFA. The ChIP assay was performed with parasites treated with 0.5 and 1.2 nM atovaquone along with the untreated control. (B) Western blot analysis showed no significant difference in the endogenous levels of PfSpo11, PfTopoVIB, and PfCytc in the atovaquone-treated culture compared to the untreated condition. (C) Graph displayed the relative band intensities of PfTopoVIB, PfSpo11, and PfCytc, from the Western blots with two independent protein preparations and calculated using ImageJ software. (D and E) Indirect immunofluorescence assay showed that there was a significant reduction in the colocalization (yellow) of Cytc (green) and PfTopoVIB/PfSpo11 (red), respectively, in the parasites treated with 0.5 nM atovaquone compared to the untreated parasites. The mean PCC values were determined from 25 individual cells from each of the IFA, and the average value is presented at the bottom of merged image. (F) The recruitment of PfTopoVIB on the mitochondrial genome was significantly decreased in the presence of atovaquone in a dose-dependent manner. (G) Quantitation of PfTopoVIB recruitment (percentage of occupancy/input) was calculated by real-time PCR analysis with two independent sets of experiments, and the data were presented. (H) Quantitation of PfSpo11 on the mitochondrial genome was also decreased with increasing concentrations of atovaquone. (I) Quantitation of PfSpo11 recruitment (percentage of occupancy/input) was calculated by real-time PCR analysis with two independent sets of experiments, and the data were presented. P values were calculated using a two-tailed Student's t test (\*\*, P < 0.01; \*, P < 0.05; N.S., not significant).

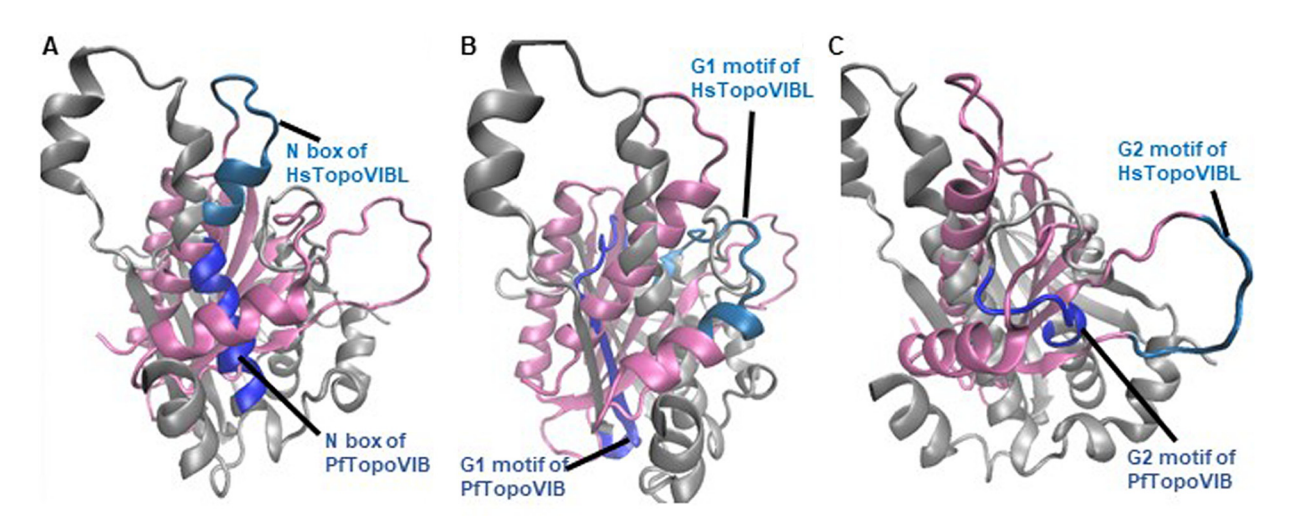


FIG 8 Structural alignment of the Bergerat fold region of PfTopoVIB (shown in silver) and HsTopoVIBL (shown in pink) shown from different angles: The core elements of the Bergerat fold are shown in blue. The difference in spatial orientation of these core elements can be seen in the figure. (A) N box; (B) G1 motif; (C) G2 motif.

PfTopoVIB/PfSpo11 and DAPI. However, in the present work we didn't explore the nuclear function of PfTopoVI, if any.

The other type II topoisomerase transcripts were detected in most stages, including the LS stage of the parasite. It is likely that these topoisomerases could be involved in various cellular function involving DNA transactions at all the stages. Alternatively, it could be possible that the transcript of other topoisomerases is very stable, having a longer half-life, and hence they are detected even at the LS stage.

Plasmodium topoisomerase VI is a type IIB topoisomerase, which can be exploited as a novel antimalarial target due to its absence in humans. The cross-reactivity of human Spo11 antibody with PfSpo11 indicates that there could be structural conservation between human and Plasmodium Spo11. On the contrary, there is much less sequence identity (10%) between PfTopoVIB and mouse/human TopoVIBL protein. Predicted structures of these two subunits show that the ATP binding pocket of PfTopoVIB, namely, the Bergerat fold, does not superimpose with the similar fold present in human TopoVIBL protein. Thus, a specific inhibitor that binds to the ATP binding pocket of PfTopoVIB is less likely to block the function of the TopoVIBL protein of human. Our earlier work demonstrated that radicicol inhibits the decatenation activity of PfTopoVI. Radicicol is a pan-inhibitor of heat shock protein Hsp90 and can bind to the Bergerat fold of the human heat shock protein Hsp90; however, apart from this Bergerat fold, TopoVIB and Hsp90 are very different molecules, and hence it could be possible to identify specific inhibitors of PfTopoVIB that do not inhibit human Hsp90. Future studies are required to screen small molecule inhibitors that will specifically block PfTopoVIB and not human Hsp90 (19). Any inhibitor specifically targeting the PfTopoVIB subunit will inhibit the function of the entire enzyme complex PfSpo11-TopoVIB, and would arrest the endoreduplication of the parasite.

### **MATERIALS AND METHODS**

**Generation of plasmids and yeast strains. (i) Plasmids.** Full-length *ScSPO11* was cloned in the yeast expression vector *pRS313* by amplifying yeast genomic DNA using the forward primer OSB 643 (5' GAC GGA TCC ATG GCT TTG GAG GGA TTG CG 3') with a BamHI site and the reverse primer OSB 644 (5' GAC GTC GAC TCA TTT GTA TTC AAA AAT TCT GGC 3') with a Sall restriction site. The full-length *PfSPO11* was cloned in the *pRS313* vector by nondirectional cloning at the BamHI site, using the 3D7 cDNA as a template and primer pairs OSB 645 (5' GAC GGA TCC ATG CCT CGT CTG GAT ATC 3') and OSB 646 (5' GAC GGA TCC TTA TAA AAG CTC CTT AAT GCG 3'), each having a BamHI restriction site. The *PfSpo11Y65F* mutant was also cloned in the *pRS313* vector at the BamHI site.

(ii) Site-directed mutagenesis. Point mutation (Y to F) was generated in *PfSPO11* by mutating the codon TAC to TTT using the splicing by overlap extension (SOE) PCR technique. To insert the point mutation at *PfSpo11Y65F*, the coding sequence was amplified in two segments. The first segment was amplified by using the primer pair OSB 645 (mentioned above) and OSB 652 (5' TAT AAA TAA TTT TGG ATT GGT AAA AAA TAT TTG TC 3'); the second segment was amplified using the primer pair OSB 653 (5' CAA

CTT TAA GAC AAA TAT TTT TTA CCA ATC C 3') and OSB 646 (described above). Subsequently, the full-length *PfSPO11* containing the Y65F mutation was amplified using the two segments as a template and primer pair OSB 645 and OSB 646 and cloned into the *pRS313* vector. The generation of mutation was confirmed by DNA sequencing.

(iii) Yeast strains. Empty *pRS313* vector, *pRS313-PfSPO11*, *pRS313-Pfspo11Y65F*, and *pRS313-ScSPO11* were transformed in a diploid  $spo11\Delta$  BY4743 strain (MATa/MAT $\alpha$   $his3\Delta1/his3\Delta1$   $leu2\Delta0/leu2\Delta0$   $LYS2/lys2\Delta0$   $met15\Delta0/MET15$   $ura3\Delta0/ura3\Delta0$  YHL022c/YHL022c::kanMX4) to generate the strains PSY4, PSY1, PSY2, and PSY3, respectively.

**Yeast sporulation.** Each strain was inoculated in the histidine dropout medium and allowed to grow overnight at 30°C. The next morning, the cells were inoculated in presporulation medium (1% potassium acetate, 1% yeast extract, 2% peptone, 0.003% uracil, and 0.005% leucine) and further allowed to grow for 18 h at 30°C in a shaker incubator. After 18 h, when the optical density at 600 nm (OD $_{600}$ ) reached 0.5, cells were washed 1 to 2 times with sterile Milli-Q water, further resuspended in the sporulation medium (1% potassium acetate, 0.003% uracil, 0.005% leucine), and allowed to grow in a shaking water bath at 18°C for 48 h. At the end of 48 h, cells were stained with DAPI and sporulation efficiency was calculated. We analyzed a total of 1,000 cells from each strain (by doing three independent sets of experiments) using fluorescence microscopy to count the number of cells that can form asci (3 or 4 spores). Subsequently, the sporulation efficiency was calculated using the following formula: % of sporulation = (cells containing 3 or 4 asci/total no. of diploid cells counted)  $\times$  100.

The mean values  $\pm$  standard deviation (SD) were plotted for each strain using GraphPad Prism 6. The results represent mean  $\pm$  SD. *P* values were calculated using the two-tailed Student's *t* test.

**Plasmodium falciparum culture.** *P. falciparum* 3D7 parasites were maintained with 5% hematocrit in RPMI 1640 medium (Himedia) supplemented with 0.5% (wt/vol) Albumax (Thermo Fisher Scientific) and 0.005% (vol/vol) hypoxanthine (Sigma). Parasites were maintained at 37°C using the candle jar method (20). Parasite growth was monitored by microscopic examination of Giemsa-stained slides. Cultured parasites were synchronized at the ring stage by treatment with 5% sorbitol (Sigma, St. Louis, MO, USA) as discussed earlier (21). We harvested the synchronized parasites that were grown for 35 to 36 hpi as early schizont (ES), 39 to 40 hpi as mid-schizont (MS), and 44 to 45 hpi as late schizont (LS). Each of the ES, MS, and LS stage-specific Giemsa-stained cultures was also confirmed according to its morphology under the microscope.

**Western blot analysis.** ES, MS, and LS stage-specific cultures were harvested at 5% parasitemia, and parasite protein was isolated. Western blot analysis was performed as described earlier (21). The blot was probed with rabbit anti-TopoVIB antibody (5) and rabbit anti-human Spo11 (anti-hSpo11) antibody (Invitrogen) at 1:500 and 1:3,000 dilutions, respectively. In order to detect PfSpo11 or ScSpo11, we used anti-human Spo11 antibody. Mouse anti-human actin 1 antibody (Abcam) was used as a normalizing control. Horseradish peroxidase (HRP)-conjugated anti-rabbit IgG (Promega) and anti-mouse (Santa Cruz Biotechnology) were used as the secondary antibodies in a 1:10,000 dilution. To probe the protein level in the presence of atovaquone, cytochrome *c* (Cytc) was used as a mitochondrial protein marker. For that, atovaquone-treated parasite proteins were probed with anti-mouse anti-Cytc (Abcam) at 1:3,000 dilutions. The Western blots were developed by using a chemiluminescence detection system (Pierce). Each experiment was repeated with three independent batches of cells, and band intensities were quantified using ImageJ software. Mean relative densities were plotted using GraphPad prism.

RNA isolation and real-time analysis. Total RNA was isolated from synchronized ES, MS, and LS stages of the 3D7 parasite as previously described (21). It was subjected to DNase I treatment (Fermentas) to eliminate DNA contamination. PCR without reverse transcriptase pretreatment was performed to confirm the absence of genomic DNA. cDNA was synthesized by using 1  $\mu g$  of total RNA by using reverse transcriptase (Qiagen), and the cDNA product was then subjected to amplification using small ARP gene-specific primers OSB 94 and OSB 95 (21). PfSPO11 expression was studied by amplifying the cDNA with gene-specific primers OSB 589 (5' TGA TAT GTC CAT CGA GAA TCT TC 3') and OSB 590 (5'CCT TAA TGC GAT TAT TTA TAT GTT C 3'). PFTOPOVIB (PF3D7\_1365600) was amplified using the gene-specific primers OSB 548 (5' GGT GTT CAG TTA GCA TCT TC 3') and OSB 549 (5' CAT TCA TCT TCA CCT TCA CC 3'). OSB 578 (5' AAA CCA AGA TTA ACC TTA TCT G 3') and OSB 579 (5' TTA AAT GTT GTA TGA ACT ATC AC 3') were used to amplify PfTOPOII (PF3D7\_1433500). OSB 580 (5' GGA AAA GGA CAT AGA ATC ATG 3') and OSB 581 (5' TCA GAT TAT GTC AAA ATA AAC C 3') were used to amplify PfGYRA (PF3D7\_1223300), and OSB 582 (5' GTG AAT GAA GAG GGT TCG AC 3') and OSB 583 (5' CTG ATA ATG AAT TTG TAT TTT CC 3') were used to amplify PfGYRB (PF3D7\_1239500). For the real-time analysis, cDNA was diluted in a 1:50 ratio and used for PCR using a TaKaRa RT-PCR kit. Real time analysis was conducted using the Applied Biosystems 7500 Fast real-time PCR system. A threshold cycle ( $C_{\tau}$ ) value of ARP transcript was used as the normalizing control for the  $C_{\tau}$  values of other TOPOII transcripts to obtain  $\Delta C_T$  values for each. The relative mRNA levels were gathered from the formula (change in mRNA level [ $2^{\Delta CT}$ ]). The mean values  $\pm$  SD were plotted using GraphPad Prism 6 software from two independent repeats.

**Chromatin immunoprecipitation assay.** Synchronized ES, MS, and LS stage-specific 3D7 parasites were harvested, each with 7 to 8% parasitemia, and we followed the standard procedure as described previously (21). Briefly, formaldehyde (37%) was added to the parasite culture so that its final concentration reached 0.5%, and then the culture was incubated at 37°C for 10 min. Subsequently, sonication (Elma; model-S-60H) was performed according to the standardized protocol (21) to generate small chromatin fragments. Protein-DNA complexes were then selectively immunoprecipitated using anti-PfTopoVIB (9) and anti-PfSpo11 antibodies (Invitrogen). Reverse cross-linking was performed using 5 M NaCl, and finally, DNA was extracted using proteinase K-phenol chloroform treatment. Recruitment of PfTopoVIB and PfSpo11 to mtDNA was quantified utilizing specific primer pairs covering different 1-kb regions (A to F) of the *Plasmodium falciparum* mitochondrial genome, as described earlier (21). Rabbit IgG was used as a control for the ChIP assay. For

Month YYYY Volume XX Issue XX 10.1128/spectrum.04980-22

quantification of the mitochondrial association, real-time qPCR analysis was performed to amplify regions A to F utilizing the following primer pairs: A, OMKB 540 (5' GAG TGG ATT AAA TGC CCA GCC 3') and OSB 596 (5' CAT TGG AAT GAG AGT TCA CCG 3'); B, OSB 493 (5' TAC TCT GTA GTT TGT AGA GAT GC 3') and OSB 597 (5' TGT ATT TTC ATC TTT AAC TTC TGG 3'); C, OMKB 615 (5' CTG GCC TAC ACT ATA AGA ACG 3') and OSB 598 (5' TGA AGA ATA TAA TTC AGT ACG TAG 3'); D, OSB 599 (5' TAC TGG TTT AGA AGT TGA TAC TAG 3') and OSB 600 (5'ATC TTG AAA TGC ACT TAC AGT TG 3'); E, OSB 601 (5' TTA TCC TCT ATT CCA GTA GCA G 3') and OSB 602 (5' ACG ATA GCA TTA TCA GGA TGT G 3'); and F, OMKB 620 (5' CGC TGA CTT CCT GGC TAA AC 3') and OSB 603 (5' GAA TTG AAG TGT GGA GAG AAT C 3'). To detect the recruitment of PfTopoVIB and PfSpo11 under the atovaquone-treated condition, tightly synchronized mid-trophozoite-treated parasite cultures (7 to 8% parasitemia) were treated with different doses of atovaquone (i.e., 0, 0.5, 1.2, and 2.4 nM) and allowed to grow until they reached the LS stage. Furthermore, LS stage-specific cultures were harvested in a similar manner as described above, and then ChIP was performed. To check the recruitment of H3K4me3 and H3K9me3 on UAS\_PfSPO11 and UAS\_PfTOPOVIB, ChIP was performed with the ES, MS, and LS stages of the parasites. We determined the recruitment of both the subunits toward its C-terminal end (CTE), as shown schematically in Fig. 3A, which acts as a negative control in our assay. We used the antibodies against H3K4me3 (Millipore) and H3K9me3 (Millipore). Quantification of the recruitment was done using primer pairs OSB 463 (5' AGC GGT ACC GTG GCA CCT TGT ATG TTT AC 3') and OSB 464 (5' AGC ATG CAT TAT TAT ACA CAA CAT AAA TAT ATA TA 3') on PfTOPOVIB<sub>IAS</sub> and OSB 563 (5' TTC CCC TAG TGT TAC ATT TGG 3') and OSB 564 (5' TAG GAA ATC ATA TTT TCA TTT TTA C 3') on PfSPO11<sub>IJAS</sub>. To check the recruitment of activation and repression mark to CTE\_PfTOPOVIB and CTE\_PfSPO11, we used the primer pairs OSB 548 and OSB 549 and OSB 589 and OSB 590, respectively. Rabbit IgG was used as a negative control.

Formaldehyde-assisted isolation of regulatory elements. The FAIRE (formaldehyde-assisted isolation of regulatory elements) assay was performed according to the previously published protocol (22). Briefly, synchronized parasite culture was divided into two parts (one as a reference and one as a test sample) and centrifuged at 3,000 rpm for 10 min. Briefly, 37% formaldehyde was added (final concentration of 1%) to the test culture, and the culture was incubated at 25°C at 80 rpm in an orbital shaker for 20 min. Glycine was added to a final concentration of 125 mM for 10 min at the same temperature to quench the formaldehyde. Cells were rinsed with phosphate-buffered saline (PBS) containing phenylmethylsulfonyl fluoride (Sigma), and the culture was then rinsed two more times. The cells were spun at 3,500 rpm for 15 min and frozen using liquid nitrogen. Cells were resuspended in 1 mL of lysis buffer (2% Triton X-100, 1% SDS, 100 mM NaCl, 10 mM Tris-HCI [pH 8.0], 1 mM EDTA) per 0.4 g of cells and incubated for 1 h for both reference and test samples. Samples were then sonicated for six sessions of 10-s bursts, followed by 5 min on ice. Cells were then spun at  $16,000 \times g$ for 20 min at 4°C. The supernatant obtained was subjected to phenol chloroform isoamyl alcohol (PCIA) treatment. After PCIA treatment, the aqueous layer was transferred into a new tube and precipitated using 2 volumes of 100% ethanol and 1/10 volume of sodium acetate. PCR analysis was performed using PFTOPOVIB and PfSPO11 promoter-specific primer pairs OSB 463 and OSB 464 and OSB 563 and OSB 564, respectively (as mentioned above). PfCOX promoter-specific primers OSB 177 and OMKB 418 (22) were used as normalizing controls.

**Coimmunoprecipitation.** Coimmunoprecipitation (co-IP) was performed using the Pierce cross-link immunoprecipitation kit (Thermo Scientific) according to the manufacturer's protocol. Briefly, the anti-PfSpo11antibody was coupled to Pierce protein A/G Plus agarose beads (provided in the kit). Cross-linking of the beads and antibody was done using disuccinimidyl suberate (DSS) solution. Furthermore, washing of the beads was performed as per the protocol to quench the cross-linking. Tightly synchronized LS stage parasites were harvested using 0.15% saponin treatment and were lysed using the immunoprecipitation (IP) lysis buffer (0.025 M Tris, 0.15 M NaCl, 0.001 M EDTA, 1% NP-40 and 5% glycerol [pH 7.4]). Centrifugation was performed to separate lysate from the cell debris. The precleaned lysate was incubated overnight with antibody-bound beads. The column was placed in a collection tube, and flow-through was collected. The antigen antibody-bound beads were then subjected to washing with the washing and conditioning buffer. Bound antigen was eluted using elution buffer and further subjected to the Western blot analysis. All buffer used was provided in the kit.

Indirect immunofluorescence assay. *Plasmodium* cultures were grown (6% parasitemia) with synchronous stage-specific cultures at the ES, MS, and LS stages, washed with  $1 \times PBS$ , and subsequently fixed using 4% paraformaldehyde for 15 min. Subsequently, the culture was washed with PBS and permeabilized using a 1:3 ratio of ice-cold acetone and methanol mixture for 15 min. Bovine serum albumin (BSA [3%]) was used as the blocking solution; subsequently, anti-mouse anti-cytochrome c (Abcam), anti-rabbit anti-TopoVIB (9), and anti-rabbit anti-Spo11 primary antibodies were used at 1:50, 1:25, and 1:25 dilutions, respectively, to probe the parasites for 1 h at 37°C. Slides were washed 3 times using  $1 \times PBS$ ,  $1 \times PBS$ -Tween 20 (PBST), and  $1 \times PBS$  for 15 min each. The secondary antibody cocktail containing Alexa Fluor 488-conjugated goat anti-mouse IgG (green) and Alexa Fluor 594-conjugated chicken anti-rabbit IgG (red) at a 1:250 dilution and DAPI (blue) (Invitrogen) at a 1:50 dilution was used and successively washed three times. At the end, parasites were mounted with antifade (Life Technologies). Nikon Eclipse NiE AR fluorescence microscope was used for analyzing and capturing the green and red fluorescence of PfCytc and PfTopoVIB/PfSpo11, respectively. The Pearson correlation coefficient (PCC) and the Manders' overlap coefficient (MOC) were calculated for immunofluorescence antibody (IFA) images using the JaCoP plugin in ImageJ (v.1.52s) software.

Fixed-ratio isobologram method to determine interaction between radicicol and atovaquone. To understand the *in vitro* interaction between radicicol (Sigma) and atovaquone (Sigma), a fixed-ratio isobologram method was used. The  $IC_{50}$  of radicicol was determined by treating the synchronous schizont stage-specific 3D7 parasites with different concentrations of radicicol for 48 h at 37°C. In order to determine the  $IC_{50}$  of atovaquone, synchronous trophozoite-specific 3D7 parasites were treated with different concentrations of atovaquone for 48 h at 37°C. Both Giemsa and SYBER green-based staining

Month YYYY Volume XX Issue XX 10.1128/spectrum.04980-22

(using a plate reader) were used to determine the percentage of parasite inhibition. The  $IC_{50}$  was calculated by plotting the percentage of inhibition against the concentration of the drug on a semilog graph using GraphPad Prism 6.

To check the interaction between radicicol and atovaquone, we used the protocol described in reference 23. Radicicol and atovaquone were combined in four fixed ratios (4:1, 3:2, 2:3, and 1:4). The effects of each of the drug combinations (along with their 2-fold serial dilutions) on the development of the parasite were assayed in triplicate. A 96-well plate was used, in which each well contained a total of 200  $\mu$ L of reaction volume with 100  $\mu$ L of culture (1% parasitemia and 5% hematocrit) and 100  $\mu$ L of medium with or without drug. After setting the reaction, plates were incubated at 37°C for 48 h, followed by an assessment of parasite count by the SYBR green I-based method. The IC $_{50}$  for each combination was calculated by plotting the semilog graph. The fractional inhibitory concentration (FIC) for each drug was determined by using the equation FIC = IC $_{50}$  of the drug in mixture/IC $_{50}$  of the drug alone. The interaction between radicicol and atovaquone was identified by computing  $\Sigma$ FIC, which was determined by using the formula  $\Sigma$ FIC = (IC $_{50}$  of radicicol in mixture/IC $_{50}$  of radicicol alone) + (IC $_{50}$  of atovaquone in mixture/IC $_{50}$  of atovaquone alone). The isobologram was prepared by using GraphPad Prism software. An  $\Sigma$ FIC value of <1 represents synergism,  $\Sigma$ FIC values of ≥2 represents antagonism. In a similar way, the interaction between radicicol and chloroquine (Sigma) was determined.

Sequence- and structure-based comparison of PfTopoVIB and HsTopoVIBL. The sequences of TopoVIB/TopoVIBL proteins were retrieved from the UniProt database (24). The UniProt ID numbers for S. shibatae, P. falciparum, Plasmodium berghei, Mus musculus, and Homo sapiens were O05207, Q8ID53, A0A509AMZ8, J3QMY9, and Q8N6T0, respectively. A multiple-sequence alignment was performed using ClustalV (25). The structures of PfTopoVIB and HsTopoVIBL were retrieved from the AlphaFold database (26). Structure alignment was performed using VMD (27).

### **SUPPLEMENTAL MATERIAL**

Supplemental material is available online only.

**SUPPLEMENTAL FILE 1**, TIF file, 10.5 MB.

### **ACKNOWLEDGMENTS**

The work was supported by the grants from the Department of Science and Engineering Research Board (DST-SERB), India (EMR/2017/001173) to S.B. and DBT-SAHAJ/BUILDER BT/INF/22/SP41176/2020 to School of Life Sciences, University of Hyderabad. P.S. and N.F. were supported by the Senior Research Fellowships from CSIR, India, and W.T. was supported by a postdoctoral fellowship from DST-SERB (CRG/2020/000552), India to M.K.B.

We declare no conflict of interest.

### **REFERENCES**

- World Health Organization. 2021. World malaria report 2021. https://www.who.int/teams/global-malaria-programme/reports/world-malaria-report-2021.
- Singh P, Rani K, Gotmare A, Bhattacharyya S. 2022. A tale of topoisomerases and the knotty genetic material in the backdrop of Plasmodium biology. Biosci Rep 42:BSR20212847. https://doi.org/10.1042/BSR20212847.
- Sugimoto-Shirasu K, Stacey NJ, Corsar J, Roberts K, McCann MC. 2002. DNA topoisomerase VI is essential for endoreduplication in Arabidopsis. Curr Biol 12:1782–1786. https://doi.org/10.1016/s0960-9822(02)01198-3.
- van Dooren GG, Marti M, Tonkin CJ, Stimmler LM, Cowman AF, McFadden GI. 2005. Development of the endoplasmic reticulum, mitochondrion and apicoplast during the asexual life cycle of Plasmodium falciparum. Mol Microbiol 57:405–419. https://doi.org/10.1111/j.1365-2958.2005.04699.x.
- Chalapareddy S, Chakrabarty S, Bhattacharyya MK, Bhattacharyya S. 2016.
   Radicicol-mediated inhibition of topoisomerase VIB-VIA activity of the human malaria parasite Plasmodium falciparum. mSphere 1:e00025-15. https://doi.org/10.1128/mSphere.00025-15.
- Bergerat A, Gadelle D, Forterre P. 1994. Purification of a DNA topoisomerase II from the hyperthermophilic archaeon Sulfolobus shibatae. A thermostable enzyme with both bacterial and eucaryal features. J Biol Chem 269:27663–27669. https://doi.org/10.1016/S0021-9258(18)47037-8.
- Buhler C, Lebbink JH, Bocs C, Ladenstein R, Forterre P. 2001. DNA topoisomerase VI generates ATP-dependent double-strand breaks with two-nucleotide overhangs. J Biol Chem 276:37215

  –37222. https://doi.org/10.1074/jbc.M101823200.
- Bergerat A, de Massy B, Gadelle D, Varoutas PC, Nicolas A, Forterre P. 1997. An atypical topoisomerase II from Archaea with implications for meiotic recombination. Nature 386:414–417. https://doi.org/10.1038/386414a0.
- Chalapareddy S, Bhattacharyya MK, Mishra S, Bhattacharyya S. 2014. Radicicol confers mid-schizont arrest by inhibiting mitochondrial replication

- in Plasmodium falciparum. Antimicrob Agents Chemother 58:4341–4352. https://doi.org/10.1128/AAC.02519-13.
- Keeney S. 2008. Spo11 and the formation of DNA double-strand breaks in meiosis. Genome Dyn Stab 2:81–123. https://doi.org/10.1007/7050\_2007 026.
- Neiman AM. 2005. Ascospore formation in the yeast Saccharomyces cerevisiae. Microbiol Mol Biol Rev 69:565–584. https://doi.org/10.1128/MMBR .69.4.565-584.2005.
- Sarkar C, Gupta S, Sinha H, Jalan S. 2017. Fundamental principles governing sporulation efficiency: a network theory approach. bioRxiv https:// www.biorxiv.org/content/10.1101/068270v2.
- Perrin AJ, Bisson C, Faull PA, Renshaw MJ, Lees RA, Fleck RA, Saibil HR, Snijders AP, Baker DA, Blackman MJ. 2021. Malaria parasite schizont egress antigen-1 plays an essential role in nuclear segregation during schizogony. mBio 12: e03377-20. https://doi.org/10.1128/mBio.03377-20.
- Karmodiya K, Pradhan SJ, Joshi B, Jangid R, Reddy PC, Galande S. 2015. A
  comprehensive epigenome map of Plasmodium falciparum reveals unique
  mechanisms of transcriptional regulation and identifies H3K36me2 as a
  global mark of gene suppression. Epigenetics Chromatin 8:32. https://doi.org/
  10.1186/s13072-015-0029-1.
- Srivastava IK, Rottenberg H, Vaidya AB. 1997. Atovaquone, a broad spectrum antiparasitic drug, collapses mitochondrial membrane potential in a malarial parasite. J Biol Chem 272:3961–3966. https://doi.org/10.1074/jbc.272.7.3961.
- Preiser PR, Wilson RJ, Moore PW, McCready S, Hajibagheri MA, Blight KJ, Strath M, Williamson DH. 1996. Recombination associated with replication of malarial mitochondrial DNA. EMBO J 15:684–693. https://doi.org/ 10.1002/j.1460-2075.1996.tb00401.x.

- 17. Wilson R, Williamson DH. 1997. Extrachromosomal DNA in the Apicomplexa. Microbiol Mol Biol Rev 61:1–16. https://doi.org/10.1128/61.1.1-16.1997.
- Raghu Ram EV, Kumar A, Biswas S, Kumar A, Chaubey S, Siddiqi MI, Habib S. 2007. Nuclear gyrB encodes a functional subunit of the Plasmodium falciparum gyrase that is involved in apicoplast DNA replication. Mol Biochem Parasitol 154:30–39. https://doi.org/10.1016/j.molbiopara.2007.04.001.
- Bansod S, Raj NRA, Nair AS, Bhattacharyya S. 2022. Molecular docking and molecular dynamics simulation identify a novel radicicol derivative that predicts exclusive binding to Plasmodium falciparum topoisomerase VIB. J Biomol Struct Dyn 40:6939–6951. https://doi.org/10.1080/07391102.2021.1891970.
- 20. Moll K, Ljungström I, Perlmann H, Scherf A, Wahlgren M (ed). 2013. Methods in malaria research, 6th ed. EVIMalaR, Glasgow, United Kingdom.
- Bansod S, Bung N, Singh P, Suthram N, Choudhury H, Roy A, Bulusu G, Bhattacharyya S. 2020. Elucidation of an essential function of the unique charged domain of Plasmodium topoisomerase III. Biochem J 477:4745–4767. https://doi.org/10.1042/BCJ20200318.
- Tabassum W, Bhattacharyya S, Varunan SM, Bhattacharyya MK. 2021. Febrile temperature causes transcriptional downregulation of Plasmodium falciparum sirtuins through Hsp90-dependent epigenetic modification. Mol Microbiol 115:1025–1038. https://doi.org/10.1111/mmi.14692.

- Suthram N, Padhi S, Jha P, Bhattacharyya S, Bulusu G, Roy A, Bhattacharyya MK. 2020. Elucidation of DNA repair function of PfBlm and potentiation of artemisinin action by a small-molecule inhibitor of RecQ helicase. mSphere 5: e00956-20. https://doi.org/10.1128/mSphere.00956-20.
- McGarvey PB, Nightingale A, Luo J, Huang H, Martin MJ, Wu C, UniProt Consortium. 2019. UniProt genomic mapping for deciphering functional effects of missense variants. Human Mutat 40:694–705. https://doi.org/10 .1002/humu.23738.
- Sievers F, Wilm A, Dineen D, Gibson TJ, Karplus K, Li W, Lopez R, McWilliam H, Remmert M, Söding J, Thompson JD, Higgins DG. 2011. Fast, scalable generation of high-quality protein multiple sequence alignments using Clustal Omega. Mol Syst Biol 7:539. https://doi.org/10.1038/msb.2011.75.
- Jumper J, Evans R, Pritzel A, Green T, Figurnov M, Ronneberger O, Tunyasuvunakool K, Bates R, Žídek A, Potapenko A, Bridgland A, Meyer C, Kohl SAA, Ballard AJ, Cowie A, Romera-Paredes B, Nikolov S, Jain R, Adler J, Back T, Petersen S, Reiman D, Clancy E, Zielinski M, Steinegger M, Pacholska M, Berghammer T, Bodenstein S, Silver D, Vinyals O, Senior AW, Kavukcuoglu K, Kohli P, Hassabis D. 2021. Highly accurate protein structure prediction with AlphaFold. Nature 596:583–589. https://doi.org/10.1038/s41586-021-03819-2.
- Humphrey W, Dalke A, Schulten K. 1996. VMD: visual molecular dynamics.
   J Mol Graph 14:33–38. https://doi.org/10.1016/0263-7855(96)00018-5.

## Role of topoisomerases in mitochondrial biology of the human malaria parasite Plasmodium falciparum

by Priyanka Singh

Librarian
Indira Gandhi Memorial Libra

Central University P.O.

Submission date: 11-Jul-2023 05:21PM (UTC+0530)

Submission ID: 2129590042

File name: Priyanka\_Singh.pdf (2.77M)

Word count: 26075

Character count: 145683

Shadland Bhattachary A

Shadland Bhattachary A

Dr. SUNANDA BHATTACHARY A

Dr. SUNANDA BHATTACHARY A

Dr. SUNANDA BHATTACHAR From the selection of the selectio

### Role of topoisomerases in mitochondrial biology of the human malaria parasite Plasmodium falciparum

SIMIL	4 % ARITY INDEX	25% INTERNET SOURCES	24% PUBLICATIONS	9% STUDENT PAPERS
PRIMAF	RY SOURCES			
1	www.nc	bi.nlm.nih.gov		13,
2	Submitt Hyderal Student Pape		y of Hyderabad	7%
3	Fangari VIB and Topoiso Possible	a Singh, Wahida a, Sandeep Dey Spo11 Constitu merase in Mala e Role in Mitoch ation ", Microbio	et al. " Topoiso Ite Functional T Iria Parasite: Its ondrial DNA	omerase Type IIB
4	Singh, N an esse	li Bansod, Navn Jiranjan Suthrar ntial function of of topoisomera 2020	n et al. " Elucid the unique ch	lation of arged
	ueaepri	nts.uea.ac.uk		1 %

Scanned with CamScanner

13	www.nature.com Internet Source	<1%
14	Renu Tuteja. "Malaria�?�an overview", FEBS Journal, 9/2007 Publication	<1%
15	Submitted to University of Ulster Student Paper	<1%
16	academic.oup.com Internet Source	<1%
17	Sugith Babu Badugu, Shaik Abdul Nabi, Pratap Vaidyam, Shyamasree Laskar, Sunanda Bhattacharyya, Mrinal Kanti Bhattacharyya. "Identification of Plasmodium falciparum DNA Repair Protein Mre11 with an Evolutionarily Conserved Nuclease Function", PLOS ONE, 2015 Publication	<1%
18	dspace.uohyd.ac.in Internet Source	<1%
19	cwww.intechopen.com Internet Source	<1%
20	Giovanni Capranico, Jessica Marinello, Giovanni Chillemi. "Type I DNA Topoisomerases", Journal of Medicinal Chemistry, 2017	<1%

21	www.biorxiv.org Internet Source	<1%
22	www.cdc.gov Internet Source	<1%
23	hdl.handle.net Internet Source	<1%
24	archive.org Internet Source	<1%
25	Submitted to University of Liverpool  Student Paper	<1%
26	idoc.pub Internet Source	<1%
27	mdpi-res.com Internet Source	<1%
28	Ming Fu, Chong Wang, Feiyang Xue, James Higgins, Mingjiao Chen, Dabing Zhang, Wanqi Liang. "The DNA Topoisomerase VI–B Subunit OsMTOPVIB Is Essential for Meiotic Recombination Initiation in Rice", Molecular Plant, 2016 Publication	<1%
29	"Molecular Life Sciences", Springer Science and Business Media LLC, 2018	<1%

30	Stefano Mastrangelo, Giorgio Attina, Silvia Triarico, Alberto Romano, Palma Maurizi, Antonio Ruggiero. "The DNA-topoisomerase Inhibitors in Cancer Therapy", Biomedical and Pharmacology Journal, 2022 Publication	<1%
31	aac.asm.org Internet Source	<1%
32	www.medchemexpress.com Internet Source	<1%
33	www.thno.org Internet Source	<1%
34	Andrzej Skladanowski, Przemyslaw Bozko, Michal Sabisz. "DNA Structure and Integrity Checkpoints during the Cell Cycle and Their Role in Drug Targeting and Sensitivity of Tumor Cells to Anticancer Treatment", Chemical Reviews, 2009	<1%
35	Submitted to Chungnam National University  Student Paper	<1%
36	T. Robert, A. Nore, C. Brun, C. Maffre, B. Crimi, V. Guichard, H M. Bourbon, B. de Massy. "The TopoVIB-Like protein family is required for meiotic DNA double-strand break formation", Science, 2016 Publication	<1%

37	researchrepository.murdoch.edu.au Internet Source	<1%
38	d-nb.info Internet Source	<1%
39	Submitted to University of Birmingham  Student Paper	<1%
40	Submitted to University of Greenwich  Student Paper	<1%
41	"Remote Sensing and GIS in Support of Malaria Epidemic Early Warnings and Control. Requirements and Current Issues for an Operational Program", 55th International Astronautical Congress of the International Astronautical Federation, the International Academy of Astronautics, and the International Institute of Space Law, 2004 Publication	<1%
42	repositories.lib.utexas.edu Internet Source	<1%
43	www.freepatentsonline.com Internet Source	<1%
44	www.science.gov Internet Source	<1%
45	www.science.org Internet Source	<1%

46	Sutram, Sunanda Bhattacharyya, Mrinal Kanti Bhattacharyya. " A small-molecule inhibitor of the DNA recombinase Rad51 from synergizes with the antimalarial drugs artemisinin and chloroquine ", Journal of Biological Chemistry, 2019  Publication	<1%
47	coek.info Internet Source	<1%
48	digitalcommons.fiu.edu Internet Source	<1%
49	Jerrylaine V. Walker, John L. Nitiss. "DNA Topoisomerase II as a Target for Cancer Chemotherapy", Cancer Investigation, 2002 Publication	<1%
50	Johanna Olesk, Deborah Donahue, Jessica Ross, Conor Sheehan et al. "Peptide- conjugated phage-mimicking nanoparticles exhibit potent antibacterial action against Streptococcus pyogenes in murine wound infection models", American Chemical Society (ACS), 2023 Publication	<1%
51	etheses.dur.ac.uk Internet Source	<1%

52	Internet Source	<1%
53	www.researchsquare.com Internet Source	<1%
54	Submitted to University College London Student Paper	<1%
55	docplayer.net Internet Source	<1%
56	Submitted to Central University of Gujarat Student Paper	<1%
57	core.ac.uk Internet Source	<1%
58	Submitted to University of Queensland Student Paper	<1%
59	Wen, R "Zebrafish Mms2 promotes K63- linked polyubiquitination and is involved in p53-mediated DNA-damage response", DNA Repair, 20120201 Publication	<1%
60	www.teriin.org Internet Source	<1%

Exclude quotes On Exclude bibliography On